Declaration

This thesis is the result of the author's original research. It has been composed by the author and has not been previously submitted for examination which has led to the award of a degree.

Signed: Date:

Acknowledgements

The opportunity to study for a PhD could not be possible without the grace of God. Thank you God for giving me the good and bliss. I am grateful to Him for all the blessings that have led me to this.

Firstly, I would like to thank the Institute of pharmacy and biomedical sciences (SIPBS) department at the University of Strathclyde and the Qassim University for supporting this project.

I would like to extend sincere thanks to my supervisors Dr Marie Boyd and Prof. Alex Mullen for their efforts and enthusiasm towards the project throughout the 4 years. In particular, Dr Marie for her planning, scientific and emotional support throughout this project

I would also like to extend sincere thanks to Dr Annette Sorensen and Dr Khalid Alharbi, who have gone above and beyond to provide so much scientific, technical and emotional support throughout this project and for their patience and lengthly training to help me to understand the biological works.

Completion of this thesis would not have possible without the scientific knowledge, practical laboratory skills and the advice of members of the Boyd group both past and present at Strathclyde University, namely, Dr Tony and Dr Issrra and particular thanks given to Abdulfatah Alhazmi for his teachings in statistical analysis.

I would also like to extend sincere thanks to the members of the Alex Mullen group, in particular Racheal Donaghey for her help and support on

nanoparticles and HPLC analysis works. Also, I am thankful to Abiy Desta for his teaching and training on NGI device.

I would also like to extend sincere thanks to lab technicians Mrs Gillian Robb for her help with Confocal microscop (Biophotonics), Dr Gareth Westrop for his training on ultracentrifuge, and Lynne Kernweiss for her safety guidance through my works in the Lab.

Finally, I have been really blessed throughout this process to have had the continued support of my loving family, in particular my amazing mother Zahiya who have always been there to listen and sympathise with my science woes and for all of her help in the middle of my PhD by taking care of my beloved one, the little boy, Turkey. This would not have been possible without you, thank you and love you all.

Abstract

In the UK, there are approximately 46,403 new lung cancer cases and 35,600 deaths in 2016 due to lung cancer, with a survival rate estimated to be less than 10 years in 95% of cases. Cisplatin treatment is being considered in all stage non-small cell lung cancer patients with overall benefits of only a 1-year survival gain. Cisplatin has a number of major drawback such as toxicities and the acquisition of cisplatin resistance which undermines its potential effectiveness.

Therefore there is a great demand for effective therapeutic strategies to improve current cisplatin treatment. The overall aims of this project are to evaluate the effectiveness of cisplatin and topotecan (TPT) as a double therapy or as triple therapy with radiation. This include using a variety of molecular biology techniques to establish the cell kill potential of cisplatin in combination with TPT and radiation therapy on human lung cancer cell lines (H460 and A549). These survival studies were then underpinned to provide a mechanistic rationale. Another aim is to encapsulate cisplatin and TPT within lipid nanoparticles such as non-ionic surfactant vesicles (NIVs), as a drug delivery system for the treatment of lung cancer by inhalation. NIV formulation was developed and characterized and the efficacy of the NIVs encapsulated chemotherapeutic drugs as single agents and in combination were then compared with the efficacy of non-encapsulated agents by clonogenic assays. This study also includes studying physicochemical properties, such as particle size, surface charge, and entrapment efficiency of NIV formulations post-preparation, to determine their stability as a pulmonary drug delivery carrier.

Finally, aerosol formulations of TPT NIVs or TPT solution were nebulized using a mesh nebulizer to determine drug deposition and aerosol particle size distribution using an *in vitro* lung simulator device.

In vitro studies confirmed that the combination therapy of cisplatin and TPT with radiation as a triple therapy has the potential to increase DNA damage and to inhibit the DNA damage repair pathways of cancer cells, and achieving a greater cytotoxicity with lower doses than would be required to achieve therapeutic efficacy with a single agent while maintaining the potential antitumor activity.

The characterisation studies showed that the size and negative charge of TPT NIVs were 1264 to 1191 nm and -51 to -46, respectively over 7 days. While cisplatin NIVs size and charge values were 565.85 to 641.5 nm and -57.30 to -68.4, respectively. These results have enhanced the physicochemical characteristics and were capable of maintaining the encapsulated dug to accumulate in the target tissue. The total active drug deposited in the lung with TPT NIVs was significantly higher than TPT solution at the deeper stages (≤ 3 μm) of the lung simulator. These results indicate that NIVs encapsulating TPT provide a superior deposition efficiency when compared to free drug.

In conclusion, combination therapy of TPT and cisplatin has the potential to achieve greater cytotoxicity with lower doses than single therapy and NIVs as a vesicular delivery vehicle have a great capability of maintaining the encapsulated drug for the administration of cisplatin and topotecan to be accumulated in the target tissue.

Table of Contents

List of Figures

List of Tables

Abbreviations

ANOVA: Analysis of variance

APSD: Aerosol particle size distribution

ATM: Ataxia telangiectasia mutated

CDKs: Cyclin-dependent kinases

CHK1: Checkpoint kinase 1

CHK2: Checkpoint kinase 2

CI: Combination index

CT: Computed tomography

CTLA-4: T lymphocyte-associated protein 4

DCP: Dicetyl phosphate

DEF: Dose enhancement factor

DLS: Dynamic light scattering

DMEM: Dulbecco's modified eagle's medium

DNA: Deoxyribonucleic acid

DSBs: DNA double-strand breaks

EE: Entrapment efficiency

EGF: Epidermal growth factor

EGFR: Epidermal growth factor receptor

EPR: Enhanced permeability and retention

FACS: Fluorescence-activated cell sorting analysis

FPF: Fine particle fraction

GPs: Gelatine nanoparticles

HPLC: High performance liquid chromatography

HRR: Homologous recombination repair

ICH: International conference on harmonization

ISCs: Interstrand cross-links

LET: Linear energy transfer

LNPs: Lipid nanoparticles

mAb: Monoclonal antibodies

MMAD: Mass median aerodynamic diameter

NER: Nucleotide excision repair

NGI: Next generation impactor

NHEJ: Non-homologous end joining

NIVs: Non-ionic surfactant vesicles

NPs: Nanoparticles

NSCLC: Non-small cell lung carcinoma

PBS: Phosphate buffer solution

PD1: Anti-programmed cell death protein 1

PDGF: Platelet-derived growth factor

PDI: Polydispersity index

PI: Propidium iodide

PS: Phosphatidylserine

Rb: Retinoblastoma

RNA: Ribonucleic acid

SCLC: Small cell lung carcinoma

SF: Fraction of cells surviving

SSBs: Single-strand breaks

TFA: Trifluoroacetic acid

TFR: Transferrin receptor

TKI: Tyrosine kinase inhibitors

TPT: Topotecan

VEGF: Vascular endothelial growth factor

XBR: External beam radiation

ZP: Zeta potential

Chapter 1 : Introduction

1.1 Incidence and aetiology of cancer

According to the most recent statistics from UK Cancer Research, there are 360,000 new cancer cases in the UK every year, which equates to approximately 990 cases a day (Cancer Research UK, 2015). The most commonly diagnosed cancers are breast, prostate, lung and bowel cancers, and together these accounted for approximately 53% of all new cancer cases in the UK (Cancer Research UK, 2015). Despite the significant progress in cancer treatment that has been achieved to date, cancer is still responsible for 164,000 deaths in the UK every year, which is equivalent to 450 deaths per day (Cancer Research UK, 2016). Figure 1.1 demonstrates the number of cancer cases by type in the UK in 2015.

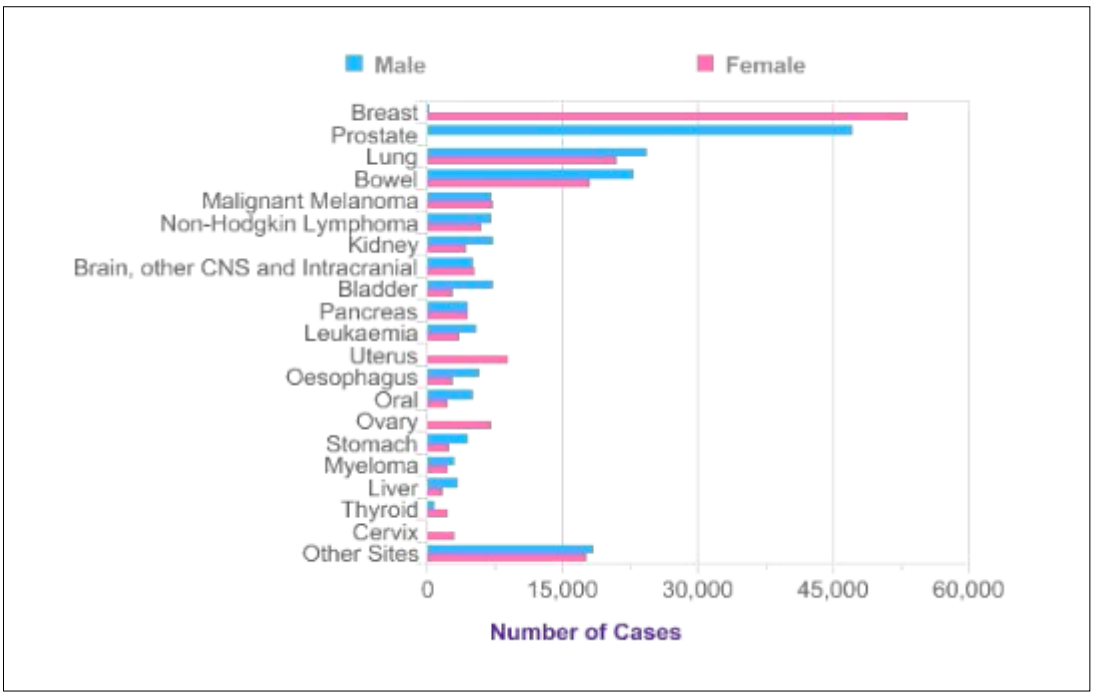

Figure 1.1 The number of cancer cases by cancer type in the UK in 2015, from UK Cancer Research (2015).

Cancer causes are many but the main underlying reasons are genetic mutations. Mutations can be caused by two main sources, inherited genetic mutations and environmental factors which have essential implications for cancer prevention (Tomasetti *et al*., 2017). Environmental factors include exposure to air pollution, sunlight, chemical and physical agents (such as tobacco), diet and obesity, infections (such as bacterial and onco-viruses), and radiation (both ionizing and non-ionizing) (Anand *et al*., 2008).

These causative factors can typically induce cancer by causing cells to acquire DNA alterations and genetic mutations during cell division (Lopez, 2015). Theoretically, the process of carcinogenesis is divided into three stages: initiation, promotion, and progression. The initiation stage encompasses an irreversible genetic change, while during the promotion stage the proliferation of initiated cells is increased, leading to a high population of initiated cells (Stewart, 2010). Progression is the accumulation of some mutated genes leading to a malignant or invasive phenotype (Bush and Moore, 2012).

1.2 Molecular basis of cancer

Cell division is a complex process which consists of multiple tightly regulated subroutines that control the cell cycle, including a series of checks that monitor cell growth, nutritional status, presence or absence of growth factors, and integrity of the genome (Barnum and O'Connell, 2014). These cell cycle regulatory pathways and the signal transduction pathways are populated with genes whose protein products are crucial to maintaining this tight control of cell division and if these genes are mutated this contributed to formation of cancer (Velez and Howard, 2015). Therefore, the uncontrolled cancer cell growth occurs as a result of mutated genes that accelerate growth and prevent normal growth inhibition (Stratton *et al.*, 2009, Broustas and Lieberman, 2014). The main genes categories that targets for mutagenesis are the oncogenes, tumour suppressor genes, and DNA repair genes (Sever and Brugge, 2015).

During cancer, the cell cycle division and the genome are disrupted by endogenous or exogenous insults, for example ionizing radiation, that causes alteration the chemical structure of DNA, such as a base missing from the backbone of DNA leading to a cellular DNA damage (Jackson and Bartek, 2009, Visconti and Grieco, 2009).This altered genome can be transmitted to daughter cells and this transmission can be avoided by activation of S and G2/M checkpoints in response to this DNA damage (Visconti *et al*., 2016, Katzung *et al.*, 2009). These checkpoints have the ability to arrest cell cycle progression and activate DNA damage repair pathways or, in case of unrepairable damage, stimulate cell death (Visconti and Grieco, 2009). This checkpoint mechanism is usually impaired in cancer cells leading to a genetic instability with resistance to

apoptotic cell death, hence contribute to neoplastic transformation (Jackson and Bartek, 2009). Much research has been undertaken to study genes which are most often mutated in cancers and understand the role of these genetic mutations in altering cell growth (Gerhards and Rottenberg, 2018). Identification of these mutated genes in cancers and interpretation of their mechanism of action is a key in identifying targets for development of novel therapeutic agents to treat cancer (Ojini and Gammie, 2015).

1.2.1 DNA damage response

The DNA damage response (DDR) involves a group of sensor proteins (checkpoint kinases) such as CHK1 (Checkpoint Kinase 1), ATM (Ataxia Telangiectasia Mutated), and CHK2 (Checkpoint Kinase 2) that identify and signal DNA damage to arrest cell cycle progression in order to repair this damage by activating cell cycle checkpoints in G1 phase, S phase and at the G2/M transition (Kastan and Bartek, 2004, Bartek and Lukas, 2007, Fujikane *et al.*, 2016). In particular, ATM kinase is activated by DNA double strand breaks (DSBs) that triggers the G1 checkpoint to activate the Chk2 and upon activation of Chk2 cells will be prevented from proceeding into S phase (Falck *et a*l., 2001, Matsuoka *et al*., 1998, Hein *et al*., 2014). Of note, the G1 checkpoint is mainly dependent on p53 and when ATM induces phosphorylation of p53 to be stabilized leading to induction of p21 that further inhibits the DNA repair proteins to promote apoptotic cell death (Banin *et al*., 1998, Vousden and Lu, 2002).

Most of cancer therapies target the DNA and this DNA damage induced cell death is attributed for most of the side effects experienced with cancer therapies such

as bone marrow suppression, gastrointestinal toxicities, and hair loss. Therefore, DNA damage causes the disease, it is used to treat the cancer, and it is responsible for the toxicity of cancer treatments (Kastan and Bartek, 2004).

1.3 Hallmarks of cancer

The hallmarks of cancer explain six biological capabilities developed during tumorigenesis. The hallmarks provides an understanding of cancer biology complexities (Figure 1.2) (Hainaut and Plymoth, 2013). The main cause of these hallmarks are genome instability and theses hallmarks are sustaining proliferative signalling, evading growth suppressors, resisting cell death, enabling replicative immortality, inducing angiogenesis, and activating invasion and metastasis (Gutschner and Diederichs, 2012).

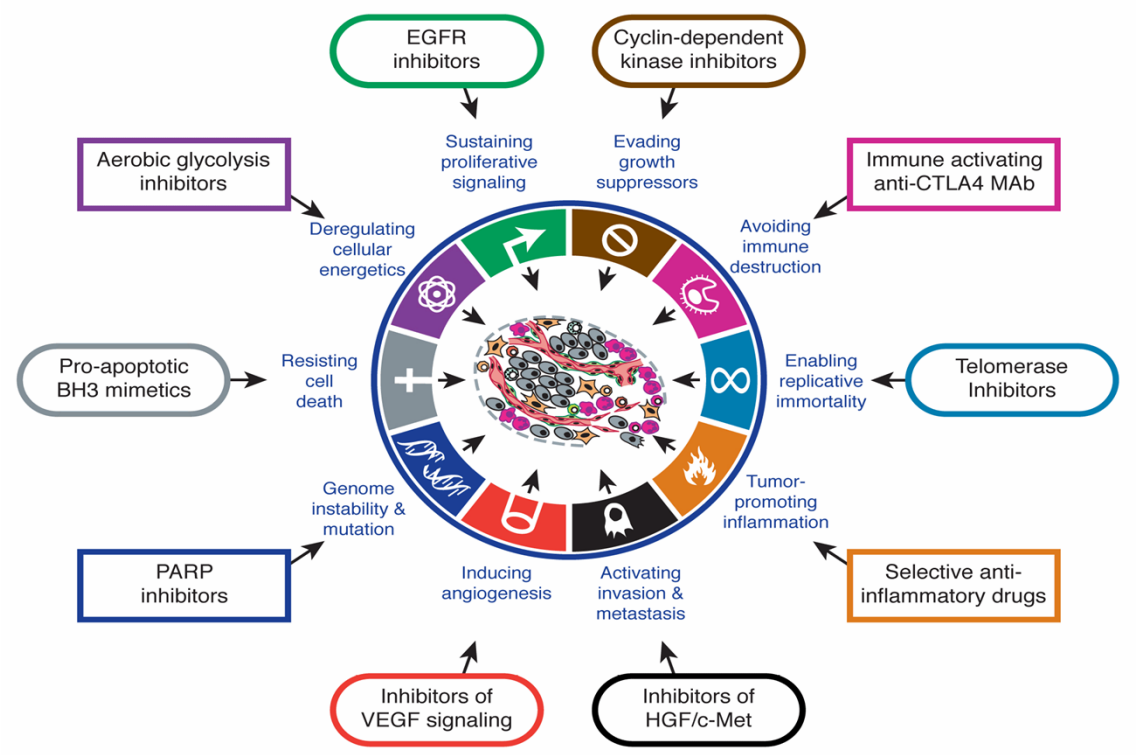

Figure 1.2 The hallmarks of cancer, from (Hanahan and Weinberg, 2011a)

1.3.1 Sustaining proliferative signalling

Cancer cells can constantly proliferate, this proliferation is achieved by the production of growth factor ligands, which send signals to normal cells to supply growth factors, increasing receptor proteins on the cancer cell surface to make them sensitive to growth factor ligand (Cheng *et al.*, 2008). An extensively studied growth factor is epidermal growth factor (EGF) and its receptor EGFR. EGF binds to an extracellular ligand, and a signalling pathway is triggered leading to activation of cell growth, proliferation, motility, and survival (Vivanco and Sawyers, 2002). Constant proliferation also activates components of the downstream signalling pathways or inhibits various pathways (Collado and Serrano, 2010). Mutations in EGFR are noticed in non–small cell lung cancer (NSCLC) in about 25% of cases (Zhang *et al*., 2016).

A tyrosine receptor kinase such as KIT, a type III receptor kinase, after ligand binding, KIT causes phosphorylation resulting in activation of downstream members of signalling pathways that control cell proliferation, apoptosis, chemotaxis, and metabolism (Rubin *et al.*, 2001).

1.3.2 Evading growth suppressors

Cancer cells have to evade regulation of cell proliferation. Tumour suppressors act in several ways to inhibit cell proliferation and growth. Mutations in tumour suppressors mean cancer cells have no checkpoints to regulate the cell-cycle division, and therefore persistent cell proliferation occurs (Aguirre-Ghiso, 2007). Cancers corrupt the pathway to redirect signals and activate another cellular program that can lead to abnormalities associated with high-grade malignancy

(Aguirre-Ghiso, 2007). Cyclins and cyclin-dependent kinases (CDKs) are responsible for maintaining control of the cell cycle division. Progression through the G1 and S phases needs the retinoblastoma (Rb) protein to be phosphorylated by CDKs and the dysregulation of these CDKs may result in uncontrolled cell cycle (Mayer, 2015, Finn *et al.*, 2016).

1.3.3 Activating invasion and metastasis

Metastasis occurs by two main steps, the first is physical spread of cancer cells from the primary tumour; the second step is the effective colonization in which transplanted cancer cells grow in a new setting, making micrometastases and later on become macroscopic tumours. The epithelial-mesenchymal transition is a step where epithelial cells develop the ability to invade and spread (Yilmaz and Christofori, 2009).

1.3.3 Enabling replicative immortality

There are two main barriers, senescence and crisis, to the proliferation of cancer cells in order to develop into macroscopic tumours (Baerlocher *et al*., 2015). Senescence cause irreversibly nonproliferative state of cancer cells, and crisis controls cell death. The unlimited proliferation is regulated by telomeres which protects the ends of chromosomes from fusion, progressive shortening of telomeres to lose their protective function leading to cell death (Hanahan and Weinberg, 2011b). Telomerase is a DNA polymerase that adds telomere repeat segments to the ends of telomeric DNA. It is over expressed in cancer cells and mainly absent in normal cells, and telomerase inhibitors may be a targeted therapy (Baerlocher *et al*., 2015).

1.3.4 Inducing angiogenesis

Cancer cells require nutrients and oxygen to function similar to normal cells to eliminate metabolic waste and carbon dioxide. Angiogenesis is constantly activated in tumour cells as a common denominator of several tumour types being induced early during the development of neoplasia (Hanahan and Folkman, 1996, Raica *et al*., 2009). Signalling proteins, including vascular endothelial growth factor (VEGF), basic fibroblast growth factor, and platelet-derived growth factor (PDGF), bind to endothelial surface receptors on the cell to regulate this angiogenic step (Tirumani *et al*., 2015). Due to rapid tumorigenesis, Hypoxia will be resulted causing the tumour to outgrow its blood supply. The well-known proangiogenic factor is VEGF-A which encodes ligands to induce new blood vessel growth and VEGF signalling by means of three receptor tyrosine kinases (Tirumani *et al*., 2015, Hanahan and Folkman, 1996). Tumour neovasculature is often abnormal with enlarged vessels that are abnormal branching, leaky capillaries, and microhemorrhage. Once angiogenesis is activated, tumours display diverse neovascularization patterns (Hanahan and Folkman, 1996).

1.3.5 Resisting cell death

Apoptosis is a natural defence mechanism against cancer development which involves upstream regulators and downstream effectors including TP53 and BCL-2 (tumour suppressors) during DNA damage or chromosomal abnormalities to induce apoptosis (Bartek *et al*., 2007). Loss of TP53 tumour suppressor can bypass apoptosis (Aubrey *et al*., 2017). BCL-2 inhibits apoptosis by binding to and suppressing BH3 proapoptotic proteins (Adams and Cory, 2007). As an

example of cancer where apoptosis induces resistance is lymphocytic leukaemia, in which BCL-2 protein expression is elevated (Adams and Cory, 2007).

1.4 Current treatment for cancer

There are three main conventional treatment methods used in cancer therapy namely; surgery, radiotherapy, and chemotherapy. The combination of these cancer treatment methods is widely practiced commonly to achieve maximum destruction of the tumour (Zappa and Mousa, 2016).

1.4.1 Surgery

Surgery is an effective treatment for cancer with significant outcomes in some cancer such as breast, colorectal and cervical cancers, and is usually used as a primary option during an early stage of cancer after being confirmed through diagnostic procedures such as biopsies where the presence and stage of the cancer can be determined (Wright, 2013). Surgery in cancer treatment is typically used in combination with either radiation or/and chemotherapy (Agnantis *et a*l., 2004, Huang *et al*., 2017) .

Therefore, in order to define whether cancer can be amended by surgery, the location and extent of the tumour are two main factors to differentiate between palliative and curative resections (Lefemine and Sweetland, 2012). A curative resection means an entire removal of tumours with the aim of leaving no cancer behind, whereas palliative resections is used in the management of cancer complications to ease and to reduce the severity of symptoms and the patient quality of life (You *et al*., 2007).

1.4.2 Radiation therapy

The effectiveness of radiation depends on the linear energy transfer (LET), total dose, fractionation rate and radio-sensitivity of the targeted cells or tissues. Low LET radiation deposits a relatively small quantity of energy whilst high LET radiation deposits higher energy on the targeted areas (Hall, 2007, Baskar, 2010, Kim *et al*., 2017).

Radiation therapy targets predominantly the DNA of cancer cells through directly or indirectly causing DNA double-strand breaks (DSBs) or single-strand breaks (SSB) which if unrepaired eventually lead to cell cycle arrest and apoptosis (Figure 1.3) (Baskar *et al*., 2014). The direct effect is achieved when radiation directly interacts with cellular DNA, causing damage. Indirect effects occur due to free radicals from the ionization or excitation of the water component of the cells. Double strand DNA breaks are more difficult to repair than SSBs and are more responsible than the single strand DNA breaks for apoptosis of cancer cells (Kurashige *et al*., 2016, Wang *et al*., 2018).

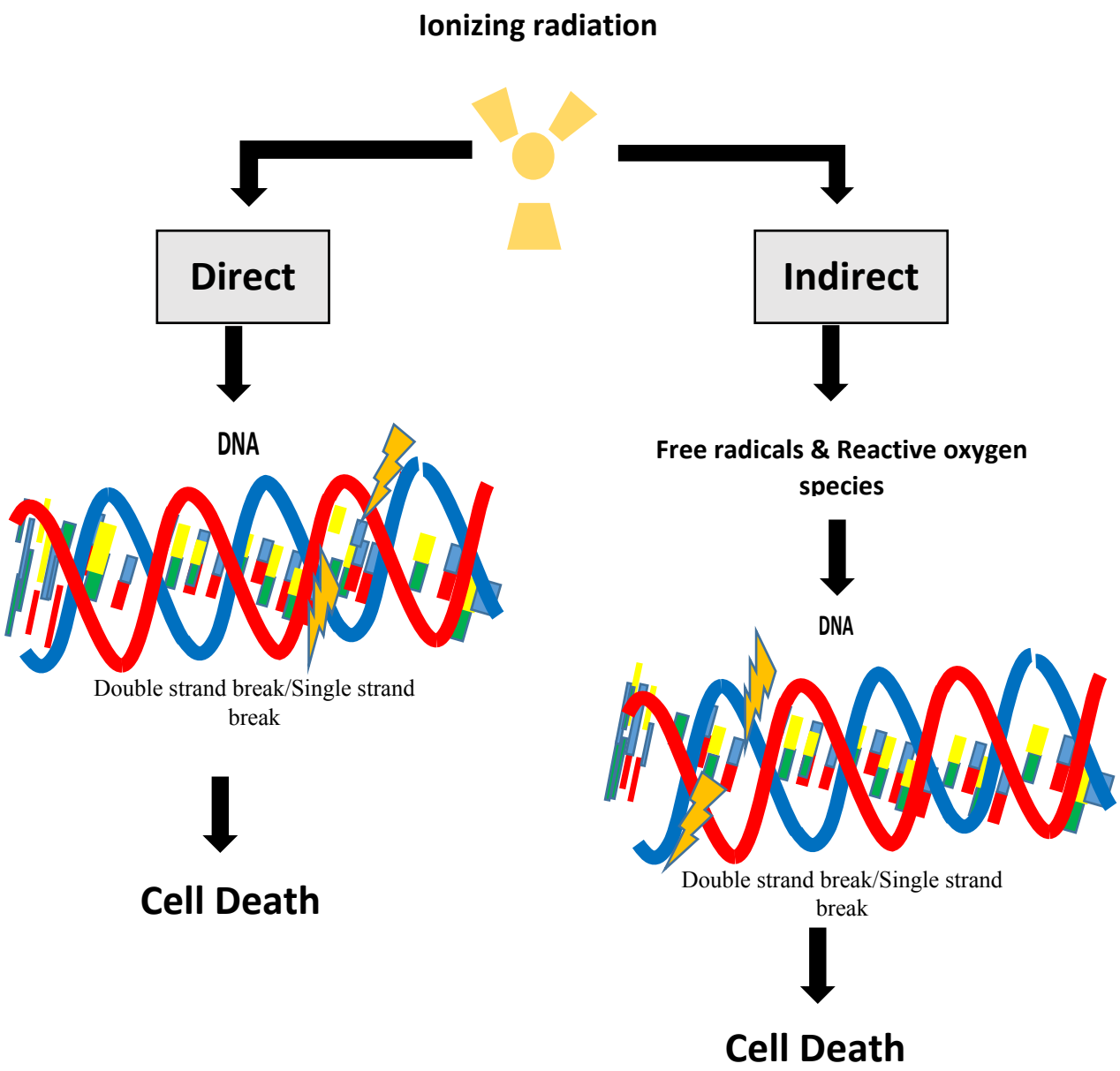

Figure 1.3 Direct and indirect DNA during apoptosis. Reproduced and modified from Baskar (2010).

1.4.3 Chemotherapy

Chemotherapy usually refers to the use of cytotoxic drugs, and have dominated systemic cancer therapy for the last 50 years, and their use has resulted in significant improvements in survival outcome for some cancers (Katzung *et al*., 2012, Palumbo *et al*., 2013).

There are a variety of different classes of cytotoxic drugs, including alkylating agents (such as cyclophosphamide and temozolomide), antimetabolites (such as methotrexate), topoisomerase I inhibitors (such as topotecan), microtubule-targeting chemotherapies (such as vinca alkaloids and taxanes), tyrosine kinase inhibitor (such as gefitinib) and platinum analogues (such as cisplatin) (Mihlon *et al*., 2010).

These cytotoxic drugs (Figure 1.4) are classified according to their mode of action but the main function of these cytotoxic agents is to disrupt the process of mitosis, which can be achieved in a variety of ways (Wells *et al.*, 2009). Conventional cytotoxic chemotherapy inhibits the growth of cancer cells by either damaging DNA, interfering with DNA synthesis, or otherwise inhibiting cell division (Priestman, 2008). Agents that affect cells only during a specific phase of the cell cycle are often called phase-specific agents or schedule-dependent agents, while agents that act on cells during any phase of the cell cycle are often called phase-nonspecific agents (Wells *et al*., 2009).

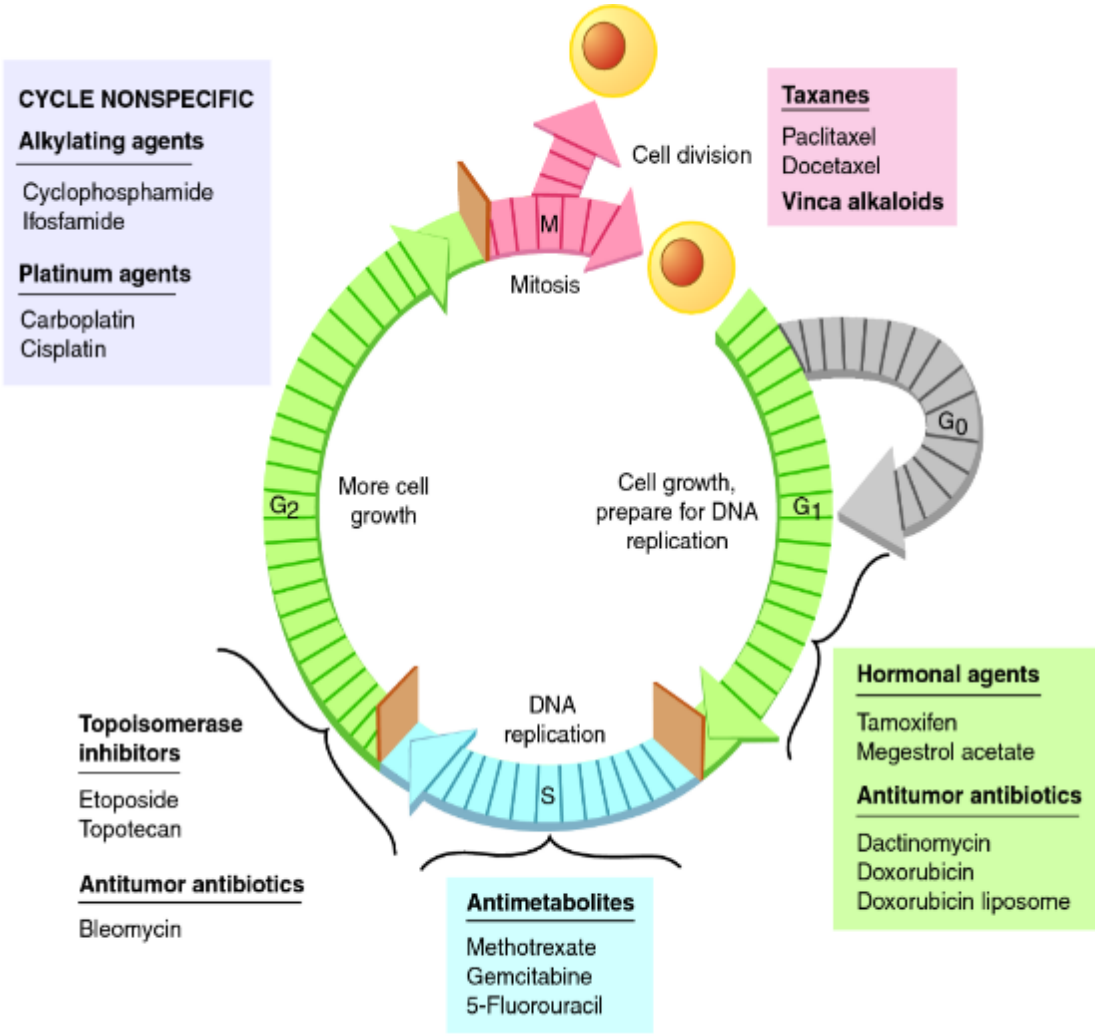

Figure 1.4 Diagram of the cell cycle and chemotherapeutic agents.

Chemotherapeutic agents are organized according to the cell cycle stage in which they have most effective on tumor control (Hoffman *et al.*, 2016) .

Chemotherapeutic agents potentially target cancer cells and have improved therapeutic outcomes for cancer patients. However, their numerous side effects have undesirable effects that may affect patient survival and also quality of life (Khawaja *et al*., 2013). Kastan and Bartek (2004) have significantly linked DNA damage, as a main mechanism of action of many cancer treatments, to induce side effects such as bone marrow suppression, gastrointestinal toxicities, and hair

loss, in particular when the recommended dose of a cytotoxic drug has to be lethal to tumour and consequently unsafe to the patient if not adjusted upon each patient considerations (Gurney, 2002). In addition, the lack of selectivity for targeting cancer cells over normal cells cause insufficient drug concentrations at tumour sites, and this result in systemic toxicities and inducing drug-resistant tumour cells (Xu and McLeod, 2001, Padma, 2015, Weyel *et al*., 2000).

Consequently, there is a great demand for more effective therapeutic strategies capable to reduce these treatment issues. Therefore, a number of effective strategies have been used for improving tumour selectivity, including alternative formulations and resistance modulation by using combination therapy (Padma, 2015).

The therapeutic and toxic properties of some chemotherapeutic drugs enable them to interfere with DNA function and integrity to induce cell death (apoptosis) in rapidly proliferating tissues (Liu *et al*., 2014, Katzung *et al.*, 2012), because many agents affect the cell cycle, their lethal effects are not realized until the cells proceed through the cycle. These drugs are most cytotoxic to tumour cells with a high growth fraction and least cytotoxic to tumour cells arrested in the G_0 phase (Koda-Kimble *et al*., 2008).

1.4.4 Immunotherapy

Recently, various components of the immune system have been identified by their pivotal roles in protecting humans from cancer, immunotherapy in treating cancer has recently had a significant improvement (Farkona *et al*., 2016), in particular after the approval of the autologous cellular immunotherapy, sipuleucel-T, for the treatment of prostate cancer (Sharma *et al.*, 2011) and the approval of the anti-cytotoxic T lymphocyte-associated protein 4 (CTLA-4) antibody, ipilimumab, and of anti-programmed cell death protein 1 (PD1) antibodies for the treatment of melanoma (Sharma and Allison, 2015b).

Immunotherapies in treating cancers work in various approaches, firstly, by stimulating and activating effector immune cells through vaccination with tumour antigens or augmentation of antigen existence to improve the patient's own immune system to response against cancer cells (Yaddanapudi *et al*., 2013). Secondly, immunotherapies have a stimulatory effect to enhance T cell activity, this activation involve using an adoptive cellular therapy (ACT) in which immune cells directly administered to patients (Sharma and Allison, 2015a). Additionally, oncolytic viruses (OVs) can be administered to activate the systemic antitumor immunity (Farkona *et al.*, 2016).

1.5 Lung cancer

According to statistics from UK Cancer Research, there are 46,700 new cancer cases in the UK every year, which equates to approximately 130 cases a day (Cancer Research UK, 2015). In the UK, lung cancer is the most common cause of deaths with 35,600 every year and accounted for 21% of all cancer deaths in 2016 (Cancer Research UK, 2016). Approximately 10% of patients diagnosed with lung cancer survive their disease for five years or more and around 32% survive their disease for one year or more. With the significant progress in lung cancer treatment that has been achieved to date, only 5% survive their disease for ten years and this percentage is the same since 1970s (Cancer Research UK, 2016). These death rates indicate a great necessity for further improvements in cancer therapies aiming to reduce cancer related mortality (Cancer Research UK, 2015).

Lung cancer occurs as a result of the exposure of epithelial cells to carcinogens, which leads to chronic inflammation originating from genetic and cytological changes which eventually leads to a solid tumour (Wells et al., 2009). From a biological and histopathological perspective, lung cancer is considered to be a complex carcinoma with different histological types, namely, small cell lung carcinoma (SCLC) and non-small cell lung carcinoma (NSCLC) (Oser et al., 2015). Metastatic lung cancer can cause neurologic deficits, bone pain and liver dysfunction (Rygiel et al., 2017). Chest x-ray and computed tomography (CT) scan are used as valuable diagnostic tools to establish the diagnosis, in addition

to the other pathologic examinations such as sputum cytology, tumour biopsy, mediastinoscopy, and open-lung biopsy (van Beek et al., 2015).

Due to the advancement in the field of molecular technologies, we now have a better understanding of the biological progressions involved in the pathogenesis of lung cancer (Hanahan. and Weinberg., 2000). A recent clinical trial indicated that lung cancers result from the accumulation of many genetic and epigenetic variations, resulting in abnormalities whereby tumour suppressor genes are inactivated and oncogenes are activated (Minna *et al*., 2002). In addition to these molecular abnormalities, the pathogenesis of lung cancer includes abnormalities in sustained angiogenesis, self-sufficiency of growth signals, insensitivity to antigrowth signals, limitless replicative potential, evasion of apoptosis, and tissue invasion and metastasis (Hanahan. and Weinberg., 2000). These molecular advances have demonstrated significant opportunities for the discovery and development of new targeted anticancer therapies as novel treatments for lung cancer (Minna. *et al*., 2002). These advances have resulted in the evolution and discovery of a new area of anticancer therapies that takes advantage of cancer-specific molecular abnormalities (Fong *et al.*, 2003). In this circumstance, understanding the mechanism of these molecular defects of lung cancer becomes even more important, and this leads to an interesting challenge in how to adequately integrate the predictable pathological and molecular investigations into the diagnosis, classification, and selection of appropriate therapeutic options to treat lung cancer effectively (Hanahan. and Weinberg., 2000).

1.5.1 Non-small-cell lung carcinoma

Non-small-cell lung carcinoma (NSCLC) is the commonest form of lung cancer cells and accounts for 75-80% of all lung cancer it is subdivided into three main histological types, namely, adenocarcinoma (45%), squamous cell carcinoma (30%), and large cell carcinoma (9%) (Gazdar and Brambilla, 2010). Moreover, there are some other unspecified and mixed cell types that occur less frequently (Brambilla *et al*., 2004). Due to the high resistance patterns of NSCLC when treated with chemotherapy, treatment with surgery is considered primarily at early stages of diagnosis (Brambilla *et al.*, 2004).

1.5.2 Small-cell lung carcinoma

Small-cell lung carcinoma (SCLC) is a malignant tumour that accounts for nearly 15% of all lung cancers and is less common but grows more rapidly than NSCLC. Therefore, patients are often diagnosed with SCLC at an advanced stage due to difficulty in diagnosing the disease (Jin *et al*., 2012, Lantuejoul and Brambilla, 2018). SCLC incidence is strongly related to cigarette smoking (Stewart and Wild, 2014). In contrast to NSCLC, SCLC is treated mainly by combined therapies such as chemotherapy and radiotherapy due to its chemo-radio sensitivity (Travis *et al*., 2004).

1.6 Clinical features and staging

Lung cancer staging determines the extent of the tumour, its location, and the severity of cancer according to the size of the original tumour and the extent of metastasis (Chheang and Brown, 2013). Furthermore, staging lung cancer has a key role in determining prognosis and selecting the appropriate approach for treatment (Tsim *et al*., 2010). The TNM staging system is used widely to classify lung cancer, and explains the extent of the tumour (T), the extent of spread to the lymph nodes (N), and the presence of metastasis (M) (Table 1.1). However, SCLC is usually staged and classified as either limited or extensive disease in accordance with the International Association for the Study of Lung Cancer (IASLC) (Travis *et al.*, 2004, Kalemkerian, 2011).

Table 1.1 The TNM staging system adapted from (Kalemkerian, 2011).

Category	Description
T	The original or primary tumour
TX	Primary tumour cannot be evaluated
T0	No evidence of primary tumour
T1–T4	Size and/or extent of primary tumour
N	Cancer tumour has extended to reach the lymph nodes
NX	Regional lymph nodes cannot be assessed
N0	Lymph nodes do not contain cancer cells
N1-N3	Involvement of lymph nodes (number and/or extent of spread)
M0	No distant metastasis
M1	Distant metastasis (cancer has spread to distant parts of the body)

1.7 Lung cancer treatment

In terms of SCLC treatment, radiation therapy alone is recommended for limited disease and combination therapy of radiation and chemotherapy (platinum based therapy) is the standard treatment for extensive SCLC; around 60-70% of patients with extensive disease and 70-90% of patients with limited disease have experienced at least temporary remission with this standard treatment (Gabriela and Daniela, 2016). As shown in Figure 1.5, the vast majority of patients (71%) with early stage NSCLC undergo surgery and around 18% also receive chemotherapy or radiation (Siegel *et al.*, 2012). Patients with advanced stage NSCLC are treated with chemotherapy alone (20%), radiation therapy alone (17%), or a combination of the two treatments (35%) (Siegel *et al.*, 2012).

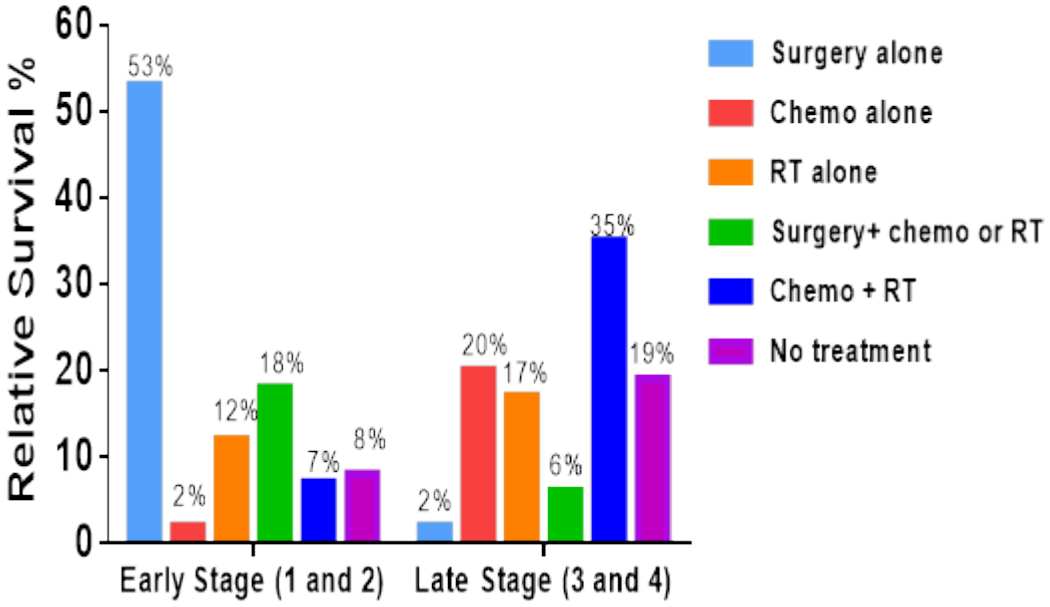

Figure 1.5 Non-Small Cell Lung Cancer Treatment Patterns by Stage.

Reproduced and modified from Siegel *et al*. (2012). Chemo = chemotherapy; RT = radiation therapy.

In recent years, the use of targeted therapy for management of patients with NSCLC has revolutionized the treatment of lung cancer. NSCLC is now classified by driver mutation in which these mutations can be inhibited by targeted therapy such as monoclonal antibodies (mAb) or tyrosine kinase inhibitors (TKI). Whereas chemotherapy with a platinum compound, such as cisplatin, either alone or in combination with other cancer therapy, remains the gold standard treatment for NSCLC without a known driver mutation (Camidge *et al*., 2014, Chan and Hughes, 2015).

1.7.1 Targeted Therapy: monoclonal antibodies (mAb) and tyrosine kinase inhibitors (TKIs)

The NSCLC with a known oncogenic driver mutation and mutant EGFR (Epidermal growth factor receptor) in receptors or protein kinases have the potential to stimulate a complex cascade of cross signalling pathways leading to uncontrolled growth. Therefore, these up-regulated pathways can be treated by either TKIs or mAb. This mutant EGFR can be inhibited either by TKI (such as gefitinib) or mAb (such as cetuximab) (Alamgeer *et al*., 2013, Savas *et al*., 2013).

Gefitinib was the first EGFR TKIs to be approved and act as a reversible competitive inhibitor of ATP for the tyrosine kinase domain of EGFR resulting in blockade of downstream pathways (Krawczyk *et al*., 2017). Gefitinib also acts on upregulating the cell cycle inhibitor (p27) and downregulation of a transcription factor causing G1 phase arrest of the cell cycle (Ahn *et al*., 2014).

Gefitinib is administered orally and inhibits the phosphorylation and tyrosine-kinase activity of the intracellular ATP-binding domain of EGFR over a

competitive biding to this site (Huang and Fu, 2015). This inhibition and its related downstream action is achieved by a daily dose of 250 mg, while the maximum dosage is 700 mg/day. Pharmacokinetic investigations indicated that gefitinib is adsorbed slowly and it reaches peak plasma concentration between 3–7 hours and have a half-life of about 28 hours that is why gefitinib is administered once daily (Nurwidya *et al*., 2016).

Cetuximab (mAb) has the potential to downregulate EGFR on the cell membrane and specifically binds to the extracellular domain of EGFR as a competitive antagonist of the endogenous ligands (Cho *et al*., 2013). This binding effect of cetuximab results in internalization of the EGFR and effectively leading to blocking EGFR-mediated signalling resulting in cell cycle arrest in G1, and pro-apoptotic processes. Cetuximab also can affect EGFR-dependent transcriptional processes, which reduces angiogenesis, tumour invasiveness, and metastasis (Kol *et al*., 2017).

Cetuximab is administered intravenously in a dose of 400 mg/m2, with a subsequent weekly dose of 250 mg/m2. The cetuximab is associated with many serious side effects such as cardiopulmonary arrest, dermatologic toxicity and radiation dermatitis, sepsis, renal failure, interstitial lung disease, and pulmonary embolus (Martinelli *et al*., 2009).

1.7.2 Cisplatin

Cisplatin usage in cancer has shown to be effective in treating malignancies either alone or in combination with other anticancer therapies and it is considered to be the first line treatment for testicular, ovarian, head and neck, bladder, cervical and lung cancer (Dasari and Tchounwou, 2014). Cisplatin treatment is being considered in all stage NSCLC patients however, it has overall benefits of only a 1-year survival gain and 1.5-month absolute increase in median survival were reported in a meta-analysis study (Delbaldo *et al*., 2004). Figure 1.6 shows chemical structure of cisplatin.

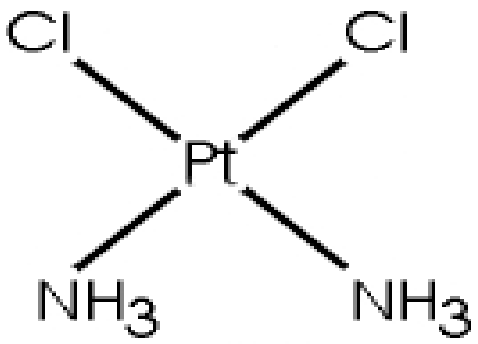

Figure 1.6 Cisplatin chemical structure (Florea *et al.,* 2011).

Cisplatin has at least one N-H group, which controls the hydrogen-bond donor properties and considered to the approach of its biological target (Florea and Büsselberg, 2011). Cisplatin has the general formula cis-[$PtX_2(NHR_2)_2$] and acts in several ways to cause intrastrand crosslink of DNA (Figure 1.7) and interfere with cell division (Katzung *et al*., 2012), mainly by formation of platinum–DNA adducts incorporated into DNA at the N7 binding site, consequently inhibiting the

DNA repair mechanisms which activate apoptosis if the repair is unable to be completed (Tanida *et al*., 2012).

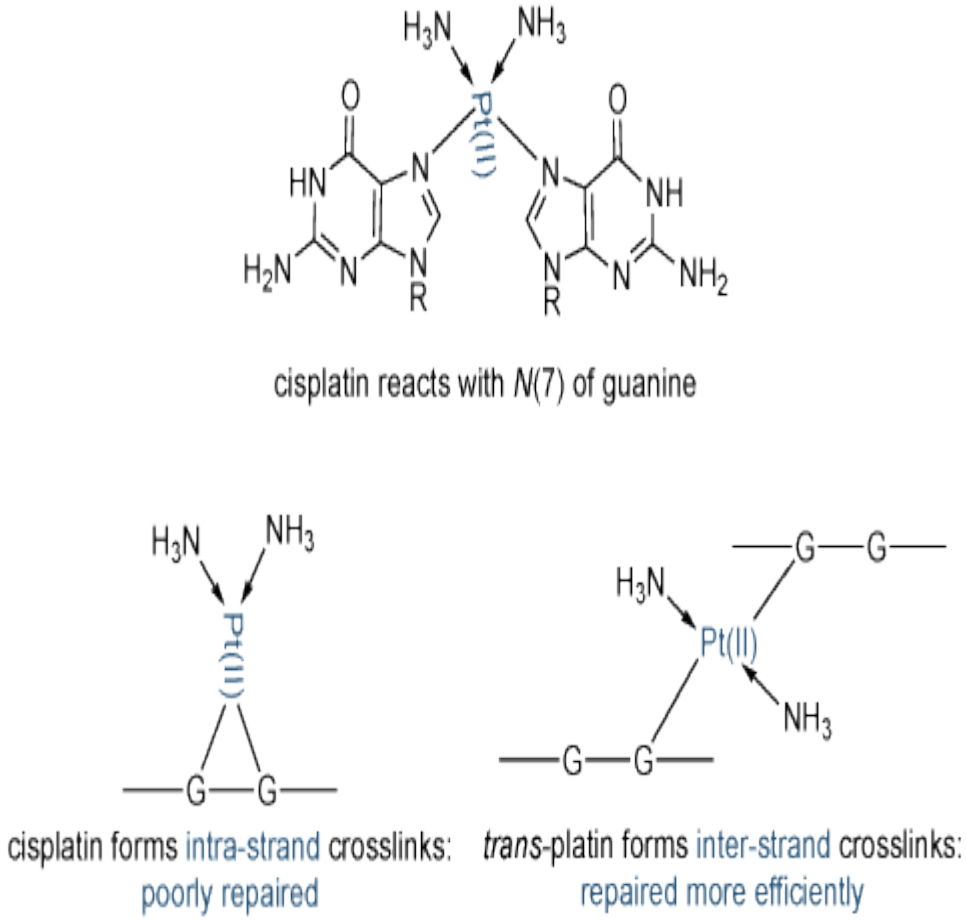

Figure 1.7 Pathways for intrastrand crosslinking of DNA caused by cisplatin. The figure displays the structure of guanine and the position of N7 (major Pt binding site) from Kostova (2006).

Cisplatin is only administered intravenously, and about 90% of cisplatin in the blood is bound to plasma proteins. The highest concentrations of cisplatin is found in the kidney, liver, intestine, and testes, but with poor CNS penetration.

Approximately 25% of the drug is excreted by the kidney after 24 hours, and up to 43% of the administered dose is recovered in the urine within five days (Visacri *et al*., 2017).

Cisplatin produces responses in all forms of carcinoma of the lung and is proven to sensitize cells to radiation therapy and improve control of locally advanced lung, oesophageal, and head and neck tumours when administered in combination with irradiation (Wells *et al*., 2009, Dasari and Tchounwou, 2014). While DNA is the ultimate target of all platinum agents including cisplatin, resistance to alkylating agent may develop rapidly when it is used as a single agent in the presence of specific biochemical changes involved in this resistance (Ettinger *et al*., 2013, Housman *et al*., 2014). These biochemical changes include decreased permeation of actively transported platinum drugs and increased intracellular concentrations of nucleophiles. Nucleophiles can linked with electrophilic intermediates and increased activity of DNA repair pathways, which, eventually, increases the activity of the complex nucleotide excision repair (NER) pathway that seems to correlate with resistance to most platinum adducts (Shen *et al*., 2012, Basourakos *et al*., 2017).

Cisplatin-induced nephrotoxicity and ototoxicity tend to be more frequent and severe with repeated doses given intravenously and prolonged treatment at high doses, which may cause progressive peripheral motor and sensory neuropathy, myelosuppression, transient leukopenia and thrombocytopenia with electrolyte imbalances, including hypomagnesemia, hypocalcaemia, and hypophosphatemia (Miller *et al*., 2010, Karasawa and Steyger, 2015).

1.7.3 Topotecan

Topotecan (TPT) is a semisynthetic chemotherapeutic agent approved by the FDA as a treatment for SCLC in 2000 and is a water-soluble analogue of camptothecin, and works as a topoisomerase I inhibitor (Vennepureddy *et al*., 2015). The chemical structure of TPT is shown in Figure 1.8.

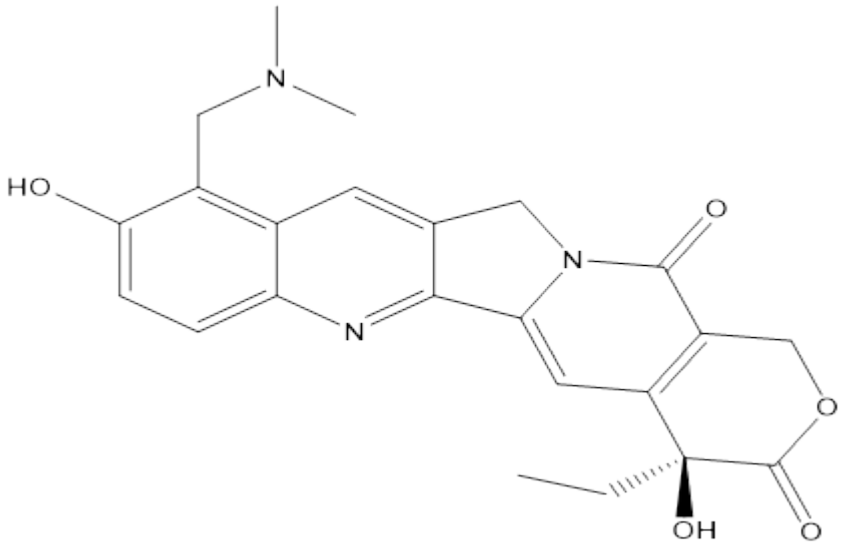

Figure 1.8 Topotecan chemical structure.

DNA topoisomerase I is a nuclear enzyme that plays a vital role in relaxing and supercoiling double-stranded DNA and is significantly involved in DNA-related functions, such as replication, recombination, and RNA transcription (Pommier *et al*., 2016). Topoisomerase I repairs single-stranded DNA break when it

preferentially binds to supercoiled duplex DNA to form a short catalytic intermediate (cleavable complex) where the topoisomerase I enzyme is covalently bound to a tyrosine residue (Figure 1.9) (D'Annessa *et al*., 2014).

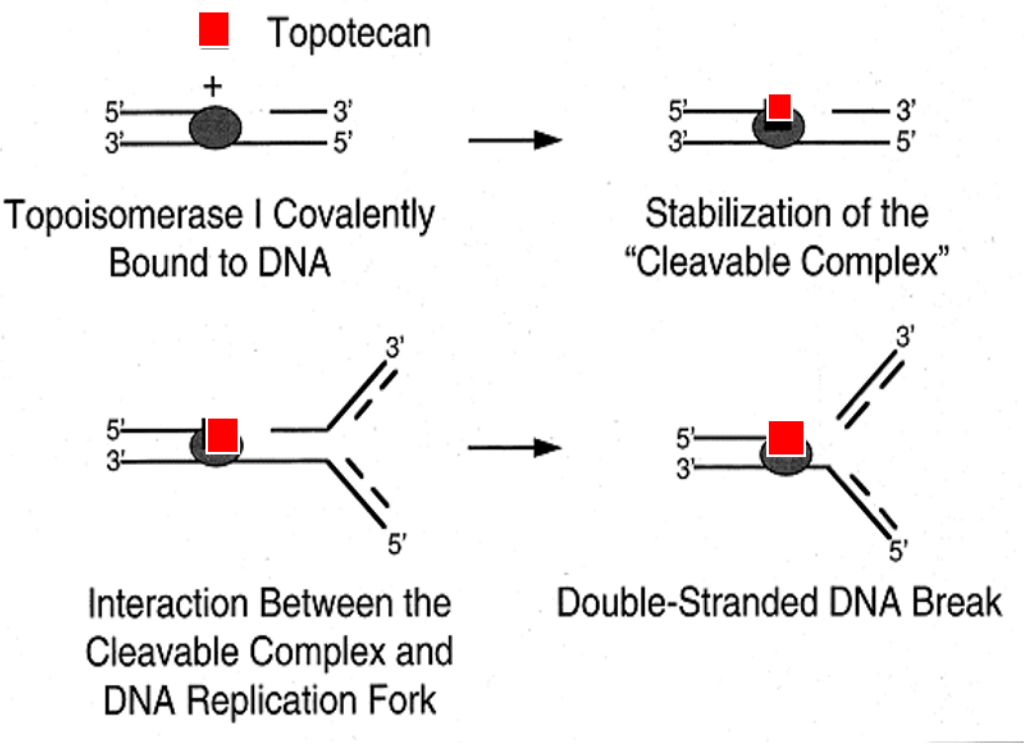

Figure 1.9 Topotacan mechanism of action. Topoisomerase I cleavable complex during DNA replication leading to DNA damage (Takimoto and Arbuck, 1997)**.**

This complex, permits for the relaxation of the torsional strain by facilitating passage of the intact strand through the single-stranded DNA, or by rotating around the remaining intact DNA phosphodiester bond (Capranico *et al.*, 2017). Rapid DNA relegation followed by enzyme dissociation regenerates a torsionally relaxed, intact double helix. However, in the presence of topotecan

topoisomerase I inhibitor) the relegation reaction by binding noncovalently to the topoisomerase I-DNA cleavable complex will be inhibited, consequently, the single-strand DNA breaks accumulate within the cell (Zhao and Darzynkiewicz, 2017, Capranico *et al*., 2017). Thereby disrupting the DNA duplication process and preventing DNA replication, which eventually leads to cell death (Staker *et al*., 2002).

TPT has a serum half-life of 3 hours with a high volume of distribution and high tissue uptake associated with low protein binding. These properties enable TPT to penetrate the blood-brain barrier (Wong and Berkenblit, 2004). The serious haematological side effects, such as neutropenia, thrombopenia, and anaemia, are more commonly experienced with TPT. Other side effects include fatigue, anorexia, and dyspnoea (Horita *et al*., 2015).

1.8 Rationale behind combination therapy

The most compelling rationale for combination chemotherapy, is firstly tumour cell heterogeneity that initiate drug resistance, and secondly the success of combination chemotherapy in the clinic in minimizing cytotoxicity and maximizing the therapeutic effectiveness in different malignant tumours. Therefore, the combination therapy in cancer is aiming to, exposure cancer cells to cytotoxic drugs in combination with radiation that could cause DNA double strand breaks whereby cancer cell DNA damage cannot be repaired, whereas it can be repaired when a DNA single strand is caused by a cytotoxic effect (Hall, 2007, Asaka-Amano *et al*., 2007). .

The effect of radiosensitisation on the efficacy of chemotherapy coupled with the discovery of targeted forms of radiotherapy that has been at the forefront of radiation therapy research. As a therapeutic strategy to overcome the current toxicities associated with cancer therapy, it has been reported by previous studies that sublethal doses of multiple chemotherapeutic agents and radiation in various cancer cells can limit normal cell toxicity while enhancing toxicity to cancer cells (Gelbard *et al*., 2006). In addition, chemotherapy expected to modify cancer cells response to radiation by altering and repairing the inherent cellular radiosensivity and function as a selective radiosensitiser targeting especially those resistant cells to radiation (Alcorn *et al*., 2013). Hence, using agents directed against DNA repair pathways and pathways associated with tumour cell survival have the potential to enhance radiotherapy (Mairs and Boyd, 2011).

Cisplatin appears to be a particularly good candidate to be combined with radiation (Figure 1.10) (Liu *et al*., 2014).

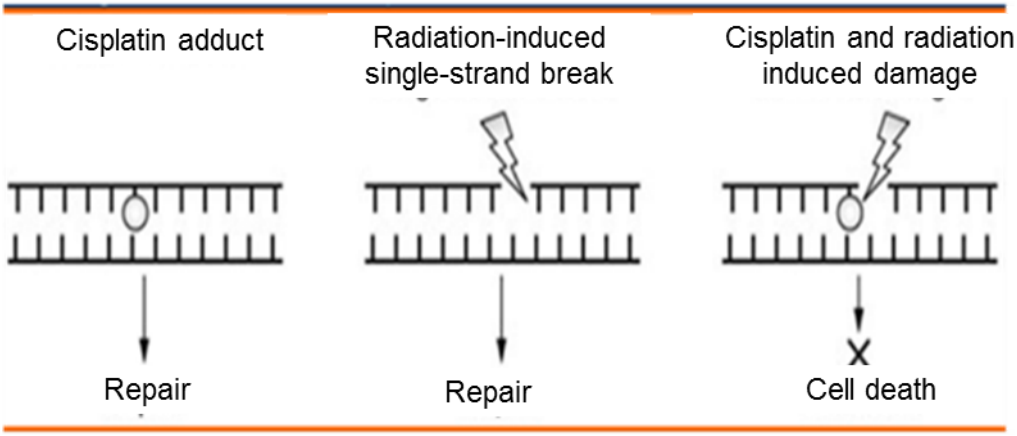

Figure 1.10 Increased DNA damage by addition of cisplatin to radiation. Data from (Seiwert *et al*., 2007).

Numerous in *vivo* and in *vitro* studies concluded that the combination of ionizing radiation and cisplatin provide a synergetic effect (Akudugu and Slabbert, 2008, Molerón, Hermann *et al.*, 2008, Boeckman *et al*., 2005a, Rose *et al.*, 1999, 1999, Dolling *et al*., 1998, Utsumi and Elkind, 2001, Calsou and Salles, 1993, Allalunis-Turner *et al.*, 1993, Asaka-Amano *et al*., 2007). As an attempt to understand the molecular basis in which cisplatin induce radiosensitisation, some previous studies concluded that the combination of ionizing radiation and cisplatin provides a clear synergetic effect in cancer cells proficient in non-homologous end joining (NHEJ) catalysed repair of DNA DSB and revealed that a site-specific cisplatin-DNA lesion results in complete abrogation of NHEJ catalysed repair of the DSB

(Boeckman *et al.*, 2005a). In addition, Dong *et al.* (2017a) provide an explanation of the molecular mechanism of cisplatin radiosensitisation in which cisplatin enhancement effects on DNA base damage and contributes significantly to radiosensitisation process. According to Dong *et al*. (2017a), there are two major mechanisms explaining the synergy of cisplatin with radiation, firstly, the inhibition of the DNA damage repair induced by radiation and an increase in cellular DNA damage caused by additional immediate species created by the primary radiation, both of which occur when cisplatin reacts with the purine bases and binds with DNA to form intrastrand cross-links. Furthermore, a research conducted by Sears *et al.* (2016b) to investigate the mechanism of synergism between cisplatin and radiation in NSCLC and confirmed that inhibition of DDR sensor kinases caused the persistence of γ-H2Ax foci in treated cells is independent of kinase activation and suggest that the delayed repair of DSBs in NSCLC cells treated with cisplatin combined with radiation contributes to cisplatin radiosensitisation and that alterations of the DDR process by inhibition of specific DDR kinases.

TPT is used as a radiosensitizer agent that can sensitize cancer cells to radiation and increase DNA damage by its inhibitory effects on topoisomerase I enzyme (Eyvazzadeh *et al*., 2015). Another study by Marchesini *et al*. (1996) investigated the interaction between TPT and ionizing radiation on H460 lung cancer cells and concluded that a supra-additive cell kill following this combination therapy.

Marchesini *et al.* (1996) observed that the radiosensitisation by TPT was related to a high level of topoisomerase I in H460 cells and its role as an enzyme in the DNA repair process of radiation damage.

Cisplatin could be more effective when combined with another chemotherapeutic agent, in particular topotecan (topoisomerase I inhibitor) as it has been shown that the DNA single strand breaks (DNA damage) caused by cisplatin are usually followed by induction of topoisomerase 1-dependent cleavage. This induction by topoisomerase is a DNA damage repair response to the DNA damage caused by cisplatin (Romanelli *et al*., 1998). Therefore, generally the rationale to combine topotecan with cisplatin is to increase DNA damage and to inhibit the DNA damage repair, thus driving the cells to apoptosis using lower doses than would be required to achieve therapeutic efficacy with a single agent while maintaining the potential antitumor activity.

Previous in *vitro* studies have reported synergistic effects between topotecan and cisplatin in combination in cancer cells and concluded that combination of TPT and cisplatin induced were supra additive cell kill when utilised in A549 lung cancer cell lines (Adjei *et al.* 1996). Whereas, Kaufmann *et al*. (1996) examined TPT and cisplatin as a combination on A549 cell line and found that the combination index values less than additive effects were seen at low to intermediate levels of cytotoxicity.

The combination therapy of TPT and cisplatin with radiation (triple therapy) may enhance the overall therapeutic advantages due to the nature of TPT to be a

radiosensitizer agent that can sensitize cancer cells to radiation and increase DNA damages by its inhibitory effects on topoisomerase enzyme (Eyvazzadeh *et al*., 2015). However, the effects of all these modalities as a triple therapy combination (cisplatin and TPT in combination with radiation) in *vitro* have been limited.

1.9 Delivery systems

As mentioned (Section 1.7.2), cisplatin is the first line chemotherapy in treating lung cancer and administered intravenously (systematically). However, recently, the use of targeted therapy for management of lung cancer by inhalation has revolutionized the treatment of lung cancer aiming to minimize the cytotoxicity effects associated with the intravenous route of administration in different normal and cancer cells (Camidge *et al*., 2014, Chan and Hughes, 2015).

1.9.1 Intravenous delivery system

Intravenous (IV) route is the main route of administration for chemotherapy where the entire dose enters the bloodstream and this is followed by distribution of the drug to all body tissues through the circulation. IV route has a very onset of action because of the circulation (blood) that transport medications through a network of vessels consisting of arteries, capillaries and veins in which the drug distribution depends on many factors such as the blood flow to the organs and tissue, plasma protein binding, the molecular weight of the drug, the drug lipophilicity, and the binding affinity of the drug to some tissues (Jin *et al*., 2015).

The main advantage of IV drug delivery is the fast onset of action where the therapeutic effect can be experienced after very short of times (seconds), however in terms of delivering chemotherapy in treating lung cancer, the IV route has drawbacks and complications such as short duration of action, infiltration, phlebitis and thrombophlebitis, and extravasation at injection site (Rivera *et al*., 2005, Barsoum and Kleeman, 2002). One of the most important drawback is that the IV route is unable to differentiate between cancer and normal cells, and so the inhibition of cell division in both cancer and normal cells are being occurred, this lead to the adverse reactions and side effects (Stewart, 2010). Hence, there is a great demand for an alternative route of administration such as the pulmonary route where chemotherapy can be delivered as a targeted therapy targeting cancer cells alone.

1.9.2 Respiratory System

The main function of the respiratory system is gas exchange where oxygen, which is needed for our cells to function, is transferred into our bloodstream from external environment while carbon dioxide which is a waste product of cellular function is exhaled into the outside air (Bates, 2009).

1.9.2.1 Physiology of the respiratory system

The respiratory tract has two main parts (Figure 1.11): the upper respiratory tract, consisting of the nose, nasal cavity and the pharynx; and the lower respiratory tract consisting of the larynx, trachea, bronchi and alveolar duct (Smola *et al*., 2008). During the inhalation, the oxygenated air first enters the nose passes

through the larynx and the trachea where then trachea divides into two bronchi. Each bronchus splits into two small branches creating bronchial tubes. These tubes terminate with a tiny sacs called alveoli where the gas exchange takes place.

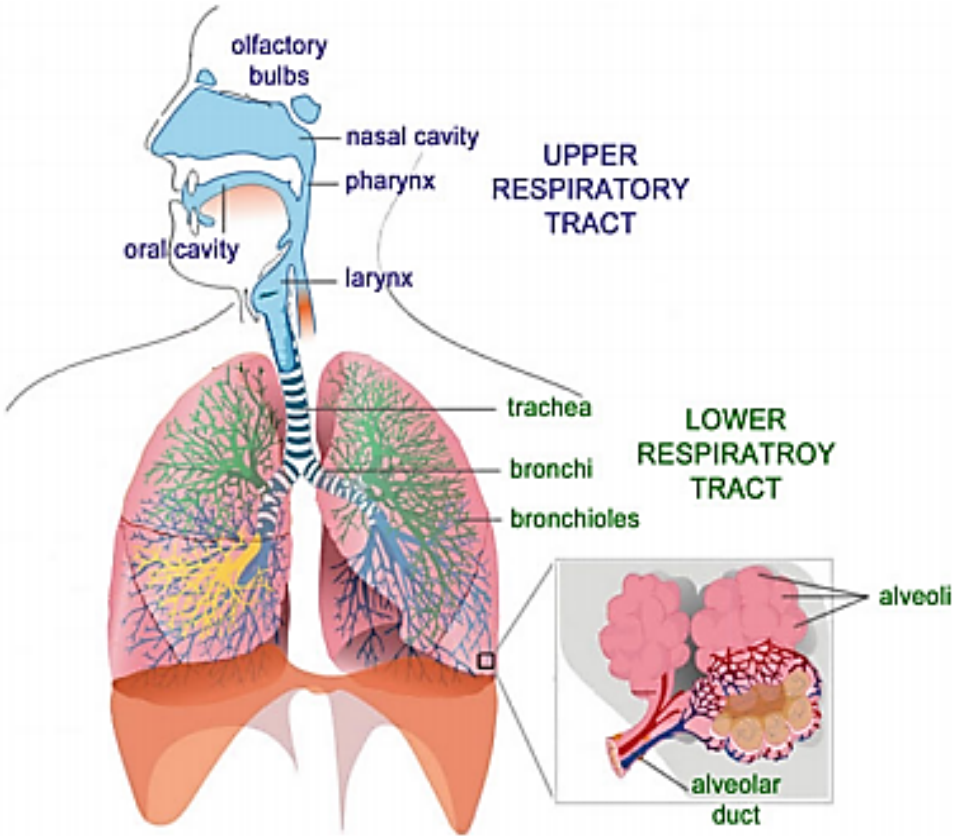

Figure 1.11 Diagram demonstrating respiratory tract regions in humans. Data from Ionescu (2013b).

During gas exchange oxygen (O_2) diffuses into the lung capillaries in exchange for carbon dioxide (CO_2). Exhalation starts after the end of gas exchange in which the air containing CO_2 begins to pass the bronchial pathways into the external environment by either the nose or mouth (Mader, 2004). The inhaled air during

the inhalation undergoes multifunction such as filtering, warming, and humidifying Brown (2015). The respiratory system is divided into different regions according to their function or anatomy and consists of organs that form a path to conduct the inhaled air into the deep lung region (alveoli) which is connected with respiratory tracts by the tracheobronchial tree (Shagam, 2010).

The tracheobronchial tree deliver the inspired air to and from the alveoli and is important for facilitating inspiration. The epithelial variations in the bronchi control the physiological functions of the airway (Mader, 2004). For instance heating, conditioning and filtering of the air are permitted by the ciliated columnar epithelium in the early branches through mucociliary action that remove mucous secretions towards the oesophagus. In the inner branches, the epithelium becomes cuboidal to permit gas exchange. The early branches and cartilage covering the trachea also change and progressively diminishing to maintain patency of the smaller airways. Oxygen is carried into the lungs and is exchanged with carbon dioxide that has resulted from cell metabolism (Windmaier, 2004). This exchange occurs in the alveolar capillaries (Figure 1.12) which are a dense mesh-like network of respiratory bronchioles, the alveolar ducts, and the pulmonary capillary bed. The alveoli gas exchange membrane has a thickness of 1–2 μm where O_2 and CO_2 passively diffuse from and into plasma and red blood cells. This diffusion occurs within less than one second between the alveolar gas and blood in the pulmonary capillaries (Ionescu, 2013a).

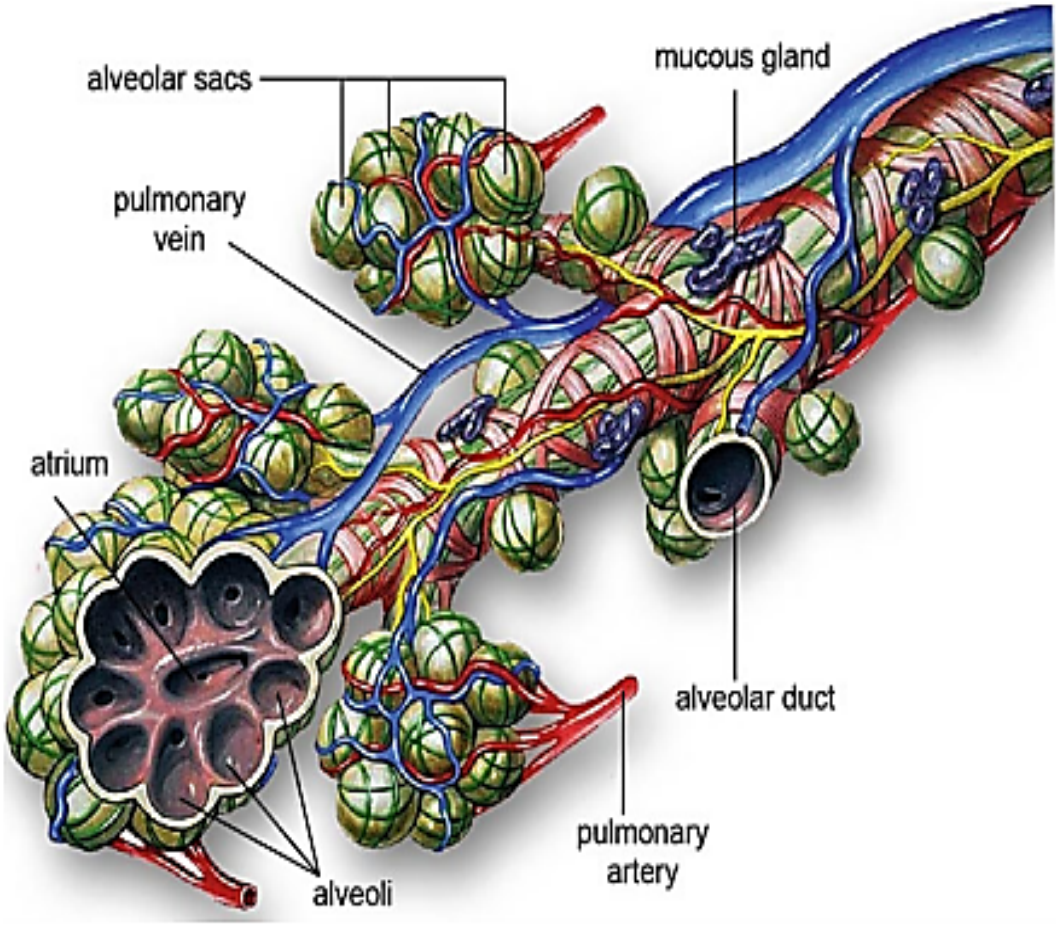

Figure 1.12 Diagram demonstrating the alveolar ducts, and a cutaway of the alveolar. Data from Shagam (2010).

1.9.2.2 Pulmonary drug delivery system

Pulmonary drug delivery has many advantages compared with oral and intravenous systems, in particular rapid drug uptake in the lung, a large surface area for drug transport (Muralidharan *et al*., 2015). The large surface area for drug deposition and high vascularization for the systemic delivery of numerous therapeutic agents have made pulmonary drug delivery (inhalation) an effective route of administration into the lungs (Paranjpe and Muller-Goymann, 2014, Patton and Byron, 2007).

Chemotherapy by inhalation could be more effective than parenteral injection due to its ability to target lung diseases and avoid first pass metabolism by the liver (Patil and Sarasija, 2012). Despite these advantages, pulmonary drug delivery has some limitation associated with its innate defence mechanisms in the lungs, such as mucociliary clearance and macrophage uptake of some drugs before it reaches its target site of action within the lungs (Evans and Koo, 2009). Furthermore, drugs delivery in the upper airways of the lungs is inadequate due to smaller surface area and minimal blood flow, as well as the presence of ciliated cells that cause propulsion of mucus out of the lung to clear foreign substances, resulting in a high capacity to filter and remove up to 90% of delivered drug particles (Evans and Koo, 2009). In contrast, systemic delivery of chemotherapy for treating lung diseases has demonstrated low efficiency and many toxic adverse effects on other organs in most treated cases (Kuzmov and Minko, 2015).

The deposition of drug particles in the lungs are influenced by physiological and physical factors (Patton and Byron, 2007, Peng *et al*., 2016). Physiological factors include the lung defence system whereby dynamic particles larger than 5μm can be trapped in the mucous lining of the tracheobronchial region (such as mouth and throat) (Elder *et al*., 2009, Peng *et al*., 2016). These trapped particles are likely to be cleared by the mucociliary escalator and eventually the ciliated epithelium moves them towards the pharynx to be swallowed and degraded by the stomach acid (Ahsan *et al*., 2002, Tilley *et al*., 2015). Particles of 0.5μm or

smaller are mainly unable to be deposited in the lungs as they are likely to be exhaled due to their very small size. Other physiological factors include the diameter of airway passages, respiratory rate, and presence of excess mucous (Fishler *et al*., 2015). Physical factors such as particle size, velocity, charge, density and properties of the aerosol also play an important role in the deposition of drug particles (Brown, 2015).

Figure 1.13 demonstrates a comparison of organ distribution between pulmonary delivery system (inhalation) and Intravenous administration of lipid nanoparticles (LNPs). The figure illustrates that the drug deposition of LNPs by inhalation was more concentrated in the lungs compared to intravenous administration which accumulated a small amount of lipid NPs in the lungs. Furthermore, 75% of the administered IV dose will likely be lost for the treatment of lung diseases resulting in a poor treatment efficacy (Kuzmov and Minko, 2015).

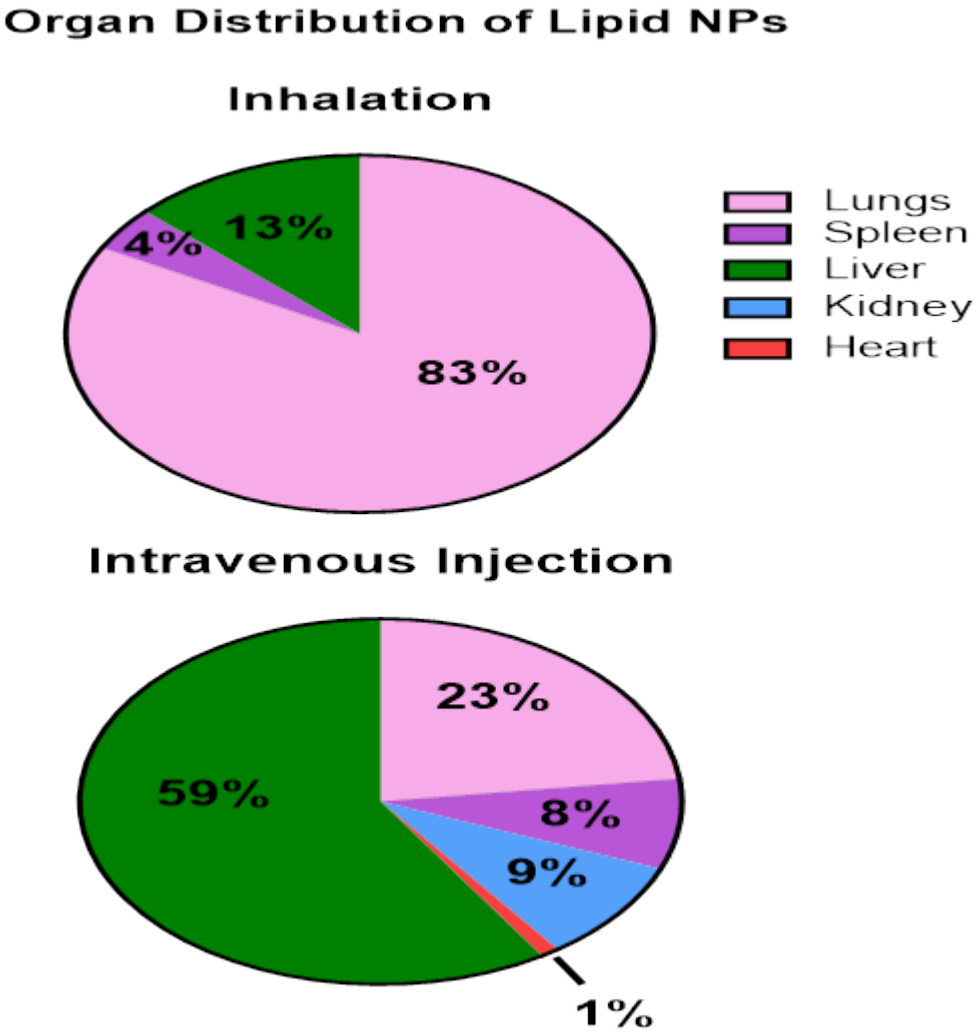

Figure 1.13 Advantages of pulmonary drug delivery.

Organ distribution of lipid NPs by inhalation compared to intravenous administration. Data reproduced and modified from Kuzmov and Minko (2015).

1.10 Nanotechnology as drug delivery system

Nanoparticles (NPs), such as polymeric nanoparticles and lipid nanoparticles (liposomes and niosomes) (Figure 1.14), focus on the design and characterization of ultra-small particles (100-2500 nm) that are widely used in pharmaceutical and medical applications due to their unique size and large surface-to-volume ratios (Duncan, 2003).

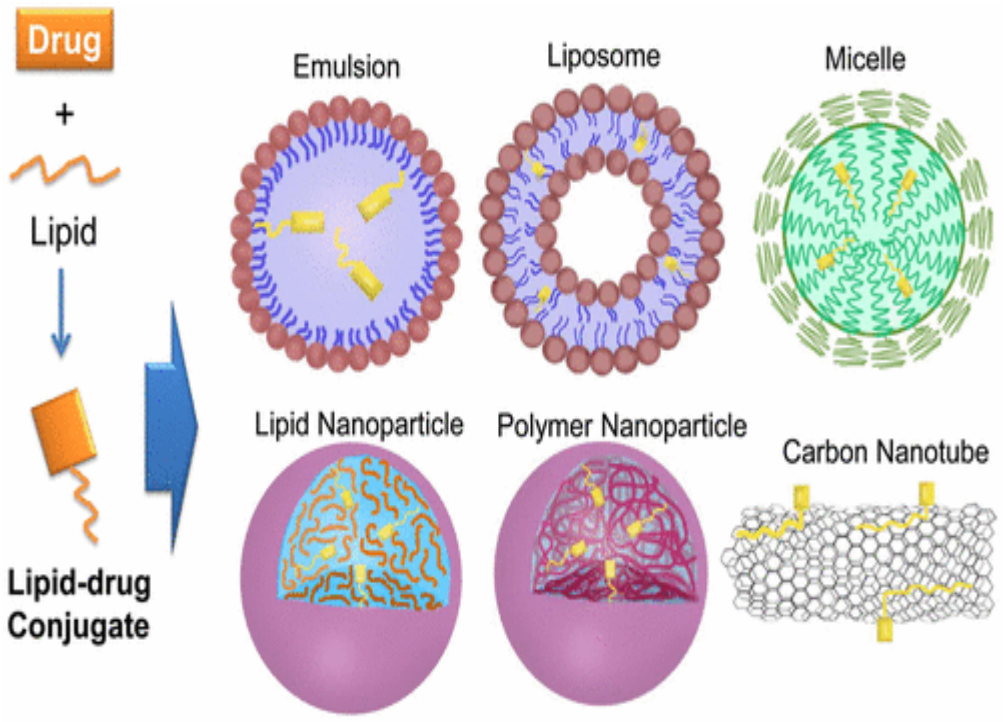

Figure 1.14 Illustration of different types of nano-carriers including lipid nanoparticles. Data from Irby *et al*. (2017).

NPs have many other properties such as stability, self-assembly, specificity, ability to encapsulate drugs, and biocompatibility (Fenske *et al*., 2008, Kearney and Mooney, 2013). Furthermore, NPs have the potential to enhance drug bioavailability due to their nanoscale properties that can increase the extent and the rate of drug absorption and therefore the field of nanotechnology can significantly improve drug manufacturing technologies, leading to better health outcomes and have significantly impacted cancer therapies (Buxton, 2009, Fenske *et al*., 2008, Shi *et al*., 2010, Gunasekaran *et al*., 2014).

Size and diameter are the main criteria to consider when classifying NPs and there are two major classifications: fine particles and ultrafine particles (Devalapally *et al.*, 2007). The size range of fine particles is 100 to 2500 nm while the size range of ultrafine is 1 to 100 nm (Byrne *et al.*, 2008).

In terms of drug discovery, this new technology will be an effective treatment option for many chronic diseases, including diabetes, Alzheimer's, neurological disorders, osteoporosis, heart disease, tuberculosis and cancer malignancies (Lin *et al.*, 2017). In terms of cancer treatment, due to their size and high bioavailability, NPs can encapsulate anticancer therapies to target cancer cells and they can be accumulated and concentrated in tumour cells rather than in the normal cells, thereby facilitating effective and novel therapeutic strategies that may replace chemotherapy (Qi et al., 2017, Kydd *et al*., 2017).

1.10.1 Approaches of nanoparticles in targeting tumour

Accumulated anticancer drugs encapsulated with NPs to the target tumour can be achieved by two approaches: active and passive (Figure 1.15). Passive targeting of the tumour site is influenced by the size of the NPs and tumour vasculature that has efficient vascular network (Byrne *et al.*, 2008, Shi *et al*., 2017). During passive targeting, NPs can disseminate into tumours preferentially to normal tissue due to the rapid and chaotic process of angiogenesis that occurs in tumour cells. Tumours require to grow vasculature rapidly to enable sufficient oxygen and nutrients to be recruited for tumour growth and the resultant vasculature is abnormal with respect to deficiency in pericytes and aberrant basement membrane formation (Siegler *et al*., 2016). These abnormalities initiate a gap size of approximately 1.2 μm between endothelial cells which results in leaky vasculature which does not occur in normal vessels and thus facilitates the extravasations of NPs in to the extravascular system in tumours (Ngoune *et al*., 2016). As a result of this process, these NPs will be more prevalent in and targeted to the tumour through the leaky vasculature and the enhanced permeability and retention (EPR) effect will accumulate the NPs at the tumour site, whereas active targeting of the tumour site can be achieved by conjugate targeting moieties with NPs to interact with the surface receptors of the tumour cells and eventually accumulate NPs in tumour sites (Byrne *et al.*, 2008, Shi *et al*., 2017).

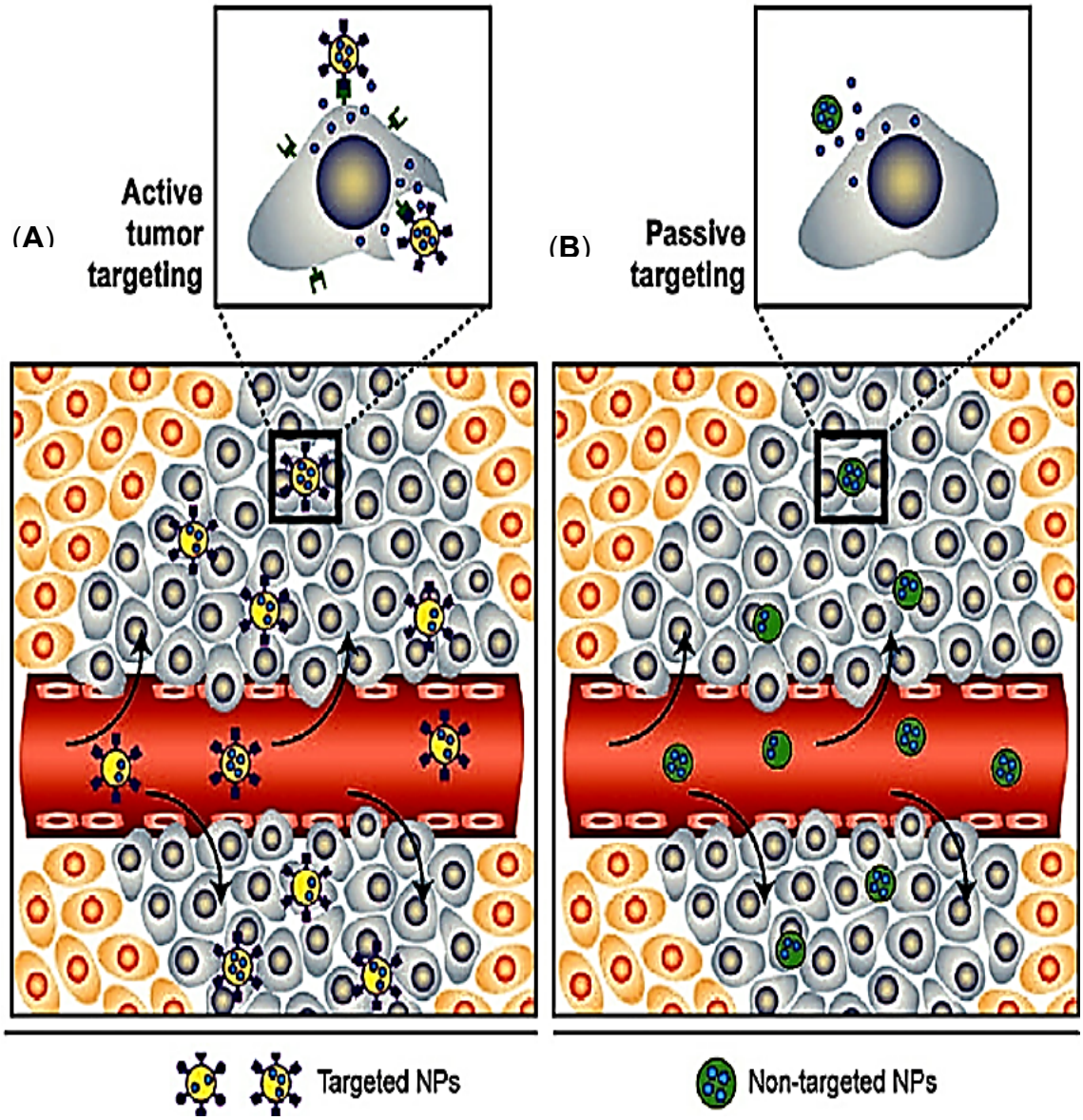

Figure 1.15 Representation of passive and active targeting of NPs.

(**A**) Active targeting. Tumour cells exhibit more receptors than normal cells. Following extravasation of the actively targeted NPs into the tumour interstitium, the NPs interact with the surface receptors of the tumour cells

(**B**) Passive targeting: extravasation of nanoparticles through the gap junctions of the blood vessels, known as the enhanced permeability and retention effect. from (Upponi and Torchilin, 2014).

As an example for active targeting an in *vitro* study conducted by Anabousi *et al*. (2006) to assess the uptake level and toxicity of transferrin (TF) conjugated liposomes as a novel pulmonary drug delivery system in treating lung cancer. It was found that transferrin receptor (TFR) has a high level of expression with cancerous cells (A549) compared with other healthy lung cells, this high level of TFR expression is correlated with an enhanced uptake of TF liposomes encapsulated with chemotherapeutic agents administered by inhalation. Anabousi *et al.* (2006) therefore concluded that TF conjugated liposomes as a novel pulmonary drug delivery system are a good candidate for delivering chemotherapeutic agents by inhalation to treat lung cancer.

There has been significant technological advantages made with NPs that may enhance their utility in cancer therapy. For example lipid NPs can be designed to incorporate both hydrophobic and hydrophilic drugs enabling drug to be distributed within the dispersion medium. Secondly, NPs can have a high carrier capacity enabling high drug entrapment efficiency. Finally NPs can also be delivered by different routes of administration including inhalation, intravenous and oral application taking into account targeting different diseases at specific sites (Irby *et al.*, 2017).

One of the most significant role of NPs in drug delivery is that NPs can avoid targeting normal cells and significantly reduce the systematic distribution side effects of conventional chemotherapeutics (Buzea *et al.*, 2007). For example, Leiva *et al*. (2017) conducted an *in vitro* study evaluating the antitumor activity of solid lipid nanoparticles loaded with paclitaxel (PTX) in human breast (MCF7, MDAMB231, SKBR3 and T47D) and lung (A549, NCI-H520 and NCI-H460)

cancer cells. Leiva *et al*. (2017) confirmed that NPs loaded with PTX showed an excellent hemocompatibility, significantly enhanced PTX antitumor activity and significantly decreased the volume of breast and lung multicellular tumour spheroids.

Chang *et al.* (2009) conducted an *in vivo* study evaluating the effectiveness of liposomes loaded with a chemotherapeutic agent (doxorubicin) as a novel pulmonary drug delivery using a peptide targeting ligand to bind to lung cancer cells (NSCLC) but without targeting normal cells. They employed a method to enhance the amount of an anticancer drug delivered to the lung cancer cells in which the targeting peptide was coupled to liposomes loaded with doxorubicin. As a result of using this novel peptide drug delivery, the survival rate and therapeutic index of doxorubicin significantly increased. Further more, this novel drug delivery vehicle enhanced the accumulation of doxorubicin in lung cells by 7.5 fold when compared with free drugs. Chang *et al*. (2009) concluded that in treating NSCLC, liposomal loaded with chemotherapies with a peptide drug delivery may be used to specifically target lung tumour cells.

Tseng. *et al.* (2011) developed gelatine nanoparticles (GPs) as carriers incorporated with cisplatin (CDDP) to improve the efficacy and reduce the side effects of cisplatin in treating lung cancer. The GPs-cisplatin nanocomplex (GP-Pt) *in vivo* was studied by injecting GP-Pt into mice strain that had been injected with human lung cancer cells (A549 cells). Tseng. *et al*. (2011) revealed that GP-Pt significantly decreased the tumour size, and improved the survival rate of the mice treated with GP-Pt compared with those treated with free CDDP. Tseng. *et al*. (2011) concluded that the GP-Pt nanocomplex was effective in reducing the

tumour size, less toxic than the free drug, and may be used as a potential drug delivery system for chemotherapy.

1.11 Vesicles as a delivery system: liposomes and niosomes

Vesicular drug delivery systems are characterized by being highly ordered assemblies made up of one or more concentric lipid bilayers. These lipid nanoparticles (LNPs) are vesicles formed from a diverse range of amphiphillic building blocks and provide several advantages to candidate drugs with which they can be encapsulated (Jain *et al*., 2014b). One of the most attractive factor of using phospholipid-based carriers (e.g., liposomes and niosomes) as a pulmonary drug delivery system is the fact that lung surfactant naturally contains phospholipids and, therefore, should not expose the lungs to toxicological risk (Danaei et al., 2018b). Furthermore, lipid nanoparticles have the capability to be well transferred into aerosols and support nebulization forces (Beck-Broichsitter *et al.*, 2012). LNPs can avoid mucociliary clearance and lung phagocytic mechanisms and, therefore, prolonging the presence of the therapeutic drug within the pulmonary system (Abdelaziz *et al.*, 2018). Other advantages include prolonged drug existence within the systemic circulation, minimization of toxicity if selective uptake is achieved due to the delivery of drug directly to the tumour, enhanced absorption and bioavailability of poorly soluble drugs, and incorporation of both hydrophilic and lipophilic particles which function as a sustained release system (Kubik *et al.*, 2005).

1.11.1 Liposomes

Liposomes are concentric bilayered vesicles with an aqueous region entirely enclosed by a natural or synthetic lipid bilayer membrane, this membrane result from interactions between phospholipids and aqueous region (Kraft *et al*., 2014, Shaker *et al.*, 2017). As a result of having lipophilic and hydrophilic portions, these lipid vesicles (liposomes) can entrap substances with different polarities either in the phospholipid bilayer or in the aqueous part (Joshi and Muller, 2009). The liposomal drug delivery system consists of essential components: phospholipids (phosphatidylcholine) and cholesterol. Cholesterol's main role is to act as a fluidity buffer but not to participate in bilayer formation (Lian and Ho, 2001). Liposomal nanoparticles are developed to act as delivery vehicles for many therapeutic drugs by encapsulating and incorporating drugs such as chemotherapeutic agents for cancer treatment (Jain, 2009, Ramishetti and Huang, 2012). A schematic diagram of a liposomal structure and design is shown in Figure 1.16.

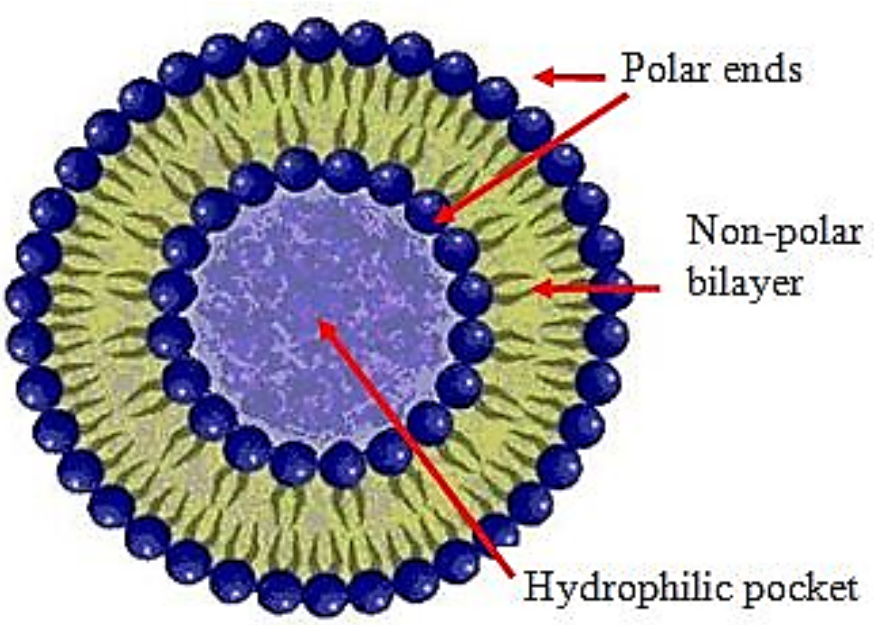

Figure 1.16 Structure and design of liposomal drug delivery. Data obtained from (Çağdaş. *et al*., 2014).

Liposomal drug delivery has several advantages such as the ability to deliver hydrophilic and lipophilic drugs, the ability to protect sensitive tissues from cytotoxic drugs, encapsulating drugs and protect drugs from the environment leading to improved drug stability, target-specific delivery can be achieved with liposomal formulation, and improved pharmacokinetic properties due to reduced elimination and increased circulation lifetime (Kraft *et al*., 2014, Shi *et al*., 2017, Torchilin, 2005, Allen and Cullis, 2013).

As an example of how liposomes can improve stability and bioavailability, an anticancer drug such as β-elemene which has an anti-lung cancer activity but

was limited because of its hydrophobic, poor stability, and low bioavailability properties (Chen *et al*., 2012). Xiaodan *et al*. (2007) evaluated physical properties of liposomal formulation encapsulating β-elemene in *in vivo* (in rats) and displayed great advantages in terms of stability of hydrophobic when compared to non-liposomal formulations for β-elemene.

Disadvantages of liposomes as vesicular drug delivery system are firstly, liposomes are leaky in nature, leading to premature drug release, secondly, poor encapsulation efficiency drugs than niosomes and finally are considered to be expensive formulation technique (Kraft *et al*., 2014, Shi *et al*., 2017, Torchilin, 2005, Allen and Cullis, 2013).

1.11.2 Niosomes

Niosomes were developed and patented for the first time by L'Oreal in 1975 and were first used in drug delivery for anticancer drugs in 1985 (Abdelkader *et al*., 2014). Niosomes are non-ionic surfactant vesicles (NIVs) and formed when non-ionic surfactants (alkyl or dialkyl polyglycerol ether class) are mixed with cholesterol with subsequent hydration in aqueous media (Kaur, 2016, Ag Seleci *et al.*, 2016, Kazi *et al*., 2010). Cholesterol acts as a enhancer in the bilayer to form less permeable niosomes (bilayer membrane stabilizer), and non-ionic surfactants act as an emulsifier to increase the stability of vesicles, resulting in improved entrapment efficiency of the drug encapsulated by niosomes (Kaur, 2016, Ag Seleci *et al*., 2016, Kazi *et al*., 2010). Niosomes have a structure that is similar to liposomes but niosomes are more effective as drug carriers than

liposomes in terms of factors like cost, stability, entrapment efficiency, and bioavailability (Baillie *et al*., 1986, Kazi *et al.*, 2010). A schematic diagram of a niosome structure and design is shown in Figure 1.17.

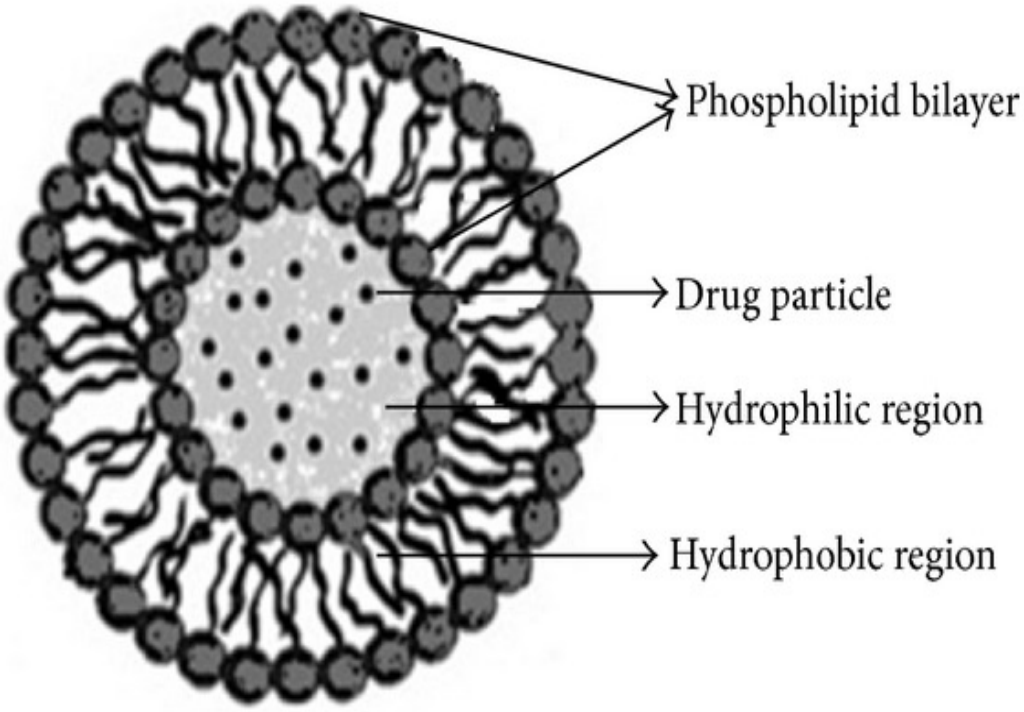

Figure 1.17 Structure of niosomes. Data obtained From (Sahoo *et al*., 2014).

Advantages of niosomes are relative more stability with very low tendency for leakage, they can serve as a depot system to release the drug slowly when require and can increase oral, topical, and parenteral bioavailability of drugs. Niosomes can improve the therapeutic performance of the entrapped drug simply

by restricting its effect to the target cells and by reducing the clearance of the drug (Sahoo *et al*., 2014, Kazi *et al*., 2010). Composition and characterization of different niosomal formulations are summarised in Table 1.2.

Table 1.2 Composition and characterization of different niosomal formulations. (Hatano and Yuksel, 2014).

Surfactant grade	**Surfactant : CHOL : DCP ratio**	**Vesicle diameter (μm)**	**Zeta potential (mV)***	**Entrapment efficiency (%)**
Sorbitan laurate	2.5:1:0.1 2:1:0.1 1.5:1:0.1 1:1:0.1 1:1.5:0.1	7.12 8.01 8.70 9.03 10.91	-91 -87 -56 -29 -25	37 48 58 78 75
Sorbitan monopalmitate	2.5:1:0.1 2:1:0.1 1.5:1:0.1 1:1:0.1 1:1.5:0.1	5.70 7.84 8.65 8.90 9.85	-61 -52 -48 -26 -22	38 52 63 83 81
Sorbitan monostearate	2.5:1:0.1 2:1:0.1 1.5:1:0.1 1:1:0.1 1:1.5:0.1	3.98 4.31 4.93 6.82 8.55	-46 -39 -28 -23 -22	48 59 71 95 89
Sorbitan oleate	2.5:1:0.1 2:1:0.1 1.5:1:0.1 1:1:0.1 1:1.5:0.1	2.95 4.17 4.59 6.31 8.42	-45 -37 -25 -21 -16	52 62 74 96 89

1.11.3 Pre-clinical evaluation of niosomal formulation

The niosomal delivery of cisplatin is largely undocumented compared to liposomes. A single study has been found evaluating the effectiveness of niosomal formulation of cisplatin in comparison to free cisplatin in a murine B16-F10 melanoma model (Gude *et al*., 2002). The niosomes were prepared from Span 60 and contained a cisplatin concentration of 1mg/ml. The study suggested significant efficacy of niosomal cisplatin in inhibiting lung tumour nodules, with lower associated toxicity in the form of myelosuppression and weight loss.

Amiri *et al.* (2018) Conducted an *in vitro* and *in vivo* study evaluating the increased therapeutic efficacy of a PEGylated niosomal formulation of vinblastine (Pn-VB) against murine lung cancer TC-1 cells using MTT assay and its tumour inhibitory effect was further evaluated in lung tumour-bearing C57BL/6 mice. Amiri *et al.* (2018) found that a sustained release drug patterns of this niosomal formulation (Pn-VB) indicated a significant increase in toxicity against TC-I cells as compared to free vinblastine and the *in vivo* results showed that Pn-VB formulation exhibited stronger tumour inhibitory effect and longer life time in comparison to free vinblastine. Amiri *et al.* (2018) concluded that Pn-VB niosomal formulation displayed appropriate stability, high-loading efficacy, lower releasing rate, and potent cytotoxic activity enhancing drug bioavailability and therapeutic efficacy against lung cancer TC-1 cells as compared to free drug.

However, differences in characteristics exist between liposomes and niosomes, especially since niosomes are prepared from uncharged single-chain surfactant

and cholesterol, whereas liposomes are prepared from double-chain phospholipids (neutral or charged). The concentration of cholesterol in liposomes is much more than that in niosomes. As a result, drug entrapment efficiency of liposomes is less than that of niosomes. Furthermore, liposomes are expensive, and their ingredients, such as phospholipids, are chemically unstable because of their predisposition to oxidative degradation; moreover, these require special storage and handling and the purity of natural phospholipids is variable (Kazi *et al.*, 2010).

1.13 Project rationale

The research problem identified to understand the mechanistic rationale behind why certain combinations are optimal and evaluate the effectiveness of NIVs encapsulated with cisplatin and/or TPT as a drug delivery system for the treatment of lung cancer by inhalation (via the pulmonary route).

The specific aims of this project are:

I. To use a variety of cell and molecular biology techniques to establish the cell kill potential of cisplatin and topotecan, firstly as single agents on human lung cancer cell lines (H460 & A549). We will subsequently utilise these agents in combination to determine optimal combinations, then to investigate whether cisplatin and TPT as a combination therapy has a synergetic effect when tested on H460 and A549 cells by using a clonogenic cell survival assay and combination index analysis. These survival studies were then underpinned to provide a mechanistic rationale behind why certain combinations are optimal.

II. To assess the radiosensitising potential of cisplatin and topotecan in combination with XBR as a novel therapy in human lung cancer cell lines H460 and A549 (NSCLC) to determine cell survival and to investigate the DNA damage response pathway with this combination therapy.

III. To formulate NIVs encapsulating cisplatin and TPT, then to study the physicochemical properties of NIVs containing cisplatin or TPT on the basis of entrapment efficiency, size and ZP as main properties in determining the post-preparation stability. The efficacy of the drugs as

single agents and in combination encapsulated in NIVs were then compared with the efficacy of non-encapsulated agents by clonogenic assays.

IV. Finally, using an *in vitro* model to determine the lung drug deposition and aerosol particle size distribution (APSD) profiles of TPT-NIVs compared to TPT aerosol solutions.

Chapter 2 : Materials and Methods

2.1 Cell lines and cell culture condition

Two non-small cell lung cancer lines (NSCLC) A549 & H460 (purchased from ATCC, Uxhridge, Middlesex, UK) were tested in this study. Cryo tubes with aliquots of frozen H460 and A549 cells were defrosted and the contents were then added to 5ml of growth medium (Dulbecco's modified Eagle's medium – DMEM- was purchased from Sigma-Aldrich, Gillingham, UK). Growth medium supplemented with penicillin/streptomycin (10000ug/mL) and fungizone (250µg/mL) (purchased from Gibco®, Paisley, UK) plus 10% v/v heat inactivated foetal bovine serum (obtained from Biosera Ltd., East Sussex, UK). The resultant cell suspension was centrifuged at 1500 rpm for 5min using a Haraeus Multifuge 3 S-R centrifuge (DJB Labcare Ltd., Newport Pagnell, and Buckinghamshire, UK). The supernatant was discarded and the pellet resuspended in 5 ml fresh medium. The pellet was then resuspended in 15ml and cell suspension was cultured in a 75 cm_2 sterile tissue culture flask (Corning B.V, Buckinghamshire, UK) for incubation at 37°C with humidified 5% CO_2 / 95% air incubator. The cells were then harvested when 70 % confluent by discarding the medium and washing cells with 4ml of phosphate buffer solution (PBS). Cells then were detached with 5 ml Trypsin-EDTA (obtained from Gibco®, Paisley, UK) for 5 min. 6ml of fresh media was added to inactivate the trypsin. Various concentrations of cells were then prepared (1:5, 1:10 and 1:20) in three new 75cm_2 flasks containing 15ml of fresh media to maintain a stock of cells.

2.2 Treatment of H460 and A549 cell lines

2.2.1 Treatment of cells with XBR

For radiosensitisation studies (chapter 4), H460 and A549 cells were exposed to External Beam Radiation (XBR) delivered by a cell irradiation cabinet XRAD 225 (CT, USA) with a 225keV X-ray beam and dose rate of 2.2 gray/minute (Gy/min) and current of 13.00mA. For treating cells with XBR alone, dose ranging from 0 to 5Gy were used, however a dose range from 0-2Gy of XBR was used for combination treatments.

2.2.2 Treatment of cells with cisplatin

Cisplatin (obtained from Medex (Northants, UK)) stock solution was freshly prepared in 0.9% w/v NaCl from a powder stock prior to each experiment at a dose ranging from 0-5 μM used for treatment of cells as a single therapy. Cisplatin solution was prepared and filter-sterilised for the assay where its limited solubility required that its concentration not to exceed 1mg/ml in 0.9% w/v NaCl. In the cytotoxicity study, 10 μl of filter sterilised cisplatin solution was pipetted into the universal tube and doubling serial dilutions were subsequently performed with DMEM. One cell culture flask containing cells to be used as the positive control.

2.2.3 Treatment of cells with TPT

TPT (purchased from Sigma-Aldrich Inc., Dorset, UK) stock solution was freshly prepared in 5% tartaric acid in 0.9% w/v NaCl from a powder stock prior to each experiment at a dose ranging from 0-1000 nM used for treatment of cells as a single therapy. TPT solution was prepared 5% tartaric acid in 0.9% w/v NaCl. In the cytotoxicity study, 1 μl of TPT solution was pipetted into the universal tube

and doubling serial dilutions were subsequently performed with DMEM. One cell culture flask containing cells to be used as the positive control.

2.2.4 Treatment of cells with NIVs

Cisplatin NIVs and TPT NIVs were prepared as described in section 2.10. Ultracenterfiguation was employed to separate entrapped drug. In the cytotoxicity study, cells were treated under sterilised conditions using microfilter to sterilised NIVs solutions prior to cell treatment. 10 µl of filter sterilised cisplatin or TPT solution was diluted with DMEM and then pipetted into the universal tube and doubling serial dilutions were subsequently performed with DMEM.

2.2.5 Combination treatment

For combination therapy a dose range from 62.5-250 nM cisplatin combined with a dose ranging from 10-30 nM TPT was administered for 24hrs. For schedule A and B treatment (chapter 3), TPT first administered for 24hrs followed by cisplatin or vice versa (total of 24hrs), whereas, schedule C (simultaneous administration) both agents were administered for 24hrs.

2.3 Clonogenic assay

The cell survival (clonogenic) assay is used to determine cells ability to proliferate indefinitely, therefore cells will be able to undergo unlimited proliferation and form a clone, whereas damaged cells will be capable of a finite number of cell divisions and be unable to form colonies. (Hall, 2000). The survival fraction curve defines the correlation between the insult-producing antitumor agent and the proportion of cells that survive (Elkind and Whitmore, 1967). The growth of cells into a large

colony that can be visualized by eyes is evidence that cells are capable for reproduction and proliferation (Hall, 2000).

24 hours after treatment with either cisplatin, TPT and XBR alone or in combination, clonogenic assays were performed by removing cell growth medium and washing cells in PBS and then detaching cells by addition of 0.05% trypsin EDTA. Once cells detached, fresh growth medium was added, and cells were disaggregated using a 21G needle and counted using a haemocytometer. 250 cells from each treatment group were seeded into 60mm dishes (Fischer Scientific, Loughborough, UK) in triplicate for each experimental treatment.

60mm dishes were then incubated at 37^{o}C in a 5% CO_2 atmosphere for 7-10 days to allow colonies of sufficient size to form in the untreated control sample. Colonies were visualised for quantification using Giemsa's stain. Briefly, colonies were washed with PBS, fixed in 100% methanol for 10mins and stained using 10% Giemsa's stain solution (BDH Laboratory Supplies). The number of colonies was then counted by eye and the fraction of cells surviving (SF) was calculated by dividing the number of colonies of the experimental treatment group by the number of colonies of the control plates multiplied by PE. The PE and SF were calculated according to the following equations:

$$\mathrm{PE} = \frac{\text{average no. of control colonies formed}}{\text{no. of seeded cells}}$$

$$\mathrm{SF} = \frac{\text{average no. of colonies formed after treatment}}{\text{no.of seeded cells X PE}}$$

The calculated results were fitted to a dose-response curve as SF (y axis) versus treatment doses (x axis).

In each experiment analysis was carried out in triplicate for each experimental group and results reported as the mean cell survival fraction (mean ± sd) of 3 independent experiments with respect to control cells. Figure 2.1 illustrates the main steps involved in clonogenic assay.

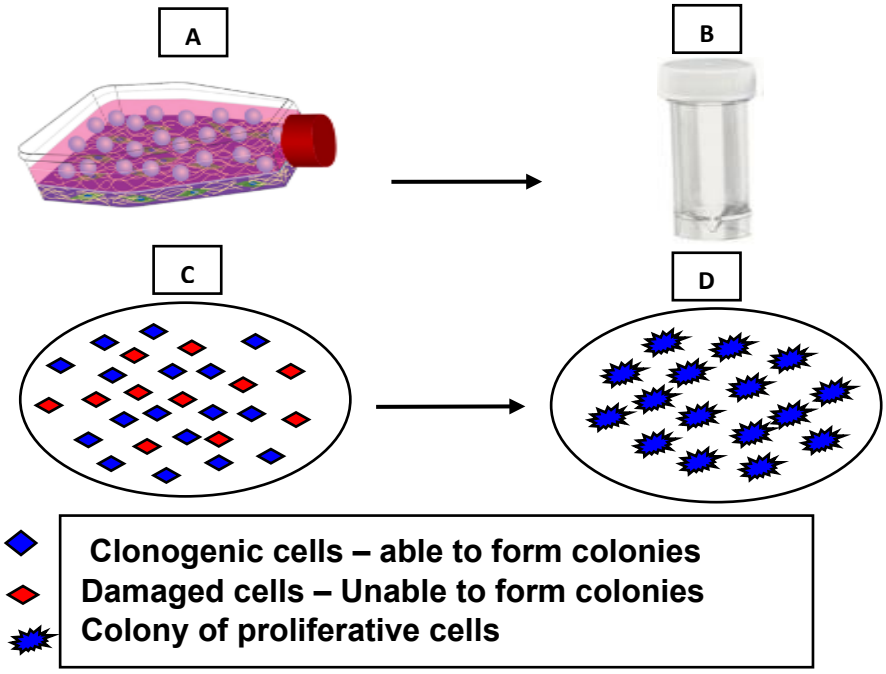

Figure 2.1: Clonoginic assay

This assay is used to evaluate the cytotoxic effects of a drug by determining the cells ability to proliferate indefinitely and to retain its reproductive to form a clone. This experiment involve multiple steps as follows:

A- Cells are plated in flasks at 37°C incubator set at 5% CO_2 and treated with cytotoxic agent.
B- Treated cells are trypsinised, placed in universal tube as a single cell suspension, and counted.
C- Treated cells are plated in petri dish at 37°C incubator set at 5% CO_2 for around 10 days to be tested for their ability for colony forming.
D- Clonogenic cells grow into colonies. Damaged cells are unable to form colonies.

2.3.1 Combination index analysis of the interaction between multiple toxic drugs

Median-effect / combination-index (CI) analysis is a software (CalcuSyn) program quantitatively used to study the potential interaction, both antagonistic and synergistic, of cells affected by combination treatment (Zhao *et al*., 2004).

CI analysis illustrates the measured effect of the combination therapy compared with the effect of single therapy using a fixed dose ratio of drug A to drug B and/or drug C in a simply additive fashion, based on their effectiveness as a single agents (Boeckman *et al*., 2005a).

The analysis of the interaction between multiple toxic drugs carried out by Chou and Talalay is based on the median-effect principle (Schinazi *et al.*, 1986).The dose-effect curves were constructed using the Equations 1 and 2 described in Equation 2.1.

Equation 1: $f_a/f_u = (D/D_m)^m$

Equation 2: $D = D_m[f_a/f_u]^{1/m}$

Equation 3: $CI = (D)_1/(Dx)_1 + (D)_2/(Dx)_2 + a(D)_1(D)_2/(Dx)_1(Dx)_2$

Equation 2.1: Equations used to analyse the interaction between multiple agents by median effect and combination index analysis.

The interaction between multiple cytotoxic drugs can be studied using the median-effect principle of Chou and Talalay, which analyses drug effect using the median-effect equation (Equation 1), which can be calculated to give Equation 2. In Equations 1 and 2, **D** is the dose, $\mathbf{D_m}$ is the IC_{50} dose, $\mathbf{f_a}$ is the fraction of cells affected, $\mathbf{f_u}$ is the unaffected fraction, and **m** is the coefficient of the sigmodicity of the dose-effect curve. The logarithmic form of equation (2).

In Equation 3, $\mathbf{(D)_1}$ and $\mathbf{(D)_2}$ are the doses of each agent which inhibit x% of cell growth when used in combination, and $\mathbf{(Dx)_1}$ and $\mathbf{(Dx)_2}$ are the doses of each drug which inhibit x% of colonies when used as single agent. If the drugs have a similar or dependent mode of action, then **a** = 0 (IC value is the sum of the first two terms). If the drugs have a different or independent mode of action, then **a** = 1 (IC value is the sum of all three terms).

A CI equal to 1 indicates no interaction while a CI greater than 1 indicates antagonist interaction. Synergistic interaction is indicated by a CI value less than 1.

2.4 H2AX foci staining and analysis

DNA single stranded breaks (SSBs) can be easily repaired, leading to inaccurate quantification of DNA damage and DNA damage repair. However, DNA double stranded breaks (DSBs) can be more accurate for quantification. The formation of DNA DSBs results in rapid phosphorylation of the histone protein H2AX (γ-H2AX), where the γ-H2AX correlates with the number of DNA DSBs formed, increasing with increased DNA DSBs formation, and decreasing as the DNA DSBs are repaired over time (Short *et al., 2007)*.

Therefore, γ-H2AX was used as a biochemical marker of the magnitude and resolution of DNA DSBs in response to cisplatin, TPT and XBR exposure as single agents and in combination.

Cells were seeded into 13mm coverslips in petri dishes at a density of 1 x 10^4 cells/coverslip and incubated for 48 hours. Cells were treated as described in section 2.2 and coverslips were taken from the dishes at two time points post treatment (2 and 24 hours). Subsequently, at each time point coverslips with its cells were washed in PBS and fixed in 4% paraformaldehyde at room temperature for 20 minutes. Cells were then washed in PBS and permeabilised in 0.5% triton X-100 for 20 minutes. Non-specific antibody binding was blocked by incubation in 0.5% BSA in PBS containing 0.15% triton X-100 for 20 minutes. The monoclonal anti-phospho-histone H2AX (ser 139) antibody (Millipore, UK) diluted 1:250 in 0.5% BSA in PBS containing 0.15% triton X-100 was added and cells incubated overnight in cold room. Cells were washed in PBS before incubation for 1.5 hours at room temperature with a goat anti-mouse alexa-488

conjugated IgG antibody (Invitrogen®, (Paisley, UK)) at a 1:1500 dilution in 0.5% BSA in PBS containing 0.15% triton X-100. A final wash with PBS followed by distilled water was carried out before the coverslips were placed on slides using Vectashield to prevent photobleaching (Vector Laboratories, Burlingame, CA). Confocal microscopy (Leica SP5 confocal) with a 63x objective lens was used to capture z-stack images of 50 cells per coverslip with a 1µm resolution. The cells per coverslip and foci in the DNA within the cell nuclei were subsequently counted using Volocity 3D Image Analysis Software (PerkinElmer, Waltham, MA). The results presented as the number of γ-H2AX foci/cell (mean ± sd) and cells were compared to control cells to determine treatment efficacy and for combination treatments foci number was compared to single treated cell alone.

2.5 Cell cycle progression by Fluorescence-Activated Cell Sorting Analysis (FACS)

The aim of the FACS method was to assess the effect of treatment agents on the cell cycle progression of H460 and A549 cells. Cells were cultured in 25cm^2 flasks until reaching 60-70% confluence and then were treated with various concentration of treatments as single agents and in combinations for 24 hours. Cells then were detached by addition of 1ml of trypsin (0.05%). The cell suspension was then spun down at 1500 RPM for 5 minutes, the supernatant was removed, and cells were washed with PBS and re-pelleted at 1500rpm, for 5 minutes. Cells were fixed with 70% cold ethanol and stored at -20C^o until analysis. On the day of analysis, cells were centrifuged at 1500rpm for 10 minutes, the ethanol layer was removed and cells were then washed twice with cold PBS. The PBS was then poured off and the pellet was resuspended with

300µL PBS containing 10µg/mL Propidium Iodide (PI) (Sigma-Aldrich, Gillingham, UK) and 50ug/mL RNase (Sigma-Aldrich, Gillingham, UK). Tubes containing cell suspensions were incubated on ice in the dark for at least 1 hour. Cell cycle analysis was carried out using a FACScan (Becton Dickinson Systems, Cowley, UK) and data were analysed using BD CellQuestTM Pro software (version 5.1.1). Three independent experiments were carried out with a minimum of 1000 cells/sample and results presented as the percentage of the cell cycle phases (mean ± sd).

2.6 Annexin V protein detection and analysis assay

During apoptosis, the appearance of phosphatidylserine (PS) on the surface of the cell membrane is an early event in apoptosis, and therefore can be used as a marker of apoptosis (Elmore, 2007). Annexin V has a potential affinity for PS and based on their Annexin V affinity, apoptotic cells can be distinguished from Annexin V-negative cells (Demchenko, 2013). Therefore, Annexin V can be used as a tool for detecting apoptosis. Cells were grown to a density of 1 x 10^6 cells/mL and were either left untreated or treated with increasing concentrations of the following agents: cisplatin, TPT, and XBR either alone or in combinations. After 48 hours cells were analysed using FITC Annexin V Apoptosis Detection Kit I (BD Pharmingen, USA). Cells then were washed twice with cold PBS and then resuspended in 1X binding buffer at a concentration of 1 x 10^6 cells/ml. 100 µl of the solution (1 x 10^5 cells) was then transferred to a 5 ml culture tube. 5 µl of FITC Annexin V conjugate and 5 µl PI was added in each tube and incubate for 15 min at RT (25°C) in the dark. 400 µl of 1X Binding Buffer was added to each tube and

analysed by flow cytometry. The level of apoptosis induction was assessed by depicting cell staining by PI vs Annexin V.

2.7. HPLC analysis of cisplatin

An isocratic reverse-phase high performance liquid chromatography (HPLC) method developed and modified from Alsaadi *et al*. (2013) was used to analyse cisplatin solution and cisplatin NIVs. This method was also employed in the analysis of cisplatin content of all NIVs. In this method, validation characteristics such as linearity, accuracy, precision (repeatability and intermediate precision), were studied aiming to present an evidence showing a high level of assurance that this method can consistently produce results that precisely reflect the quality characteristics of cisplatin.

For detection of cisplatin by HPLC, internal standard $NiCl_2$ and chelating agent Sodium diethyldithiocarbamate trihydrate (DDTC) were obtained from Sigma-Aldrich Inc. (Dorset, UK) and used in this analysis. The internal standard NiC_{l2} (Nickel chloride) and chelating agent DDTC (diethyldithiocarbamate) were needed as cisplatin cannot be detected alone within the UV normal wave length. The addition of DDTC to cisplatin is to form a complex (Pt(DDTC)2) and with $NiCl_2$ (Ni(DDTC)2) to be absorbed by UV detector Standard concentrations of cisplatin ranging from 1.56-150 µg/ml were prepared in serial dilutions from a freshly prepared 1mg/ml cisplatin in 0.9% w/v NaCl. A 0.1mg/ml solution of NiCl2 was prepared from a freshly prepared 1mg/ml solution in 0.9% w/v NaCl. The chelating agent DDTC was prepared in a concentration of 100mg/ml in 0.1N

NaOH. From each standard concentration or unknown sample, 85µl was spiked with 5µl of NiCl2 and reacted with 10µl of DDTC reagent in a 37ºC water bath for 30min. A blank sample using 85µl 0.9% w/v NaCl solution was prepared in the same way. The reactant material (such as DDTC, $NiCl_2$, and cisplatin) was extracted with 80µl chloroform by vortexing for 1min and then the chloroform layer was separated by centrifugation at 13000rpm and 4ºC for 5min in a Biofuge fresco centrifuge, obtained from DJB labcare Ltd. (Buckinghamshire, UK).

2.7.1. HPLC instrumentation and chromatographic conditions

The HPLC system consisted of a Gynkotek® HPLC pump series P580 and autosampler model GINA 50 (Macclesfield, Cheshire, UK) operated by Chromeleon™ software version 6.30 SP3 Build 594, Dionex (Surrey, UK). Separation was carried out on a Luna C_{18} (150 × 4.6mm i.d. and 3µm particle size). Phenomenex® column (Macclesfield, Cheshire, UK) connected to a UV detector set at 254nm. Mobile phase was pumped through the system at a flow rate of 1.4 ml/min and consisted of water, acetonitrile and methanol in a ratio of 29:31:40 v/v/v, respectively. Solvents were measured separately, mixed and degassed by vacuum filtration using Millipore vacuum filtration kit (Watford, UK) and Phenomenex® 0.22µm membrane filters (Macclesfield, Cheshire, UK). A calibration curve was established from the standard concentrations of cisplatin used. Area under the curve (AUC) ratio was plotted against the concentration of cisplatin. AUC was calculated by dividing the AUC of detected cisplatin by the AUC of the internal standard used.

2.8. HPLC analysis of topotecan

An isocratic reverse-phase high performance liquid chromatography (HPLC) method, adapted and modified from (Saini et al., 2010, Jain *et al*., 2014a) and used to analyse both TPT solution and TPT NIV formulations. Standard concentrations of TPT ranging from 1.25-80 µg/ml were prepared in serial dilutions from a freshly prepared 1mg/ml solution of TPT in 5% tartaric acid in 0.9% w/v NaCl. The hydroxylactone ring of TPT in alkaline conditions undergoes a rapid pH-dependent hydrolysis, this hydrolysis would deactivate the carboxylate form of TPT, leading to a decrease in the antitumor activity of TPT following dissolution in aqueous media (Souza et al., 2011a, Fassberg and Stella, 1992). Therefore, in this analysis TPT was prepared in 5% tartaric acid and 0.1% TFA was added to the mobile phase to maintain and stabilize the lactone ring in an acidic condition.

2.8.1. HPLC instrumentation and chromatographic conditions

The HPLC system consisted of a Gynkotek® HPLC pump series P580 and autosampler model GINA 50 (Macclesfield, Cheshire, UK) operated by Chromeleon™ software version 6.30 SP3 Build 594, Dionex (Surrey, UK). Separation was carried out on a Luna C18 (150 × 4.6mm i.d. and 3µm particle size) Phenomenex® column (Macclesfield, Cheshire, UK) connected to a UV detector set at 227nm. Mobile phase was pumped through the system at a flow rate of 0.4 ml/min and consisted of water, and acetonitrile in a ratio of 50:50, 0.1% TFA v/v/v, respectively. Solvents were measured separately, mixed and degassed by vacuum filtration using Millipore vacuum filtration kit (Watford, UK)

and Phenomenex® 0.22µm membrane filters (Macclesfield, Cheshire, UK). A calibration curve was established from the standard concentrations of topotecan used. Area under the curve (AUC) ratio was plotted against the concentration of topotecan.

2.9 HPLC analysis of lipids

A gradient normal phase HPLC unpublished method, was developed by Prof Alex Mullen (University of Strathclyde) and a modified and published method by Alsaadi (2011) used in this study. NIV formulations were prepared for lipid analysis as described (Section 2.7). Standard concentrations ranging from 0.025-250µg/ml of the lipid mixture (cholesterol, surfactant VIII and DCP) were prepared. Each lipid mixture was dissolved separately in chloroform stabilised with ethanol to prepare a 1mg/ml solution. From each lipid solution (1mg/ml), 12ml were taken and mixed together and additional 12ml chloroform was added to prepare 250µg/ml lipid mixture solution. Serial dilutions were considered to prepare the rest of the standard concentrations and 10ml volumes were taken from each concentration. 400µl of prednisolone (2mg/ml in methanol) as the internal standard was added to each 10ml of prepared standard or unknown sample, and then mixed to ensure a complete miscibility. 400µl of prednisolone was also added to a 10ml volume of chloroform to prepare a blank sample. From each sample, 100µl was taken and evaporated at 35ºC under using a vacuum centrifuge - SpeedVac™ (UK) for 40min until samples become dried. 100µl chloroform was added to each dried sample to reconstitute with chloroform and 20µl of the resultant solution was analysed by HPLC.

2.9.1 HPLC instrumentation and chromatographic conditions

The lipid analysis was carried out on a YMC-PVA Silica column (100 × 3.0mm i.d. and 5µm particle size) from Hichrom Limited (Berkshire, UK) attached to a guard column with PVA-Sil (10 ×3.0mm i.d. and 5µm particle size) from Hichrom Limited (Berkshire, UK). Detection was obtained by an evaporative light scattering detector model 500 (Alltech, UK) supplied with 5l of nebulisation gas by a compressor and optimised at 80°C and gas flow rate of 2.90 standard litres per minute (SLPM).

A gradient ternary elution was used for separation of the lipids, where solvent A was isohexane, solvent B was ethyl acetate and solvent C was 60% propan-2-ol, 30% acetonitrile, 10% methanol, 142µl/100ml glacial acetic acid and 378µl/100ml triethylamine (Table 2.1). The gradient elution was run for 15min at a flow rate of 1ml/min where ingredients eluted within 10min and the final 5min was for column regeneration.

Table 2.1 Gradient elution sequence used in lipid analysis. In this analysis 100% isohexane (A), 100% ethyl acetate (B) and a mixture of 60% propan-2-ol, 30% acetonitrile and 10% methanol, 142µl/100ml glacial acetic acid and 378µl/100ml triethylamine (C) were used.

Time	**Solvent channel**		
(min)	**A**	**B**	**C**
0	80	20	-
2	72	25	3
3	64	30	6
4	56	35	9
5	48	40	12
6	35	45	20
7	35	45	20
8	35	45	20
9	72	25	3
10	80	20	-
15	80	20	-

2.10 Preparation of NIVs

Lipid components containing surfactant VIII (Tetra-ethylene glycol mono n-hexadecyl ether (Cruz Biotechnology, USA)), cholesterol (obtained from Croda Chemicals Ltd, East Yorkshire, UK) and DCP (Dicetyl phosphate (obtained from Sigma-Aldrich Inc., Dorset, UK)) were weighed in a 3:3:1 molar ratio, respectively, to prepare 750μmol/5ml. The contents were placed in glass tube and melted at 130ºC in an oil bath for 5min. The temperature was then reduced to 70ºC and hydrated with either 1mg/ml cisplatin in 0.9% w/v NaCl or 1mg/ml TPT in 5% tartaric acid in 0.9% w/v NaCl preheated to 70ºC in a water bath. The mixture was then homogenised at 8000 rpm for 15min using a Silverson L4R SU rotor fitted with a five-eighth inch tubular work head (Chesham, Buckinghamshire, UK).

2.10.1 Characterisation of NIVs

2.10.1.1 Sizing and zeta potential (ZP) of NIVs

The ZP is surface charge of particle within the media in which it is dispersed. For the measurement of particles size and zeta potential (ZP), a Nano ZS® (Malvern, UK) was used. Approximately 0.1ml of each NIV preparations was suspended in 2.5ml distilled water. The suspension then was sampled in a triplicates and placed in a cuvette to measure the size and ZP of each sample at 25°C. Each measurement was the average of three runs. These measurements were taken on the same days as entrapment efficiency.

2.10.1.2 Entrapment efficiency of NIVs

For both formulations cisplatin NIVs and TPT NIVs, 0.5 ml from each formulation was suspend in either 4.5 ml of 0.9% w/v NaCl for cisplatin NIVs or 4.5 ml of 5%

tartaric acid in 0.9% w/v NaCl w/v for TPT-NIVs. XL-90 ultracentrifuge (Beckman optima, U.S.A.) then was used to ultracentrifuge each NIV formulations at 60000rpm for an hour. The supernatant containing unentrapped drug was discarded and pellet was resuspended in 0.1N NaOH for cisplatin NIVs or 4.5 ml of mobile phase (50:50 Acetonitrile:H_2O, 0.1% TFA) for TPT NIVs to disrupt the vesicles and release their entrapped drug contents. From each formulation, triplicate HPLC samples were prepared and diluted to a suitable concentration within the calibration range. Cisplatin NIVs and TPT NIVs samples were analysed for entrapment efficiency by the described HPLC method in Section 2.7 and Section 2.8, respectively.

Entrapment efficiency was calculated using the following equation:

$$\% \text{ Entrapment} = \frac{\text{Concentration of drug entrapped (mg)}}{\text{Initial hydrating concentration of drug (mg)}} \times 100$$

2.11 Stability study

In this study TPT NIVs were prepared in batches of 20 ml. Surfactant VIII, cholesterol and DCP were weighed in a 3:3:1 molar ratio, respectively, to prepare 750µmol/5ml (Table 2.2).

Table 2.2. The weighed amount of lipids used in the preparation of NIVs hydrated with 1mg/ml TPT in batches of 20 ml.

Material	Theoretical wt. in 20 ml	Actual wt. in 20 ml
Surfactant VIII	537.6 mg	536.5 mg
Cholesterol	497.6 mg	495.5 mg
DCP	234.4 mg	233.8 mg

Aggregation or precipitation of the formulation was determined by the changes in the vesicle diameter using the DLS technique. The formulations were assessed for changes in entrapment efficiency, size and ZP at two different temperatures (4°C and 25°C) on a weekly basis for one month post preparation.

2.12 Determination of TPT NIVs in *vitro* pulmonary drug deposition

The nebulization efficiency of TPT NIVs and TPT solution were evaluated using an in *vitro* simulated lung model, Next Generation Impactor (NGI) provided by Copley Scientific Ltd., Nottingham, UK. NGI was used to determine the aerodynamic particle size distribution (APSD) of TPT NIVs and TPT solution. TPT NIVs were prepared, as described (section 2.7), as an aerosol formulation containing 200 µg of either TPT NIVs or TPT solution prepared in 5% tartaric acid in 0.9% w/v NaCl w/v was nebulized over 1.20 minutes using a mesh nebulizer AeronebGo (Aerogen LTD, Galway, Ireland). 7 ml of mobile phase (50:50 H_2O: acetonitrile, 0.1% TFA) was then added to each stage (stage 1 to micro-orifice collector (MOC), including the invented breath simulator throat) of the NGI to quantify TPT particles. The resultant solution was then analysed by HPLC as described (Section 2.8) for particle size distribution, two major indexes were determined: Mass Median Aerodynamic Diameter (MMAD) and Fine Particle Fraction (FPF%) represented the particle amount in which the diameter was less than or equal to 5 µm. Particles of this size were considered to be respirable.

2.13 Statistical analysis

2.13.1 Analysis of variance (ANOVA)

All experiments were carried out in triplicate, with results reported as the mean (± sd). Statistical analysis of the differences in clonogenic survival following drug dose exposure as a single therapy compared with untreated control cells, was carried out using one-way ANOVAs. Two-way ANOVA with Bonferroni test was used to statistically compare means of treated samples as a combination therapy with treated cells as a single therapy.

2.13.2 Linear quadratic analysis

To assess mathematically the radiosensitisation effect of either cisplatin or TPT and their ability to sensitise H460 and A549 cells to XBR, the clonogenic survival data for cells exposed to XBR alone and in combination was fitted to a linear quadratic model which defines the relationship between XBR dose and cell survival.

The linear quadratic model contains two key components of cell kill. The linear component, defined by the α coefficient, (equation 1) describes the initial slope of the survival curve in the low dose area, and the cell death which results from the α component increases linearly with radiation dose. As the administered radiation dose increases, the cell death resulting from the quadratic component, defined by the β coefficient increases in proportion to the square of the dose (equation 1).

It is suggested that the linear component, defined by the α coefficient represents cell death caused by single particle ionisation events, and that the quadratic component, defined by the β coefficient describes damage in cells as a result of accumulation of lesions resulting from two independent ionisation events at higher radiation doses. However, the contribution of single and multiple ionisation events to the relationship is still to be fully understood (Scheidegger *et al*., 2013, Franken *et al*., 2013)

The linear quadratic model is defined by equation 1;

$SF = \exp(-\alpha D - \beta D^2)$ Equation 1

Where; SF denotes the fraction of colonies which survive a given dose D of radiation.

GraphPadPrism software, version 6.01, 2014 (CA) was used to fit the experimental clonogenic survival fractions to the linear quadratic model (equation 1), and to obtain the values for the α and β coefficients.

The radiation dose required to induce 50% clonogenic cell kill (IC_{50}) was calculated using equation 2 for cells exposed to XBR alone from 0-2Gy and in combination with cisplatin at 62.5nM, 125nM and 250nM or TPT at 10nM, 20nM, and 30nM respectively.

$IC_{50} = [-\alpha + \sqrt{(\alpha^2 - 4\beta \ln 0.5)}] / 2\beta$ Equation 2

Following calculation of the IC_{50} for XBR alone and with TPT or cisplatin concentration, the dose enhancement factor at 50% clonogenic cell kill (DEF_{50}) was calculated using equation 3. The DEF is defined as the ratio of effect

observed following exposure of cells to radiation in combination with cisplatin or TPT to that of radiation alone at a given survival fraction (Roeske et al., 2007). Therefore, if the effect of AuNPs in combination with XBR results in the same amount of clonogenic cell kill as XBR alone the DEF equals 1. A DEF > 1 indicates that cisplatin or TPT act as a radiosensitisers and increase the effect compared to radiation alone, whilst a DEF < 1 suggests the cisplatin and TPT are acting as a radioprotector.

DEF_{50} = IC_{50} radiation alone / IC_{50} radiation + TPT or Cis **Equation 3**

2.13.3 T-test

To determine if the effects of particle size, ZP, or encapsulation efficiency for cisplatin NIVs, TPT NIVs, or empty NIVs were statistically significant different over time compared with day 0, t-test was used. T-test was used to determine if the drug deposition of TPT NIVs was statistically significantly different to the effects of the TPT solution during the NGI experiment. All statistical tests were carried out using GraphPad Prism software, version 6.0, 2014 (CA).

Chapter 3 : *In Vitro* Antitumor Evaluation of Cisplatin and TPT as Single or Combination Treatments

3.1 Introduction

Since its introduction into clinical practice, cisplatin has had a significant impact on cancer therapy, changing the course of treatment for numerous tumour types (Barr *et al*., 2013). To date, the most effective systemic chemotherapy for NSCLC is platinum-based compound, in particular cisplatin that is still the standard first-line chemotherapy for NSCLC. While an understanding of the mechanism of action is desirable in refining therapeutic strategies that can further enhance the antitumor activity of this platinum drug, cisplatin has a number of major drawbacks, one of which is the acquisition of cisplatin resistance which undermines its potential effectiveness (Sears *et al*., 2016a).

Cisplatin could be more effective when combined with another chemotherapeutic agent, in particular topotecan (topoisomerase I inhibitor) as it has been shown that the DNA single strand breaks caused by cisplatin is usually followed by induction of topoisomerase 1-dependent cleavage. This induction by topoisomerase 1 is a DNA damage repair response to the DNA damage caused by cisplatin (Capranico *et al*., 2017). Therefore, the rationale to combine topotecan with cisplatin is to increase DNA damage caused by cisplatin and to inhibit the DNA damage repair caused by topoisomerase 1, thus driving the cells to apoptosis using lower doses than would be required to achieve therapeutic efficacy with a single agent while maintaining the potential antitumor activity.

Some previous *in vitro* studies have reported synergistic effects between topotecan and cisplatin in combination in cancer cells and concluded that combination of TPT and cisplatin induced were supra additive cell kill when

utilised in A549 lung cancer cell lines (Adjei *et al.* 1996). Whereas, Kaufmann *et al.* (1996) examined TPT and cisplatin as a combination on A549 cell line and found that the CI values less than additive effects were seen at low to intermediate levels of cytotoxicity.

However, there is no consensus with respect to the optimum order of delivery of these chemotherapeutic agents. It is unclear whether possible synergistic effects resulting from a combination of these agents would be effective because of the order of delivery, and possibly greater cytotoxicity would occur only when one agent was administered prior to exposure to the second. Three treatment schedules (schedule A, schedule B, and schedule C) were investigated in this study in order to determine for the first time the dependence of sequencing of these agents on cell kill efficacy. In schedule A TPT first administered for 24hrs followed by cisplatin or vice versa in schedule B (total of 24hrs), whereas, schedule C (simultaneous administration) both agents were administered for 24hrs.

In addition, Fluorescence-Activated Cell Sorting (FACS) analysis was used in this chapter to provide a description of the cell cycle of lung cancer cells distribution following treatment. Previous studies concluded that TPT increased the proportion of NSCLC cells in S and G2/M phases after exposure to topotecan in high dose (50nM) whereas at high dose (1000 nM) TPT induced G1 arrest (Ohneseit *et al*., 2005), whereas cisplatin induced G2/M cell cycle arrest in NSCLC (Sarin *et al*., 2017). In this study, the effects of cisplatin and TPT, either alone or in combination, were examined to evaluate how cell cycle distribution

was perturbed by utilising the agents in combination and how this could be optimised to maximise treatment.

3.2 Aims

The primary aim of this chapter was to determine the cell line sensitivity and dose range of cisplatin and TPT as a single agent on H460 and A549 cell lines, then to investigate whether cisplatin and TPT as a combination therapy has a synergetic effect with respect to cell kill on H460 and A549 cells by using a clonogenic cell survival assay and combination index analysis. Secondly, we aimed to determine the most effective combination schedule by identifying the order of delivery that achieves greater cytotoxicity with lowest concentration of each agent. The second aim was to determine the mechanistic of this combination by analysis of the progression of cells through the cell cycle, and the DNA double stranded damage and repair, and to measure Annexin V expression as an indicator of apoptosis by cisplatin and TPT as single and combination treatments on H460 and A549 cell lines.

3.3 Results

3.3.1 Determining the cytotoxic effect of cisplatin and TPT on clonogenic survival of H460 and A549 cell lines

In this study the clonogenic assays were performed as described in section 2.3 The effect of cisplatin and TPT as single agents on clonogenic survival of H460 and A549 cells was firstly investigated to determine the dose response relationship of the cell lines to cisplatin to be used in combination with TPT, and with radiation in subsequent chapters. The results of clonogenic survival, following cisplatin alone in a dose range of 0-5 μM, are shown in Figures 3.1 for H460 cells and in Figures 3.2 for A549 cell lines, there was a dose-responsive reduction in survival fraction with the administered dose of cisplatin in both cell lines, where the clonogenic cell survival reduced proportionally with increasing cisplatin doses.

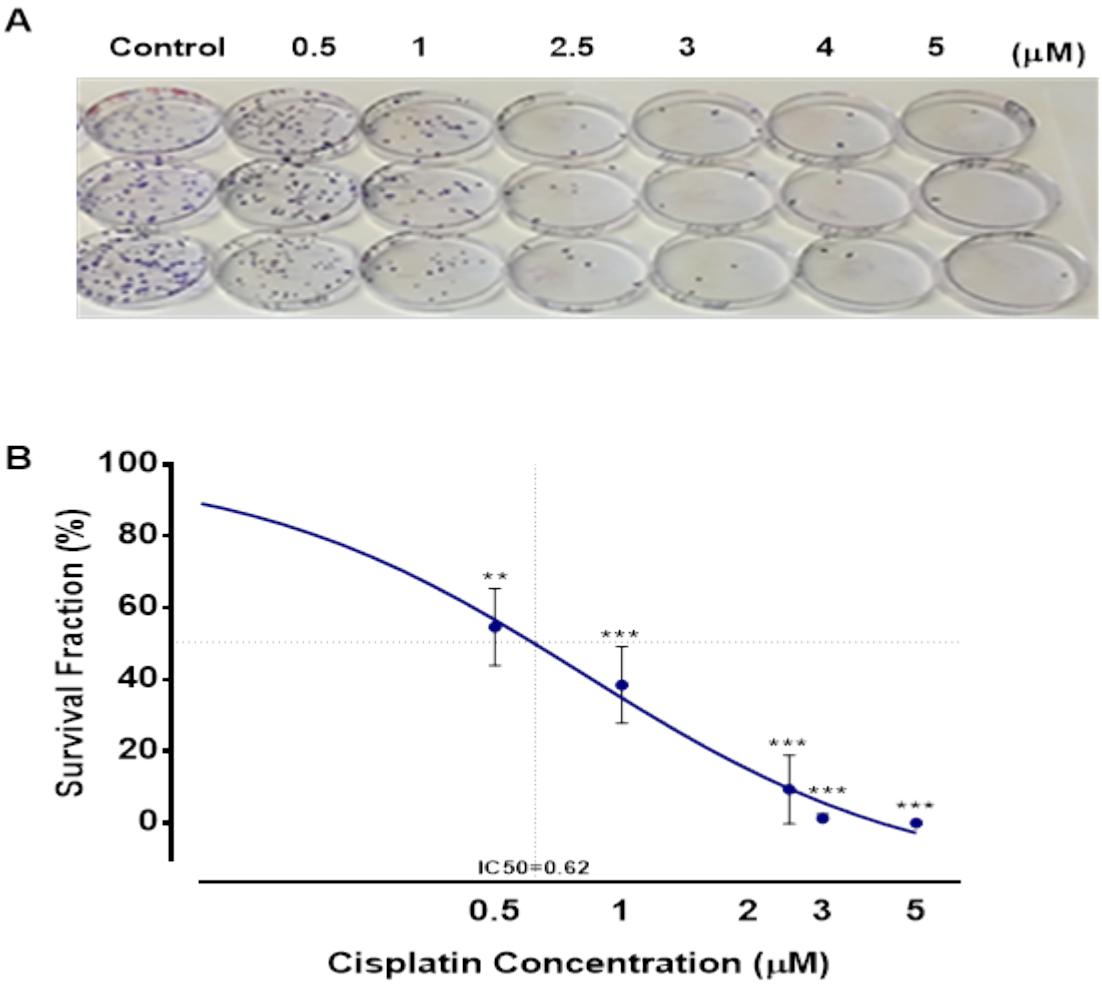

Figure 3.1: The effect of increasing doses of cisplatin on H460 cells survival.
Figure **A**) Demonstrates the number of colonies in petri dishes for each dose used in the cisplatin experiment. **B)** Demonstrates the effect of cisplatin across a concentration range of 0-5 μM on H460 for 24 hours. Statistical analysis of the differences in clonogenic survival following exposure to each dose, compared with untreated control cells, was carried out using one-way ANOVAs with Bonferroni corrections with 95% C.I. Data points are averages of triplicate experiments and are shown ± STD. ** = $p < 0.01$; *** = $p < 0.001$.

H460 cells exposure to the lowest dose of cisplatin (0.5 μM) indicated a significant reduction in the cell survival fraction compared to the untreated control with an average cell survival of 0.54 ± 0.1 (inhibition by 44%, $p < 0.01$). With the highest doses of 5 μM cisplatin, clonogenic survival was completely inhibited by 100% *(p* < 0.001), indicating a statistically significant reduction when compared with the untreated control. The dose of cisplatin that killed 50% of the cell population (IC_{50}) was 0.62 μM.

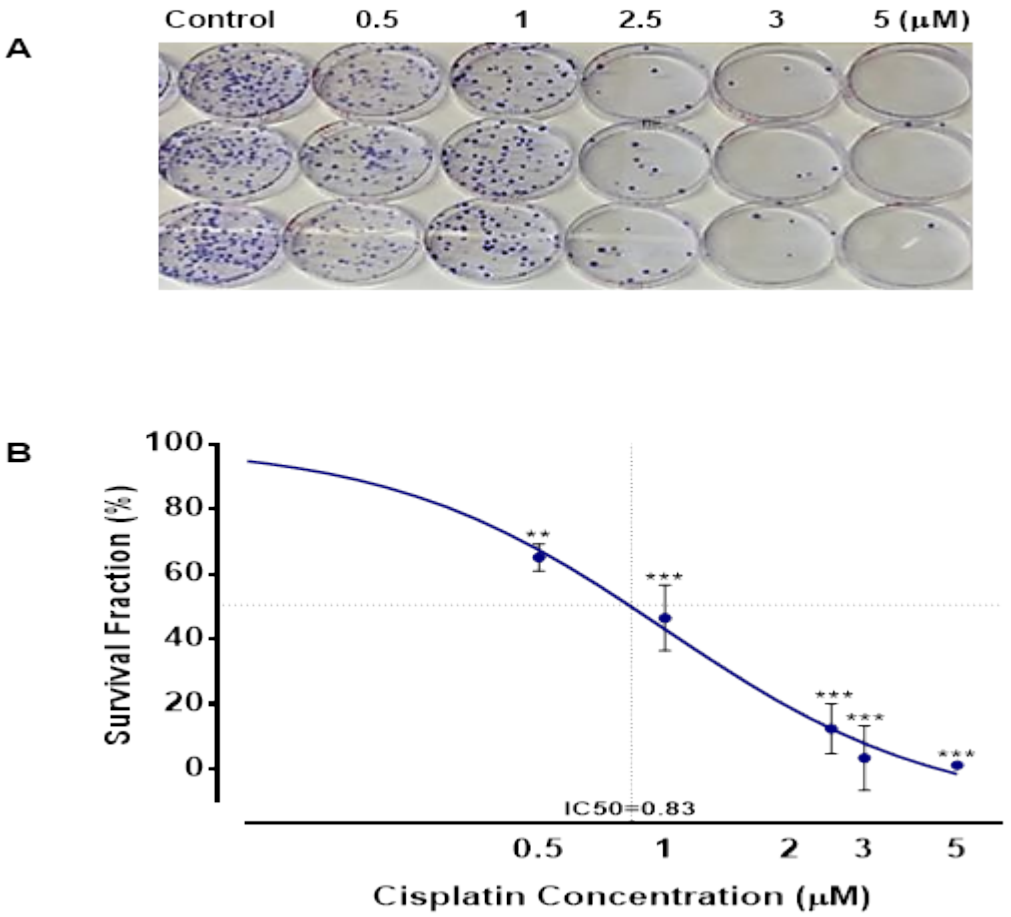

Figure 3.2: The effect of increasing doses of cisplatin on A549 cells survival.
Figure **A**) Demonstrates the number of colonies in petri dishes for each dose used in the cisplatin experiment. **B)** Demonstrates the effect of cisplatin across a concentration range of 0-5 µM on A549 for 24 hours. Statistical analysis of the differences in clonogenic survival following exposure to each dose, compared with untreated control cells, was carried out using one-way ANOVAs with Bonferroni corrections with 95% C.I. Data points are averages of triplicate experiments and are shown ± STD. ** = $p < 0.01$; *** = $p < 0.001$.

Similarly, A549 cells exhibited a dose-dependent reduction in survival fraction following exposure to cisplatin over the 0.5-5 µM dose range (Figure 3.2). Cell

exposure to the lowest dose of cisplatin (0.5 μM) inhibited the cell survival fraction significantly from 1 in the untreated control to 0.65 ± 0.04 (inhibition by 35%, $p < 0.01$). With the highest dose of 5 μM cisplatin, the cell survival fraction was completely inhibited by 100% ($p < 0.001$), indicating a statistically significant reduction when compared with the untreated control. The dose of cisplatin that killed 50% of the cell population (IC_{50}) was 0.95 μM. A549 cells were observed to be less sensitive to cisplatin than H460 cells.

TPT alone in a dose range of 100-1000 nM in both cell lines are demonstrated in Figure 3.3, there was a dose-responsive reduction in survival fraction with increasing the administered dose of TPT in both cell lines, where the clonogenic cell survival reduced proportionally with increasing TPT doses.

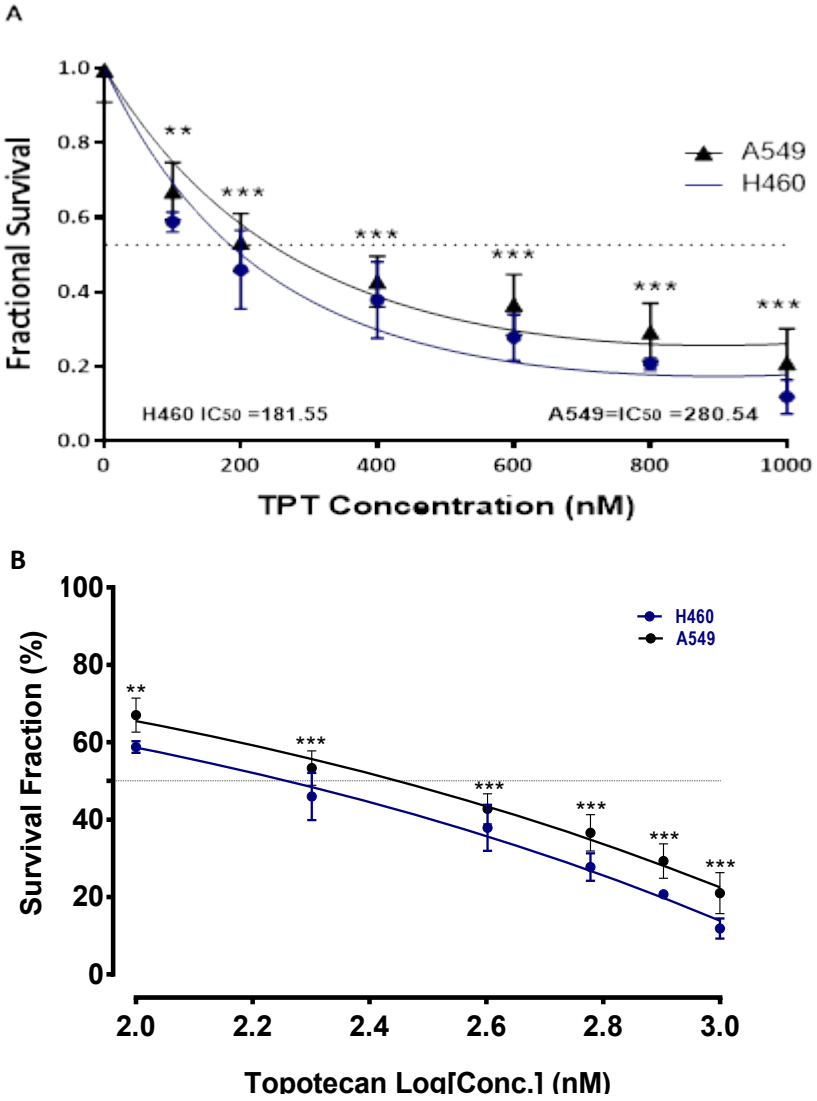

Figure 3.3: The effect of increasing doses of TPT on H460 and A549 cells survival. Figure **A**) Demonstrates the effect of TPT alone across a concentration range of 100-1000 nM on H460 and A549 for 24 hours. **B**) Clonogenic survival data presented in (A) was fitted to the linear quadratic model using GraphPad Prism version 6.0.1.Statistical analysis of the differences in clonogenic survival following exposure to each dose, compared with untreated control cells, was carried out using one-way ANOVAs with Bonferroni corrections with 95% C.I. Data points are averages of triplicate experiments and are shown ± STD. ** = $p < 0.01$; *** = $p < 0.001$.

H460 cells exhibited a dose-dependent reduction in survival fraction following exposure to TPT over the 100-1000 nM dose range (Figure 3.3), with a 50% (IC_{50}) reduction in clonogenic survival observed after administration of 181 nM TPT. H460 cells exposure to the highest dose of 1000 nM TPT resulted in cell survival fraction inhibition by 89% from 1 in untreated control to 0.11 ± 0.045 *(p* < 0.001), indicating a statistically significant reduction when compared with the untreated control.

Similarly, after 24 hours of TPT treatment A549 cells exhibited a dose-dependent reduction in survival fraction following exposure to TPT over the 100-1000 nM dose range (Figure 3.3), with a 50% (IC_{50}) reduction in clonogenicity observed at 280 nM. A549 cells exposure to the highest dose of 1000 nM TPT resulted in survival fraction inhibited by 0.79% from 1 in the untreated control to 0.21 ± 0.09 (*p* < 0.001), indicating a statistically significant reduction when compared with the untreated control. Again, based on the survival results, A549 cells are less sensitive to TPT than H460 cells (IC_{50} = 280nM).Table 3.1 summarises the IC_{50} values obtained from the clonogenic data for cisplatin and topotecan in H460 and A549 cell lines.

Table 3.1: IC50 values from clonogenic experiments of cisplatin and TPT on H460 and A549 cell lines.

Agent	Cell Line	IC50
Cisplatin	H460	0.62 μM
	A549	0.83 μM
TPT	H460	181.55 nM
	A549	280.54 nM

These results indicate that there is a dose dependant reduction in cell survival in both H460 and A549 cell lines to TPT and cisplatin as a single agent. However, it was noticed the A549 cells are less sensitive to cisplatin and TPT than H460 cells, this deference is mainly related to the cell line characteristics, for example, A549 cells is well known to have a P53 genes that play a significant role as a cyto-protective agent. Thesrefore, the IC_{50} value of A549 cells is higher than H460 cells.

Based on the effect of cisplatin and TPT alone in H460 and A549 cell lines, the cisplatin dose range from 62.5-250 nM and TPT dose range from 10-30 nM were used for subsequent combination studies, using lower doses than IC_{50} values of each agent as this allow for detection of any potential decreases in survival fraction that would be required to achieve therapeutic efficacy with a single agent while maintaining the potential antitumor activity.

3.3.2 Assessing the cytotoxic effects of cisplatin and TPT alone or in combination treatments against H460 cell lines by using clonogenic (cell survival) assays

In this study the clonogenic assays were performed as described in section 2.3. From the survival data of H460 discussed in section 3.3.1 a lower dose range of cisplatin and TPT were generated taking into account that dose range to be lower than IC_{50} to achieve greater cytotoxicity with lowest concentration of each agent as per our hypothesis. These lower dose ranges then were tested to assess the chemosensitisation potential of TPT in combination with cisplatin on H460 cells, the effect of TPT with an administered dose range of 10-30 nM and the effects of cisplatin with an administered dose range of 62.5-250 nM were investigated either alone or in combination in three different treatment schedules (schedule A, schedule B, and schedule C) to determine the dependence of sequencing of these agents on cell kill efficacy. In schedule A TPT was administered before cisplatin for 24hrs, in schedule B cisplatin was administered before TPT for 24hrs, and in schedule C cisplatin and topotecan were administered simultaneously for 24 hours. The results are shown in Figure 3.4 and indicating significant differences in favour of schedule C (simultaneous administration) to be more effective in achieving greater cytotoxicity when compared to schedule A and B when tested on H460 cells.

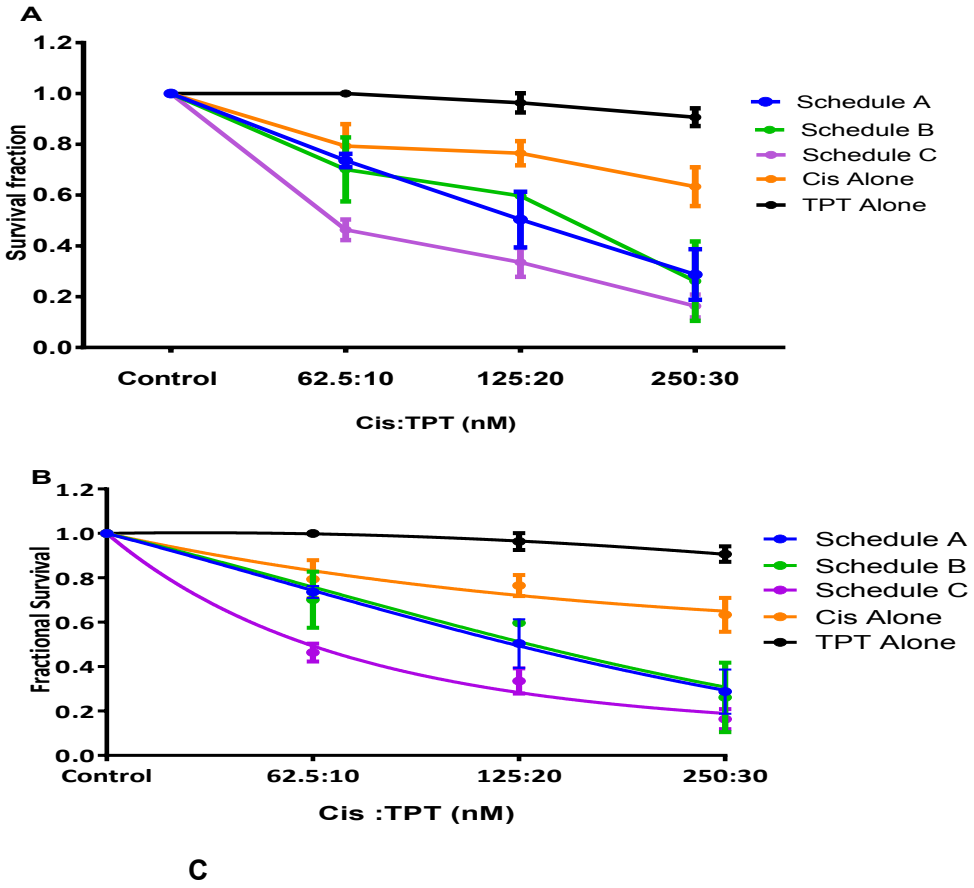

C

Schedule **A** vs. **B**	ns
Schedule **A** vs. **C**	$p < 0.0001$
Schedule **B** vs. **C**	$p < 0.0001$
Schedule **A** vs. **Cis** Alone	$p < 0.0001$
Schedule **A** vs. **TPT** Alone	$p < 0.0001$
Schedule **B** vs. **Cis** Alone	$p < 0.0001$
Schedule **B** vs. **TPT** Alone	$p < 0.0001$
Schedule **C** vs. **Cis** Alone	$p < 0.0001$
Schedule **C** vs. **TPT** Alone	$p < 0.0001$
TPT Alone vs. **Control**	ns
Cis Alone vs. **Control**	$p < 0.01$

Figure 3.4: The effect of increasing doses of cisplatin and TPT in combination on H460 survival.

A) The effects of cisplatin and TPT alone and in combination on H460 cells. Based on data from A, cells were dosed with cisplatin and TPT in the following quantities (Cis:TPT): 0:0, 62.5:10, 125:20, and 250:30 nM. **B)** Clonogenic survival data presented in (A) was fitted to the linear quadratic model using GraphPad Prism version 6.0.1. **C)** Two-way ANOVA with Bonferroni test was used to statistically compare means of treated samples with either untreated controls or cis/TPT alone. Tests were performed with 95% C.I

90% survival (IC_{10}) was observed at the highest concentration of 30 nM TPT tested on H460 (Figure 3.4). Whereas, concentration of 20 nM or less had no effect on H460, there was no statistically significant effect over the dose range 10-30 nM TPT when compared to untreated control. Whereas, H460 cell survival decreased in the 62.5-250 nM cisplatin dose range. There was a statistically significant decrease in clonogenic survival (63%, $p < 0.01$) of H460 at the highest concentration of 250 nM cisplatin when compared to untreated control.

However, after combination therapy, levels of cytotoxicity greater than the IC_{50} were seen in all scheduled combinations, with a statistically significant decrease *(*$p < 0.0001$) observed in clonogenic survival of H460 cells, compared with cells exposed to TPT or cisplatin alone. In the case of the schedule C 10 nM TPT administered simultaneously with 62.5 nM cisplatin, a survival fraction of 46% was observed, compared with 100% survival for 10 nM TPT alone or 79% survival fraction for 62.5 nM cisplatin alone. In contrast, for schedules A and B the clonogenic survival rates were 73% and 69% respectively, with no significant difference between schedules A and B. Whereas, schedule C resulted in a statistically significant reduction in survival fraction compared with schedules A and B *(*$p < 0.0001$). These clonogenic survival results indicate that combining TPT and cisplatin achieved better cytotoxicity than the cell kill induced for TPT or cisplatin alone (Figure 3.4) on H460 cell line.

3.3.2.1 Combination-index analysis of the interaction between cisplatin and TPT on H460 cell lines

To analyse the synergy of TPT in combination with cisplatin on H460 cells, the survival fractions from different scheduled combinations of TPT and cisplatin shown in Figure 3.4 were used to construct the combination index (CI values) as described in section 2.3.1. These are shown in Figures 3.5.

The CI values in Figure 3.5 correspond to the modes of action of the two agents at different levels of cytotoxicity, where CI < 1, CI = 1 and CI >1 indicate synergism, additivity and antagonism, respectively.

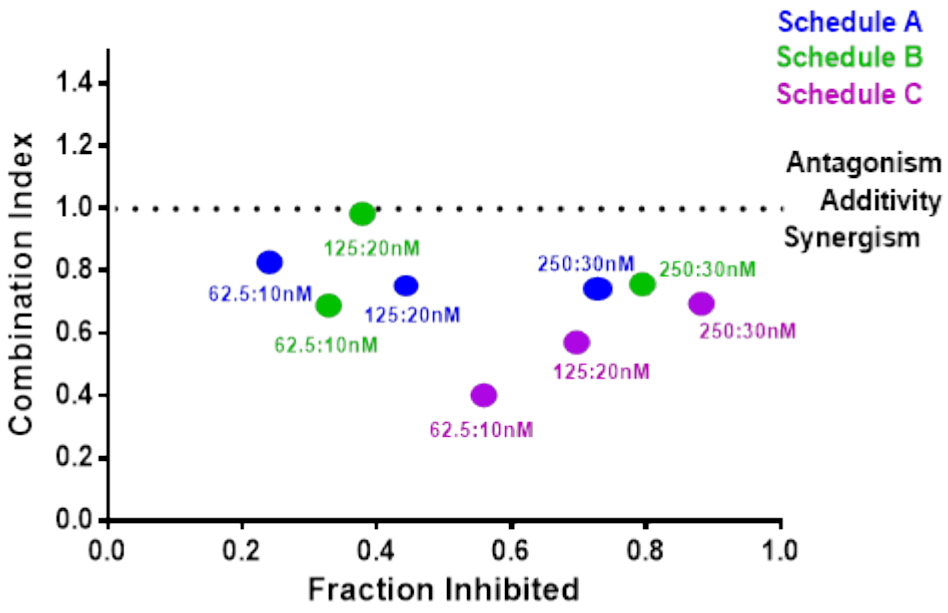

Figure 3.5: Combination index (C.I.) combined effect of cisplatin and TPT on clonogenic survival of H460 cells. Schedule **A,** schedule **B**, schedule **C**. Clonogenic survival data were analysed using combination index analysis, where CI < 1, CI = 1 and CI > 1 indicated synergism, additivity and antagonism respectively. Each value represents the CI of three separate experiments

Supra-additive kill of H460 cells after treatment with all combination schedules resulted in CI values < 1 that indicates a synergetic effect in between TPT and cisplatin when tested in combination. At the lowest combination dose of 10 nM TPT combined with 62.5 nM cisplatin, treatment by schedules A, B and C resulted in the following CI values: schedule A = 0.825; schedule B = 0.689; schedule C = 0.349. At the highest combination dose of 30 nM TPT and 250 nM cisplatin, treatment by schedule A, B and C resulted in the following CI values: schedule A = 0.849; schedule B = 0.823; schedule C = 0.738. Thus, administration of TPT after cisplatin (schedule B) or before cisplatin (schedule A) showed no significant change, whereas simultaneous administration (schedule C) of two agents produced a more synergistic effect with CI value of 0.738 compared to schedule A (CI = 0.849) and schedule B (CI = 0.823).

3.3.3 Assessment of the cytotoxic effects of cisplatin and TPT alone or in combination treatments against A549 cell lines using clonogenic (cell survival) assays

Clonogenic assays were performed as described in section 2.3. From the survival data of A549 discussed in section 3.3.1 a lower dose range of cisplatin and TPT were generated taking into account that dose range to be lower than IC_{50} to achieve greater cytotoxicity with lowest concentration of each agent alone. These lower dose ranges then were tested to assess the chemosensitisation potential of TPT in combination with cisplatin on A549 cells, the effect of TPT with an administered dose range of 10-30 nM and the effects of cisplatin with a dose range of 62.5-250 nM were investigated either alone or in combination in three different treatment schedules (schedule A, schedule B, and schedule C) on A549. In schedule A TPT was administered before cisplatin for 24hrs, in schedule B cisplatin was administered before TPT for 24hrs, and in schedule C cisplatin and topotecan were administered simultaneously for 24 hours. The results are shown in Figure 3.6 and indicating significant differences in favour of schedule C (simultaneous administration) to be more effective in achieving more cytotoxic effect when compared to schedule A and B when tested on A549 cells.

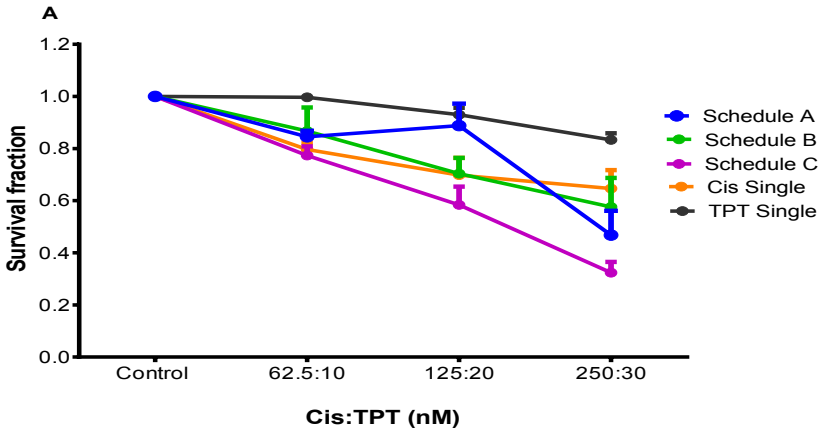

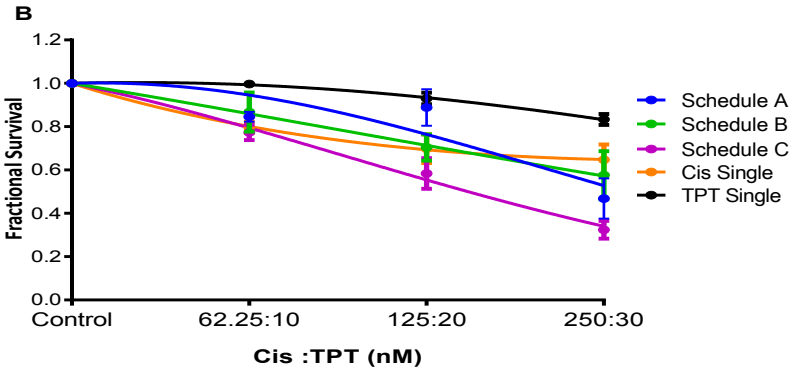

C

Schedule **A** vs. **B**	ns
Schedule **A** vs. **C**	$p < 0.0001$
Schedule **B** vs. **C**	$p < 0.0001$
Schedule **A** vs. **Cis** Single	ns
Schedule **A** vs. **TPT** Single	$p < 0.0001$
Schedule **B** vs. **Cis** Single	ns
Schedule **B** vs. **TPT** Single	$p < 0.0001$
Schedule **C** vs. **Cis** Single	$p < 0.05$
Schedule **C** vs. **TPT** Single	$p < 0.0001$
Cis Single vs. **Control**	$p < 0.01$
TPT Single vs. **Control**	*ns*

Figure 3.6: The effect of increasing doses of cisplatin and TPT on A549 cells survival fraction.

A) The effects of cisplatin and TPT alone and in combination on A549 cells. Based on data from A, cells were dosed with cisplatin and TPT in the following quantities (Cis:TPT): 62.5:10, 125:20, and 250:30 nM. **B)** Clonogenic survival data presented in (A) was fitted to the linear quadratic model using GraphPad Prism version 6.0.1. **C)** The effects of cisplatin and TPT alone and in combination on A549 cells. Two-way ANOVA with Bonferroni test was used to statistically compare means of treated samples with either untreated controls or cis/TPT alone. Tests were performed with 95% C.I.

A549 cells showed no statistically significant decrease in cell survival over the 10-30 nM TPT dose range compared to untreated control when used as a single agent. 83% survival was observed at the highest concentration of 30 nM (Figure 3.6), whereas 10 nM TPT had no effect with 100% survival fraction. A549 cells survival decreased statistically significant in the 62.5-250 nM cisplatin dose range; 64% survival was observed at the highest concentration of 250 nM compared to untreated control ($p < 0.01$) (Figure 3.6).

After combination therapy on A549 cells, levels of cytotoxicity greater than IC_{50} were seen in only schedule A (TPT before cisplatin) and schedule C (simultaneous administration) whereas schedule B resulted in no significant difference when compared with cisplatin alone. There was no significant difference in survival between schedule A and schedule B when compared with schedule C, whereas schedule C had a statistically significant decrease ($p < 0.0001$) in clonogenic survival of A549 cells when compared with survival data of schedules A and B. In the case of schedule C (simultaneous administration), the combination of 10 nM TPT with 250 nM cisplatin resulted in survival fractions of 32%, compared with 83% survival for 10 nM TPT alone ($p < 0.0001$) or 64% ($p < 0.05$) survival with 62.5 μM cisplatin alone. These clonogenic survival results indicate that TPT is chemosensitising to cisplatin (Figure 3.6) when tested on the A549 cell line.

3.3.3.2 Combination-index analysis of the interaction between cisplatin and TPT on A549 cell lines

To analyse the chemosensitisation of TPT in combination with cisplatin on A549, from the survival results of different scheduled combinations of TPT and cisplatin shown in Figure 3.6, the combination index (CI values) and median effect plots were constructed as described (Section 3.1.1). These are shown in Figures 3.7. The CI values in Figure 3.7 correspond to the modes of action of the two agents that are dependent or distinct at different levels of cytotoxicity, where CI < 1, CI = 1 and CI > 1 indicate synergism, additivity and antagonism, respectively. An additive to infra additive effect was observed only in schedule C (simultaneous administration) whereas schedule A and B were seen to produce an antagonistic effect in A549 cells.

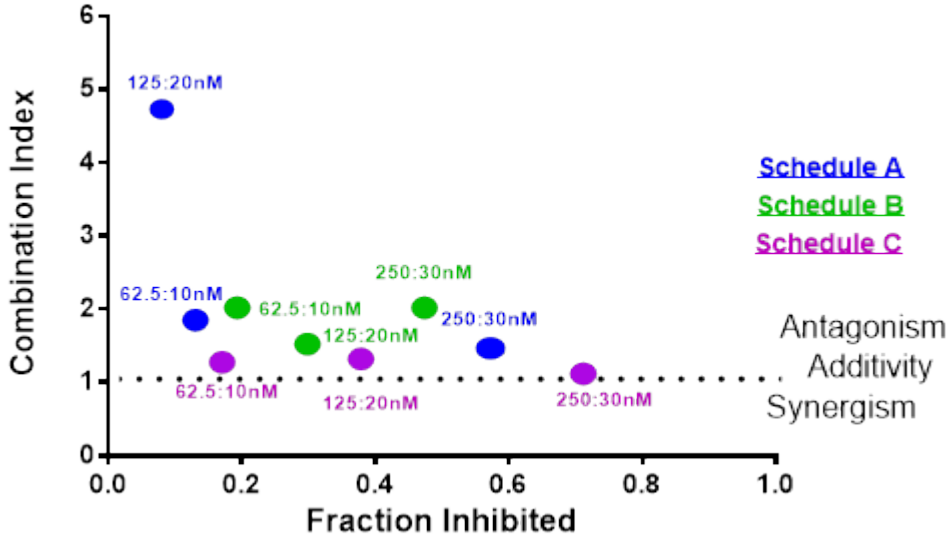

Figure 3.7: Combination index (C.I.) combined effect of cisplatin and TPT on clonogenic survival of A549 cells. Schedule **A**, Schedule **B**, Schedule **C**

Clonogenic survival data were analysed using combination index analysis, where CI < 1, CI = 1 and CI > 1 indicated synergism, additivity and antagonism, respectively. Each value represents the CI of three separate experiments.

Additive to infra-additive kill effect of A549 cells after treatment was only observed in combination doses of schedule C, which resulted in CI values = 1 at the highest combination dose of cisplatin 250nM and TPT 30nM. In contrast, an antagonism effect was observed in schedules A and B, which resulted in CI values > 1. This may due to induction of p53 expression that could be induced in a time- and concentration-dependent manner, irrespective of the cytotoxic compound used. At the lowest combination dose of 10 nM TPT and 62.5 nM cisplatin, treatment by schedules A, B and C resulted in CI values of 1.679, 1.952, and 1.143, respectively. At the highest combination dose of 30 nM TPT and 250 nM cisplatin, treatment by schedules A, B and C resulted in CI values of 1.526, 2.070, and 1.039, respectively.

Administration of TPT simultaneously with cisplatin (schedule C) produced an additive effect and in agreement with the clonogenic data discussed in section 3.3.2, whereas, TPT before or after cisplatin (schedules A and B) showed to be inferior to schedule C.

3.3.5 Investigation of the induction and repair of DNA damage by measurement of γ-H2AX foci assessment following cisplatin and topotecan alone or in combination treatments on H460 cells

As discussed in section 1.4, treating cells with chemotherapy results in different types of DNA damage, such as SSBs and DSBs. DNA SSBs though induced, can be easily and rapidly repaired, leading to inaccurate quantification of initial DNA damage and DNA damage repair. However, DNA DSBs are more difficult for the cell to repair and can therefore be more accurate for quantification of significant DNA damage which can lead to cell death.

The mean number of γ-H2AX foci/cell of H460 cells was therefore measured, as described in section (2.4), following incubation with cisplatin alone across a dose range of 125-250 nM, TPT alone across a dose range of 20-30 nM, and both in combination. The results are shown in Figure 3.8 at 2 and 24 hours after treatment.

With cisplatin treatment, the data shows a significant dose-dependent increase in γ-H2AX levels at all doses across the time period when compared with untreated control cells, however, γ-H2AX levels decreased at 24hrs compared to 2hrs indicating that DNA damage is being repaired. In contrast there was no significant difference with 20-30 nM TPT at 2 hours but at 24 hours there was a significant increase in γ-H2AX levels when compared with untreated cells. The combination therapy shows a significant dose-dependent increase in γ-H2AX levels at all doses across the time period when compared with cisplatin alone treatment group.

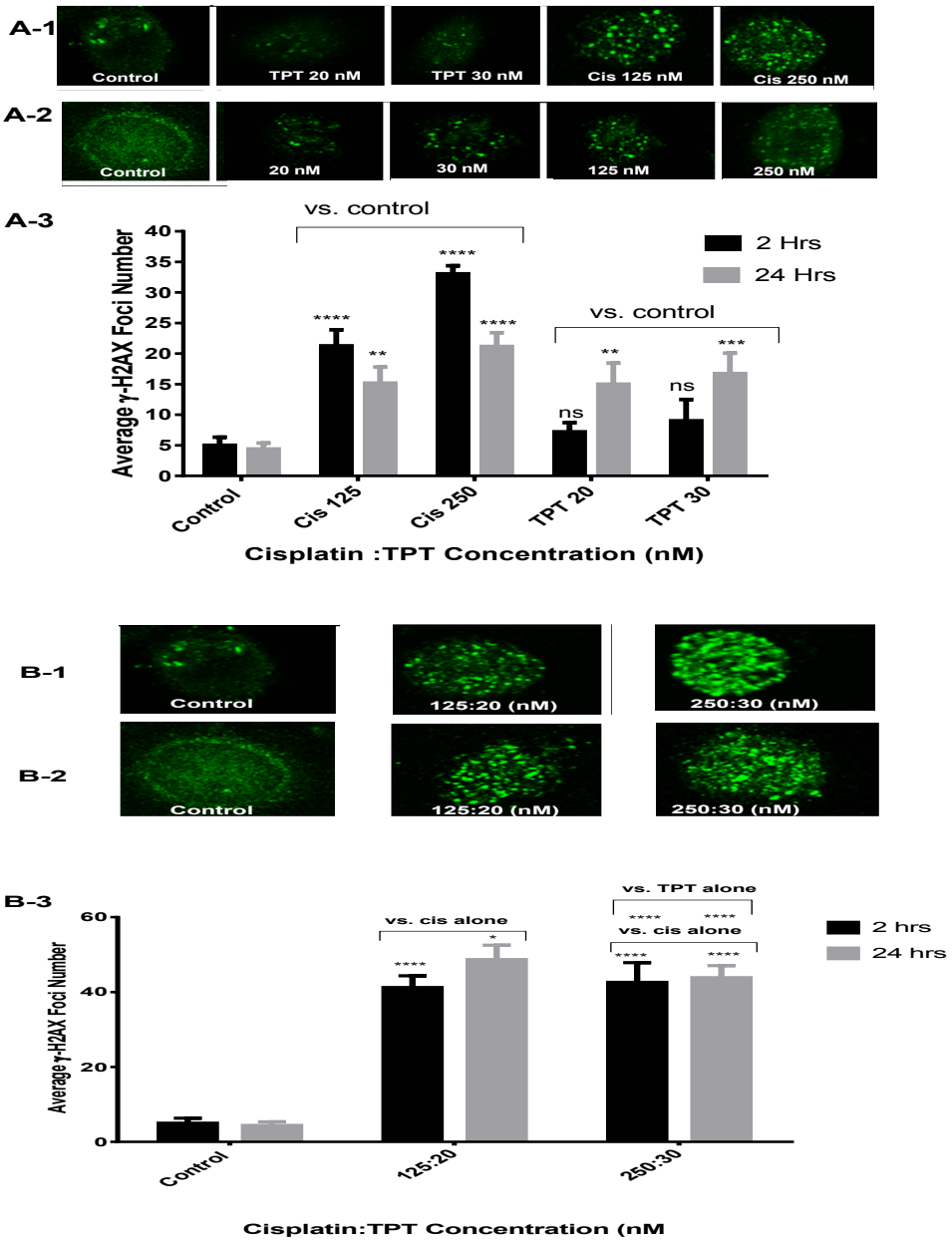

Figure 3.8: The effects of cisplatin and TPT alone (A) and in combination (B) on H460 cells formation and residual of DNA-DSB.

The mean number of γ-H2AX foci/cell was assessed at 2 hours and 24 hours after treatment. Results presented are the mean number of γ-H2AX foci/cell (mean ± sd) of 3 independent experiments for cisplatin and TPT alone (A3), and in combination (B3) in H460 cells respectively. Two-way ANOVA was used to determine if statistically significant changes in the number of γ-H2AX foci/cell resulted. All tests were performed at a 95% C.I. * = $p < 0.05$; *** = $p < 0.001$; **** = $p < 0.0001$. Representative images of γ-H2AX foci in each treatment group at 2 hours (A/B/-1) and 24 hours (A/B/-2) are presented.

Based on the effect of cisplatin and TPT alone on H460 cells, the formation of γ-H2AX foci increased as the dose increased. With cisplatin treatment doses of 125 nM or 250 nM, at 2 hours there was a statistically significant increase in the number of γ-H2AX foci from 5 foci/cell ± 1.32 in untreated controls to 21 foci/cell ± 2.6 ($p < 0.0001$) and 33 foci/cell ± 1.3 ($p < 0.0001$), respectively. At 24 hours compared with 2 hours with cisplatin treatment, the number of γ-H2AX foci decreased to 15 foci/cell ± 2.6 and 21 foci/cell ± 2.2, respectively, but this level was still significantly higher than untreated controls (4 foci/cell ± 9.6 vs. 15 foci/cell ± 2.6 and 21 foci/cell ± 2.2 ($p < 0.0001$), respectively). .

In contrast, at 2 hours there was no significant difference in the number of γ-H2AX foci/cell induced by 20 nM and 30nM of TPT alone (5 foci/cell ± 1.32 vs. 7.2 foci/cell ± 1.5 and 9 foci/cell ± 3.5 ($p > 0.05$), respectively) compared with untreated controls. However, after 24 hours there was a statistically significant increase in the average number of foci/cell from 4 foci/cell ± 9.6 in untreated controls to 15 foci/cell ± 3.4 with 20 nM TPT ($p < 0.0001$) and 17 foci/cell ± 3.3 ($p < 0.0001$) with 30 nM TPT.

After 2 hours of combination treatment, at the lowest combination dose (125 nM cisplatin with 20 nM TPT) there was a statistically significant increase the number of γ-H2AX foci compared with the same dose of each agent alone at 2hrs (41 foci/cell ± 1.3 ($p < 0.0001$) in the treated cells vs. 21 foci/cell ± 2.6 and 7.2 foci/cell ± 1.5 in control cells, respectively). Similarly, at 24 hours the three was a statistically significant increase in the number of γ-H2AX foci compared with the same dose of each agent alone at 24hrs (48 foci/cell ± 3.8 ($p < 0.0001$) vs. 15 foci/cell ± 2.6 and 15 foci/cell ± 3.4, respectively). After 2 hours of combination

treatment, at the highest combination dose (250 nM cisplatin: 30 nM TPT) three was a statistically significant increase in the number of γ-H2AX foci compared with the same dose of each agent alone (44 foci/cell ± 5.25 *(p* < 0.0001) vs. 33 foci/cell ± 1.3 and 9 foci/cell ± 3.5, respectively). Similarly, at 24 hours the number of γ-H2AX foci increased statistically significantly compared with the same dose of each agent alone at 24hrs (44 foci/cell ± 3.22 (*p* < 0.0001) vs. 21 foci/cell ± 2.2 and 17 foci/cell ± 3.3, respectively).

The results of the measurement of γ-H2AX foci in this section confirmed a significant dose-dependent increase in γ-H2AX levels in H460 cells following cisplatin treatment alone or in combination with TPT at all doses across the time period when compared with untreated control cells or cisplatin alone. Furthermore, the DNA repair seen at 24hrs after cisplatin alone was inhibited when the combination treatment introduced. The nature of this interaction suggests that cisplatin treatment increases the susceptibility of cells to TPT-induced toxicity. Supporting our data are several studies which suggest a clear role for cisplatin impairing DNA DSB repair (Sears et al., 2016a).This result was in agreement with the clonogenic survival data described in section (3.3.2.1) that showed a synergism following treatment with cisplatin and TPT in combination in H460 cells.

3.3.6 Investigation of the induction and repair of DNA damage by measurement of γ-H2AX foci assessment following cisplatin and topotecan alone or in combination treatments on A549 cells

In this study the formation and repair of DNA DSBs was investigated by measuring γ-H2AX foci numbers (described in section 2.4) in the A549 cell line to evaluate the effects of cisplatin and TPT as single treatments and in combination. The mean number of γ-H2AX foci/cell was measured in A549 cells following incubation with cisplatin (125-250 nM) alone, TPT (20-30nM) alone, and in combination, and is shown in Figure 3.9 at 2 and 24 hours after treatment. With cisplatin, the data show a significant increase in γ-H2AX levels at all doses across the time period when compared with untreated control cells, however at 24 hrs there was a statistically significant decrease in γ-H2AX level compared to 2hrs but still significantly increased compared to control cells indicating that some of the DNA damage being repaired . Whereas TPT showed a significant difference with 20-30 nM TPT at 24 hours when compared with 2hrs or untreated cells. The combination treatment of cisplatin and TPT results in a significant increase in γ-H2AX levels at all doses when compared to either cisplatin alone or TPT alone treatment group.

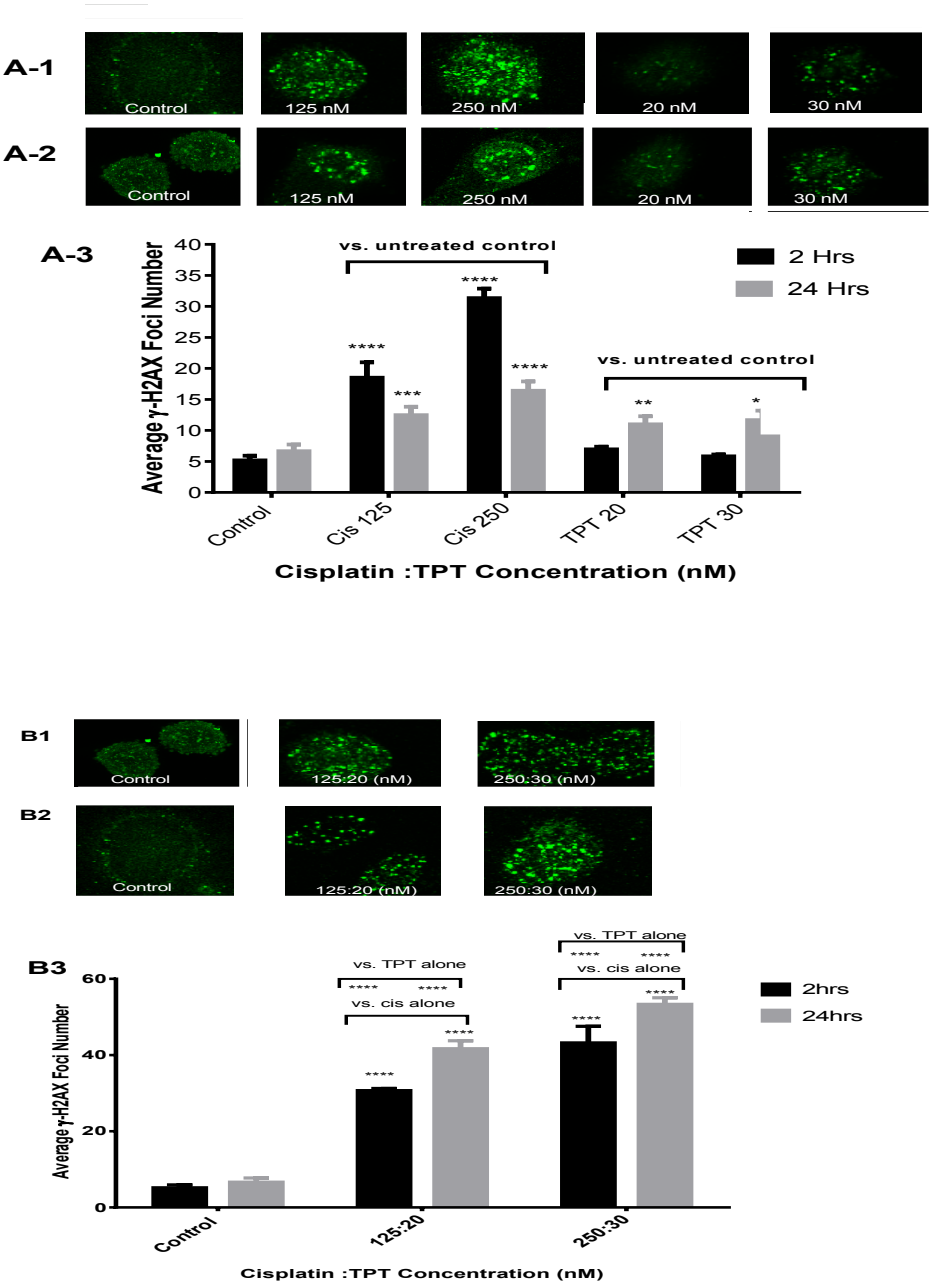

Figure 3.9: Effects of cisplatin TPT alone (A) and in combination (B) on A549 cells' residual DNA-DSB.

The mean number of γ-H2AX foci/cell was assessed at 2 hours and 24 hours after treatment. Results presented are the mean number of γ-H2AX foci/cell (mean ± sd) of 3 independent experiments for cisplatin and TPT alone (A3), and in combination (B3) in A549 cells respectively.All tests were performed at a 95% C.I. *** = $p < 0.001$; **** = $p < 0.0001$. Representative images of γ-H2AX foci in each treatment group at 2 hours (A/B/-1) and 24 hours (A/B/-2) are presented.

At 2 hours post treatment with two different cisplatin doses (125 and 250 nM), A549 cells showed a statistically significant increase in number of γ-H2AX foci to 18.50 ± 2.5 and 31.33 ± 1.52 ($p < 0.01$ and $p < 0.0001$, respectively) compared with untreated controls (5.16 ± 0.76) (Figure 3.9). At 24 hours, the number of γ-H2AX foci still remained significantly increased compared with untreated control cells. However, in comparison with the cisplatin-treated cells between 2 hours and 24 hours, the number of γ-H2AX foci/cell decreased from 18.50 (± 2.5) to 12.48 (± 1.34, $p < 0.01$) at 125 nM and with dose of 250 nM from 31.33 (± 1.52) to 16.40 (± 1.50, $p < 0.0001$).

At 2 hours post treatment with two different TPT doses (20 and 30 nM), A549 cells showed no significant increase in number of γ-H2AX foci when compared with untreated controls (Figure 3.9). In contrast, at 24 hours, there was a statistically significant increase in the number of γ-H2AX foci compared with untreated control cells or 24hrs TPT treatment group; the number of γ-H2AX foci/cell increased from 6.95 (± 0.42) to 11.00 (± 1.3, $p < 0.01$) at 20 nM and with a dose of 30 nM from 5.83 (± 0.288) to 11.66 (± 1.52, $p < 0.001$).

The number γ-H2AX foci was measured in A549 cells following combination treatment of cisplatin (125 and 250 nM) and TPT (20 and 30 nM) at 2 and 24 hours (Figure 3.9).

At 2 hours post combination treatment, A549 cells in both combination doses (125 and 25 nM of cisplatin with 20 and 30 nM of TPT) showed a statistically significant increase in number of γ-H2AX foci from 30.66 ± 0.57 to 41.66 ± 2.08 and from 43.2 ± 4.35 to 53.3 ± 1.73 ($p < 0.0001$ and $p < 0.0001$, respectively) compared

with untreated controls (5.16 ± 0.76 to 6.64 ± 1.08). At 24 hours, with this combination therapy, the number of γ-H2AX foci still remained significantly increased, indicating that the DNA damage repair process was being inhibited due to the effect of the combined TPT while cisplatin alone showed a decrease in the number of γ-H2AX foci between 2 and 24 hours. In contrast, TPT had no significant effect at 2 hours when compared with untreated control cells and treated cells at 2 hours.

The results of the measurement of γ-H2AX foci in this section confirmed a significant increase in γ-H2AX levels following cisplatin treatment alone or in combination at all doses across the time period when compared with untreated control cells or cisplatin alone. This result was in agreement with the clonogenic survival date described in section (3.3.3) that showed cisplatin and TPT induced an additive to infra additive cell kill (simultaneous administration schedule) in A549 cells, supporting our data are several studies which suggest a clear role for cisplatin impairing DNA DSB repair (Sears et al., 2016a). However, A549 cells were less susceptible than H460 cells to TPT-induced toxicity.

3.3.7 Analysis of cell cycle progression following exposure to cisplatin and TPT

During the cell cycle, there are two pathways for repairing DNA DSBs. Repair by homologous recombination has been shown to occur during late S and G2 phases of the cell cycle whilst NHEJ repair occurs in all phases of the cell cycle particularly in the G0 and G1 phases (Tolis *et al*, 1999). The effect of cisplatin and TPT as combination treatments of NSCLC remain unresolved. In this study, the effects of cisplatin and TPT, either alone or in combination, were examined using fluorescence-activated cell sorting (FACS) analysis discussed (Section 2.5) to identify several mechanisms involved in this interaction.

3.3.7.1 The effect of cisplatin and TPT alone or in combination on cell cycle progression in H460 cells

The proportion of H460 cells in different phases of the cell cycle described (section 2.5), after treatment with various concentrations of cisplatin alone, TPT alone, or in combination, was assessed by flow cytometry and data are shown in Figure 3.10.

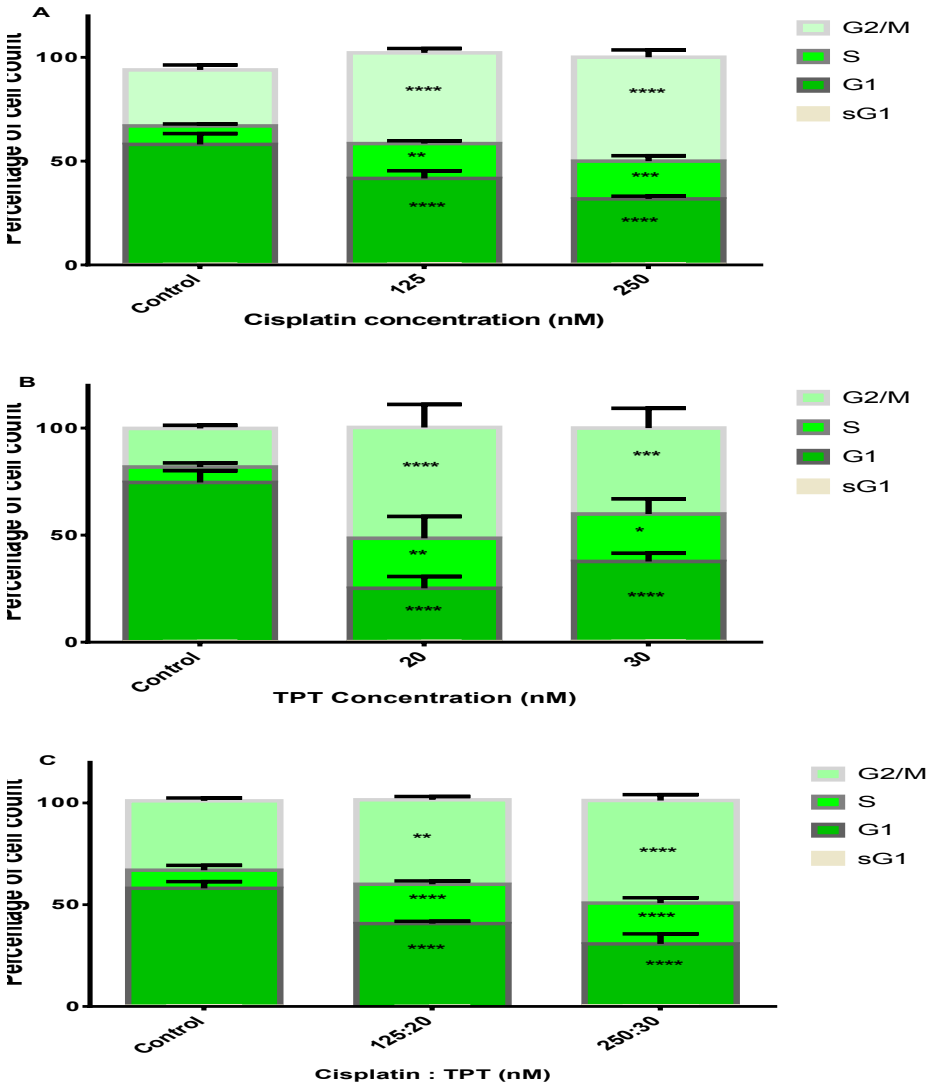

Figure 3.10 Effect of cisplatin alone, TPT alone, and in combination on cell cycle progression in H460 cell lines.

Effect of cisplatin alone **(A),** TPT alone **(B),** and in combination **(C)** on cell cycle progression in H460 cell lines. Cells were treated with different doses of cisplatin alone (125-250 nM), TPT alone (20 and 30 nM) or in combination for 24 hours. The cell cycle was then assessed by flow cytometry using propidium iodide (PI) for the determination of total DNA content. The chart demonstrates the distribution of cells in the different phases of the cell cycle following treatment. Two-way ANOVA was used to determine if there were statistically significant changes in the distribution of cells throughout the cell cycle. Bonferroni correction was used to compare with untreated controls. Each value represents the mean (± sd) of three separate experiments. *** = $p < 0.001$ compared with the non-treated control group.

As shown in Figure 3.10, exposure of H460 cells to 125-250 nM of cisplatin for 24 hours caused significant changes in cell cycle distribution of G0/G1, G2/M and S phases. With the highest dose of 250 nM cisplatin there was a statistically significant increase ($p < 0.0001$) in the percentage of cells in G2/M phase from 27% (± 2.4) in the control cells to 50% (± 3.5) in the treatment cells while the proportion of cells in S phase increased from 8.8% (± 1) in the control cells to 18.2% (± 2.6, $p < 0.001$) in the treatment cells. However, it was observed that increasing doses did not cause any additional significant changes in cell cycle distribution ($p > 0.05$).

Exposure of H460 cells to 20-30 nM TPT resulted in a statistically significant increase in the accumulation of cells within the G2/M and S phases of the cell cycle when compared with untreated cells after 24 hours treatment. With the highest dose of 30 nM the percentage of cells within G2/M increased from 18% (± 1.4) in the control cells to 40% (± 9.2, $p < 0.001$) in the treatment cells while the proportion of cells in S phase increased from 7.2% (± 1.9) in the control cells to 22.2% (± 7.1, $p < 0.05$) in the treatment cells.

Exposure of H460 cells to cisplatin (125-250 nM) and TPT (20-30 nM) in combination resulted in a statistically significant increase in the accumulation of cells within the G2/M and S phases of the cell cycle when compared with untreated cells after 24 hours treatment. With the highest dose of 250 nM cisplatin: 30 nM TPT the percentage of cells within G2/M increased from 34% (± 1.4) in the control cells to 50.4% (± 2.8, $p < 0.0001$) in the treatment cells while the proportion of cells in S phase increased from 8.8% (± 2.4) in the control cells to 20% (± 2.6, $p < 0.0001$) in the treatment cells.

The results of the cell cycle analysis reported in this section confirmed that exposure H460 cells to cisplatin alone resulted in G2/M arrest in a higher percentage of the cell population, whereas exposure to TPT alone resulted in S-phase and G2/M arrest in H460 cells. This finding is in agreement with previous data on increased proportions of NSCLC cells in S and G2/M phases after a 4 hour exposure to topotecan (Tolis *et al*, 1999).

3.3.7.2 The effect of cisplatin and TPT alone or in combination treatments on cell cycle progression in A549 cells

After treatment with various concentrations of cisplatin alone, TPT alone, or in combination, was assessed by flow cytometry and data are shown in Figure 3.11.

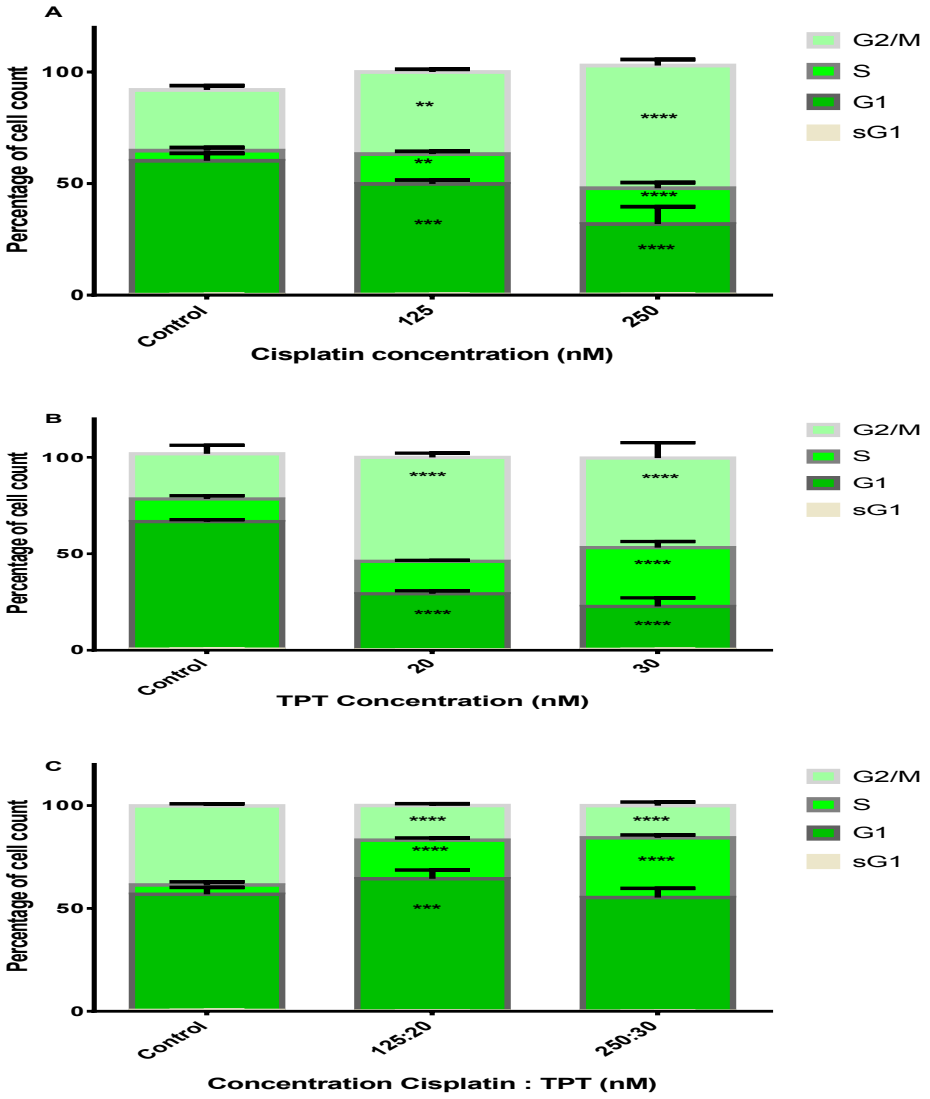

Figure 3.11: Effect of cisplatin alone, TPT alone, and in combination on cell cycle progression in A549 cell lines.

Effect of cisplatin alone (A), TPT alone (B), and in combination (C) on cell cycle progression in A549 cell lines. Cells were treated with different doses of cisplatin alone (125-250 nM), TPT alone (20 and 30 nM) or in combination for 24 hours, then the cell cycle assessed by flow cytometry using propidium iodide (PI) for the determination of total DNA content. The chart demonstrates the distribution of cells in the different phases of the cell cycle following treatment. Two-way ANOVAs with Bonferroni corrections were used to determine if there were statistically significant changes in the distribution of cells throughout the cell cycle. Each value represents the mean (± sd) of three separate experiments. *** = $p < 0.001$ compared with the control group.

As shown in Figure 3.11, exposure of A549 cells to 125-250 nM cisplatin alone and 20-30 nM TPT alone for 24 hours causes significant changes in cell cycle distribution of G0/G1, G2/M and S phases. With the highest dose of 250 nM cisplatin, there was a statistically significant decrease in the percentage of cells in G2/M phase from 38.4% (± 1.0) in the control cells to 15.6% (± 1.7, $p < 0.0001$) in the treatment cells while the proportion of cells in S phase increased from 4.5% (± 1.5) in the control cells to 29% (± 1.4, $p < 0.001$) in the treatment cells.

Exposure of A549 cells to 20-30 nM TPT resulted in a statistically significant increase in the accumulation of cells within the G2/M and S phases of the cell cycle when compared with untreated cells after 24 hours treatment. With the highest dose of 30 nM, the percentage of cells within G2/M increased from 23.4% (± 4.4) in the control cells to 46.4% (± 7.9, $p < 0.0001$) in the treatment cells, while the proportion of cells in S phase increased from 11.7% (± 1.6) in the control cells to 30.5% (± 3.1, $p < 0.0001$) in the treatment cells.

Exposure of H460 cells to cisplatin (125-250 nM) and TPT (20-30 nM) in combination resulted in a statistically significant increase in the accumulation of cells within the G2/M and S phases of the cell cycle when compared to untreated cells after 24 hours treatment. With the highest dose of 250 nM cisplatin : 30 nM TPT the percentage of cells within G2/M decreased from 38.4% (± 1.0) in the control cells to 15.6% (± 1.7, $p < 0.0001$) in the treatment cells while the proportion of cells in S phase increased from 4.5% (± 1.5) in the control cells to 29% (± 1.4, $p < 0.0001$) in the treatment cells.

The results of the cell cycle analysis reported in this section confirmed that exposure A549 cells to cisplatin alone resulted in G2/M arrest in a higher

percentage of the cell population, whereas exposure to TPT alone resulted in S-phase and G2/M arrest. However, after combination treatment, a significant population of A549 cells were arrested in G1 and S phase. The arrest of cells at G1 phase in A549 cells minimises the population of cells that will enter S and G2/M phase. This observation was in line with the results of previous studies, such as a study performed by Tolis *et al*. (1999) which revealed that an increased number of cells arrested in the G1 in A549 cells when TPT was combined with a DNA damage agent. Furthermore, this result was in line with the clonogenic survival data that showed an additive kills described in section (3.3.3.2).

3.3.8 The effect of cisplatin and topotecan treatments on Annexin V protein expression

In order to determine whether the changes in H2Ax and cell cycle distribution were inducing apoptosis the next set of experiments were designed to examine the rates of apoptosis in various treatment groups. During apoptosis, the appearance of phosphatidylserine (PS) on the surface of the cell membrane is an early event in apoptosis, and therefore can be used as a marker of apoptosis (Elmore, 2007). Annexin V has a potential affinity for PS and based on their Annexin V affinity, apoptotic cells can be distinguished from Annexin V-negative cells (Demchenko, 2013). Therefore, Annexin V can be used as a tool for detecting apoptosis. As described (Section 2.6) for quantitative measurement of apoptosis, after treatment with cisplatin alone, TPT alone, or in combination for 48 hours, followed by FACS analysis to identify several mechanisms involved in this interaction. 48 hours treatment duration was selected instead of 24 hours

treatment duration because 24 hours did not show any significant expression on Annexin V protein in all treatment group when compared to the control cells. Therefore, longer duration was decided.

3.3.8.1 The effect of cisplatin and topotecan alone or in combination on Annexin V expression in H460 cells

The expression of Annexin V-negative cells (described in section 2.6) in H460 cell lines, after treatment with various concentration of cisplatin alone, TPT alone, or in combination, was assessed by flow cytometry and the results are shown in Figure 3.12. Treatment with cisplatin and TPT alone on H460 results in significant differences in Annexin V expression when compared to untreated control. The combination therapy induce further significant increase in the percentage of apoptotic cells when compared to cisplatin alone.

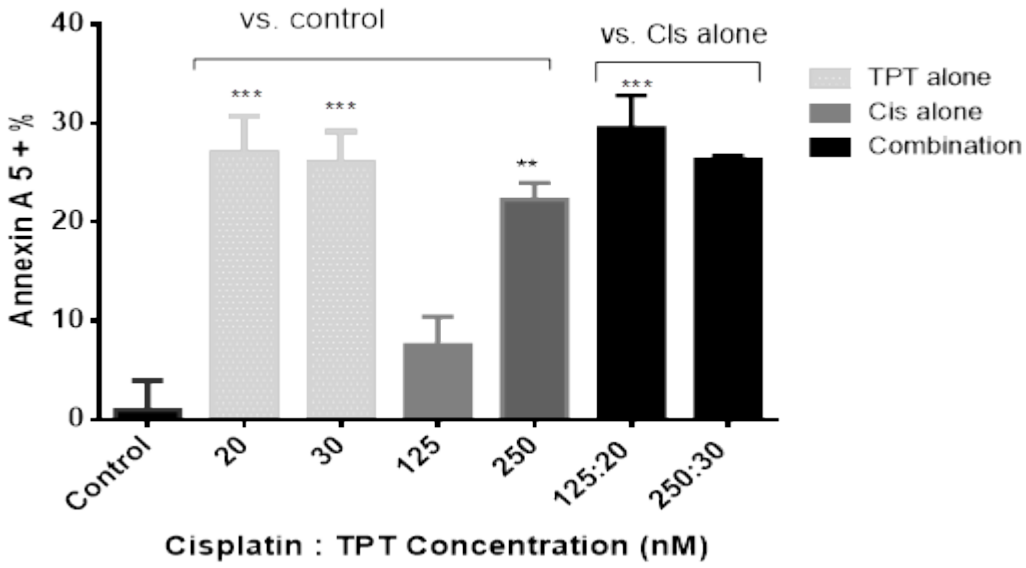

Figure 3.12: Cisplatin and TPT alone or in combination induce Annexin V protein expression in H460.

Cells were treated with cisplatin alone or TPT alone for 48 h. Two-way ANOVA was used to determine if there were statistically significant differences in the Annexin 5 expression. Each value represents the mean (± sd) of three separate experiments. Bonferroni post-test to compare treated cells to untreated control or cisplatin/TPT alone. Each value represents the mean (± sd) of three separate experiments. ** = $p < 0.01$; *** = $p < 0.001$; **** = $p < 0.0001$.

Exposure of H460 cells to 125-250 nM cisplatin alone and 20-30 nM TPT alone for 48 hours caused significant increases in Annexin V expression (Figure 3.12) when compared with untreated control cells. With the highest dose of 250 nM cisplatin, there was a statistically significant increase in the percentage of apoptotic cells from 1% (± 5.11) in the control cells to 22.28% (± 2.8, $p < 0.01$) in the treatment cells, whereas 125 nM cisplatin did not cause any significant increase in the percentage of Annexin V when compared with control cells ($p > 0.05$).

At doses of 20 nM and 30 nM TPT, there was a statistically significant increase in the percentage of apoptotic cells, from 1% (± 5.11) in the control cells to 27% (± 6.4, $p < 0.01$) and 26% (± 5.4, $p < 0.01$) in the treatment cells, respectively.

After the combination treatments, there was a statistically significant increases in the percentage of apoptotic cells in the treatment groups when compared with cisplatin alone. At the combination dose of 125nM cisplatin with 20nM TPT, the percentage of apoptotic cells, increase significantly from 7.53% (± 4.96) in the cisplatin alone treated cells to 29.5% (± 5.7, $p < 0.01$) in the combination treated cells.

The significant increase in Annexin V expression reported in this section confirmed a high a rate of apoptosis following treatment with cisplatin and TPT alone in H460 cells, whereas the combination had an additional significant effect when compared to cisplatin alone. This apoptotic results confirmed the synergism effect seen on H460 cells (3.3.2) resulted from the DNA damage that was reported in section 3.3.5.

3.3.8.2 The effect of cisplatin and topotecan alone or in combination treatments on Annexin V in A549 cells

The expression of Annexin V-negative cells (described in section 2.6) in A549 cell lines, after treatment with various concentrations of cisplatin alone, TPT alone, or in combination, was assessed by flow cytometry and results are shown in Figure 3.13. Treatment with cisplatin and TPT alone on H460 results in significant differences in Annexin V expression when compared to untreated control. The combination therapy induce further significant increase in the percentage of apoptotic cells when compared to cisplatin alone.

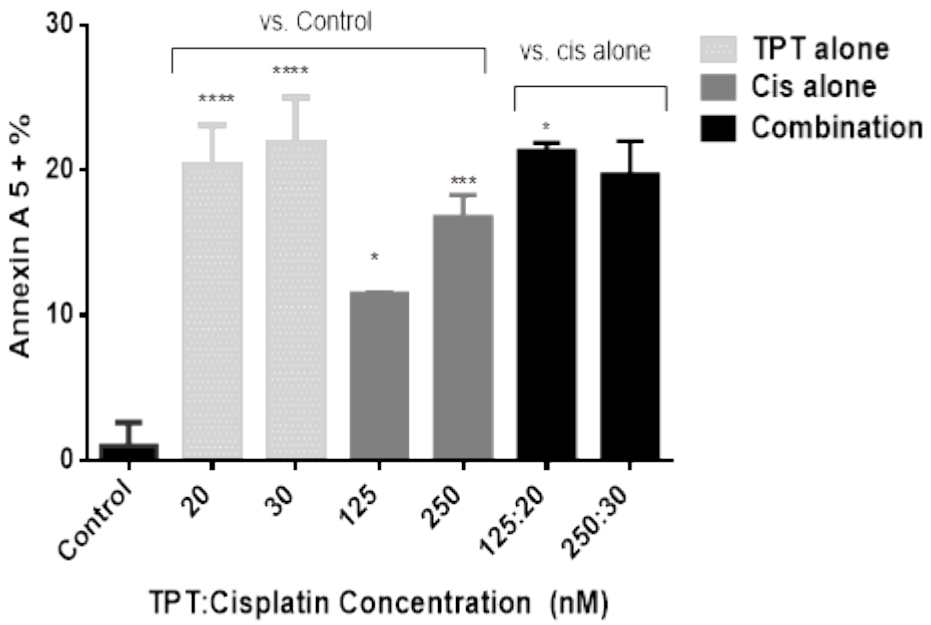

Figure 3.13: Cisplatin and TPT alone or in combination induce Annexin V protein expression in A549. Cells were treated with cisplatin alone or TPT alone for 48 h. Two-way ANOVA was used to determine if there were statistically significant differences in the Annexin 5 expression. Each value represents the mean (± sd) of three separate experiments. Bonferroni post-test to compare treated cells to untreated control or cisplatin/TPT alone. Each value represents the mean (± sd) of three separate experiments. . * = $p < 0.05$; *** = $p < 0.001$; **** = $p < 0.0001$.

Exposure of A549 cells to 125-250 nM cisplatin alone and 20-30 nM TPT alone for 48 hours (Figure 3.13) caused significant increases in Annexin V expression when compared to untreated control. With the highest dose of 250 nM cisplatin, there was a statistically significant increase in the percentage of apoptotic cells, from 1% (± 5.11) in the control cells to 22.28% (± 2.8, $p < 0.01$) in the treatment cells.

At doses of 20 nM and 30 nM TPT, there was a statistically significant increase in the percentage of apoptotic cells, from 1% (± 5.11) in the control cells to 27% (± 6.4, $p < 0.01$) and 26% (± 5.4, $p < 0.05$) in the treatment cells, respectively.

After the combination treatments, there was a statistically significant increases in the percentage of apoptotic cells at the combination dose of 125nM cisplatin with 20nM TPT, where the apoptotic percentage increased from 11.46% (±0.20) in the cisplatin alone treated cells to 21.33% (±0.92, $p < 0.01$) in the combination treated cells.

The significant increase in Annexin V expression reported in this section confirmed a high a rate of apoptosis following treatment with cisplatin and TPT alone in A549 cells and the combination treatment had an additional significant effect when compared to cisplatin alone. This apoptotic results are in agreement with the additive effect seen by the clonogenic survival data described in section 3.3.3 that thought to be due DNA damage that was reported in section 3.3.6.

3.4 Discussion

The aim of this study was to firstly evaluate the effects of cisplatin and TPT alone and in combination on the clonogenic survival of H460 and A549 cells. In this study a significant reduction in clonogenic survival was observed in both cell lines following 24 hours incubation with cisplatin alone or TPT alone in H460 and A549 cells (Figures 3.1- 3.3). There was a dose-responsive reduction in survival fraction of H460 and A549 cells with the administered dose of cisplatin and TPT, where the clonogenic cell survival reduced proportionally with the increasing cisplatin and TPT doses and it was observed that A549 cells were less sensitive than H460 cells to the administered treatment. The results of previous studies performed to evaluate the cytotoxicity of cisplatin and TPT alone in NSCLC have demonstrated similar effects to results described in this chapter. For example, study carried out by Barr *et al*. (2013), incubation of A549 cells with cisplatin in a dose range of 0.1 μM to 100 μM resulted in a significant reduction ($p < 0.001$) in clonogenic survival ability. While, Giovannetti *et al*. (2005) reported that TPT causes a dose-dependent inhibition of cell survival of A549 cells with an IC_{50} observed at a dose of 840.2 ng $ml^{-1.}$

The combination of cisplatin across the concentration range 62.5-250 nM with 10-30 nM TPT was assessed by using different combination schedules: (A) a 24-hour period of TPT exposure followed by cisplatin treatment, (B) a 24-hour period of cisplatin exposure followed by TPT treatment and (C) a 24-hour period of simultaneous exposure to cisplatin and topotecan. The results confirmed a statistically significant decrease *(*$p < 0.05/0.001$) in the clonogenic survival of H460 (Figure 3.4) in all of three schedules when compared to cisplatin or TPT

alone groups indicating that TPT is a chemosinsitiser to cisplatin, further to this, the combination index (CI) analysis (Figure 3.5) showed a synergism interaction in all of the three schedules with CI values less than 1 (Figure 3.5). However, the survival results for the combination of cisplatin and TPT on A549 cells (Figure 3.6) showed a statistically significant difference in only schedule C (simultaneous administration of cisplatin and TPT) compared with cisplatin exposure alone. The in *vitro* investigations in this chapter of the combination interaction between cisplatin and TPT in A549 cells (Figure 3.7) underwent antagonistic effects in schedules A and B (CI > 1) and an additive to infra-additive effect was observed in schedule C. This result is in agreement with Ma *et al*.1998 found that the synergistic cytotoxicity of cisplatin and TPT during simultaneous administration were observed in seven human solid-tumour cell lines used and may at least partly be induced by the increased retention of DNA interstrand cross-links (ISCs) in the presence of topo I inhibitors.

In both cell lines, schedule C (simultaneous administration) had at least an additive effects, indicating a significant schedule-dependent synergistic cytotoxicity. On the basis of these observations at a cellular level of the molecular effect of this cisplatin-TPT interaction, it is likely that the inhibition of topoisomerase I affects the ability of cells to repair cisplatin adducts. This combination may therefore have pharmacological implications in overcoming the cisplatin-induced resistance. This observed chemosensitisation is in agreement with the results of previous studies, such as a study performed by Romanelli *et al.* (1998), which found that cisplatin and TPT have an additive to infra additive

effect in sequential schedules and supra-additive effects in a simultaneous schedule when both drugs were tested in ovarian cancer cells.

A further study by Ma *et al*. (1998) using median-effect analyses of the cytotoxicity interaction of cisplatin alone and in combination with TPT in eight solid-tumour cell lines revealed a synergistic cytotoxicity in seven of the eight cell lines used in this study including NSCLC. Another study conducted by Kaufmann *et al.* (1996) in agreement with the results described in this chapter illustrated that TPT and cisplatin administered simultaneously in A549 cells resulted in less than additive effects at low-to intermediate levels of cytotoxicity, and more than additive effects were seen at high levels of cytotoxicity. Therefore, schedule C (simultaneous administration of TPT and cisplatin) was selected to be used in all combination experiments in this chapter for the cell cycle analysis, γ-H2AX foci measurement, and Annexin V expression.

The results of the induction and repair of DNA damage by measurement of γ-H2AX foci in this chapter confirmed a significant dose-dependent increase in γ-H2AX levels on H460 and A549 (Figure 3.8 and Figure 3.9, respectively) following cisplatin treatment alone or in combination with TPT at all doses across the time period when compared with untreated control cells or cisplatin alone, however it was observed in this experiment that cisplatin induced DNA damage was significantly repaired after 24hrs, this repair may link to the activation of p53 by cisplatin-induced DNA damage that has been reported to have various effects on cellular sensitivity to cisplatin. In some studies, activation of p53 has been shown to provide cytoprotection against cisplatin (Sekiguchi *et al*., 1996, Sorenson *et al*., 1990). p53 has also been shown to have a role in regulating the G2/M

checkpoint (Tolis *et al*., 1999). This result was in agreement with a recent study conducted by Sears *et al*. (2016) investigating the DDR in A549 and H460 which revealed an increase in γ-H2Ax-positive H460 cells after treatment with cisplatin alone. The DNA-CDDP inter-strand adducts are repaired by the homologous recombination repair (HRR) pathway while intra-strand adducts are repaired by the nucleotide excision repair (NER) pathway, and hypersensitivity to cisplatin is often observed in cells deficient in either NER or HRR (Sakai *et al.* 2008; Koberle *et al.* 1999).

In contrast, our results showed that TPT alone at 2 hours did not result in any significant differences when compared with untreated control cells suggesting the mechanism of DNA DSBs is not dose dependent when tested in H460 cells (Figure 3.8) and A549 cells (Figure 3.9). This may reflect the role of TPT in relaxing and supercoiling the DNA double helix to allow the replication of chromosomes for S-phase. However, at 24 hours TPT induced a statistically significant increase in γ-H2AX levels when compared with untreated control.

After combination treatment was introduced, at 24hrs γ-H2AX levels increased significantly compared with 2hrs γ-H2AX levels of cisplatin alone or TPT alone. Furthermore, the DNA repair seen at 24hrs after cisplatin alone was inhibited when the combination treatment with TPT introduced. The nature of this interaction suggests that cisplatin treatment increases the susceptibility of cells to TPT-induced toxicity. Supporting our data are several studies which suggest a clear role for cisplatin impairing DNA DSB repair (Sears *et al*., 2016a). This result was in agreement with the clonogenic survival data described in section (3.3.2.1) that showed a synergism to additive effect following treatment with cisplatin and

TPT in combination using a simultaneous administration in H460 and A549 cells and this simultaneous administration of TPT and cisplatin have increased the level of DNA DSBs represented by the observed high level of γ-H2AX.

Recent studies have proven the importance of modulating the cell cycle to exploit the effect of drug combinations (Shah and Schwartz, 2001). Cell exposure to cisplatin commonly results in G2/M phase arrest, which is induced and sustained by the transactivation of p53 genes as a result of exposure to cisplatin (Barr *et al*., 2013) while TPT results in S-phase and G2/M arrest (Tolis *et al*., 1999). The results of the cell cycle analysis reported in this chapter confirmed that exposure to cisplatin alone resulted in G2/M arrest in a higher percentage of the cell population in H460 and A549 cell lines (Figure 3.10 and Figure 311, respectively), whereas exposure to TPT alone resulted in S-phase and G2/M arrest in H460 and A549 cells (Figure 3.10B and Figure 311B, respectively). This finding is in agreement with previous data on increased proportions of NSCLC cells in S and G2/M phases after exposure to topotecan (Tolis *et al,* 1999).

Interestingly, after combination treatment, there was a significant population of A549 cells were arrested in G1 and S-phase, and H460 cells displayed S and G2/M arrests. The arrest of cells at G1 phase in A549 cells minimises the population of cells that will enter S and G2/M phase. This observation was in line with the results of previous studies, such as a study performed by Tolis *et al*. (1999) which revealed that an increased number of cells arrested in the G1 and S phase in A549 cells when TPT was combined with a DNA damage agent such

as gemcitabine. Nonetheless, the rationale for this observation is still unclear, as combinations are often still purely empirical. The effect of the combination of TPT and cisplatin on cell-cycle distribution of A549 indicates a cell-type-dependent effect. We found that in the A549 cell line p53 expression could be induced in a time- and concentration-dependent manner, irrespective of the cytotoxic compound used, indicating a role of p53 in controlling both checkpoints.

Apoptosis has been illustrated to have a significant role in cell death following cytotoxic drug treatment in a variety of cancer cells (Wang *et al*., 2016). The significant increase in Annexin V expression reported in this chapter confirmed a high a rate of apoptosis following treatment with cisplatin and TPT alone in H460 (Figure 3.15) and A549 cells (Figure 3.16). These results are in agreement with several studies performed by Tang *et al* (2013), Wang *et al* (2016) and (2015), who reported that cisplatin alone significantly induced apoptosis in A549 cells compared with untreated cells. In contrast, another study found that cisplatin had no effect on Annexin V expression in A549 cells, which suggests that the PRRX1 gene could reduce cell apoptosis (Zhu *et al.,* 2017). The significant increase in Annexin V expression reported in this section confirmed a high a rate of apoptosis following treatment with cisplatin and TPT alone in H460 and A549 cells, whereas the combination had an additional significant effect when compared to cisplatin alone. This apoptotic results confirmed the synergism effect seen on H460 cells and the infra additive effect seen on A549 cells in this chapter that resulted from the DNA damage reported in section 3.3.5.

Chapter 4 : In *Vitro* Antitumor Evaluation of Cisplatin and TPT Effect as Radiosensitisers in Combination with External Beam Radiation (XBR)

3.1 Introduction

Radiotherapy is widely used as an effective option in treating approximately 50% of cancers (Baskar *et al*., 2012). However, radiation is associated with numerous toxicities to normal tissues in the beam path limiting its usage in clinical practice (Boeckman *et al*., 2005a). The combination of chemotherapy and radiation is the current standard of care for treatment of lung cancer (Parashar *et al.*, 2013). However, despite this intensive combination therapy, the survival rate of lung cancer is still poorly progressing (Liu *et al*., 2014).

The effect of radiosensitisation on the efficacy of chemotherapy coupled with the discovery of targeted forms of radiotherapy has been at the forefront of radiation therapy research. As a therapeutic strategy to overcome the current toxicities associated with cancer therapy, it has been reported by previous studies that sublethal doses of multiple chemotherapeutic agents in combination with radiation in various cancer cells can limit normal cell toxicity while enhancing sensitivity to cancer cells (Gelbard *et al.*, 2006).

Chemotherapy is expected to modify cancer cells response to radiation by altering and repairing the inherent cellular radiosensivity and function as a selective radiosensitiser targeting especially those resistant cells to radiation (Alcorn *et a*l., 2013). Hence, using agents directed against DNA repair pathways and pathways associated with tumour cell survival have the potential to enhance radiotherapy (Mairs and Boyd, 2011).

Therefore, the combination therapy of TPT and cisplatin with radiation as a triple therapy may enhance the overall therapeutic advantages due to the nature of TPT to be a radiosensitizer agent that can sensitize cancer cells to radiation and increase DNA damages by its inhibitory effects on topoisomerase enzyme (Eyvazzadeh *et al*., *2015*).

Marchesini *et al*. (1996) investigated the interaction between TPT and ionizing radiation on H460 lung cancer cells and concluded that a supra-additive cell kill following this combination therapy. Marchesini *et al*. (1996) observed that the radiosensitisation by TPT was related to a high level of topoisomerase I in H460 cells and its role as an enzyme in the DNA repair process of radiation damage.

As an attempt to understand the molecular basis in which cisplatin induce radiosensitisation, some previous studies concluded that the combination of ionizing radiation and cisplatin provides a clear synergetic effect in cancer cells proficient in non-homologous end joining (NHEJ) catalysed repair of DNA DSB and revealed that a site-specific cisplatin-DNA lesion results in complete abrogation of NHEJ catalysed repair of the DSB (Boeckman *et al*., 2005a). In addition, Dong *et al.* (2017a) provided an explanation of the molecular mechanism of cisplatin radiosensitisation in which they explained that the cisplatin enhancement effects of DNA base damage contributes significantly to radiosensitisation process. According to Dong *et al*. (2017a), there are two major mechanisms explaining the synergy of cisplatin with radiation, firstly, the inhibition of the DNA damage repair induced by radiation and an increase in cellular DNA damage caused by additional immediate species created by the primary radiation, both of which occur when cisplatin reacts with the purine bases and

binds with DNA to form intrastrand cross-links. Furthermore, research conducted by Sears et al. (2016b) to investigate the mechanism of synergism between cisplatin and radiation in NSCLC and confirmed that inhibition of DDR sensor kinases caused the persistence of γ-H2Ax foci in treated cells is independent of kinase activation and suggest that the delayed repair of DSBs in NSCLC cells treated with cisplatin combined with radiation contributes to cisplatin radiosensitisation and that alterations of the DDR process by inhibition of specific DDR kinases.

However, research on radiosensitisation effects of cisplatin and TPT as a triple combination has been limited. Hence, in this chapter the radiosensitisation effect of cisplatin and topotecan with radiotherapy was assessed in human lung cancer cell lines H460 and A549 (NSCLC) With respect to cell kill and the mechanistic underpinning of any observed effects.

3.2 Aims

The primary aim of this chapter was to evaluate the radiosensitisation effect of cisplatin or topotecan when combined with XBR and then the effects of cisplatin and TPT in combination with XBR as a triple therapy by investigating the clonogenic cell of A549 and H460 cell lines exposed to these combinations.

The second aim was to determine the mechanism underpinning any observed enhanced tumour toxicity of this triple combination by analysis of the progression of cells through the cell cycle, and the DNA double stranded damage and repair, and to measure Annexin V expression following administration of the triple combination on H460 and A549 cell lines.

4.3 Results

4.3.1 Determining the cytotoxic effect of XBR alone on clonogenic survival of H460 and A549 cell lines

The effect of XBR alone on clonogenic survival (described in section 2.3) of H460 and A549 cells was firstly investigated to determine suitable dose range of XBR to be used in combination with TPT, and cisplatin in this chapter. Clonogenic survival data for XBR alone in a dose range of 0.5-5 Gy in both cell lines was therefore investigated (Figure 4.1). There was a dose-dependent relationship between the administered dose of XBR where the clonogenic cell survival in H460 and A549 cells reduced proportionally with increasing XBR dose indicating statistically significant differences when compared to untreated control. H460 cells were observed to be more sensitive than A549 cells.

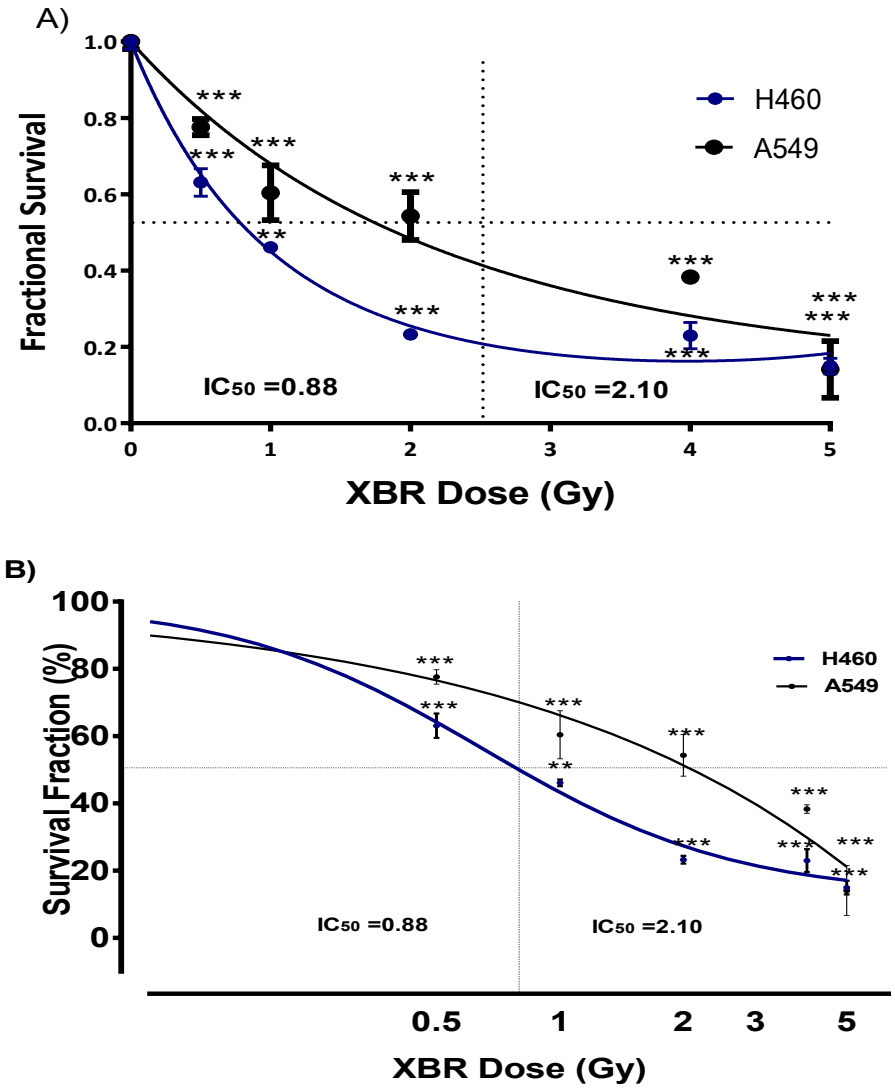

Figure 4.1: The effect of increasing doses of XBR alone on H460 and A549 survival fraction.

Figure demonstrates the effect of 24 hours treatment with XBR in dose range from 0-5 Gy against H460 and A549 survival fraction. Statistical analysis of the differences in clonogenic survival following exposure to each dose, compared with untreated control cells, was carried out using one-way ANOVAs with Bonferroni test with 95% C.I. Data points are averages of triplicate experiments and are shown ± STD. ** = $p < 0.01$; *** = $p < 0.001$.

H460 cells exhibited a dose-dependent reduction in survival fraction following exposure to XBR over 0.5-5 Gy dose range, at the lowest dose of 0.5 Gy there was a statistically significant inhibition in the cell survival fraction from 1 in the untreated control to 0.63 ± 0.036 (inhibition by 37%, $p < 0.001$). With the highest doses of 5 Gy, the congenic survival was completely inhibited by 100% *(*$p < 0.001$), indicating a statistically significant reduction when compared with the untreated control. The dose of XBR that killed 50% of the cell population (IC_{50}) on H460 cells was 0.88 Gy.

Similarly, A549 cells exhibited a dose-dependent reduction in survival fraction as H460 cells, however, A549 cells was shown to be less sensitive to the treatment than H460 cells with an IC_{50} observed at 2.10 Gy. Following exposure to XBR over the 0.5-5 Gy dose range, cell exposure to the highest dose of 5 Gy resulted in a reduction in congenic survival by 89% from 1 in untreated control to 0.14 ± 0.045 indicating a statistically significant *(*$p < 0.001$) reduction when compared to untreated control. The dose of XBR that killed 50% of the cell population (IC_{50}) on A549 cells was 2.10 Gy.

These results indicate that both H460 and A549 cell lines are sensitive to XBR alone with different levels of sensitivities. Based on the effect of XBR alone in H460 and A549 cell lines, the XBR dose of 1 - 2 Gy was used for subsequent combination studies in this chapter to determine the radiosinsitisation effect of cisplatin and TPT when combined with XBR.

4.3.2 The radiosensitisation efficacy of cisplatin or TPT in combination with XBR against H460 cell lines by using clonogenic (cell survival) assays

To assess the radiosensitisation potential of cisplatin and TPT on H460 cells, based on the results obtained in section 4.3.1 for the effects of XBR alone on the clonogenic survival (described in section 2.3) of H460 cells, XBR across the dose range 0.5-2 was employed in combination with cisplatin concentration range 62.5-250nM or TPT concentration range 10-30nM and the results are shown in Figure 4.2 for cisplatin in combination with XBR and in Figure 4.3 for TPT in combination with XBR. Two-way ANOVA was carried out to determine if the SF observed for cells treated with XBR in combination with cisplatin or TPT were significantly different from XBR alone group. H460 cells treated with XBR combined with either cisplatin or TPT demonstrated a statistically significant decrease in clonogenic cell survival compared to XBR exposure alone (Figure 4.2 and 4.3, respectively).

The clonogenic survival data of cisplatin or TPT from Figure 4.2(A) and 4.3(A) were fitted to the linear quadratic model (Figure 4.2 (C) and Figure 4.3 (C)) and values for α, β, IC_{50} and the DEF_{50} (dose enhancement factor at 50% clonogenic cell kill) were calculated (Figure 4.2(D) and Figure 4.3 (D)), respectively. DEF_{50} (described in section 2.13.2) indicates the ratio of effect observed following exposure of cells to radiation in combination with cisplatin or TPT to that of XBR alone at a given survival fraction. Therefore, if the effect of cisplatin or TPT in combination with XBR results in the same amount of clonogenic cell kill as XBR alone the DEF equals 1. A DEF > 1 indicates that cisplatin or TPT act as a

radiosensitisers and increase the effect compared to XBR alone, whilst a DEF < 1 suggests the cisplatin or TPT are acting as a radioprotector.

A)

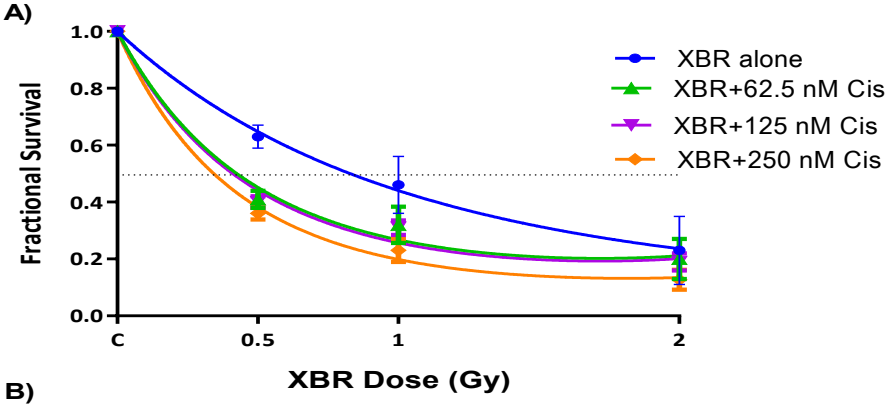

B)

Cisplatin Concentration (nM)	0.5 Gy	1Gy	2Gy
62.5	****	**	ns
125	****	**	ns
250	****	****	ns

C)

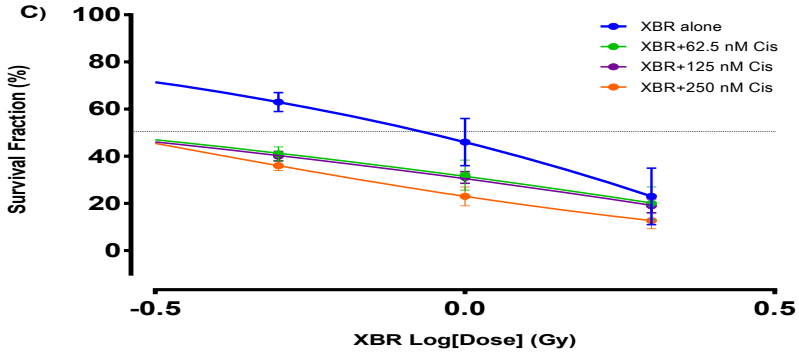

D)

	0nM	62.5nM	125nM	250nM
α (Gy^{-1})	0.9177	1.861	1.915	2.233
β (Gy^{-1})	-0.09795	-0.5416	-0.5569	-0.6154
R^2	0.9453	0.9705	0.9845	0.9916
IC_{50} (Gy)	0.8657	0.2454	0.2260	0.2550
DEF_{50}	1	3.52	3.83	3.39

Figure 4.2: The effect of increasing doses of cisplatin in combination with XBR on H460 survival fraction.

A) The effects of XBR alone in dose range 0.5-2 Gy or in combination with cisplatin across concentration 62.5-250 nM on H460 cells. **B).**Two-way ANOVA with Bonferroni test was used to statistically compare means of cisplatin in combination with XBR treatment group compared to XBR alone. **C)** Clonogenic survival data presented in (A) was fitted to the linear quadratic model using GraphPad Prism version 6.0.1. **D)** Values

calculated for the α and β coefficients and the IC_{50} and DEF50 for XBR in combination with each cisplatin concentration.

As shown in figure 4.2 following treatment of H460 cells with cisplatin 62.5-250 nM in combination with XBR in dose range 0.5-2 Gy, H460 cells demonstrated a statistically significant decrease in clonogenic cell survival at cisplatin and XBR combinations, compared to XBR exposure alone, with the exception of 2Gy XBR (Figure 4.2) . At 1 Gy XBR in combination with cisplatin across concentration range 62.5-250 nM, there was a statistically significant decrease in the survival fraction, compared to 1 Gy XBR exposure alone, the cell survival fractions were 0.32 ±0.064 ($p<0.01$), 0.31±0.025 ($p<0.01$), and 0.23±0.040 ($p<0.0001$) respectively, compared to 0.46 ±0.10. Whereas, H460 cells treated with 2 Gy XBR in combination with cisplatin across dose range 62.5-250nM demonstrated no statistically significant deference in the clonogenic survival fraction when compared to 2 Gy XBR exposure alone.

The DEF_{50} and IC_{50} values (Figure 4.2(D)) indicated that H460 cells treated with cisplatin in combination with XBR induced a concentration dependant increase in the effects of radiation. The IC_{50} values decreased from 0.86Gy for XBR alone to 0.24Gy, 0.22Gy and 0.250Gy for XBR in the presence of cisplatin at 62.5nM, 125nM and 250nM, respectively. The DEFs calculated at the 50% toxicity level (DEF_{50}) were 3.52, 3.83 and 3.39 for XBR in combination with cisplatin at 26.5nM, 125nM and 250nM, indicating that cisplatin as a radiosensitiser to radiation and had the potential to increase the effect of radiation compared to XBR alone when tested on H460 cells.

A)

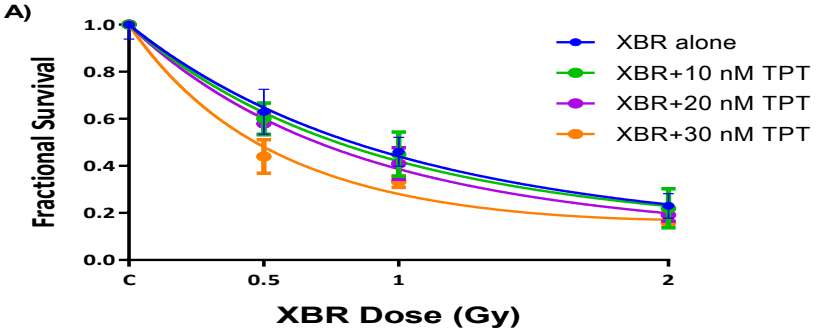

B)

TPT Concentration (nM)	0.5 Gy	1Gy	2Gy
10	ns	ns	ns
20	ns	ns	ns
30	****	*	*

C)

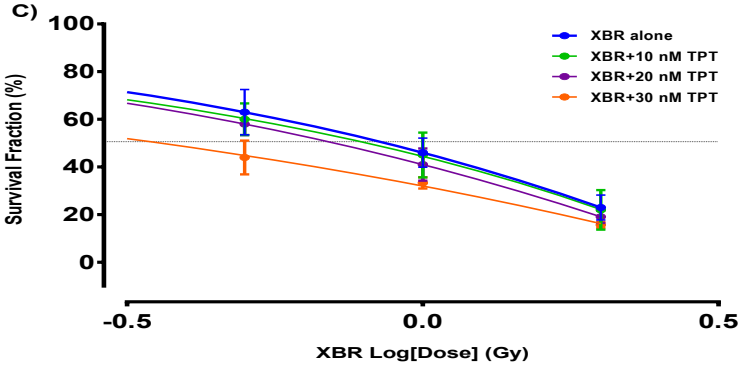

D)

	0nM	10nM	20nM	30nM
α (Gy^{-1})	0.9177	0.9995	1.092	1.659
β (Gy^{-1})	-0.09795	-0.1315	-0.1421	-0.3884
R^2	0.9587	0.9543	0.9830	0.9785
IC_{50} (Gy)	0.8657	0.8057	0.7097	0.3608
DEF_{50}	1	1.074	1.219	2.399

Figure 4.3: The effect of increasing doses of TPT in combination with XBR on H460 survival fraction.

A) The effects of XBR alone in dose range 0.5-2 Gy or in combination with TPT across concentration 10-30 nM on H460 cells. **B).**Two-way ANOVA with Bonferroni test was used to statistically compare means of TPT in combination with XBR treatment group compared to XBR alone. **C)** Clonogenic survival data presented in (A) was fitted to the linear quadratic model using GraphPad Prism version 6.0.1 **D)** values calculated for the α and β coefficients and the IC_{50} and DEF_{50} for XBR in combination with each TPT concentration.

As shown in figure 4.3 following treatment of H460 cells with TPT 10- 30 nM in combination XBR in dose range 0.5-2 Gy, A549 cells demonstrated a statistically significant decrease in clonogenic cell survival at only 30nM TPT combined with XBR, compared to XBR exposure alone. At 0.5 Gy XBR in combination with TPT across concentration 10-30nM, the cell survival fractions were 0.60 ±0.067 ($p>0.05$), 0.58±0.046 ($p>0.05$), and 0.44±0.071 ($p<0.0001$) respectively, compared to 0.46 ±0.10 (0.5Gy XBR alone). It was observed that H460 cells treated with 10 and 20nM in combination with 2 Gy XBR demonstrated no statistically significant deference in the clonogenic survival fraction when compared to all XBR alone doses.

The DEF_{50} and IC_{50} values (Figure 4.3(D)) indicated that A549 cells treated with TPT in combination with XBR induced a concentration dependant increase in the effects of radiation. The IC_{50} values decreased from 0.86Gy for XBR alone to 0.80Gy, 0.70Gy and 0.36Gy for XBR in the presence of cisplatin at 10, 20, and 30nM.The DEFs values were 1.07, 1.21 and 2.39 for XBR in combination with TPT at 10, 20 and 30nM respectively, indicating that TPT act as a radiosensitiser to radiation and had the potential to increase the effect of radiation compared to XBR alone when tested on H460 cells.

4.3.3 The radiosensitisation efficacy of cisplatin or TPT in combination with XBR against A549 cell lines by using clonogenic (cell survival) assays

To assess the radiosensitisation potential of cisplatin and TPT on A549 cells, based on the results obtained in section 4.3.2 for the effects of XBR alone on the clonogenic survival (described in section 2.3) of A549 cells, XBR across the dose range 0.5-2 was employed in combination with cisplatin concentration range 62.5-250nM or TPT concentration range 10-30nM and the results are shown in Figure 4.4 for cisplatin in combination with XBR and in Figure 4.5 for TPT in combination with XBR. Two-way ANOVA with Bonferroni post-hoc testing for multiple comparisons was carried out to determine if the clonogenic survival fractions observed for cells treated with XBR in combination with either cisplatin or TPT were significantly different from those observed following exposure to XBR alone. A549 cells treated with XBR combined with either cisplatin or TPT demonstrated a statistically significant decrease in clonogenic cell survival compared to XBR exposure alone (Figure 4.4 and 4.5, respectively).

The clonogenic survival data of cisplatin and TPT from Figure 4.4(A) and 4.5(A) were fitted to the linear quadratic model (Figure 4.4 (C) and Figure 4.5 (C)) and values for α, β, IC_{50} and the DEF_{50} were calculated (Figure 4.4(D) and Figure 4.5 (D)), respectively.

A)

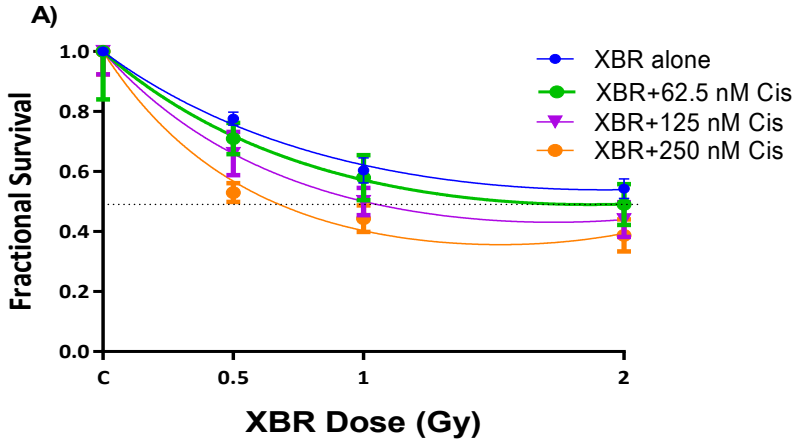

B)

Cisplatin Concentration (nM)	0.5 Gy	1Gy	2Gy
62.5	ns	ns	ns
125	ns	ns	ns
250	***	*	*

C)

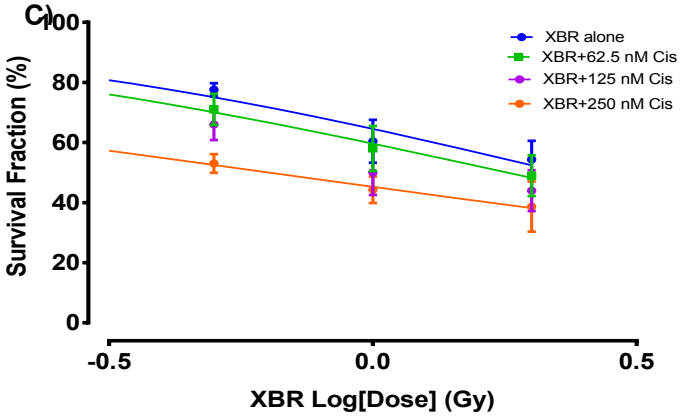

D)

	0nM	62.5nM	125nM	250nM
α (Gy^{-1})	0.6416	0.7105	0.9710	1.270
β (Gy^{-1})	-0.1665	-0.1895	-0.2796	-0.3791
R^2	0.9466	0.9623	0.9813	0.9881
IC_{50} (Gy)	2.282969	1.796801	0.800571	0.635916
DEF50	1	1.270574	2.851675	3.590046

Figure 4.4: The effect of increasing doses of cisplatin in combination with XBR on A549 survival fraction.

A) The effects of XBR alone in dose range 0.5-2 Gy or in combination with cisplatin across concentration 62.5-250 nM on A549 cells. **B)** Two-way ANOVA with Bonferroni test was used to statistically compare means of cisplatin in combination with XBR treatment group compared to XBR alone. **C)** Clonogenic survival data presented in (A) was fitted to the linear quadratic model using GraphPad Prism version 6.0.1.Tests were performed with 95% C.I. **D)** values calculated for the α and β coefficients and the IC_{50} and DEF_{50} for XBR in combination with each cisplatin concentration.

As shown in Figure 4.4 following treatment with cisplatin across concentration range 62.5-250 nM in combination with XBR in dose range 0.5-2 Gy, A549 cells demonstrated a statistically significant decrease in clonogenic cell survival at cisplatin concentration 250nM, compared to XBR exposure alone (Figure 4.4). At 2 Gy XBR combined with cisplatin 250nM, A549 cells survival fraction reduced to 0.38±0.053 ($p<0.05$), compared to 0.54 ±0.032 (2 Gy XBR alone). Whereas at 2Gy XBR combined with 62.5 or 125 nM cisplatin, survival fractions were 0.49± 0.068 ($p>0.05$) and 0.44± 0.058 ($p>0.05$) respectively, indicating no significant deference when compared to 2Gy XBR alone (0.54 ±0.032).

The DEF_{50} and IC_{50} values (Figure 4.4(D)) indicated that A549 cells treated with cisplatin in combination with XBR induced a concentration dependant increase in the effects of radiation. The IC_{50} values decreased from 2.28Gy XBR alone to 1.79Gy, 0.80Gy and 0.63Gy for XBR in the presence of cisplatin 62.5nM, 125nM and 250nM.The DEFs calculated at the 50% toxicity level (DEF_{50}) were 1.27, 2.85 and 3.5 for XBR in combination with cisplatin at 62.5nM, 125nM and 250nM, indicating that cisplatin act as a radiosensitiser to radiation and had the potential to increase the effect of radiation compared to XBR alone when tested on A549 cells.

A

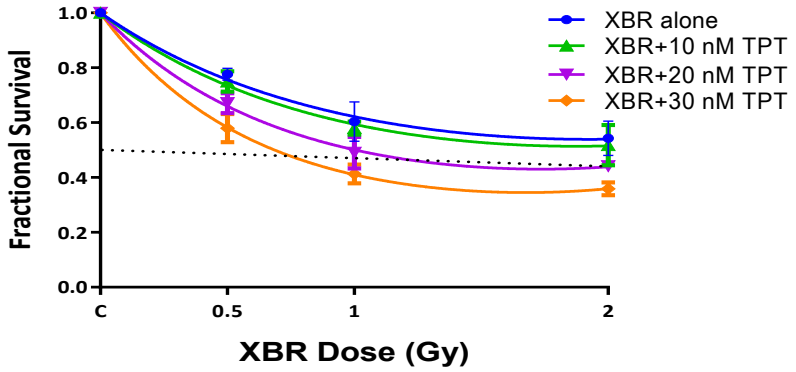

B

TPT Concentration (nM)	0.5 Gy	1Gy	2Gy
10	ns	ns	ns
20	**	**	*
30	****	****	****

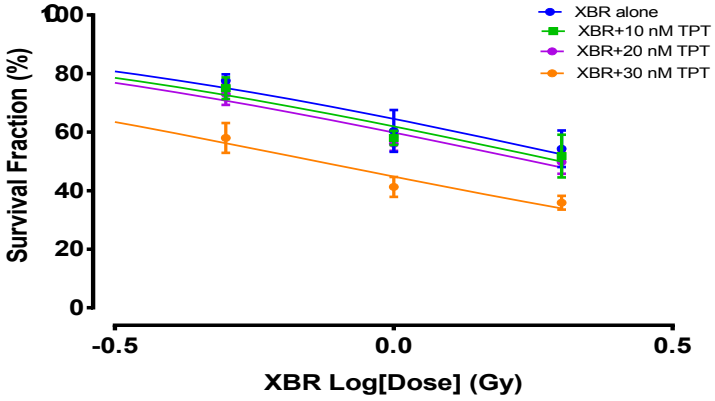

D

	0nM	10nM	20nM	30nM
	0.6416	1.052	1.780	2.382
	-0.1665	-0.3181	-0.6606	-0.8400
	0.9314	0.9483	0.9682	0.9806
	2.282969	1.992967	1.776233	0.730298
	1	1.145513	1.285287	3.126079

Figure 4.5: The effect of increasing doses of TPT in combination with XBR on A549 survival fraction.

A) The effects of XBR alone in dose range 0.5-2 Gy or in combination with TPT across concentration 10-30 nM on A549 cells. **B).**Two-way ANOVA with Bonferroni test was used to statistically compare means of TPT in combination with XBR treatment group compared to XBR alone. **C)** Clonogenic survival data presented in (A) was fitted to the linear quadratic model using GraphPad Prism version 6.0.1. **D)** Values calculated for the α and β coefficients and the IC_{50} and DEF_{50} for XBR in combination with each TPT concentration.

As shown in figure 4.5 following treatment of A549 cells with TPT 10, 20, and 30 nM in combination with XBR in dose range 0.5-2 Gy, A549 cells demonstrated a statistically significant decrease in clonogenic cell survival only at 30 and 20nM TPT combined with XBR, compared to XBR exposure alone. At 1 Gy XBR in combination with TPT across concentration 10-30nM, the cell survival fractions were 0.58±0.024 ($p>0.05$), 0.49±0.057 ($p<0.01$), and 0.41±0.034 ($p<0.0001$) respectively, compared to 0.60 ±0.071 at 1Gy XBR alone. It was observed that A549 cells treated with 10nM in combination with XBR demonstrated no statistically significant deference in the clonogenic survival fraction when compared to all XBR alone doses.

The DEF_{50} and IC_{50} values (Figure 4.5(D)) indicated that A549 cells treated with TPT in combination with XBR induced a concentration dependant increase in the effects of radiation. The IC_{50} values decreased from 2.286Gy for XBR alone to 1.99Gy, 1.77Gy and 0.73Gy for XBR in the presence of TPT at 10, 20, and 30nM.The DEFs calculated at the 50% toxicity level (DEF_{50}) were 1.14, 1.28 and 3.12 for XBR in combination with TPT at 10, 20 and 30nM, indicating that TPT act as a radiosensitiser to radiation and had the potential to increase the effect of radiation compared to XBR alone when tested on A549 cells.

4.3.4 Assessing the cytotoxic effects of cisplatin and TPT in combination with XBR against H460 cell lines by using clonogenic (cell survival) assays

To assess the cytotoxic effects of cisplatin and TPT in combination with XBR as a triple therapy on H460 cells, in this study cisplatin with a concentration range of 62.5-250 nM and TPT with a concentration range of 10-30 nM in combination with a fixed dose of 1 Gy XBR, were investigated to allow the combination index analyses in subsequent study. The 1 Gy XBR as a fixed dose was chosen in order to avoid the high level of toxicity as from the results described in section 4.3.2, the IC_{50} of either cisplatin or TPT with XBR alone (as a double therapy) indicating a dose dependent reduction relationship that may lead to a toxic effect, while our hypothesis is to use lower doses in combination to achieve similar cell kill achieved with each agent alone. There in this study the double therapy (cisplatin and TPT) survival data were compared with the triple therapy (Cisplatin:TPT+ 1 Gy XBR) on H460 cells and the results are shown in Figure 4.6. In this study, simultaneous administration of TPT and cisplatin with 1 Gy XBR for 24 hrs on H460 cells was employed as this schedule was the most effective in achieving greater cytotoxicity when tested in chapter 3. Two-way ANOVA with Bonferroni post-hoc testing for multiple comparisons was carried out to determine if the clonogenic survival fractions observed for cells treated with triple therapy were significantly different from those observed following exposure to double therapy (treated cells with only cisplatin and TPT). There was a significant decrease in the clonogenic survival of A549 cells following the triple therapy when compared to double therapy.

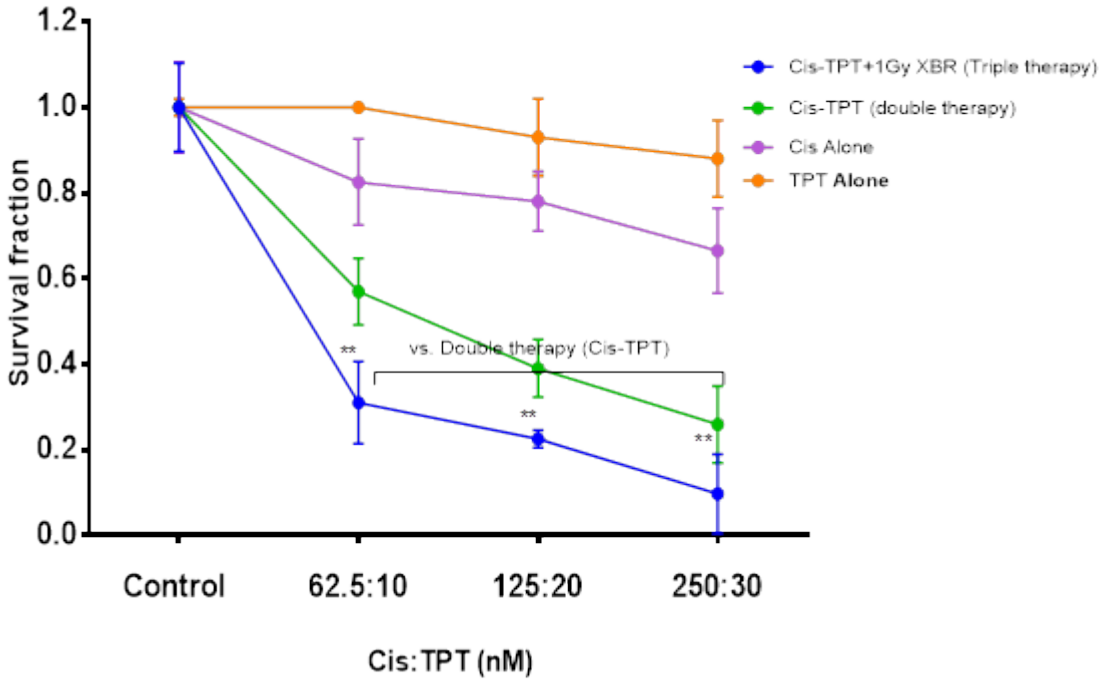

Figure 4.6: The effect of increasing doses of cisplatin and TPT in combination with XBR as triple therapy on H460 survival fraction.

The effects of cisplatin alone, TPT alone or cisplatin:TPT in combination with 1 Gy XBR as a triple therapy on H460 cells. Cells were dosed with cisplatin and TPT in the following quantities: 0:0, 62.5:10, 125:20, and 250:30 (nM).Two-way ANOVA with Bonferroni test was used to statistically compare means of treated samples with Cis:TPT treatment group compared to the triple therapy treatment group. Tests were performed with 95% C.I. ** = $p < 0.01$; *** = $p < 0.001$; **** = $p < 0.0001$.

Following the exposure to the triple therapy involving cisplatin, TPT, and XBR, as a triple therapy on H460 cells, cells showed a significant decrease in the survival fraction compared to the double therapy. At dose of 250 nM cisplatin and 30 nM TPT in combination with 1 Gy XBR, there was a statistically significant decrease in the congenic survival when compared to cisplatin and TPT (double therapy) treatment group, where the survival fraction decreased from 0.25± 0.09 ($p < 0.01$) in the double therapy group to 0.097 (± 0.093) in the triple therapy group. The results of this study demonstrated that using lower doses of triple cytotoxic agents achieved a greater or similar cytotoxicity than using a high dose of a single therapy alone.

4.3.4.1 Combination-index analysis of the interaction between cisplatin and TPT in combination with XBR on H460 cell lines

To analyse the radiosensitisation effect of TPT and cisplatin in combination with 1 Gy XBR on H460 cells, from the survival fraction results shown in Figure 4.6. The combination index (CI) values (described in section 3.1.1) were calculated and are shown in Figure 4.7. The CI values in Figure 4.7 correspond to the modes of action of the two agents, where CI < 1, CI = 1 and CI >1 indicate synergism, additivity and antagonism, respectively.

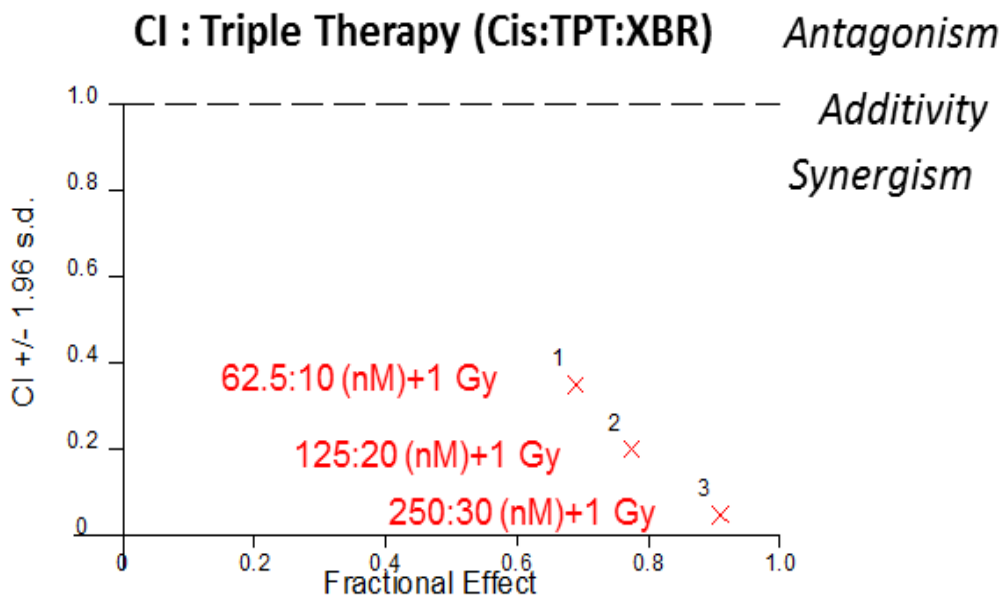

Figure 4.7: Combination index (C.I.) combined effect of cisplatin or TPT with XBR on clonogenic survival of H460 cells.

Clonogenic survival data were analysed using combination index analysis, where CI < 1, CI = 1 and CI > 1 indicated synergism, additivity and antagonism respectively. Each value represents the CI of three separate experiments.

Supra-additive effect was seen in all of the triple combination doses on H460 cells with CI values less than 0.5. With the lowest triple combination dose of 62.5 nM cisplatin and TPT 10 nM combined with 1 Gy XBR, the CI value was 0.35. In comparison with either CI values of double therapy, the triple therapy resulted in enhancing the additive (described in section 3.3.2.1) to be supra-additive effect indicating a significant interaction resulted in a supra additive effect on H460 cells.

4.3.5 Assessing the cytotoxic effects of cisplatin and TPT as a triple therapy with XBR against A549 cell lines by using clonogenic (cell survival) assays

To assess the cytotoxic effects of cisplatin and TPT in combination with XBR as a triple therapy on A549 cells, in this study cisplatin with a concentration range of 62.5-250 nM and TPT with a concentration range of 10-30 nM in combination with a fixed dose of 1 Gy XBR for 24 hours, were investigated to allow the combination index analyses in subsequent study. The 1 Gy XBR as a fixed dose was chosen in order to avoid the high level of toxicity as from the results described in section 4.3.3, the IC_{50} of either cisplatin or TPT with XBR alone (as a double therapy) indicating a dose dependent reduction relationship that may lead to a toxic effect. There in this study the double therapy (cisplatin and TPT) survival data were compared with the triple therapy (cisplatin and TPT plus 1 Gy XBR) on A549 cells and the results are shown in Figure 4.8. Two-way ANOVA with Bonferroni post-hoc testing for multiple comparisons was carried out to determine if the clonogenic survival fractions observed for cells treated with triple therapy were significantly different from those observed following exposure to double therapy (treated cells with only cisplatin and TPT). There was a significant decrease in the clonogenic survival of A549 cells following the triple therapy when compared to double therapy.

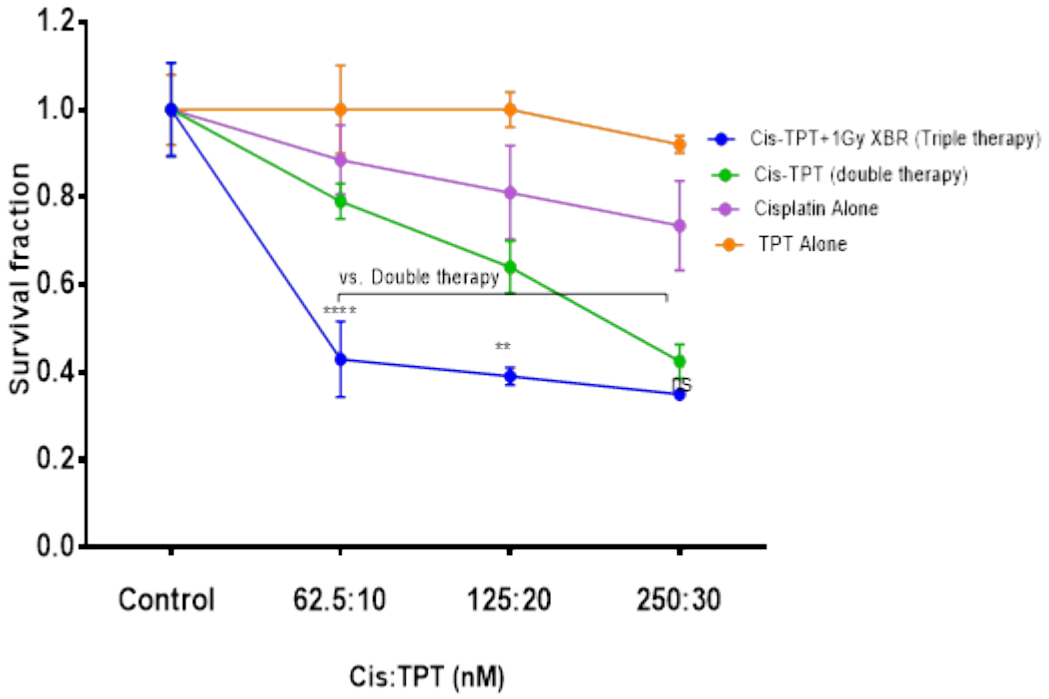

Figure 4.8: The effect of increasing doses of cisplatin and TPT in combination with XBR as triple therapy on A549 survival fraction.

The effects of cisplatin alone, TPT alone or cisplatin:TPT in combination with 1 Gy XBR as a triple therapy on A549 cells. Cells were dosed with cisplatin and TPT in the following quantities: 0:0, 62.5:10, 125:20, and 250:30 (nM).Two-way ANOVA with Bonferroni test was used to statistically compare means of treated samples with Cis:TPT treatment group compared to the triple therapy treatment group. Tests were performed with 95% C.I. ** = $p < 0.01$; *** = $p < 0.001$; **** = $p < 0.0001$.

Following the exposure to the triple therapy involving cisplatin, TPT, and XBR (Figure 4.8). A549 cells exhibited a significant decrease in the survival fraction when compared to double therapy. At dose of 250 nM cisplatin and 30 nM TPT in combination with 1 Gy XBR, there was no significant decrease in the survival when compared to cisplatin and TPT (double therapy) treatment group, wherease at dose of 125 nM cisplatin and 20 nM TPT in combination with 1 Gy XBR, there was statistically significant decrease in the survival when compared to cisplatin and TPT (double therapy) treatment group where survival fraction decreased from 0.640±0.08 ($p < 0.01$) in the double therapy group to 0.39 (± 0.02) in the triple therapy group. The results of this study demonstrated that using lower doses of triple cytotoxic agents achieved a greater or similar cytotoxicity than using a high dose of a single therapy.

4.3.5.1 Combination-index analysis of the interaction between cisplatin and TPT in combination with XBR on A549 cell lines

To analyse the effect of TPT or cisplatin in combination with 1 Gy XBR on A549 cells, from the survival fraction results of TPT and cisplatin shown in Figure 4.6, 4.7 and 4.8. The combination index (CI) values (described in section 3.1.1) were calculated and are shown in Figure 4.9. The CI values in Figure 4.9 correspond to the modes of action of the two agents, where CI < 1, CI = 1 and CI >1 indicate synergism, additivity and antagonism, respectively

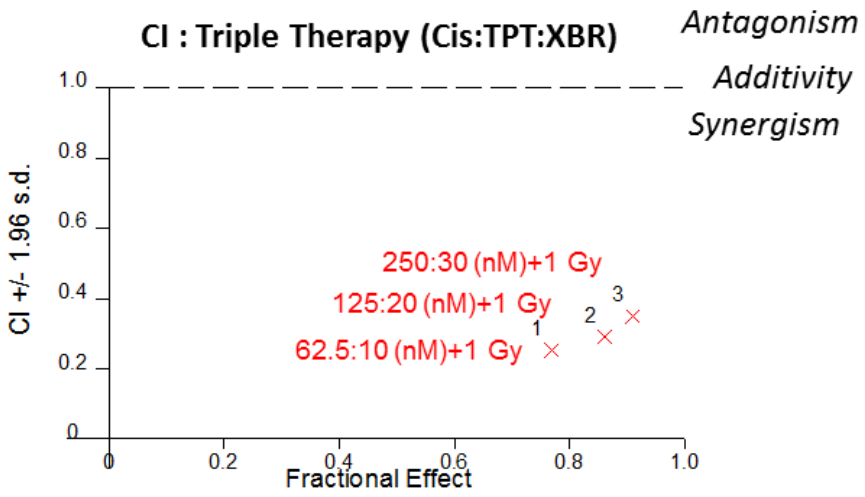

Figure 4.9: Combination index (C.I.) combined effect of cisplatin or TPT with XBR on clonogenic survival of A549 cells.

Clonogenic survival data were analysed using combination index analysis, where CI < 1, CI = 1 and CI > 1 indicated synergism, additivity and antagonism, respectively. Each value represents the CI of three separate experiments.

Supra-additive kill of A549 cells, after treatment with cisplatin and TPT in combination with 1 Gy XBR, was seen in all combination doses with CI value <0.4. With the lowest triple combination dose of 62.5 nM cisplatin and TPT 10 nM combined with 1 Gy XBR the CI value was 0.25. In comparison with CI value of double therapy, the triple therapy resulted in enhancing the infra-additive effect (described in section 3.3.3.2) to be supra-additive effect indicating a significant interaction resulted in a supra additive effect on A549 cells.

4.3.6 The efficacy of cisplatin and TPT as radiosensitisers on the induction and repair of DNA damage by measurement of γ-H2AX foci in H460 cells

The mean number of γ-H2AX foci/cell described (Section 2.4) was measured in H460 cells following incubation with 1 Gy XBR alone or in combination with two different doses of cisplatin (125-250 nM) and TPT (20-30 nM). The results are shown in Figure 4.10 at 2 and 24 hours after treatment. With XBR, the data shows a significant increase in γ-H2AX levels at 2 hrs post treatment compared to untreated control cells. Whereas, at 24 hrs γ-H2AX levels decreased significantly when compared to 2hrs time point indicating that DNA damage was being repaired at 24hrs following XBR alone . The results of cisplatin and TPT as a combination therapy were obtained from chapter 3 section 3.3.5 and compared to the triple therapy combination cisplatin in this study to determine the radiosensitisation. The triple therapy (cisplatin and TPT plus XBR) had the potential to maintain a high and significant number of γ-H2AX at 24hrs post treatment when compared to cells treated with XBR alone indicating a radiosinsitisation effect induced by cisplatin and TPT to XBR.

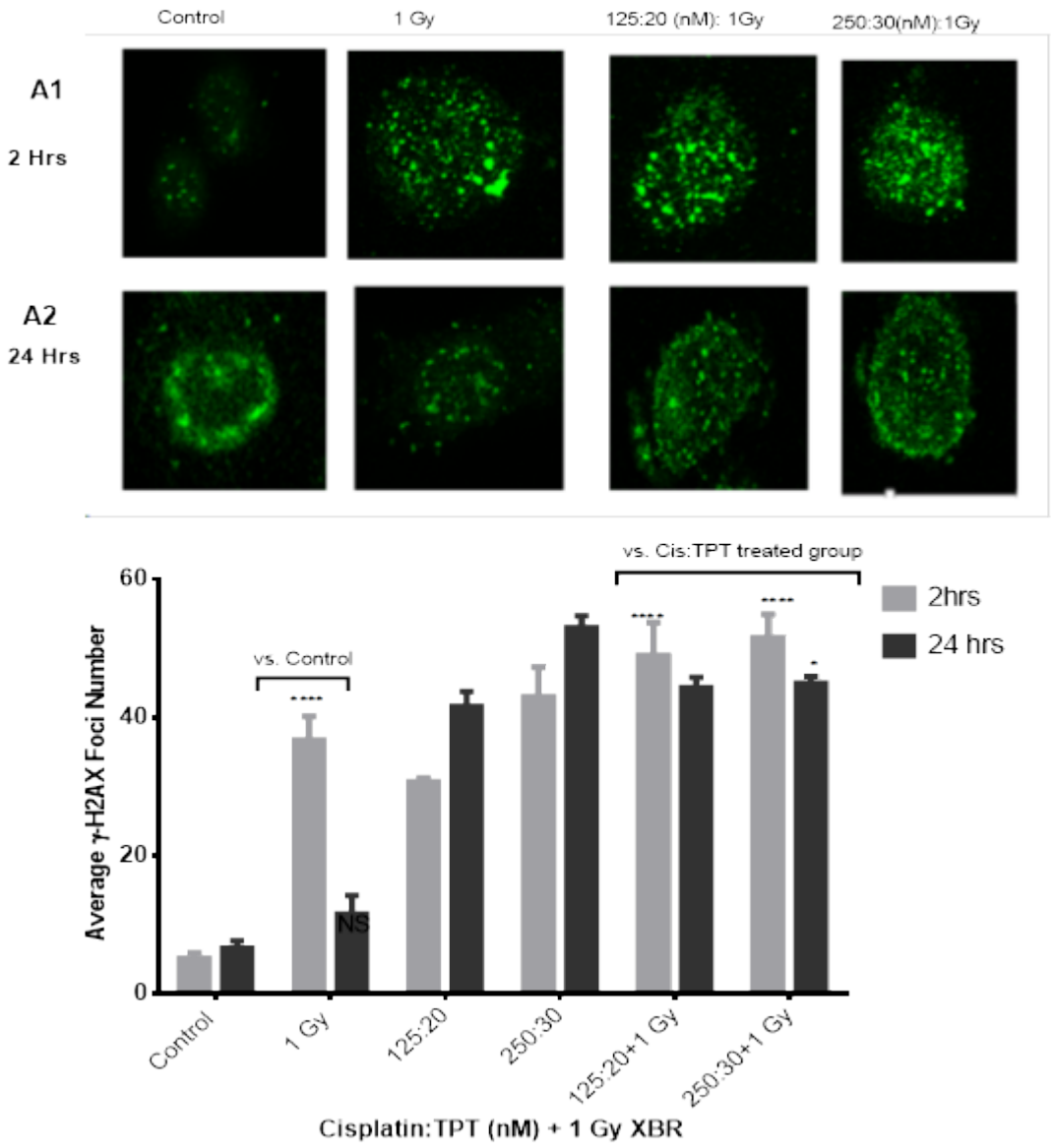

Figure 4.10: The effects of cisplatin and TPT in combination with XBR on H460 cells formation and residual of DNA-DSB.

The mean number of γ-H2AX foci/cell was assessed at 2 hours and 24 hours after treatment. Results presented are the mean number of γ-H2AX foci/cell (mean ± sd) of 3 independent experiments. Two-way ANOVA was used to determine if statistically significant changes in the number of γ-H2AX foci/cell resulted as an effect of cisplatin, TPT, and XBR in combination as triple therapy (compared with the effects of cisplatin and TPT as a double therapy). All tests were performed at a 95% C.I. * = $p < 0.05$; *** = $p < 0.001$; **** = $p < 0.0001$. Representative images of γ-H2AX foci in each treatment group at 2 hours (A-1) and 24 hours (A-2) are presented.

At 2 hours post treatment with 1 Gy XBR alone, on H460 cells, there was a statistically significant increase in number of γ-H2AX foci from 5.16 ± 0.76 (p < 0.0001) in the untreated controls to 36.7 ± 3.5 (Figure 4.10). However, at 24 hours, there was a statistically significant decrease the number of γ-H2AX foci to 11.57± 2.68 (p < 0.0001) when compared to cells exposed to 1Gy XBR at 2 hrs.

Following treatment with triple therapy of 1 Gy XBR in combination with two different doses of cisplatin and TPT (125:20 nM and 250:30 nM, respectively) at 2 hours, H460 cells presented a significant increase in number of γ-H2AX foci when compared to 1Gy XBR alone or double therapy treated cells. At 2hrs, with the lowest triple combination dose (125 nM cisplatin,20 nM TPT+ 1 Gy XBR) the number of γ-H2AX foci increased significantly to 49.0±4.75 (p < 0.0001) compared to cisplatin and TPT (double therapy) treated cells (43 ± 4.3). At 24 hours, with the same triple combination dose (125 nM cisplatin and 20nM TPT +1 Gy XBR) there was no additional significant increase in the number of γ-H2AX foci compared to cells treated with the double therapy (125 nM cisplatin + 20 nM TPT), this is not in line with the clonogenic data presented in this chapter as the clonogenic assay gives a clear picture of the effect due to the long duration of treatment incubation with cells (10 days), whereas H2AX has shorter incubation time. However, in comparison to treated cells with 1Gy XBR alone, at 24hrs the number of γ-H2AX foci was significantly increased from 11.57± 2.68 (1Gy XBR alone) to 44.33±1.52 (p < 0.0001) of treated cells with triple therapy. It was observed that the number of γ-H2AX foci at 24hrs with XBR alone decreased significantly, whereas after cisplatin and TPT treatment in combination with XBR had a significant effect on maintaining a high number of γ-H2AX foci, however at

24hrs with the highest triple dose (250:30:1) there was a significant decrease in γ-H2AX foci when compared to double therapy, indicating that the induced DNA damage at 2hrs is being repaired at 24hrs at high level of toxicity.

4.3.7 The efficacy of cisplatin and TPT as radiosensitisers on the induction and repair of DNA damage by measurement of γ-H2AX foci in A549 cells

In this study the formation and repair of DNA DSBs were investigated by measuring γ-H2AX foci numbers (described in section 2.4) in the A549 cell line after treatment with XBR to evaluate the radiosensitisation effects of cisplatin and TPT in combination. The mean number of γ-H2AX foci/cell was measured in A549 cells following incubation with cisplatin (125-250 nM) and TPT (20-30nM) in combination with 1 Gy XBR, and the results are shown in Figure 4.11 at 2 and 24 hours after treatment.. With XBR alone, the data shows a significant increase in γ-H2AX levels at 2 hrs post treatment compared to untreated control cells. Whereas, at 24 hrs γ-H2AX levels decreased significantly when compared to 2hrs time point indicating that DNA damage was being repaired at 24hrs following XBR alone . The results of cisplatin and TPT as a combination therapy were obtained from chapter 3 section 3.3.6 and compared to the triple therapy combination cisplatin in this study to determine the radiosensitisation. The triple therapy (cisplatin and TPT plus XBR) had no additional significant increase in the number of γ-H2AX at 24hrs post treatment when compared to cells treated with the double therapy, whereas a significant difference was observed in comparison to XBR.

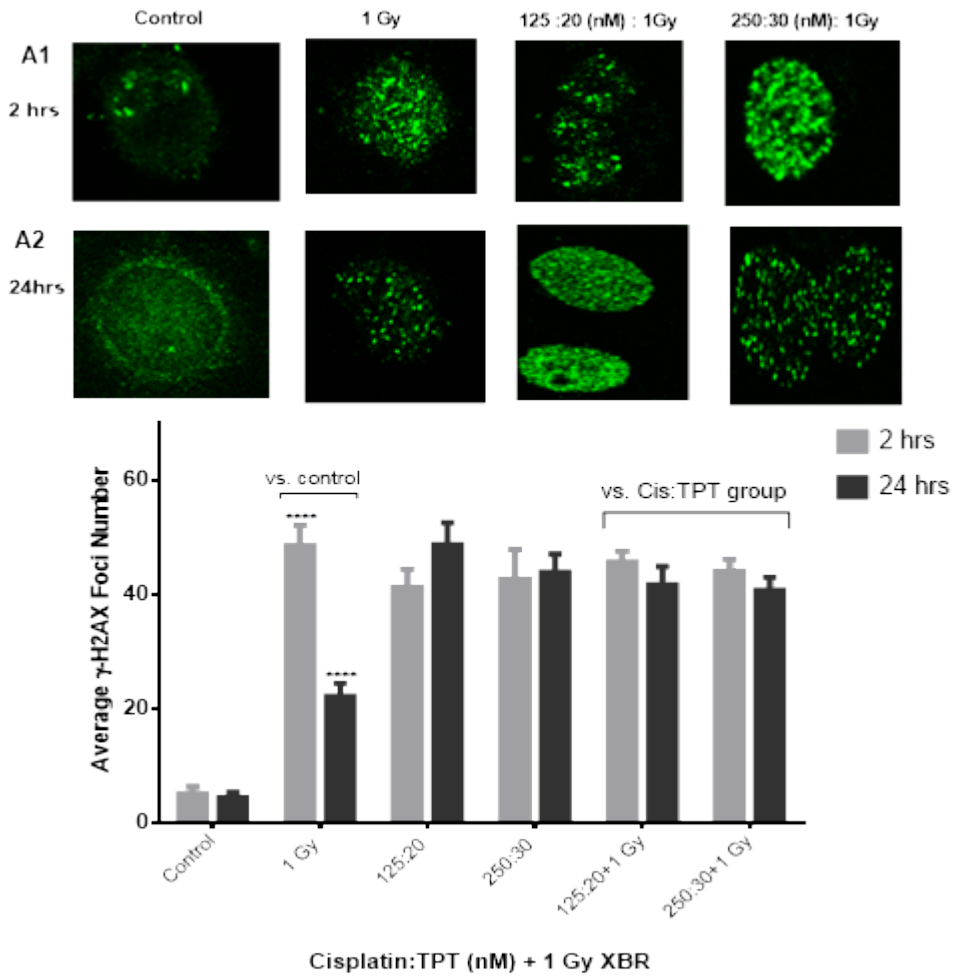

Figure 4.11: The effects of cisplatin and TPT in combination with XBR on A549 cells formation and residual of DNA-DSB.

The mean number of γ-H2AX foci/cell was assessed at 2 hours and 24 hours after treatment. Results presented are the mean number of γ-H2AX foci/cell (mean ± sd) of 3 independent experiments. Two-way ANOVA was used to determine if statistically significant changes in the number of γ-H2AX foci/cell resulted as an effect of cisplatin, TPT, and XBR in combination as triple therapy (compared with the effects of cisplatin and TPT as a double therapy). All tests were performed at a 95% C.I. * = $p < 0.05$; *** = $p < 0.001$; **** = $p < 0.0001$. Representative images of γ-H2AX foci in each treatment group at 2 hours (A-1) and 24 hours (A-2) are presented.

Based on the effect of 1 Gy XBR alone at 2 hrs post treatment on A549 cells, there was a statistically significant increase in the mean number of γ-H2AX foci, from 5 foci/cell ± 1.32 in untreated controls to 48.4 foci/cell ± 3.5 *(p* < 0.0001). Whereas, at 24 hours compared with 2 hours treatment, the number of γ-H2AX foci decreased significantly to 22.1 foci/cell ± 2.3 but still significantly higher than untreated controls *(p* < 0.001).

In contrast, there was no additional significant difference in the number of γ-H2AX foci/cell induced by 1 Gy XBR in combination with cisplatin and TPT (triple therapy) compared with cisplatin and TPT treated cells (double therapy).

4.3.8 Analysis of cell cycle progression following exposure to XBR alone and in combination with cisplatin and TPT

In this study, the effects of XBR alone or in combination with cisplatin and TPT were examined on H460 and A549 cells using fluorescence-activated cell sorting (FACS) analysis (described in section 2.5) to identify the radiosensitisation effect of cisplatin and TP involved in this interaction. XBR alone in dose range of 1-2 Gy was used, then a fixed dose of 1 Gy XBR was used with combination treatments of cisplatin and TPT. The effect of XBR alone was compared to untreated control cells whereas the effects of this triple therapy (XBR, cisplatin, and TPT) was compared to the effects of cisplatin and TPT as a combination therapy without XBR to determine the radiosensitisation. Two different doses of cisplatin and TPT across dose range of 125-250 nM and 20-30 nM, respectively were used in this study.

4.3.8.1 The efficacy of cisplatin and TPT in combination as radiosensitisers on cell cycle progression in H460 cells

The proportion of H460 cells in different phases of the cell cycle, after treatment with XBR alone in dose range 1-2 Gy, and in combination with cisplatin and TPT across dose range of 125-250 nM and 20-30 nM, respectively, was assessed by flow cytometry and data are shown in Figure 4.12.

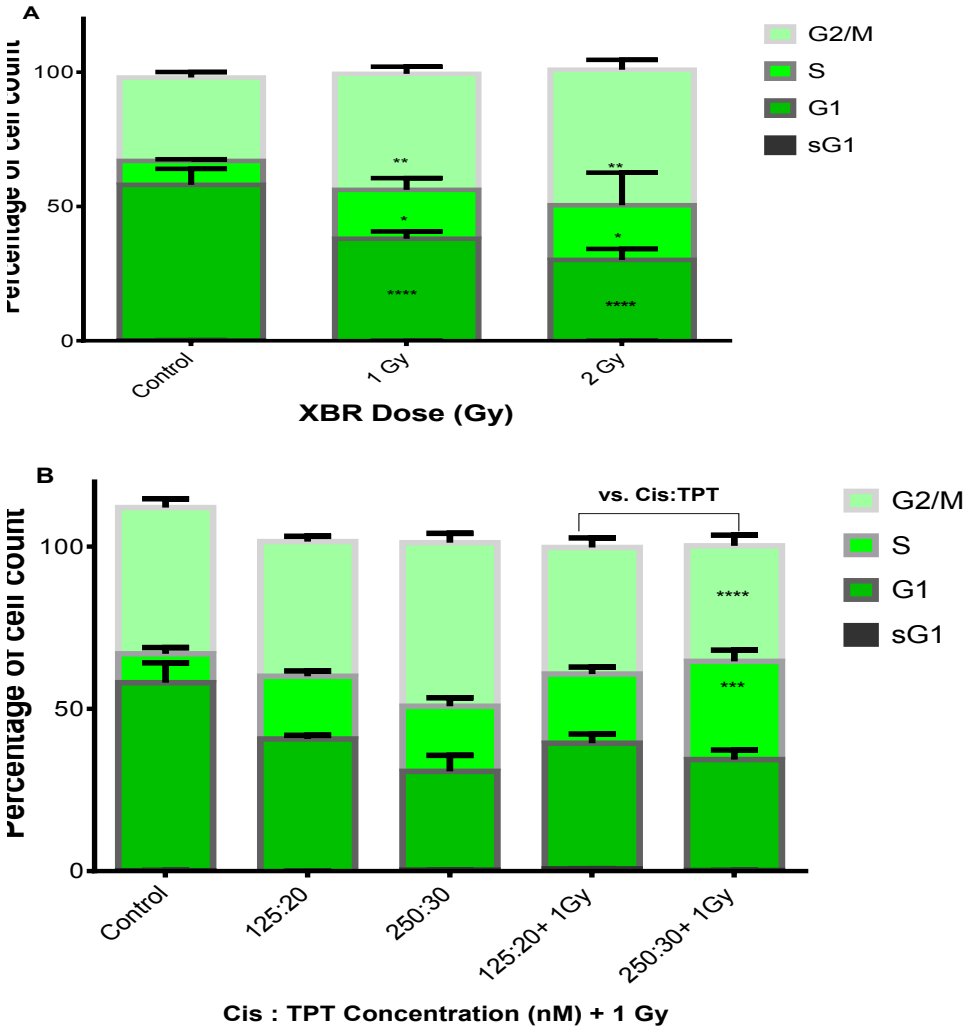

Figure 4.12 Effect of XBR alone and in combination with cisplatin and TPT as a triple therapy on cell cycle progression in H460 cell lines.

A) Effect of XBR alone across the dose range 1-2 Gy **(B)** cisplatin and TPT in combination with 1 Gy XBR. Cells were treated with cisplatin and TPT across dose range of 125-250 nM and 20-30 nM as a double therapy or in combination with 1 Gy. The cell cycle was then assessed by flow cytometry using propidium iodide (PI) for the determination of total DNA content. One-way or Two-way ANOVA was used to determine if there were statistically significant changes in the distribution of cells throughout the cell cycle compared with the either non-treated control group or double therapy treatment group. Each value represents the mean (± sd) of three separate experiments. * = $p < 0.05$, **= $p < 0.01$, *** = $p < 0.001$.

As shown in Figure 4.12, exposure of H460 cells to 1-2 Gy of XBR for 24 hours caused significant changes in cell cycle distribution of G0/G1, G2/M and S

phases. With the lowest dose of 1 Gy there was a statistically significant increase ($p < 0.001$) in the percentage of cells in G2/M phase from 31.1% (± 2.0) in the control cells to 43.2 % (± 2.64) in the treatment cells while the proportion of cells in S phase increased from 8.8% (± 1) in the control cells to 18.28% (±4.3, $p < 0.05$) in the treatment cells. However, it was observed that the highest dose of 2 Gy did not cause any additional significant changes in cell cycle distribution in comparison to 1 Gy. Therefore, 1 Gy of XBR as a single dose was used in the following combination study.

Exposure of H460 cells to triple therapy (XBR, cisplatin, and TPT) resulted in a statistically significant increase in the accumulation of cells within the S phase of the cell cycle whereas the accumulation of cells within G2/M phase significantly decreased when compared to the double combination therapy. With the highest dose (250 nM cisplatin and 30 nM TPT + 1 Gy XB) the percentage of cells within G2/M decreased to 35.6% (±3.2) in the triple therapy treated cells from 50.4% (±2.8, $p < 0.001$) in the double treatment treated cells while the proportion of cells in S phase increased significantly ($p < 0.01$) to 30.2% (± 3.4) from 20.0% (± 2.6) in the double therapy treated cells.

In summary, analysis of the progression of cells through the cell cycle demonstrated that the combination of XBR with cisplatin and TPT on H460 XBR did not result in a statistically significant increase in the proportion of cells which arrested in G2/M compared to XBR exposure alone or to double therapy (cisplatin combined with TPT). Whereas a statistically significant increase in the proportion of cells which arrested in S phases was demonstrated following exposure to triple

therapy (XBR, cisplatin and TPT) compared to XBR exposure alone or to double therapy (cisplatin combined with TPT).

4.3.8.2 The efficacy of cisplatin and TPT in combination as radiosensitisers on cell cycle progression in A549 cells

The proportion of A549 cells in different phases of the cell cycle (described in section 2.5), after treatment with XBR alone in dose range 1-2 Gy, and in combination with cisplatin and TPT as a double therapy across dose range of 125-250 nM and 20-30 nM, respectively, was assessed by flow cytometry and data are shown in Figure 4.13.

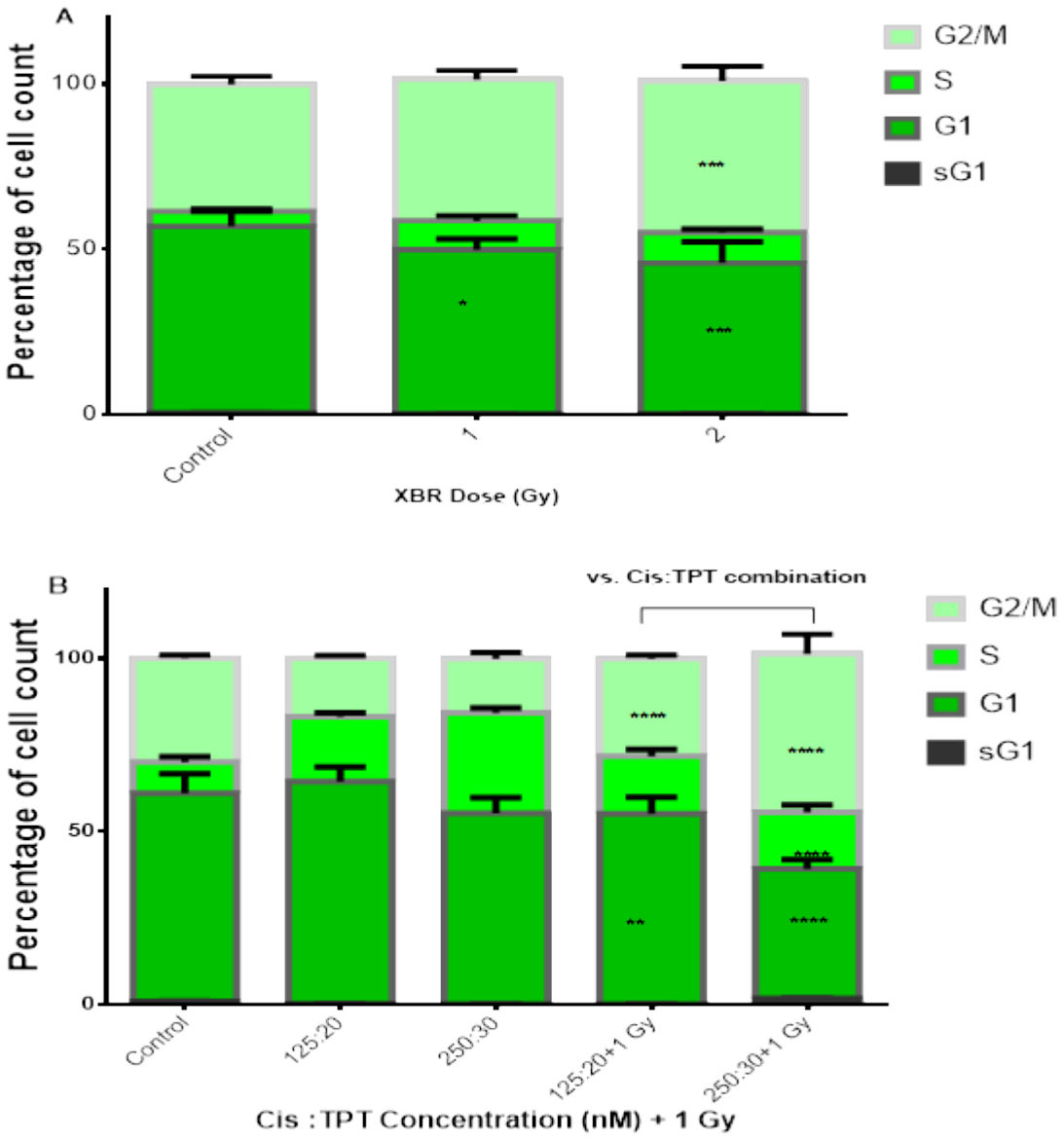

Figure 4.13: Effect of XBR alone and in combination with cisplatin and TPT as a double therapy on cell cycle progression in A549 cell lines.

(A) Effect of XBR alone across dose range 1-2 Gy. **(B)** Cisplatin and TPT in combination with 1 Gy XBR. Cells were treated with XBR 1 Gy, cisplatin and TPT across dose range of 125-250 nM and 20-30 nM as a triple therapy. The cell cycle was then assessed by flow cytometry using propidium iodide (PI) for the determination of total DNA content. One-way or Two-way ANOVA was used to determine if there were statistically significant changes in the distribution of cells throughout the cell cycle compared with the either non-treated control group or double therapy treatment group. Each value represents the mean (± sd) of three separate experiments. *** = $p < 0.001$.

As shown in Figure 4.13, exposure of A549 cells to 1-2 Gy of XBR for 24 hours caused significant changes in cell cycle distribution of G0/G1 and G2/M phases whereas S phase did not show any significant changes in the cell percentage accumulated during the treatment period. With the highest dose of 2 Gy there was a statistically significant increase ($p < 0.001$) in the percentage of cells in G2/M phase from 38.4% 2.3 (± 2.3) in the control cells to 45.8% (± 4.3) in the treatment cells while the proportion of cells in G1 phase decreased significantly from 56.4% to (± 4.6, $p < 0.001$) in the control cells to 45.5% (± 6.3, $p < 0.001$) in the treatment cells.

Exposure of A549 cells to triple therapy (XBR, cisplatin, and TPT) resulted in a statistically significant increase in the accumulation of cells within the G2/M and a significant decrease in G1 and S phases of the cell cycle when compared to the double combination therapy (cisplatin :TPT). With the highest dose (250 nM cisplatin and 30 nM TPT + 1 Gy XB) the percentage of cells within G2/M increased to 45.7% (±5.3) in the triple therapy treatment cells to 29.9% (±1.0, $p < 0.001$) in the double treatment cells while the proportion of cells in S and G1 phase decreased significantly to 16.4% and 37.4% (± 2.1 and ± 2.7, $p < 0.0001$, respectively) in the triple treatment cells

In summary, analysis of the progression of cells through the cell cycle demonstrated that the combination of XBR with cisplatin and TPT on A549 XBR result in a statistically significant increase in the proportion of cells which arrested in G2/M and a statistically significant decrease in the proportion of cells which arrested in G1 and S phases was demonstrated following exposure to triple

therapy (XBR, cisplatin and TPT) compared to XBR exposure alone or to double therapy (cisplatin combined with TPT).

4.3.7 The efficacy of XBR alone and in combination with cisplatin and TPT as radiosensitisers on Annexin V expression in H460 cells

For quantitative measurement of apoptosis as described (Section 2.6) and after treatment with 1 Gy XBR alone or in combination with cisplatin and TPT in dose range 125:20 -250:30 (nM) respectively, for 48 hours, followed by FACS analysis. The expression of Annexin V-negative cells in H460 cell lines, was assessed by flow cytometry and the results are shown in Figure 4.14. There was no additional significant increase in the percentage of apoptotic cells of H460 cells reated with triple therapy when compared to double therapy at the lowest dose, whereas there was a significant decrease in the percentage of apoptotic cells of H460 cells reated with triple therapy when compared to double therapy.

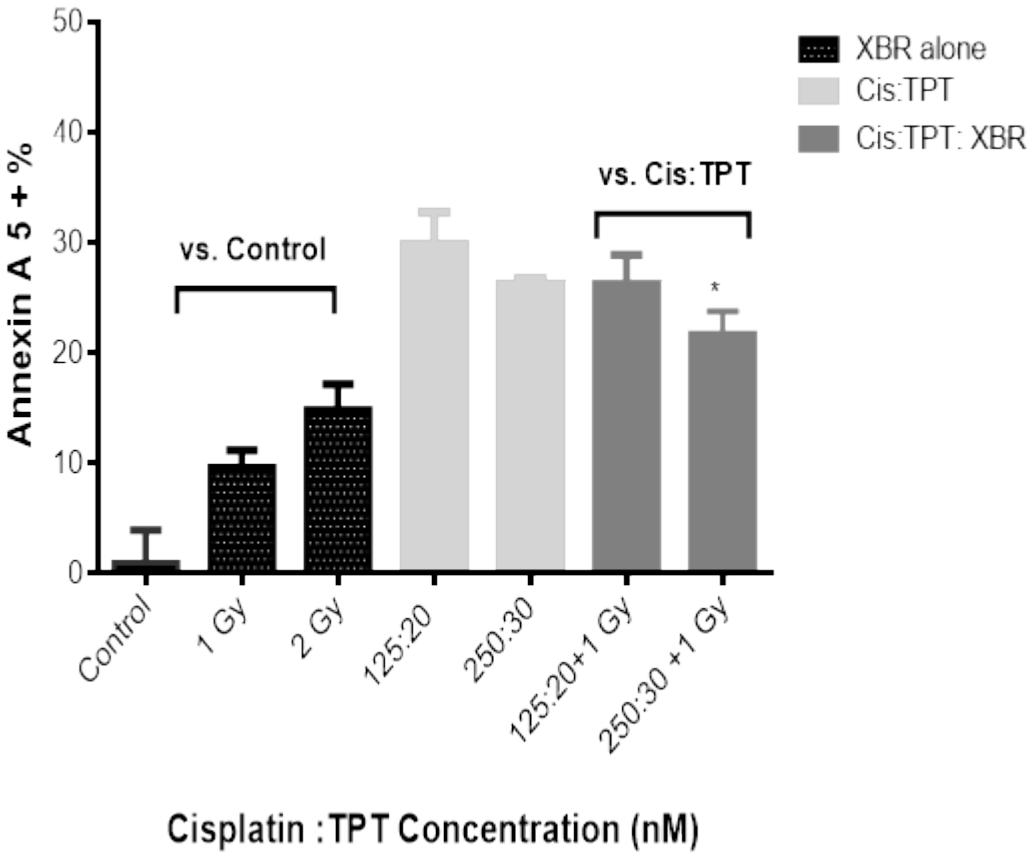

Figure 4.14: Cisplatin and TPT in combination with XBR induce Annexin V protein expression in H460.

Cells were treated with XBR alone with 1 or 2 Gy or cisplatin and TPT as a double therapy (data obtained from figure 3.12) or in combination with 1 Gy XBR as triple therapy for 48 h. One-way ANOVA or Two-way ANOVA was used to determine if XBR alone or triple therapy statistically significant in the Annexin 5 expression compared to either control group or double therapy. Each value represents the mean (± sd) of three separate experiments. Each value represents the mean (± sd) of three separate experiments.

Exposure of H460 cells to 1-2 Gy XBR alone for 48 hours caused no significant increases in Annexin V expression with either dose of 1 or Gy ($p > 0.05$) when compared to untreated control cells (Figure 4.14). After the triple combination treatments, there were no significant increases in the percentage of apoptotic cells in the triple treatment groups (XBR, cisplatin, and TPT) when compared with double treatment group at the lowest dose (cisplatin and TPT) ($p > 0.05$). Whereas the percentage of apoptotic cells in the triple treatment groups decreased significantly from 26.33 (0.68±) in the double group to 21.7 (3.5±) in triple group.

4.3.8 The efficacy of cisplatin and TPT in combination as radiosensitisers on Annexin V expression in A549 cells

The expression of Annexin V-negative cells as described (Section 2.6) in A549 cell line, after treatment with various concentrations of cisplatin alone, TPT alone, or in combination, was assessed by flow cytometry and results are shown in Figure 4.15. There was no additional significant increase in the percentage of apoptotic cells of A549 cells treated with triple therapy when compared to double therapy.

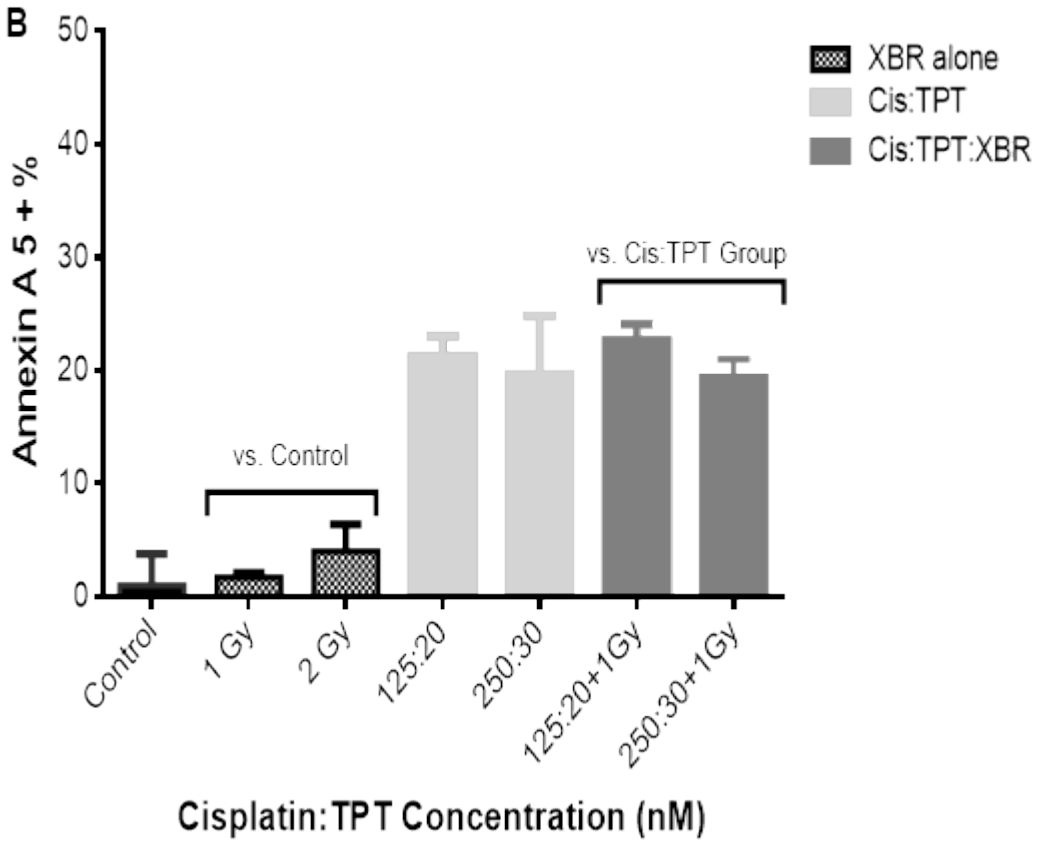

Figure 4.15: Cisplatin and TPT in combination with XBR induce Annexin V protein expression in A549.

Cells were treated with XBR alone with 1 or 2 Gy or cisplatin and TPT as a double therapy (data obtained from figure 3.13) or in combination with 1 Gy XBR as triple therapy for 48 h. One-way ANOVA or Two-way ANOVA was used to determine if XBR alone or triple therapy statistically significant in the Annexin 5 expression compared to either control group or double therapy. Each value represents the mean (± sd) of three separate experiments. Each value represents the mean (± sd) of three separate experiments.

Exposure of A549 cells to 1-2 Gy XBR alone for 48 hours caused no any significant increases in Annexin V expression (Figure 4.15) when compared with control cells ($p > 0.05$). After the triple combination treatment, there were no significant increases ($p > 0.05$) in the percentage of apoptotic cells when compared to double combination treatment group (cisplatin and TPT).

4.4 Discussion

The aim of this study was to establish the radiosensitisation potential of cisplatin and TPT to XBR. The data presented in this chapter demonstrated that the radiosensitisation induced by cisplatin and TPT was observed in both of the human lung cancer cell line, for instance with the lowest combination dose (62.5nM cisplatin or 10nM TPT) on H460 (Figure 4.2 and 4.3, respectively) the DEF50 were 3.52 and 1.07, respectively and the DEF50 with A549 (Figure 4.4 and 4.5) cells were 1.27 and 1.14, these indicate cisplatin and TPT act as radiosensitisers. This observed radiosensitisation effect of cisplatin to XBR is in agreement with the results of numerous studies, such as studies performed by Boeckman *et al*. (2005), Liu *et al.* (2014), and Zhang *et al*. (2009). The cisplatin induced radiosensitisation effect associated to an increase in cellular DNA damage caused by additional immediate species created by the primary radiation, both of which occur when cisplatin reacts with the purine bases and binds with DNA to form intrastrand cross-links (Dong *et al*., 2017a).

The induced TPT radiosensitisation effects seen in this chapter is in agreement with Eyvazzadeh *et al*. (2015) that found TPT can sensitize cancer cells to radiation by its inhibitory effects on topoisomerase I enzyme. Furthermore, the results in this chapter was in agreement with Marchesini *et al.* (1996) that found the radiosensitisation by TPT was related to a high level of topoisomerase I in H460 cells and its role as an enzyme in the DNA repair process of radiation damage. In this chapter, the triple therapy of cisplatin and TPT in combination with radiation treatment showed a supra additive effect compared to double treatment of cisplatin and TPT in both cell lines, indicating that using triple therapy

in low doses have the potential to achieve greater cell kill than with double or monotherapy.

Where radiosensitisation was observed, it was associated with a decrease in the resolution of γ-H2AX foci, but not necessarily with an increase in the number of DNA DSBs, compared to double therapy exposure with an exception of one dose (250:30:1) tested on H460 cells at 24hrs showed a significant decrease in γ-H2AX foci when compared to double therapy. In H460 (Figure 4.10) and A549 cells (Figure 4.11) at 2 hours post 1Gy irradiation, the number of γ-H2AX foci had decreased by 31.5%±3.5 and 45%±2.5 respectively, when compared to cells exposed to 1Gy XBR alone at 24hours, this indicating the repair of DNA damage after 24 hours of irradiation . However in the combination of cisplatin and TPT with XBR in H460 cells at the lowest combination dose, γ-H2AX foci/cell increased by 12.3%±4.5 at only 2hrs but at 24hrs there was no additional increase in the number of DNA DSBs. Whereas, at the highest treatment dose (250:30:1) at 24hrs there was a significant decrease in the number of H2AX foci/cell compared to douple therapy (from 53 to 45, $p < 0.05$) , indicating that the combination of cisplatin and TPT with XBR on H460 significantly increase the DNA DSBs only at the lowest used dose when compared to either the double therapy or XBR alone. In contrast, in A549 cells at either 2 or 24 hrs the triple combination therapy indicated that there was no additional significant increase resulted in the γ-H2AX foci/cell number when compared to the double therapy group. The results in this chapter was in agreement with research conducted by Sears et al. (2016b) to investigate the mechanism of synergism between cisplatin and radiation in NSCLC and confirmed that inhibition of DDR sensor kinases

caused the persistence of γ-H2Ax foci in treated cells is independent of kinase activation and suggest that the delayed repair of DSBs in NSCLC cells treated with cisplatin combined with radiation contributes to cisplatin radiosensitisation and that alterations of the DDR process by inhibition of specific DDR kinases. The results of the induction and repair of DNA damage reported in this chapter showed that the radiosensitising effect of cisplatin and TPT induced in H460 cells, but the radiosensitisation effect was not clear in A549 cells as there was no additional significant effects in the DNA damage of the triple therapy when compared to double therapy. This observation was in agreement with a report by Gupta et al. (2011) and Toulany et al. (2014) who demonstrated that the lack of cisplatin- mediated radiosensitising was related to cisplatin mediated ATM phosphorylation and Gupta *et al*. (2011) showed that cisplatin in combination with a 2-Gy XBR dose, improved the radiation efficacy of H460 cells, but not of A549 cells. p53, as a protector of the genome, is a factor of the genotoxic effects of cisplatin (Lin and Howell, 2006). The results of radiosensitisation effects in this chapter of cisplatin and TPT as a double therapy could led to p53 protein stabilization in A549. Therefore, the radiosensitising effect of cisplatin and TPT as a double therapy appears to be p53-independent, as a result cisplatin or TPT across the used doses in combination with XBR did not affect irradiation-triggered apoptosis of the radiosensitised A549 cells, cell survival after irradiation is apoptosis-independent (Brown and Wouters, 1999). Furthermore, the double combination in this study appears to mediate the phosphorylation of cytoplasmic ATM in A549 cells, but not in H460 cells. The observed synergistic radiosensitising effect of combined treatment with cisplatin and TPT in A549 cells

indicate that cisplatin could mediate ATM activity exerted a prosurvival effect. (Chaachouay *et al*., 2011). Cytoplasmic ATM signalling has the potential to activate autophagy, which is a dynamic response to this combination treatment (Alexander *et al*., 2010), and ATM can mediate the induction of autophagy after irradiation (Liang *et al*., 2013). Thus, as a results of this induced autophagy, A549 cells were protected against irradiation, where in some previous studies the targeting of autophagy showed to induce tumour cell radiosensitisation (Apel *et al.*, 2008, Chaachouay *et al.*, 2011). Toulany *et al.* (2014) showed that inhibition of autophagy via targeting ATM induced radiosensitisation in both A549 cells.

In addition, the cause of this infra additive, which was observed mainly with TPT during the combination index analysis in this chapter, could be resulted from the activation of chk1, phosphorylation of p53, or inhibition of cdc25A phosphatase that caused by a cross-talk between the two signalling pathways or the activation of the ATR pathway, the inhibition of cdc25A phosphatase activity could lead to the subsequent sensing of IR-induced DNA DSBs via ATM. ATM activation and chk2 phosphorylation would also result in p53 activation and cdc25A inhibition (Boeckman *et al.*, 2005b).

The results of the Annexin V in this chapter showed no significant effects being induced by XBR to cisplatin or TPT. This result was in agreement with previous studies of autophagy in H460 and A549 cells, provide strong and direct evidence that ionizing radiation may induce autophagic vacuoles leading to the autophagic death of A549 and H460 cells during combination treatment with ionizing irradiation *in vitro* (Groen *et al.*, 1995, Liu *et al*., 2014).

Chapter 5 . Analytical HPLC Method Development and Characterization Studies of Non-ionic Surfactant Vesicle (NIV) Formulations

5.1 Introduction

Non-targeted chemotherapy (traditional therapy) has a limited safety and efficacy due to inadequate drug delivery to the target cancer tumour or undesired severe toxic effects in healthy tissues (Wang *et al*., 2017). Both of these limitations can be avoided by encapsulating the chemotherapeutic drug inside nanocarriers (such as liquid crystals, metal–organic frameworks, and silica nanospheres) that are able to function as a targeted therapy, however a very promising method involved use of lipid vesicles (such as NIVs, simply known as niosomes) with defined and predictable physicochemical characteristics that provide maximum bioavailability and minimal side effects (Manaia *et al*., 2017, Andrade *et al*., 2015). Therefore, the rationale behind using NIVs as a vesicular delivery system is to create a carrier vehicle that is capable of maintaining the encapsulated dug and to accumulate in the target tissue to improve therapeutics outcomes and minimise toxicities of various drugs (Bulbake *et al*., 2017). The NIVs' ability, as a carrier vehicle, to achieve this target relies on the physicochemical characteristics of the NIVs and following preparation to assure their suitability and stability as a vesicular delivery system for *in vitro* and *in vivo* applications (Bulbake *et al*., 2017). These physicochemical characteristics such as particle size, particle size distribution, surface charge (zeta potential), and entrapment efficiency (Pandita and Sharma, 2013, Ruckmani and Sankar, 2010).

The optimal particles size is varied but should be limited up to 5 μm depending on endocytic pathways for nanoparticles to enter cells (Kou *et al*., 2013), whereas some research indicated a range of 50–1000 nm of NIVs would achieve optimal

delivery efficiency (Azhar Shekoufeh Bahari and Hamishehkar, 2016). The particle size has another important key in evaluating a colloidal formulation (such as NIVs) upon storage (Azhar Shekoufeh Bahari and Hamishehkar, 2016). Therefore, in this chapter the particle size characterization was studied to determine the stability of NIVs, for example, if there is a significant increase or decrease in the particle size over the time compared to day 0, this indicate the formulation developed an aggregation and has a stability issue.

Polydispersity index (PDI), also known as a heterogeneity index, is a parameter that defines the size range of the lipoic nanocarriers in which the non-uniformity of a size distribution of particles can be described (Bera, 2015, Danaei et al., 2018a). PDI values smaller than 0.05 are mainly seen with highly monodisperse standards, whereas PDI values bigger than 0.7 indicate that the formulation has a very broad particle size distribution (Stetefeld *et al*., 2016, Dong *et al.*, 2017b).

Moreover, a high charge (negative or positive) of nanoparticles indicates stability of a formulation that will resist aggregation of particles in the colloidal system, thus, NIV formulations with high charge are considered to be electrically stabilized and not tend to coagulate and able to prevent the aggregation and fusion of vesicles leading to a uniform and integrated vesicles with an improved entrapment efficiency of a formulation (Marasini *et al*., 2017, Vincent, 2012).

The non-ionic surfactants, such as alkyl or dialkyl polyglycerol ether class, act as an emulsifier to increase the stability of vesicles, resulting in improved entrapment efficiency of the drug encapsulated by niosomes. The cholesterol acts as a rigidity enhancer of the bilayer to form less permeable niosomes (Pandita and Sharma,

2013). Niosomes have a similar structure to liposomes but niosomes are more effective than liposomes as a drug carrier system in terms of factors such as cost, stability, entrapment efficiency, and bioavailability (Semalty *et al*., 2009, Bartelds *et al*., 2018).

In this chapter, the physicochemical properties such as particle size, surface charge, and entrapment efficiency post-preparation of empty NIVs, NIVs containing cisplatin (cis NIVs) and NIVs containing TPT (TPT NIVs) were studied to firstly determine their stability as a pulmonary drug delivery carrier and then to use these optimised NIVs for assessment of cell kill efficacy in comparison to free drug in chapter 6. In terms of stability, 28 days stability study only for TPT-NIVs was conducted. Cisplatin-NIVs stability was studied intensively by research colleague at SIPBS and results were published by (Alsaadi, 2011). Therefore, in this research, due to time limitation, the main focus was on studying the stability of TPT-NIVs. Venancio *et al*., 2017 conducted 30 days stability study evaluating formulation containing TPT loaded nanostructured lipid carriers for topical treatment of skin cancers in which physical characteristics such as size, charge, and EE% were studied. Venancio *et al*., 2017 found that TPT formulation was stable with no significant changes over the study period when compared to day 0.

Vesicular delivery systems (NIVs) can improve the delivery of cytotoxic drugs through improved encapsulation of the entrapped drug (Hua, 2015). Furthermore, nanoparticle technology has the potential to leverage the EPR effect to enhance the selective accumulation of cisplatin in tumour cells and to minimize toxicities (Guo *et al*., 2013). The main aim of this chapter was to determine whether the

designed NIV formulations encapsulating drugs can potentially achieve greater cytotoxicity effects than free drugs to improve cisplatin or TPT delivery in H460 and A549 cancer cells.

The zeta potential (ZP) has a significant role as an indicator of NIV formulation stability that considered to be colloidal structures where vesicles are dispersed in an aqueous medium (Bhattacharjee, 2016).

5.2 Aims

The primary aim was to study the physicochemical properties of NIVs containing cisplatin or TPT on the basis of entrapment efficiency, size and ZP as main properties in determining the post-preparation stability and conducting 28 days stability study for the TPT NIVs at two different temperature conditions (4°C and 25°C). Eventually, we aimed to determine whether NIVs loaded with cisplatin or TPT either alone or in combination have a greater cytotoxicity with possibly lower concentrations than free solutions of cisplatin or TPT when tested on H460 and A549 cells by using a clonogenic cell survival assay.

5.3 Results

5.3.1 HPLC analysis of cisplatin

HPLC method used for cisplatin quantification was described in section 2.7 and 2.7.1. This method was adopted from Lopez-Flores *et al.* (2006) and Alsaadi (2011) prior to use in this analytical study. In this method, validation characteristics such as linearity, accuracy, precision (repeatability and intermediate precision), were studied. These studied validation characteristics of cisplatin standard concentration range (1.56-150 µg/ml) were in line within the acceptance criteria set by ICH. This method showed a reliable and accurate detection of cisplatin (Appendix A.3). The chromatographic conditions used in the analysis of cisplatin are illustrated in Appendix A.1.

For detection of cisplatin by HPLC (described in section 2.7), internal standard NiCl2 (Nickel chloride) and chelating agent DDTC (diethyldithiocarbamate) were needed as cisplatin cannot be detected alone within the UV normal wave length. The addition of DDTC to cisplatin is to form a complex (Pt(DDTC)2) and with NiCl2 (Ni(DDTC)2) to be absorbed by UV detector. The method was validated and showed good separation of the analytes (DTTC, NiCl2, and cisplatin) and retention times were in the order of approximately 8, 9.8 and 12.9 min, for DDTC, Pt(DDTC)2 and Ni(DDTC)2, respectively (Appendix A.3).

The linearity of analytical procedure determines its ability to obtain test results which are directly proportional to the concentration of cisplatin in the sample. The

correlation coefficient, y-intercept, slope of the regression line and residual sum of squares were obtained over cisplatin standard concentration range (1.56-150 µg/ml) and showed a good linearity with R2 = 0.998 (Appendix A.4), the shown linearity result is consistent within the acceptance criteria set by ICH guidelines.

Chromatogram of a blank sample containing only DDTC and NiCl2 and with no cisplatin was needed to identify the cisplatin peak, the HPLC chromatogram showed excess DDTC and Ni(DDTC)2 eluting at approximately 8 and 12.9 min, respectively (Appendix A.5) with the absence of interference with the elution of cisplatin indicating no interference with the analysis of the targeted analyte (cisplatin).

Analytical variability, between different laboratories in one day or over different days, is defined as reproducibility. The intra-day (within-day variations) and inter-day (across-day variations) precision for all the standard concentrations were a percentage RSD of < 5% (Appendix A.6). ICH acceptance criteria for precision of minor components should have RSD of ± 5%.

The accuracy of an analytical procedure explain the closeness of agreement between the values. For the accuracy measurement, three concentrations (3.125, 25, and 150 µg/ml) in the calibration range were selected (Appendix A.6) as per ICH guideline recommendations and showed a percentage recovery between 94.6 and 97.8%. The acceptance criteria set by ICH indicates that the mean recovery should be within 90 to 110% for non-regulated products.

From the results of the validation characteristics studied in this chapter, it was documented that this HPLC method for cisplatin validation presented an evidence showing a good and acceptable level of assurance and consistently produce results that precisely reflect the quality characteristics of cisplatin.

5.3.1.1 HPLC analysis of cisplatin NIVs

For the quantification of the cisplatin NIV formulation, the same HPLC method for cisplatin quantification described in Sections 2.12 and 2.12.1, and the same chromatographic conditions that are illustrated in Section 5.1, were used. The chromatogram for the cisplatin NIV formulation showed good separation of the analytes where retention times were in the order of approximately 8, 11.19 and 14.9 min, for DDTC, Pt(DDTC)2 and Ni(DDTC)2, respectively (Figure 5.6). .

5.3.2 HPLC analysis of topotecan

The HPLC method for quantification of TPT was described in Section 2.8 and 2.8.1. This method was adapted from Saini *et al.* (2010) prior to use in this analytical study. In this method, validation characteristics such as accuracy, precision (repeatability and intermediate precision), detection limit, quantitation limit, and linearity, were studied aiming to present an evidence showing a high level of assurance that this method can consistently produce results that precisely reflect the quality characteristics of cisplatin. All these validation characteristics were in line with the acceptance criteria set by ICH guidelines. This method showed a reliable and accurate detection of TPT (Figure 5.1). The chromatographic conditions used in the analysis of TPT is illustrated in Table 5.1.

Table 5.1 Chromatographic conditions of the evaluated HPLC method for topotecan detection. Conditions include type of instrument and column, constituent of mobile phase, flow rate, wave lengths, and size of injected sample.

Instrument	Gynkotek® HPLC pump series P580 and autosampler model GINA 50 (Macclesfield, UK) operated by Chromeleon™ software version 6.30 SP3 Build 594, Dionex (Surrey, UK).
Column	Luna 3 µm C18(2) 100A – 150 x 4.60 mm 3 micron
Mobile phase	50:50 ACN:H2O, 0.1% TFA v/v/v
Flow rate	0.4 ml/min
Wave length	UV detector set at 227 nm
Sample size	20 µg

The method was validated and showed a good separation of the analyte with a clear and sharp peak at a retention time of 3.28 min (Figure 5.1).

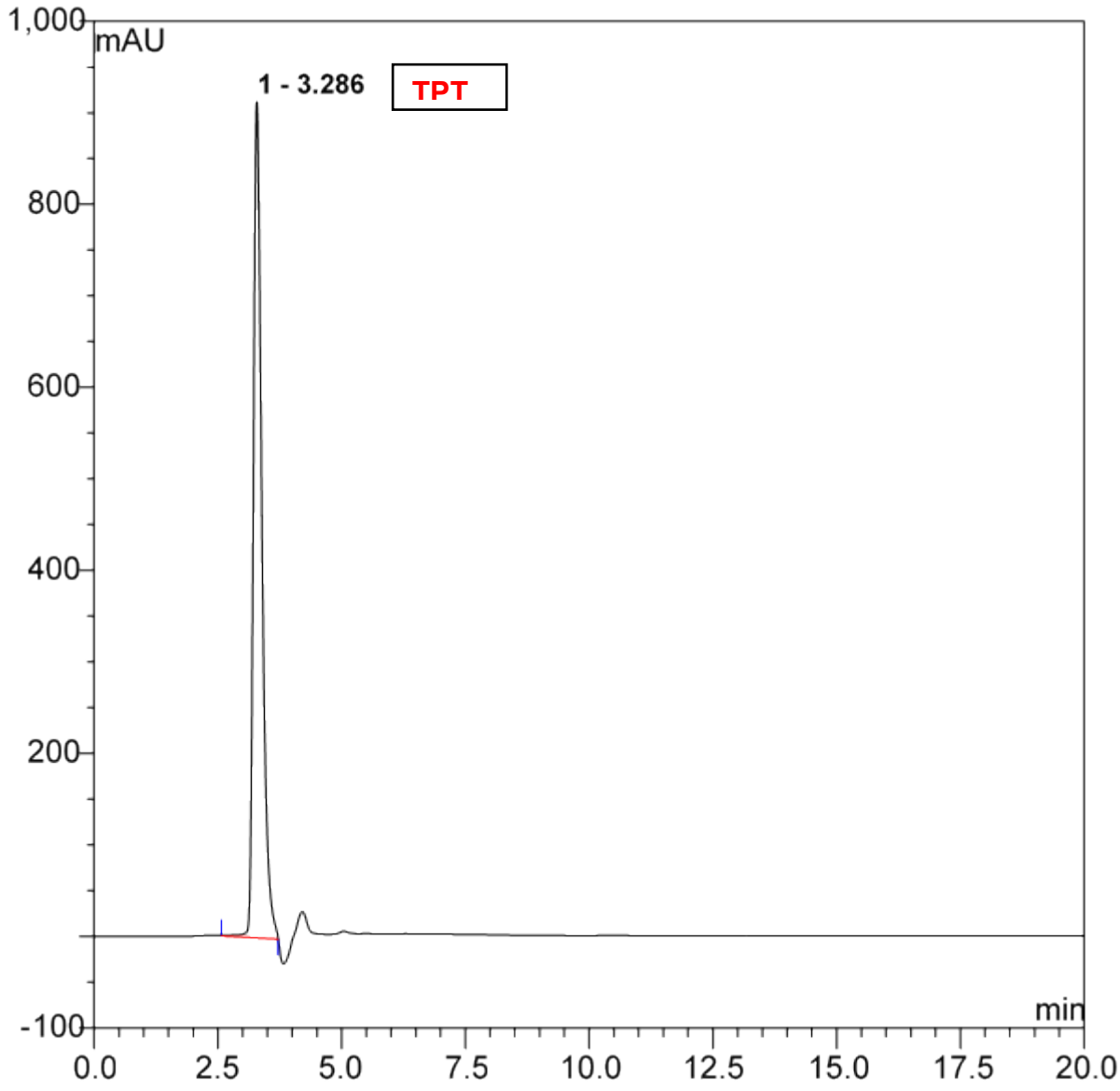

Figure 5.1. A chromatogram illustrating the separation and elution of topotecan at 3.28 min. TPT powder was dissolved in a solution of 5mg/ml of tartaric acid in distilled water and the sample was prepared from the mobile phase (ACN:H20 50:50, 0.1% TFA) containing 80 µg/ml topotecan, at a pH of 2.5 and a flow rate of 0.4 ml/min.

The linearity of analytical procedure determines its ability to obtain test results which are directly proportional to the concentration of cisplatin in the sample. The correlation coefficient, y-intercept, slope of the regression line and residual sum of squares were obtained over cisplatin standard concentration range (0-80 µg/ml) .The concentration range used showed good linearity with R2 = 0.999 (Figure 5.2).

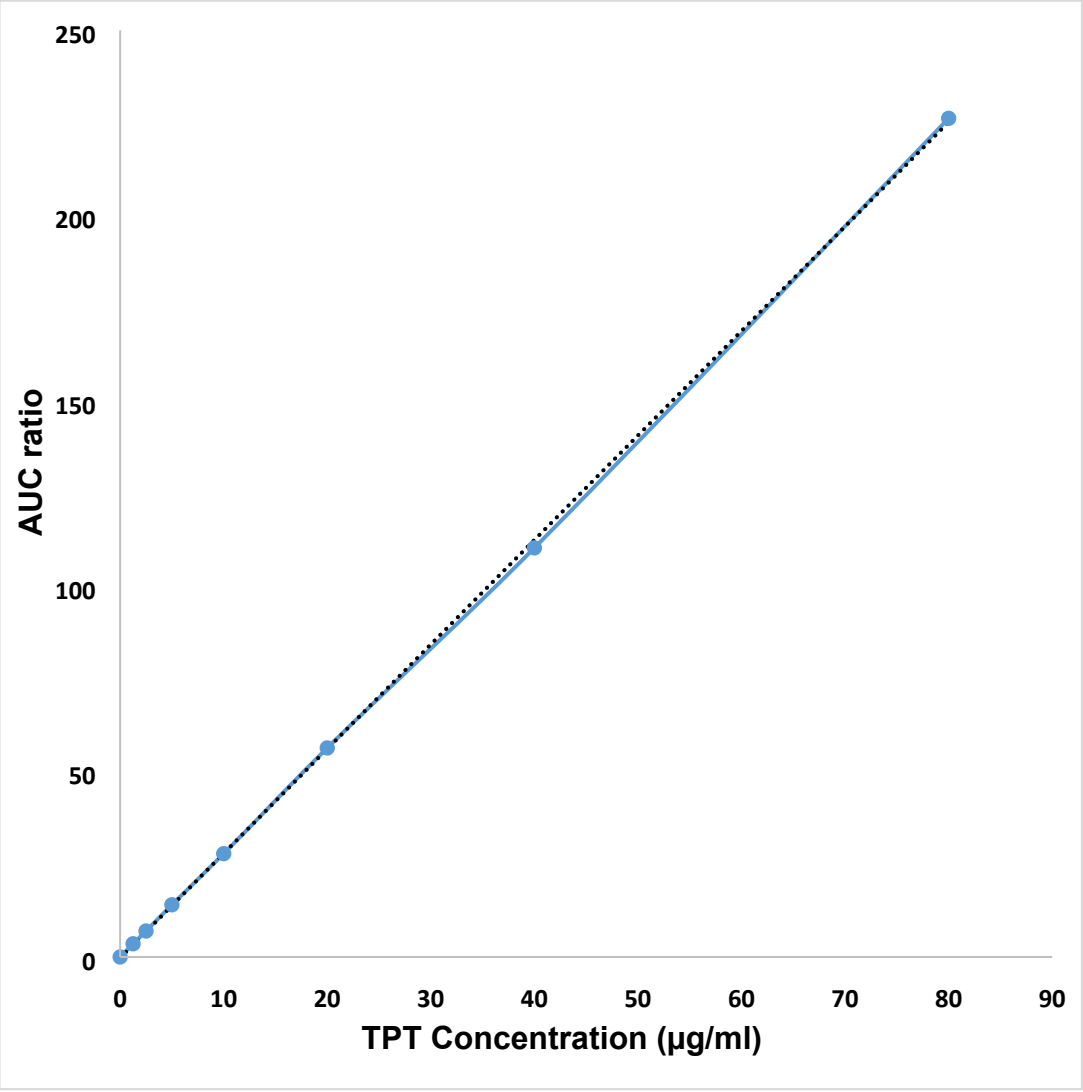

Figure 5.2 A typical calibration curve obtained for the quantification of topotecan. Concentrations used to establish the calibration curve were 0, 1.25, 2.5, 5, 10, 20, 40 and 80 µg/ml.

However, at the beginning of this analytical study, the peak occasionally had a retention time of 1.2 min at a flow rate of 1 ml/min that could make the quantification unreliable as this peak may not be that of topotecan (Figure 5.3). This led to the change in the current method where the flow rate was changed from 1 ml/min to 0.4 ml/min. This change in the flow rate resulted in shifting the HPLC peak of topotecan from 1.2 min to 3.28.

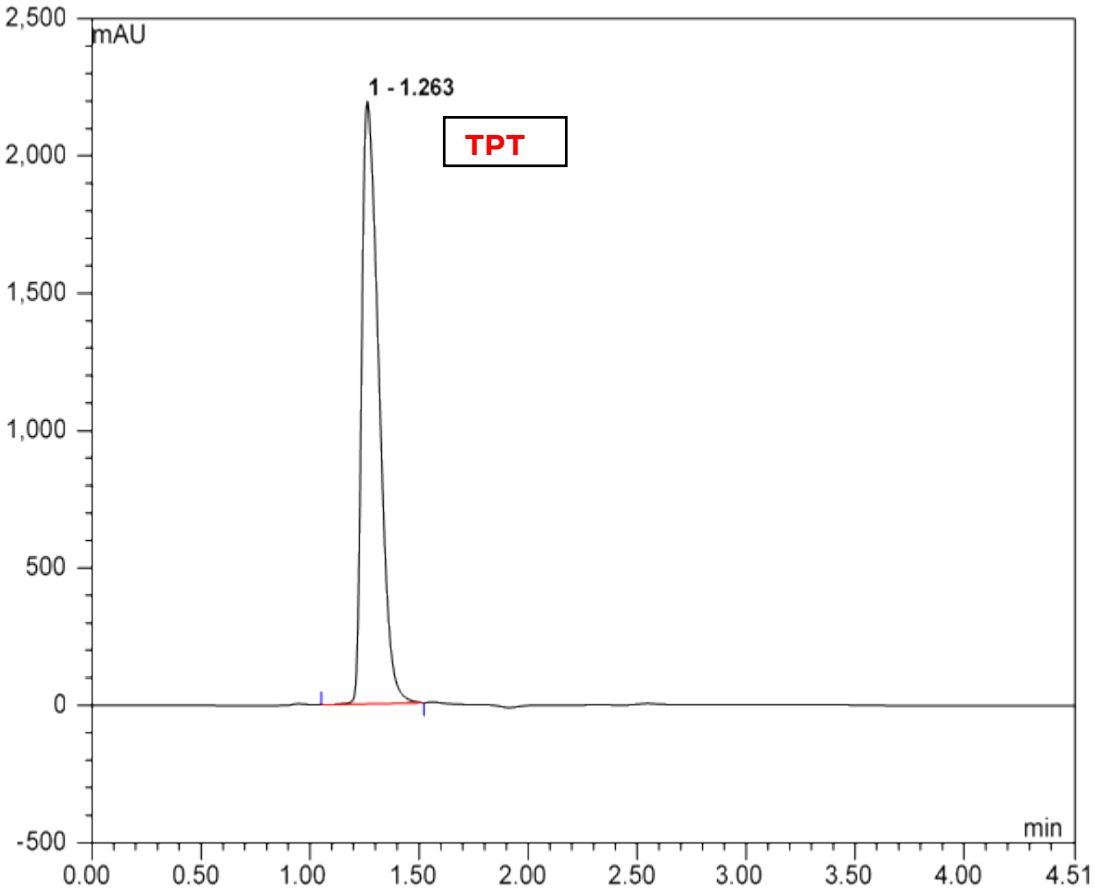

Figure 5.3 A chromatogram illustrating the separation and elution of topotecan at 1.26 min. TPT powder was dissolved in the mobile phase (ACN:H2O 50:50, 0.1% TFA).The sample was prepared from the mobile phase containing 80 µg/ml of TPT at a pH of 2.5 and a flow rate of 1 ml/min.

Moreover, the lactone ring of topotecan is responsible for its biological activity; the hydrolysis of this lactone ring would occur if the pH is more than 4. Due to this hydrolysis issue, the topotecan was analysed at a pH of 5.4 (Figure 5.4) to identify this hydrolysis reaction and to detect the degradation products resulting from this hydrolysis reaction.

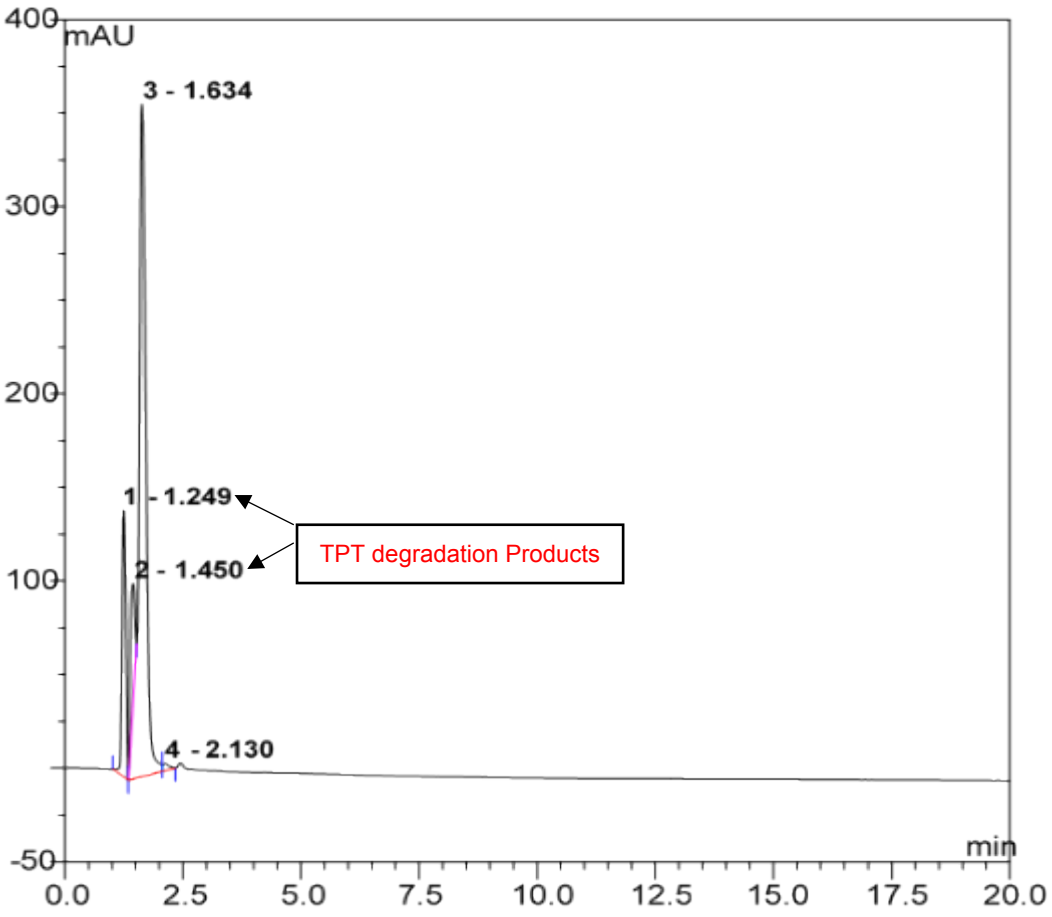

Figure 5.4 A chromatogram illustrating the separation and elution of topotecan with its degradation products at a pH of 5.4. The sample was prepared from the mobile phase (ACN: H20 50:50) without TFA and containing 2.5 µg/ml topotecan.

The peak characteristics of topotecan at different standards concentrations are illustrated in Table 5.2.

Table 5.2 Peak characteristics of TPT standard concentrations when elution was carried out at flow rate of 0.4 ml/min in triplicate.

Con. (µg/ml)	Mean retention time (min) ± SD	Mean AUC (mV*min) ± SD	Mean height (mV) ± SD	Asymmetry
1.25	3.23 (± 0.0125)	3.56 (± 0.40)	357.55 (± 1.78)	2.2
2.5	3.27 (± 0.0693)	7.00 (± 0.12)	413.86 (± 0.11)	1.9
5	3.23 (± 0.0017)	14.08 (± 0.72)	441.40 (± 3.62)	1.95
10	3.23 (± 0.00231)	27.87 (± 0.17)	532.14 (± 2.57)	1.35
20	3.24 (± 0.0017)	56.39 (± 0.86)	657.32 (± 4.93)	1.30
40	3.25 (± 0.0011)	110.37 (± 2.23)	831.87 (± 8.64)	1.15
80	3.26 (± 0.0005)	226.25 (± 1.93)	1078.85 (± 5.71)	1.35

Analytical variability, between different laboratories in one day or over different day, is defined as reproducibility. The intra-day (within-day variations) and inter-day (across-day variations) precision for all the standard concentrations were a percentage RSD of < 5% (Table 5.3). ICH acceptance criteria for precision of minor components should have RSD of ± 5%.

Table 5.3 The intraday and interday precision of the analysis of topotecan standard concentrations. Values are representative of % RSD. Two sets of standards were analysed in triplicate for intraday precision and three sets of standards were analysed in triplicate for interday precision. Values are representative of % RSD = (SD ×100%)/mean.

Concentration (µg/ml)	Intraday precision (% RSD) (n = 2)	Interday precision (% RSD) (n = 3)
40	1.49	1.69
20	3.21	2.0
10	0.29	0.617
5	1.06	1.52
2.5	0.87	2.02
1.25	1.06	0.853

The accuracy of an analytical procedure explain the closeness of agreement between the values. For the accuracy measurement, three concentrations (5, 20, and 80 µg/ml) in the calibration range were selected (Table 5.4) as per ICH guideline recommendations and showed a percentage recovery between 101.6 and 100.42%.

Table 5.4 Accuracy of HPLC method used in the detection of topotecan using three concentrations prepared in 35% w/v tartaric acid and analysed in triplicate.

Concentration (µg/ml)	Mean % recovery ± SD (n = 1)	Precision (% RSD)
5	101.6633 (± 5.107)	5.02
20	100.4567 (± 1.525)	1.51
80	100.42 (± 0.840)	0.83

The Low Limit of Detection (LLD) was 0.072 µg/mL and the Low Limit of Quantitation (LLQ) was 0.41 µg/ml.

From the results of the validation characteristics studied in this chapter, it was documented that this HPLC method for TPT validation presented an evidence showing a good and acceptable level of assurance and consistently produce results that precisely reflect the quality characteristics of TPT tested.

5.3.2.1 HPLC analysis of TPT NIVs

For the quantification of the topotecan NIV formulation, the same HPLC method for topotecan quantification (described in Sections 2.13 and 2.13.1) and the same chromatographic conditions (illustrated in Section 5.5) were used. The chromatogram for the topotecan NIV formulation showed good separation of the analyte where the retention time was at 3.2 min (Figure 5.5).

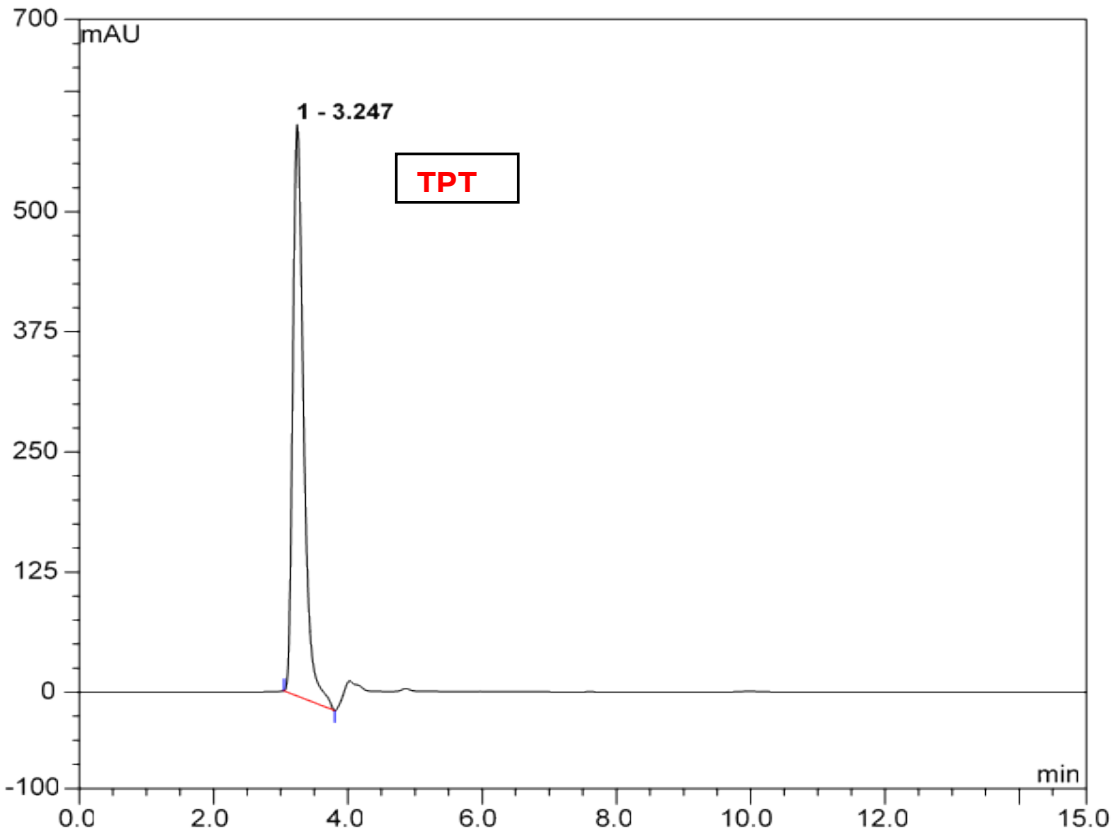

Figure 5.5 A chromatogram illustrating the separation and elution of topotecan NIV at 3.37 min on day 0 post preparation. TPT powder was dissolved in a solution of 5 mg/ml of tartaric acid in distilled water and the sample was prepared from the mobile phase (ACN:H20 50:50, 0.1% TFA) containing 80 µg/ml topotecan at a pH of 2.5 and at a flow rate of 0.4 ml/min.

5.3.3 Lipid analysis by HPLC

The method used in the analysis of lipid content was described (Section 2.9 and 2.9.1.). This method was developed and modified by Prof Alex Mullen and Dr Manal Alsaadi, (University of Strathclyde) and published by (Alsaadi et al., 2013). In this HPLC method, the ternary gradient elution consisted of the same mobile phase composition with a 15min run and a gradient flow rate at 1ml/min as shown (Table 5.5).

Table 5.5 Gradient elution sequence used in lipid analysis. In this analysis. 100% isohexane (A), 100% ethyl acetate (B) and a mixture of 60% propan-2-ol, 30% acetonitrile and 10% methanol, 142µl/100ml glacial acetic acid and 378µl/100ml triethylamine (C), were used.

Time (min)	**Solvent channel**		
	A	**B**	**C**
0	80	20	-
2	72	25	3
3	64	30	6
4	56	35	9
5	48	40	12
6	35	45	20
7	35	45	20
8	35	45	20
9	72	25	3
10	80	20	-
15	80	20	-

The analysis was carried out for surfactant, cholesterol and DCP. The lipids had clear separation (Figure 5.6) and a linear relationship for all three lipids in the concentration range 0.015-0.5mg/ml.

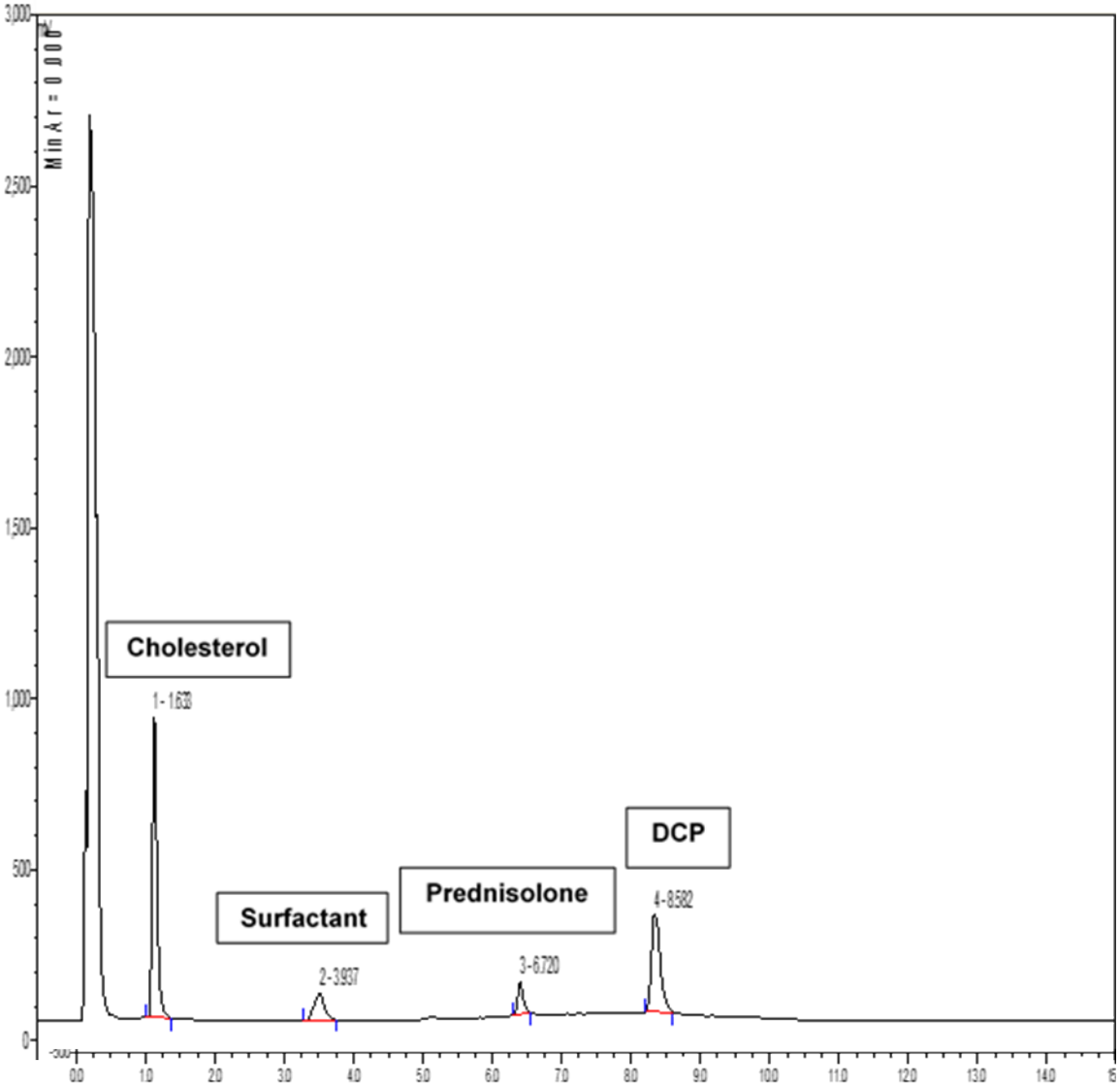

Figure 5.6 A chromatogram illustrating the separation and elution of cholesterol, surfactant and prednisolone and DCP at 2, 4, 7 and 9 min.

5.3.4 Determination of entrapment efficiency, size, ZP, and PDI values of empty NIVs, cisplatin NIVs and TPT NIVs

.

For the formulations of cisplatin NIVs and TPT NIVs, the size and ZP, and entrapment efficiency were measured as described in Sections 2.10.1.1 and 2.10.1.2, respectively. Size and ZP measurements for empty NIVs, cisplatin NIVs, and TPT NIVs were determined and are shown Sections 5.3.3.1, 5.3.3.2, and 5.3.3.3, respectively.

5.3.4.1 Empty NIVs

5 ml empty NIV formulations were prepared as described in Section 2.10.The formulations were characterised on the basis of entrapment efficiency, size and ZP on days 0, 4, 7 and 10 post preparation. The mean particle size, PDI, and ZP results are summarised in Table 5.6 and Figure 5.7.

Table 5.6 Corresponding particle size, PDI and ZP values of empty NIVs. Each point is representative of triplicate readings (n=3).

Days post preparation	Empty NIV ± SD		
	Mean Size (nm)	Mean PDI	Mean ZP
0	259.933 (± 3.052)	0.328 (± 0.019)	-73.766 (± 1.276)
4	259.255 (± 5.634)	0.400 (± 0.049)	-72.266 (± 1.362)
7	260.088 (± 4.368)	0.404 (± 0.036)	-72.844 (± 1.267)
10	276.788 (± 12.169)	0.436 (± 0.073)	-64.511 (± 2.496)

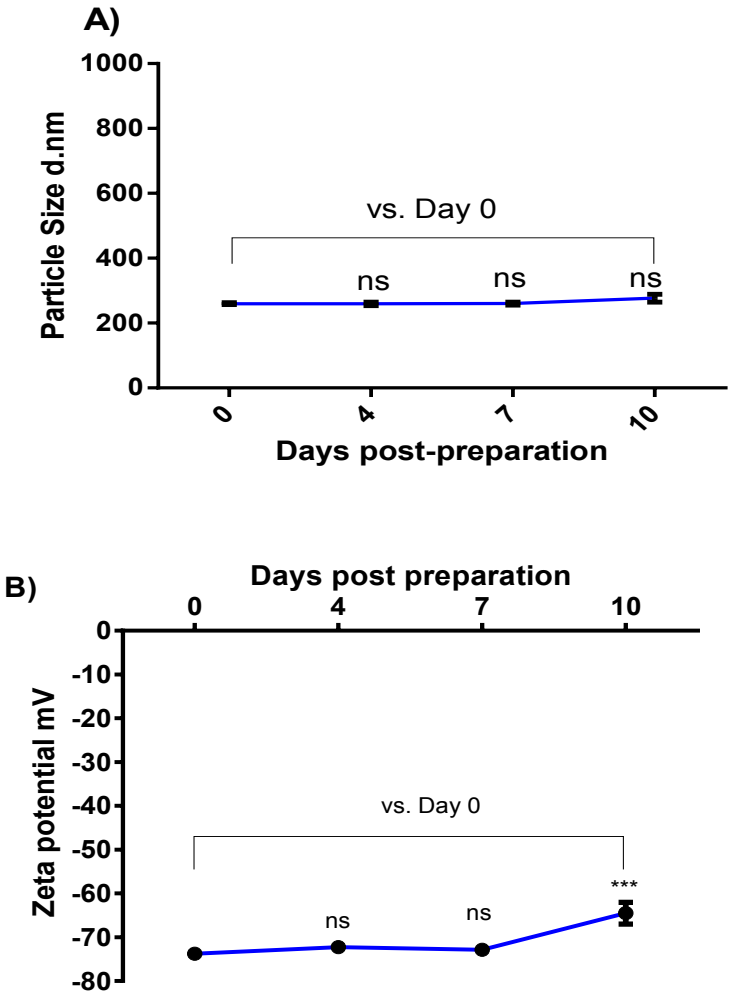

Figure 5.7 The particle size and ZP measurements of empty NIVs over 10 days post preparation. A) Particle size. B) ZP of empty NIVs. Statistical analysis was carried out using t-test comparing day 0 with the other days. Each point is representative of triplicate readings (n = 3). 0.1 ml of the niosomal formulation was suspended in 2.5 ml distilled water and sampled in a cuvette. The measurements of the size of prepared samples was performed using a Zetasizer (Malvern, UK) at 25°C.

The size and ZP results of empty NIVs illustrated a stable formulation without any statistically significant increase or decrease over time ($P > 0.05$) of either size or ZP, except for the ZP value on day 10 when compared to size on day 0. The size ranged from 259.933 nm (± 3.052) on day 0 to 276.788 nm (± 12.169) on day 10. The zeta potential values were approximately similar without a statistically significant decrease or increase in the negative charge ($P > 0.05$) on day 0, 4, and 7 when compared to charge on day 0 with a charge of -73.766 (± 1.276), -72.266 (± 1.362), and -72.844 (± 1.267) respectively. On day 10 there was a statistically significant decrease ($P < 0.01$) in the negative charge to -64.511 (± 2.496). This negative charge of empty NIVS on day 10 does not indicate instability as the charge is still less than -60 which resist the aggregation of formulation within the colloidal system.

The PdI values indicated that the empty NIV formulation has a heterogeneous size distribution ranging from 0.328 (± 0.019) on day 0 to 0.436 (± 0.073) on day 10. Empty NIVs in this study, exhibit a monodisperse distribution indicating a stable formulation. The lower PdI value is much closer to achieving monodisperse system, values less than 0.7 indicate greater stability for a colloidal system.

5.3.4.2 Cisplatin NIVs

5 ml empty NIV formulation was hydrated with 1 mg/ml cisplatin and then processed as described in Section 2.10.The formulations were characterised on the basis of size, ZP and entrapment efficiency as described (Section 2.10.1 and 2.10.2) on days 0, 1, 3, 4 and 7 post preparation. The mean particle size, PDI, and ZP results are summarised in Table 5.7 and Figure 5.8.

Table 5.7 Corresponding particle size, PDI and ZP values of cisplatin NIVs (1 mg/ml). Each point is representative of triplicate readings (n = 3).

Days post preparation	Cisplatin NIV ± SD		
	Mean Size (nm)	Mean PDI	Mean ZP
0	565.85 (± 23.19)	0.216 (± 0.012)	- 57.30 (± 4.73)
1	616.53 (± 37.47)	0.157 (± 0.017)	- 60.80 (± 4.53)
3	527.1 (± 4.01)	0.476 (± 0.10)	- 55.23 (± 3.36)
4	693.51 (± 47.49)	0.227 (± 0.013)	- 48.20 (± 5.34)
7	641.5 (± 23.9)	0.569 (± 0.037)	- 68.7 (± 1.45)

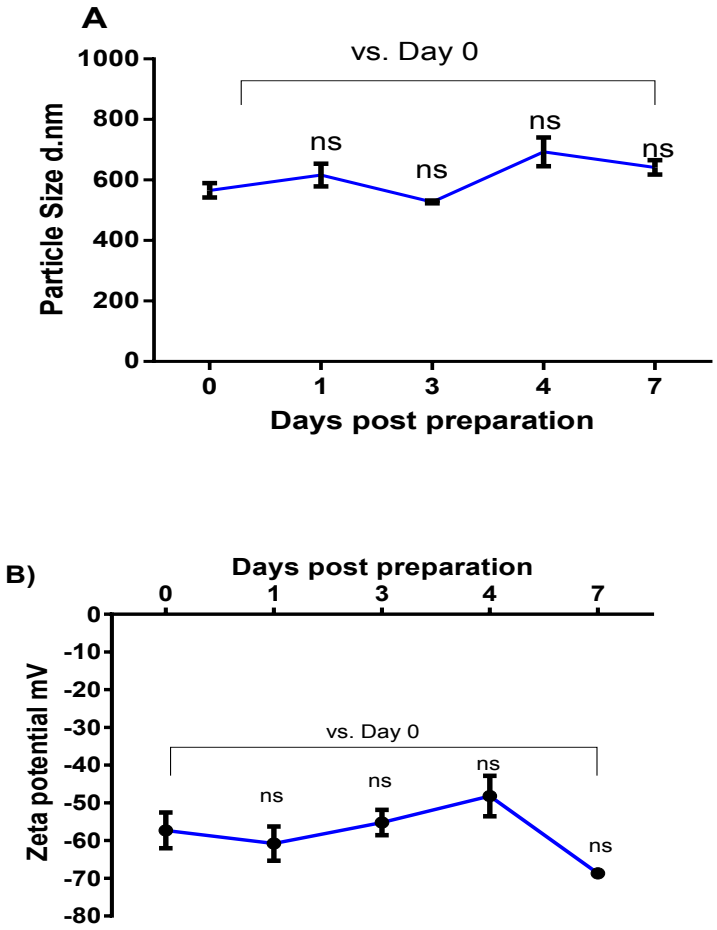

Figure 5.8 The particle size and ZP measurements of cisplatin NIVs over 7 days post preparation. A) Particle size of cisplatin NIVs B) ZP of cisplatin NIVs. Statistical analysis was carried out using t-test comparing day 0 with the other days. Each point is representative of triplicate readings (n = 3). 0.1 ml of the niosomal formulation was suspended in 2.5 ml distilled water and sampled in a cuvette. The measurements of the size of prepared samples was performed using a Zetasizer (Malvern, UK) at 25°C.

The size results of cisplatin NIVs ranged from 565.85 nm (± 23.19) on day 0 to 641.5 nm (± 23.9) on day 7. The formulation was stable without any statistically significant increase or decrease ($P > 0.05$) over time when compared to size on day 0. The zeta potential values were approximately similar without any statistically significant change ($P > 0.05$) over time; ZP values ranged from -57.30 (± 4.73) on day 0 to -68.4 (± 1.31) on day 7.

.The PdI results indicated that cisplatin NIV formulation has a heterogeneous size distribution ranging from 0.216 (± 0.012) on day 0 to 0.56 (± 0.037) on day 7, this indicate cisplatin NIVs exhibit a monodisperse distribution indicating a stable formulation.

.

The percentage entrapment results over time are shown in Figure 5.9.

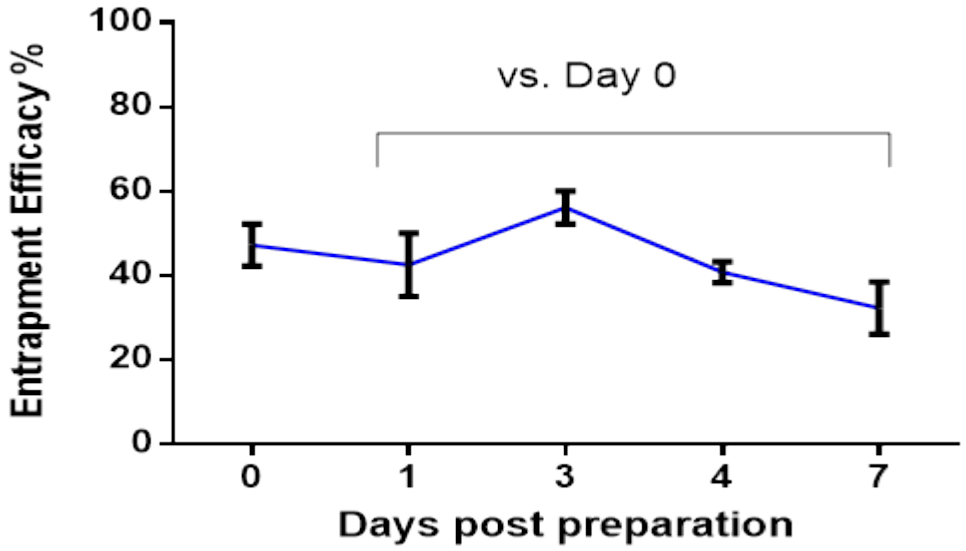

Figure 5.9 The entrapment efficiency (EE) of cisplatin NIVs (1mg/ml) over 7 days post preparation (n = 3). From the NIV suspension 0.5ml was taken and suspended in 4.5ml 0.9% w/v NaCl, then ultracentrifuged at 60,000 rpm for an hour using a Beckman Optima™ XL-90 Ultracentrifuge (GMI, U.S.A.).

The percentage entrapment results over time (Figure 5.9) showed greater entrapment efficiency of cisplatin NIVs on day 3 (56%) in comparison with days 0 and 7. There was no statistically significant reduction in the entrapment efficiency of cisplatin NIVs on day 1, 3, and 4 when compared to day 0. However the EE was significantly reduced from 47.17% (± 5.00) on day 0 to 32.27% (± 6.20, $P < 0.05$) on day 7.

5.3.4.3 TPT NIVs

5 ml of empty NIV formulations as described (Section 2.10) were hydrated with 1 mg/ml TPT and then characterised on the basis of entrapment efficiency, size and ZP as described in Sections 2.10.2.and 2.10.1. on days 0, 1, 3 and 7 post preparation. The particle size results, PDI and ZP values are summarised in Table 5.8 and Figure 5.10.

Table 5.8 Corresponding size, PDI, and zeta potential values of TPT NIVs 1 mg of 5% tartaric acid in 0.9% NaCl w/v. Each point is representative of triplicate readings (n = 3).

Days post preparation	TPT NIV ± SD		
	Mean Size (nm)	Mean PDI	Mean Zeta Potential
0	1264.55 (± 81.21)	0.665 (± 0.048)	-51.84 (± 1.84)
2	1200.44 (± 46.57)	0.689 (± 0.074)	-47.04 (± 2.38)
4	1141.44 (± 35.90)	0.626 (± 0.046)	-48.32 (± 2.80)
7	1191.88 (± 50.50)	0.681 (± 0.097)	-46.055 (± 3.34)

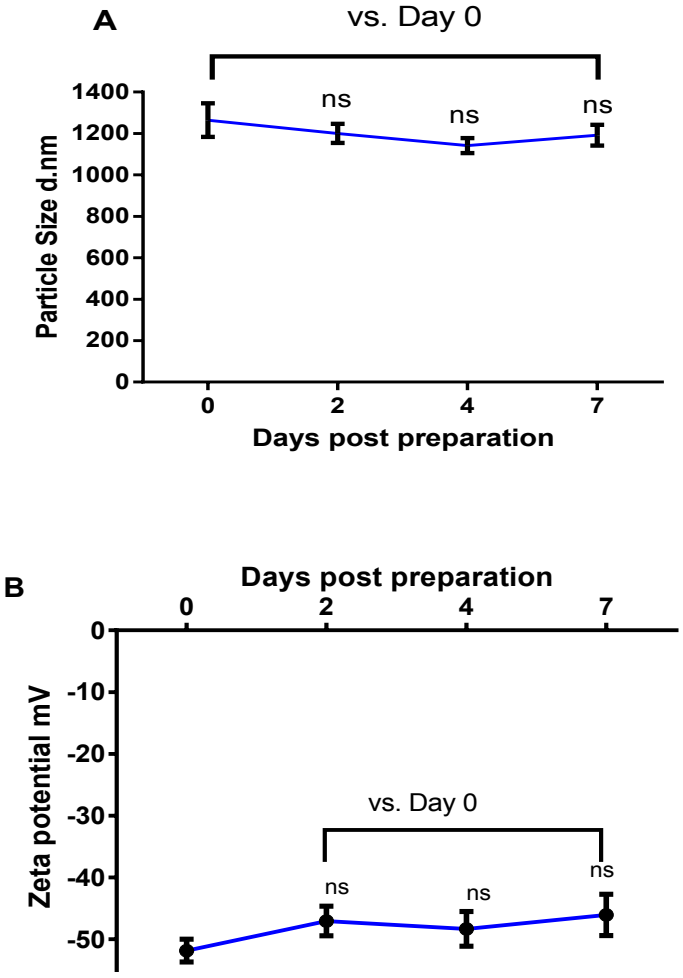

Figure 5.10 The particle size and ZP measurements of TPT NIVs over 7 days post preparation. A) Particle size of TPT NIV B) ZP of TPT NIV. Statistical analysis was carried out using t-test comparing day 0 with the other days. TPT 1 mg was prepared in 5% tartaric acid in 0.9% NaCl w/v. Each point is representative of triplicate readings (n = 3). 0.1 ml of the niosomal formulation was suspended in 2.5 ml distilled water and sampled in a cuvette. The measurements of the size of prepared samples was performed using a Zetasizer (Malvern, UK) at 25°C.

The size and ZP results of TPT NIVs (Figure 5.10) illustrated a stable formulation without any statistically significant change over time when compared to either size or ZP on day 0 ($P > 0.05$). However, it was observed from this study that the size range was higher than that of empty NIVs. The size ranged from 1264.55 nm (± 81.21) on day 0 to 1191.88 nm (± 50.50) on day 7. The zeta potential values were approximately similar without any statistically significant change ($P > 0.05$) and the negative charge ranged from -51.84 (± 1.84) on day 0 to -46.055 (± 3.34) on day 7 post preparation. This negative charge indicates a stable formulation that resists the aggregation within the colloidal system.

The PdI values indicated that TPT NIV formulation has a heterogeneous size distribution ranging from 0.665 (± 0.048) on day 0 to 0.681 (± 0.097) on day 7. This indicates that TPT NIVs exhibit a monodisperse distribution indicating a stable formulation.

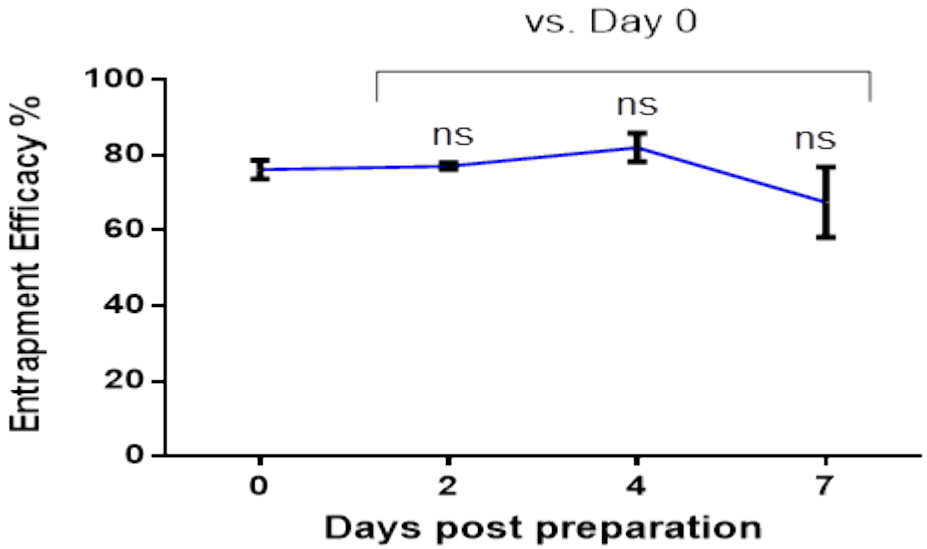

Figure 5.11 The entrapment efficiency of TPT NIVs 1mg /ml in 5% tartaric acid in 0.9% NaCl w/v (n = 3). From the NIV suspension 0.5ml was taken and suspended in 4.5ml of 5% tartaric acid then ultracentrifuged at 60,000 rpm for an hour using a Beckman Optima™ XL-90 ultracentrifuge (GMI, U.S.A.).

The percentage entrapment efficiency results (Figure 5.11) showed a good entrapment efficiency of TPT NIVs over time. The entrapment efficiency of TPT NIVs ranged from 76.22% (± 2.50) on day 0 to 67.54% (± 9.372) on day 7. The percentage entrapment efficiency was slightly decreased from 76.22% on day 0 to 67.54% on day 7 but without a statistically significant decrease ($P > 0.05$).

The data from Figures 5.7, 5.8, and 5.10 were utilized to plot Figure 5.12 where TPT NIVs and cisplatin NIVs are compared with empty NIVs in terms of particle size and ZP values.

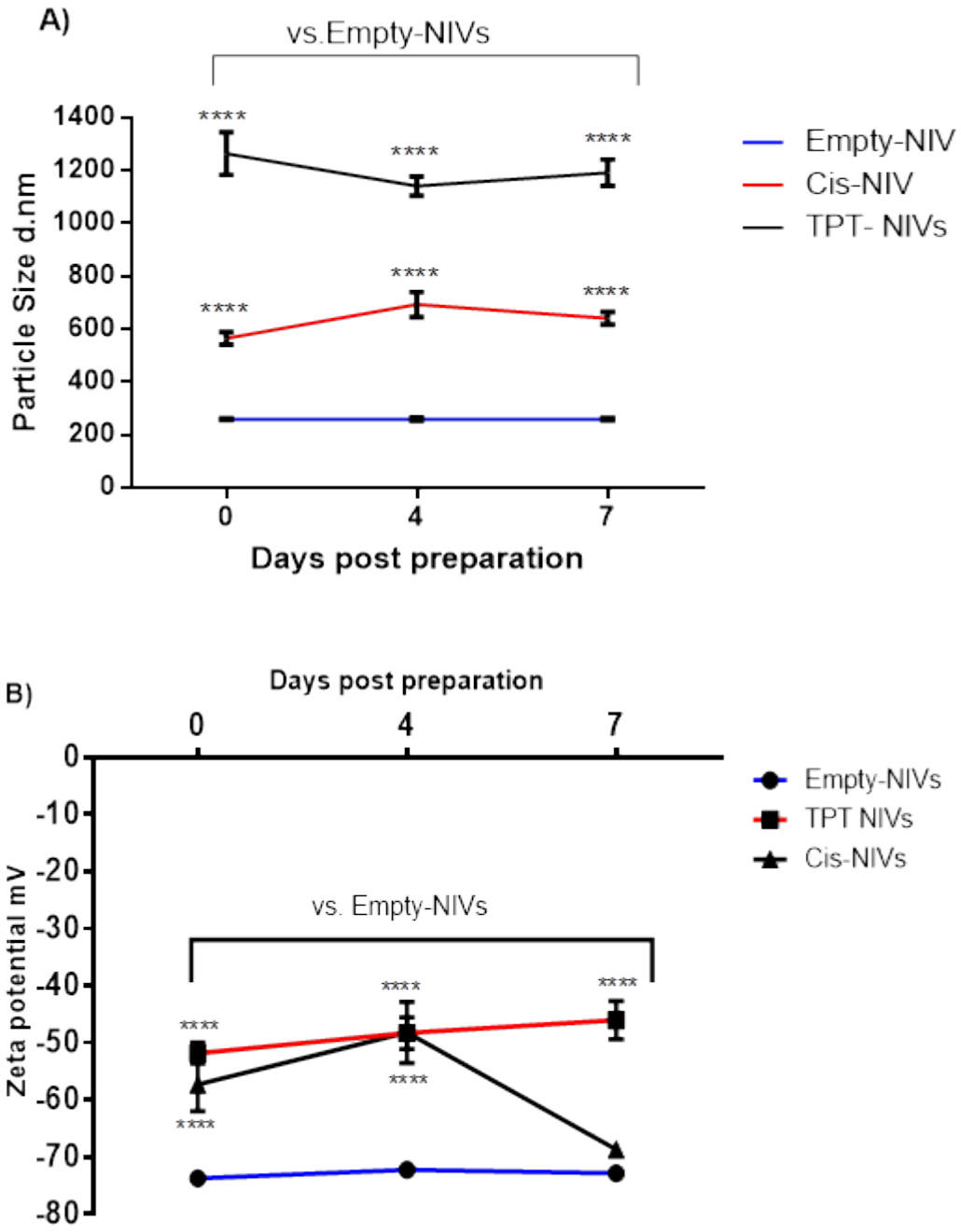

Figure 5.12 The particle size and ZP values of empty NIVs, TPT NIVs and cisplatin NIVs over 7 days post preparation. Data were obtained from Figures 5.7, 5.8, and 5.10.

In Figure 5.12 A, it can be seen that there was a statistically significant increase ($P > 0.001$) in the particle size of TPT NIVs and cis NIVs when compared with empty NIVs over 7 days post preparation. The size of TPT NIVs and cisplatin NIVs were increased from 1264.55 nm (± 81.21) and 565.80 nm (± 23.90) respectively, whereas the size of empty NIVs was 259.93 (± 3.05). This significant increase in the particle size of NIVs after encapsulation with either TPT or cisplatin.

In addition, the negative charge (Figure 5.12 B) showed a statistically significant change ($P > 0.001$) of TPT NIVs and cisplatin NIVs when compared with empty NIVs. On day 0, the ZP value of empty NIVs was -73.76 (± 1.27) whereas the ZP values of TPT NIVs and cisplatin NIVs were -57.30 (± 4.73) and -51.84 (± 1.84) respectively. Empty NIVs were shown to be more stable than TPT NIVs and cisplatin NIVs.

5.3.5 Stability studies of TPT NIVs

20 ml of empty NIV formulation were hydrated as described (Section 2.11) with 20 mg/ml TPT and then processed as described in Section 2.10.1 and 2.10.2. The stability studies were performed to examine entrapment efficiency, size and ZP of TPT NIVs at two different temperatures (4°C and 25°C) on a weekly basis over 28 days post preparation.

The particle size, PDI and ZP results of the TPT NIV formulation is summarised in Table 5.9 and Figure 5.13.

Table 5.9 Corresponding size, PDI, and ZP values of TPT NIVs (1 mg/ml) at 2 different temperatures (4°C and 25°C) measured on a weekly basis over 28 days post preparation. Each point is representative of triplicate readings (n = 3).

Days post prep.	TPT NIV ± SD					
	Mean Size (nm)		Mean PDI		Mean ZP	
	4°C	25°C	4°C	25°C	4°C	25°C
0	1264.55 (± 81.21)	1264.55(± 81.21)	0.865 (± 0.048)	0.865 (± 0.048)	-51.84 (± 1.84)	-51.84 (± 1.84)
7	1191.88 (± 50.50)	1259.88 (± 45.72)	0.681 (± 0.097)	0.767 (± 0.084)	-46.055 (± 3.34)	-55.24 (± 2.54)
14	1232.11 (± 48.26)	1281.44 (± 53.55)	0.656 (± 0.06)	0.689 (± 0.03)	-46.74 (± 1.85)	-51.15 (± 1.97)
21	1331.55 (± 80.51)	1311.66 (± 71.94)	0.763 (± 0.044)	0.739 (± 0.065)	-46.98 (± 3.15)	-47.12 (± 2.14)
28	1190.33 (± 8.09)	1339.33 (± 37.74)	0.6456 (± 0.024)	0.616 (± 0.017)	-43.82 (± 1.203)	-41.25 (± 2.72)

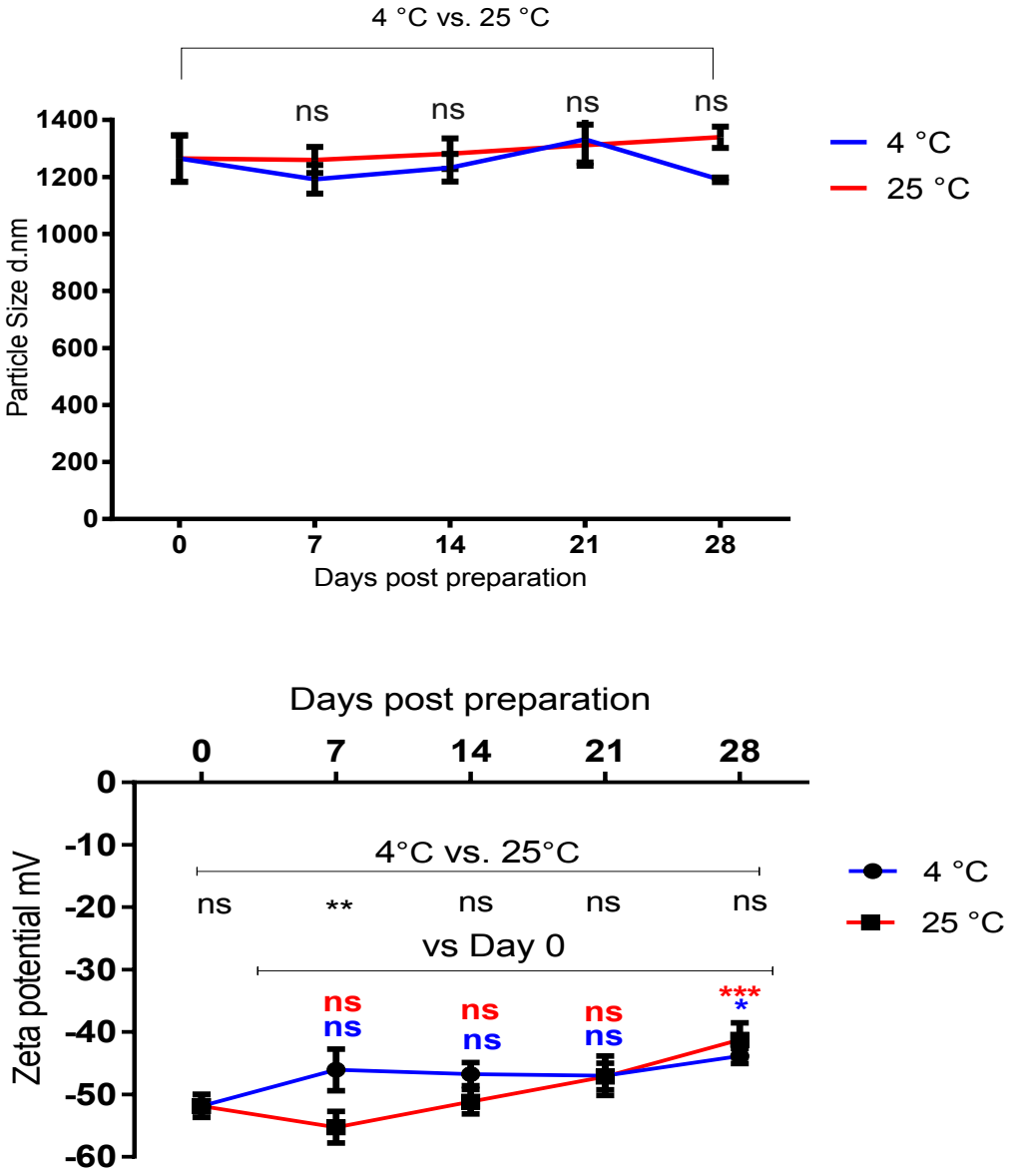

Figure 5.13 The particle size and ZP values of TPT NIVs at 4°C and 25°C over 28 days post preparation. 1 mg/ml of 5% tartaric acid in 0.9% NaCl w/v. Statistical analysis was carried out using t-test comparing TPT NIVs stored at 4°C with TPT NIVs stored at 25°C over 28 days. Each point is representative of triplicate readings (n = 3). 0.1 ml of the niosomal formulation was suspended in 2.5 ml distilled water and sampled in a cuvette.

As seen in Figure 5.13, the size results of TPT NIVs at 4°C and 25°C over 28 days post preparation illustrated a stable formulation without no statistically significant change in size ($P > 0.05$) when the two conditions were compared with each other over 28 days. The size ranged from 1264.55 nm (± 81.21) on day 0 to 1191.88 nm (± 50.50) at 4°C, and 1339.33 nm (± 37.74) at 25°C on day 28. The zeta potential values were approximately similar without a significant change between the two temperatures (4°C and 25°C) except on day 7 where the negative charge was significantly different at -46.055 (± 3.34) for 4°C compared with -55.24 (± 2.54) for 25 °C ($P<0.001$). The ZP values over the 28 days ranged from -51.84 (± 1.84) on day 0 to -43.82 (± 1.203) for 4°C and -41.25 (± 2.72) for 25 °C on day 28.

The PdI values (Table 5.9) indicated that both TPT NIV formulations had a heterogeneous size distribution ranging from 0.865 (± 0.048) on day 0 to 0.6456 (± 0.024) for 4°C and 0.616 (± 0.017) for 25 °C on day 28. The percentage entrapment efficiency results of TPT NIVs at 4°C and 25°C over the time course are shown in Figure 5.14.

Table 5.10 Corresponding entrapment efficacy values of TPT NIVs (1mg/ml) at 4°C and 25°C over 28 days post preparation. Each point is representative of triplicate readings (n = 3).

Days post preparation	TPT NIV ± SD	
	Mean EE ± ST.D	
	4°C	25°C
0	76.22% (±4.51)	76.22% (±4.51)
7	71.54% (±9.37)	74.16% (± 7.59)
14	68.89% (± 4.31)	65.95% (±7.63)
21	66.47% (± 4.65)	67.49% (±3.99)
28	56.32% (± 3.97)	52.85% (±2.99)

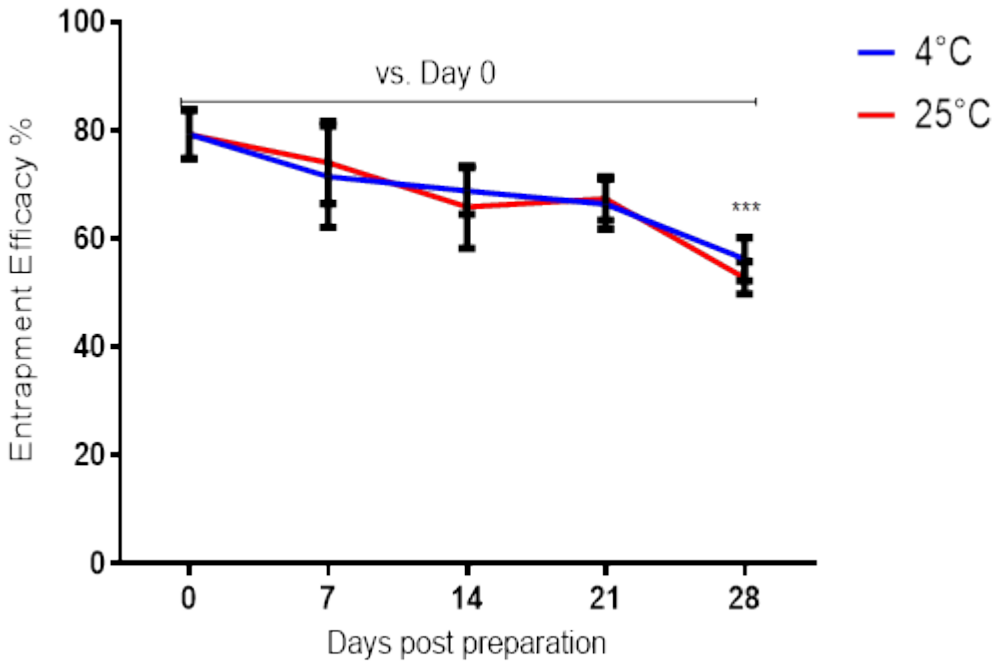

Figure 5.14 The entrapment efficiency of TPT NIVs 1mg /ml of 5% tartaric acid in 0.9% NaCl w/v (n = 3). From the NIV suspension 0.5ml was taken and suspended in 4.5ml of 5% tartaric acid 0.9% NaCl w/v then ultracentrifuged at 60,000rpm for an hour using a Beckman Optima™ XL-90 ultracentrifuge (GMI, U.S.A.).

The percentage entrapment efficiency results over the time course (Figure 5.14) showed a good entrapment efficiency of TPT NIVs. There was only a statistically significant decrease in the entrapment efficiency of TPT NIVs from 76.22% (± 4.51) on day 0 to 56.32% (± 3.97) on day 28 for 4°C and 52.85% (±2.99) for 25°C. However, there was no significant change of the entrapment efficiency TPT NIVs on day 7, 14, 21 when compared to day 0. The percentage entrapment efficiency results of formulation stored at 4°C did not show any significant changes when compared with formulation stored at 25°C. These results indicate that temperature has no influence on formulation entrapment efficiency over time.

5.3.5.1 Physical appearance of TPT NIVs

The physical appearance of TPT NIVs was evaluated (Figure 5.15 A) to demonstrate that formulations at 4°C and 25°C do not have unacceptable changes in physical properties such as homogenization, appearance, clarity, or colour of solution. Over the 28 days TPT NIV formulations appeared to be homogenized and consistent in their milky colour, appearance and clarity. There were no signs of flocculation or sedimentation observed in any of the NIVs that could indicate gross colloidal instability. Figure 5.15B shows photographs of ultracentrifugation tubes containing TPT NIV pellets.

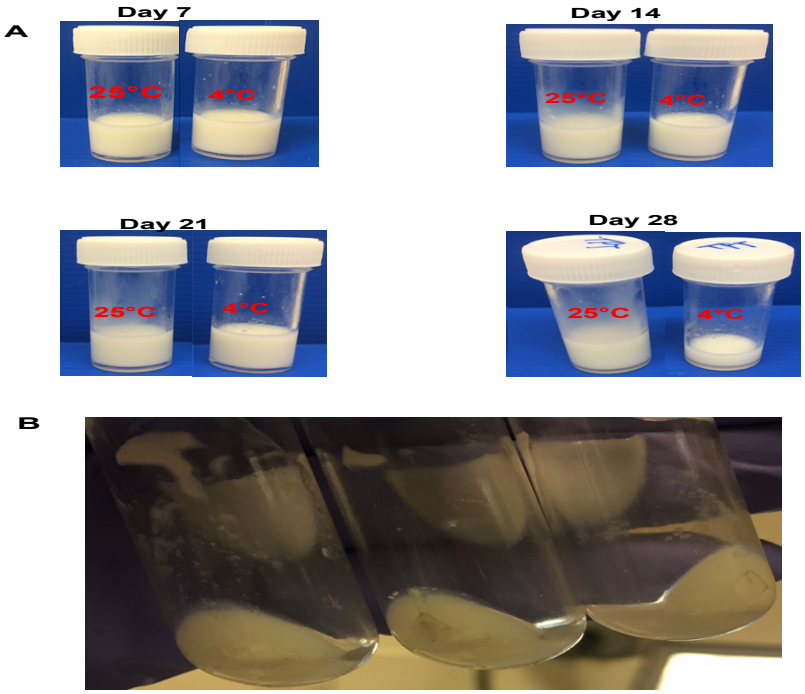

Figure 5.15 The physical appearance of TPT NIVs. A) Formulation stored at 25°C and 4°C. All formulations were homogenized and appeared to be consistent in their colours, appearance and clarity. B) Ultracentrifugation tubes showing TPT NIV pellets before pellet disruption for analysis by HPLC.

5.3.6 Assessing the cytotoxic effects of cisplatin NIVs and TPT NIVs using clonogenic (cell survival) assays

The effect of cisplatin NIVs and TPT NIVs either as single agents or in combination therapy on clonogenic survival (as described in Sections 2.3) of H460 and A549 cells was investigated to compare cytotoxicity with NIV formulations verses the free solutions of cisplatin or TPT and empty NIVs. 1 mg/ml of either cisplatin NIVs or TPT NIVs were prepared as described in Sections 2.10. Cells were incubated cisplatin NIVs or TPT NIVs alone for 24 hours over a dose range of 62.5-250 nM and 10-30 nM respectively were tested. The cytotoxicity results of the single agents (Cis-NIVs and TPT-NIVs) are shown in Figure 5.16. There was a statistically significant difference in toxicity of the TPT-NIVs versus the free TPT at the higher doses. This was approximately two fold difference and suggests that the TPT-NIVs were more toxic to the monolayer cells than the free TPT. Similarly with cisplatin, there was only significant deference in toxicity of the cisplatin-NIVs versus the free cisplatin at the administered dose of 125nM, whereas the other administered doses were non-toxic.

A1

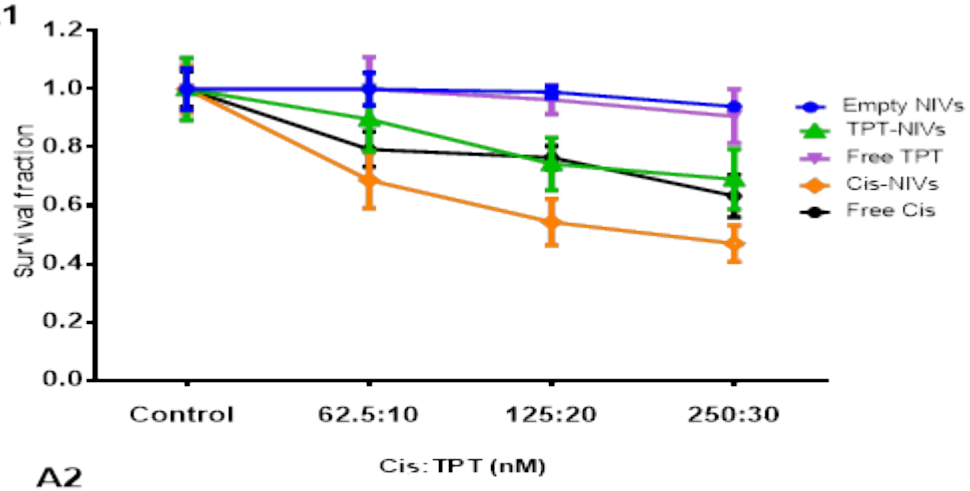

A2

62.5:10 nM		125:20 nM		250:30 nM	
TPT-NIVs vs. Free TPT	ns	TPT-NIVs vs. Free TPT	$p < 0.05$	TPT-NIVs vs. Free TPT	$p < 0.05$
Cis-NIVs vs. Free Cis	ns	Cis-NIVs vs. Free Cis	$p < 0.05$	Cis-NIVs vs. Free Cis	ns

B

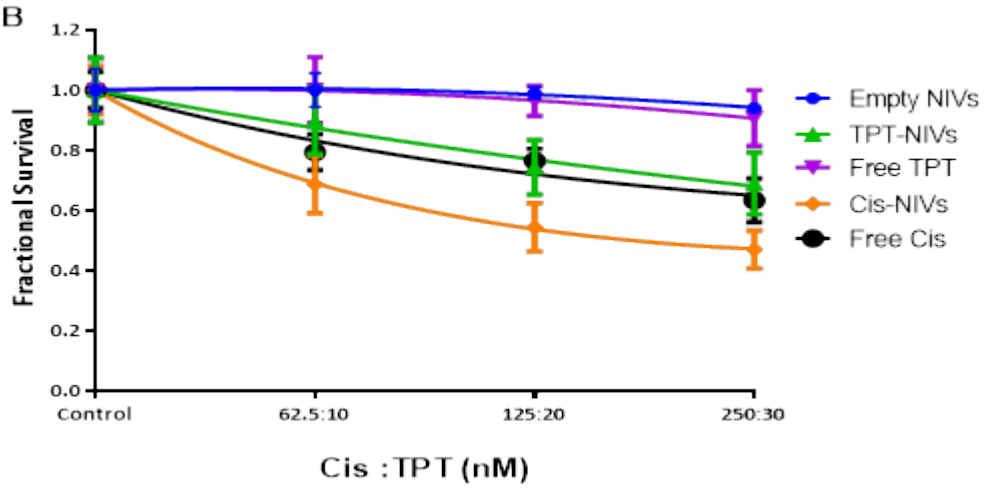

Figure 5.16 The effect of increasing doses of cisplatin NIVs and TPT NIVs alone on H460 cell survival fraction. A1) The effects of cisplatin NIVs and TPT NIVs or cisplatin and TPT as free drugs alone on H460 cells. Cells were dosed with cisplatin alone either encapsulated with NIVs or as free solution over dose range 62.5-250 nM and TPT alone either with NIVs or as free solution over dose range 10-30 nM. A2) Table with the test significances comparing NIV formulations with free drugs. B) Clonogenic survival data presented in (A1) was fitted to the linear quadratic model using GraphPad Prism version 6.0.1. Two-way ANOVAs with Bonferroni test were used to statistically compare the means of NIV formulation with free drugs. Tests were performed at 95% C.I. * = $p < 0.05$; ns = no significance.

Following exposure of H460 cells to empty-NIVs, there was no significant differences in the clonogenic survival fraction of empty-NIVs when compared to untreated control indicating the used NIVs doses have no toxic effects on H460 cells. Following exposure of H460 cells to cisplatin-NIVs alone and free cisplatin alone, there was no significant decrease in the clonogenic survival fraction of cisplatin-NIVs when compared to free cisplatin at treatment doses of 62.5 and 250 nM ($p > 0.05$), whereas, there was a statistically significant deference in the survival fraction of H460 cells when exposed to cisplatin-NIVs at dose of 125nM (inhibition by 45.67%, $p < 0.05$) when compared to free cisplatin 125nM (inhibition by 23.5%). Following exposure of H460 cells to TPT NIVs and free TPT at a dose of 20 and 30 nM, there was a statistically significant reduction in H460 cells clonogenic survival fraction from 0.96±0.050 and 0.90 ±0.093, respectively in free TPT treatment group to 0.74±0.090 and 0.69±0.10 ($p < 0.05$, inhibition by 22% and 21%, respectively) for TPT NIVs treatment group. Whereas, at dose of 10nM there was no significant deference in clonogenic survival fraction of free TPT when compared to TPT-NIVs.

The effects of cisplatin NIVs in combination with TPT NIVs versus free dugs were tested on H460 cells for 24 hours and the results are shown in Figure 5.17. The combination treatment group encapsulated with NIVs showed no significant differences in the clonogenic survival of H460 cells when compared to free drug treatment group.

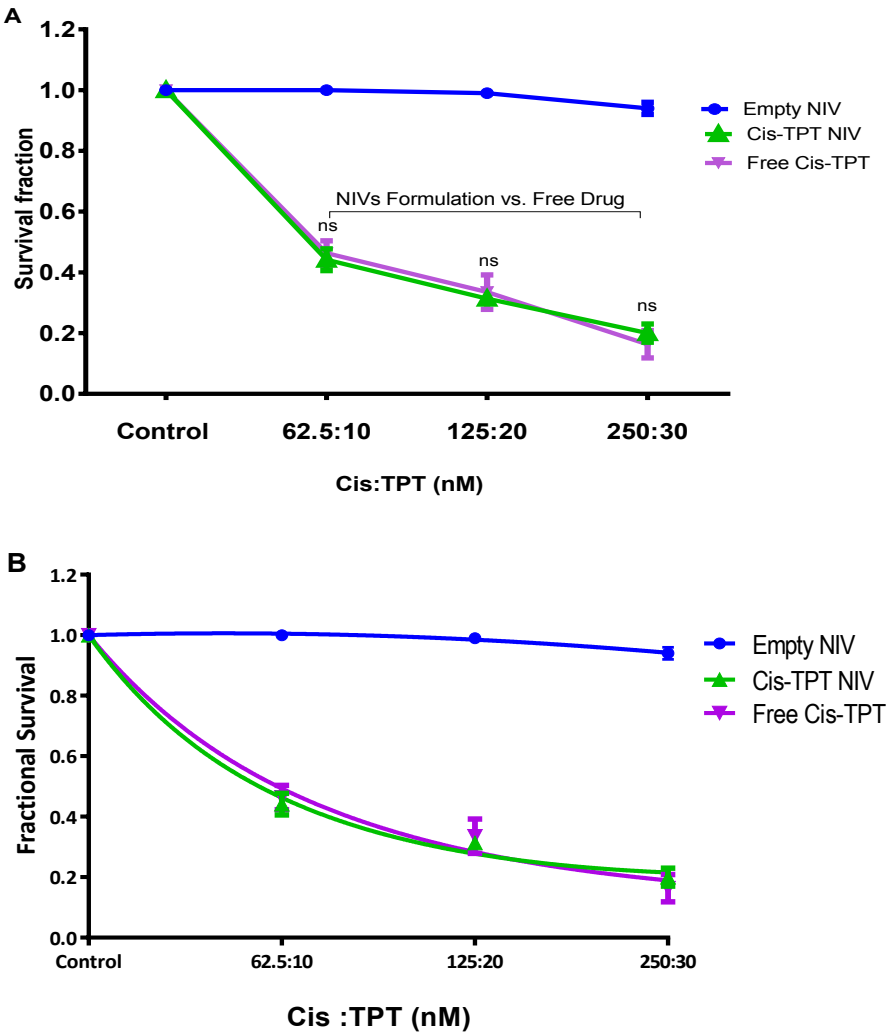

Figure 5.17 The effect of increasing doses of cisplatin NIVs and TPT NIVs in combination on H460 cell survival fraction.

A1) The effects of cisplatin NIVs and TPT NIVs or free cisplatin and TPT in combination on H460 cells. Cells were dosed with cisplatin over dose range 62.5-250 nM and TPT over dose range 10-30 nM in combination. **B)** Clonogenic survival data presented in (A1) was fitted to the linear quadratic model using GraphPad Prism version 6.0.1Two-way ANOVAs with Bonferroni test were used to statistically compare the means of NIV formulation with free drugs. Tests were performed at 95% C.I. ns = no significance.

In contrast to the results from single agent NIVS, there was no statistically significant difference in clonogenic survival when both TPT and cisplatin in combination were administered as NIVS or as free drugs as is shown Figure 5.24. For example, at a combination dose of 250nM cisplatin-NIVs combined with TPT-NIVs 30 nM, the survival fraction was inhibited to 0.31 (± 0.015, inhibition by 69%) from 0.335 (± 0.05, inhibition by 66.5%).

Next the effects of cisplatin NIVs or TPT NIVs alone on clonogenic survival were tested on A549 cells after treatment with NIVs for 24 hours and results are shown in Figure 5.18.

A1

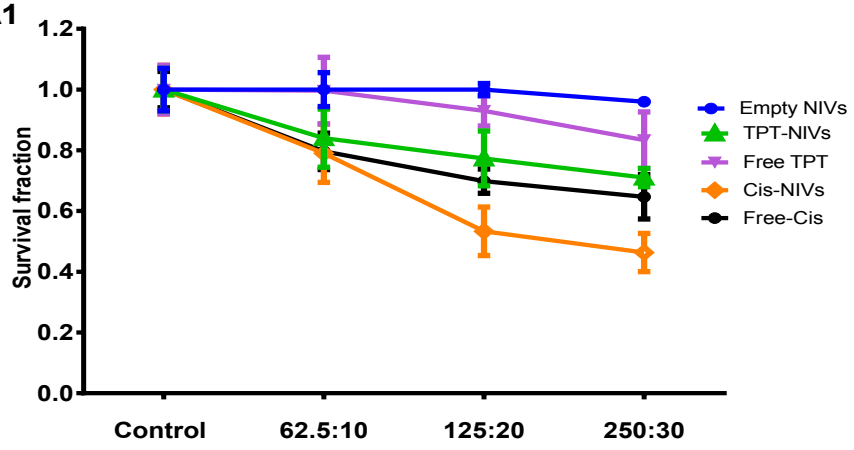

A2

61.25:10 nM		125:20 nM		250:30 nM	
TPT-NIVs vs. Free TPT	ns	TPT-NIVs vs. Free TPT	ns	TPT-NIVs vs. Free TPT	ns
Cis-NIVs vs. Free Cis	ns	Cis-NIVs vs. Free Cis	ns	Cis-NIVs vs. Free Cis	p < 0.05

B

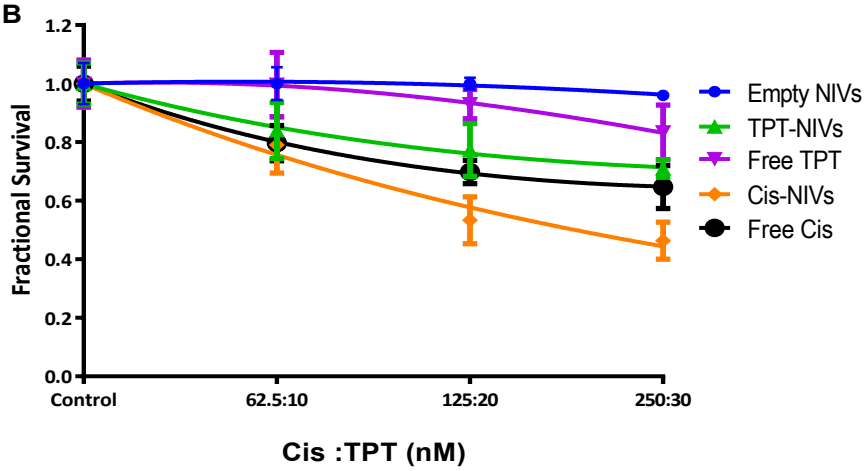

Figure 5.18 The effect of increasing doses of cisplatin NIVs and TPT NIVs alone on A549 cell survival fraction. A1) the effects of cisplatin NIVs and TPT NIVs or cisplatin and TPT as free drugs alone on A549 cells. Cells were dosed with cisplatin alone either encapsulated with NIVs or as free solution over dose range 62.5-250 nM and TPT alone either with NIVs or as free solution over dose range 10-30 nM. A2) Table with the test significances comparing NIV formulations with free drugs. B) Clonogenic survival data presented in (A1) was fitted to the linear quadratic model using GraphPad Prism version 6.0.1. Two-way ANOVAs with Bonferroni test were used to statistically compare the means of NIV formulation with free drugs. Tests were performed at 95% C.I. * = $p < 0.05$; ns = no significance.

From figure 5.18 it was apparent that the free NIVS were again non-toxic to the A549 cells over the dose range tested. Following exposure of A549 cells to TPT NIVs and free TPT alone or cisplatin-NIVs and free cisplatin alone, there were no significant differences in the clonogenic survival fraction of A549 cells with TPT-NIVs and cisplatin-NIVs when compared to free drugs with an exception of only the highest administered dose of cisplatin-NIVs (250nM) where there was a statistically significant reduction in the congenic survival fraction from 0.64±0.073 in the free cisplatin group to 0.46±0.063 in the cisplatin-NIVs treatment group inhibition by 18%, $p < 0.05$.

The effects of cisplatin NIVs in combination with TPT NIVs versus free dugs were tested on A549 cells for 24 hours and the results are shown in Figure 5.19. The combination treatment group encapsulated with NIVs showed no significant differences in the clonogenic survival of A549 cells when compared to free drug treatment group.

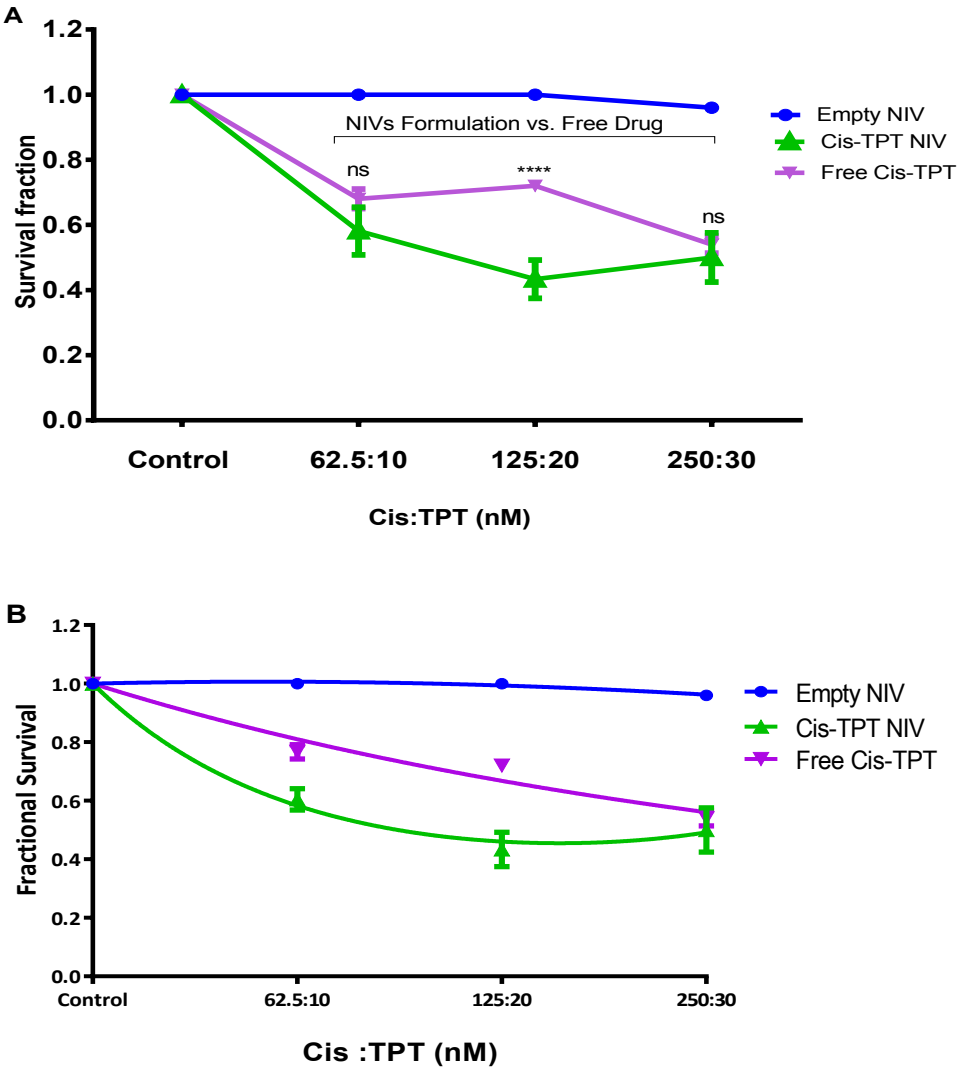

Figure 5.19 The effect of increasing doses of cisplatin NIVs and TPT NIVs in combination on A549 cell survival fraction.

A1) The effects of cisplatin NIVs and TPT NIVs or free cisplatin and TPT in combination on A549 cells. Cells were dosed with cisplatin over dose range 62.5-250 nM and TPT over dose range 10-30 nM in combination. **B)** Clonogenic survival data presented in (A1) was fitted to the linear quadratic model using GraphPad Prism version 6.0.1Two-way ANOVAs with Bonferroni test were used to statistically compare the means of NIV formulation with free drugs. Tests were performed at 95% C.I. *** = $p < 0.001$; ns = no significance.

In contrast to the H460 cells there was a statistically significant difference in clonogenic survival at some administered doses. At administered dose of 125

nM cisplatin in combination with 20nM TPT, A549 cells exhibited a statistically significant deference in the survival fraction from 0.72± 0.03 in free dugs treatment group to 0.43 ±0. 0.097 in the NIV drug formulation treatment group (inhibition by 29%, $p < 0.001$) indicating once again a superior toxicity with the NIV encapsulated drugs given in combination at this dose. However a statistically sig difference was only seen at some doses.

5.4 Discussion

In this chapter, the HPLC methods were validated to allow the measurement of entrapment efficiency of cisplatin NIVs and TPT NIVs. The HPLC method for the quantification of cisplatin (platinum compound) was adopted from Lopez-Flores et al. (2006) and Alsaadi (2011). In this method, DDTC was used to form a complex with cisplatin (Pt(DDTC)2) as the UV range cannot absorb cisplatin alone and this make it difficult to quantify a platinum compound such as cisplatin, hence this complex compound formed by the addition of DDTC has a strong capability to be absorbed and detected easily by the HPLC UV range. In this HPLC method, ICH acceptance criteria of the validation characteristics were in line with results shown in this chapter where cisplatin concentration range was shown to be linear, with R2 values of 0.99 and the retention times of the peaks of interest were precise, and the %RSD of the concentrations analysed was within the intraday and interday precision with %RSD < 5% (Appendix A). Furthermore, the accuracy values were as per ICH guideline recommendations and showed a percentage recovery between 94.6 and 97.8 %.

A sensitive and reliable method was required for the quantification and validation of TPT to avoid the hydrolysis of the lactone ring which is responsible for the biological activity of TPT (Souza et al., 2011a, Fassberg and Stella, 1992). In this chapter, the method for TPT quantification and validation was adopted from a published method by Saini *et al*. (2010). Saini *et al.* (2010) reported TPT peak detected at retention time of 1 minute while the retention time in this chapter was detected at 3.28 minutes. This variation in the retention time was due to

modification in this HPLC method as an attempt to shift the peak to a longer retention time. The modified HPLC method used in this chapter seems to be more reliable than the published methods used by Saini *et al.* (2010), having a precise peak at a retention time of 3.28 minutes. However, at the beginning of this analytical study, the peak occasionally had a retention time of 1.2 min at a flow rate of 1 ml/min. This could make the quantification unreliable as this peak may not belong to topotecan and misinterpreted as a solvent peak. This led to the flow rate being changed from 1 ml/min to 0.4 ml/min. This change in the flow rate resulted in a shift in the HPLC peak of topotecan from 1 min to 3.28 (Figure 5.1). Moreover, the hydroxylactone ring of TPT in alkaline conditions usually undergoes a rapid pH-dependent hydrolysis. This hydrolysis would deactivate the carboxylate form of TPT, leading to a decrease in the antitumor activity of TPT following dissolution in aqueous media (Souza et al., 2011a, Fassberg and Stella, 1992). Therefore, in this research TPT was prepared in 5% tartaric acid in 0.9% NaCl w/v and the addition of 0.1% TFA to the mobile phase was beneficial to maintain and stabilize the lactone ring in an acidic condition. The hydrolysis of this lactone ring would occur if the pH is more than 4. Due to this hydrolysis issue, the topotecan was analysed at a pH of 5.4 (Figure 5.4) to identify this hydrolysis reaction and to detect the degradation products resulting from this hydrolysis reaction. With regards to the TPT method validation characteristics, the concentration range used showed a good linearity with R2 = 0.999 (Figure 5.2) and the intraday and interday precision for all the standard concentrations had a %RSD of < 5%. For the accuracy measurement, three concentrations (5, 20, and

80 µg/ml) in the calibration range were selected and showed a percentage recovery between 101.6 and 100.42% in line with the ICH acceptance criteria.

One of the aims in this chapter was to formulate a stable lipid nanoparticle formulation (NIVs) capable of delivering either cisplatin or TPT effectively. For specific drug distribution into solid tumours and to maximize cell exposure, stable formulations are vital (Drummond *et al*., 2010). The use of niosomal formulations is very advantageous to overcome some of the limitations associated with liposomes (Müller *et al*., 2000). Physical properties such as uniform size distribution, charge and minimal leakage are required for stability purposes (Liu *et al*., 2002). In comparison with liposomes, NIVs have a minimal degradation rate leading to a better control of drug release and greater protection of the encapsulated drug (Vivek *et al*., 2007).

In this chapter, the results showed particle size and zeta potentials for empty NIVs, cisplatin NIVs and TPT NIVs formulations having a high negative charge with no significant differences over the time course (Figure 5.7 A, 5.8 A, and 5.10 A, respectively) when compared to day 0. Due to the chemical nature of the lipid matrix (DCP/cholesterol) and surfactants used, all formulations had a high negative residual charge. From the results it was observed that the incorporation of cisplatin or TPT with lipid nanoparticles (NIVs) decreased the zeta potential values ($p < 0.001$) when compared with empty NIVs. This is because the drugs used in this study, particularly TPT, present a positive residual charge at the pH values used for the nanoparticle dispersion (Souza et al., 2011a), however, this

decrease in the charge is still considered to be high and suitable in making TPT NIVs or cisplatin NIVs as a stable formulations. The results of this study are in agreement with Souza et al. (2011a).

In addition, the particle size results (Figure 5.14 B, 5.15 B, and 5.17 B, respectively) show all formulations over the time course (7 days) to be consistent with no significant differences when compared with day 0. However, it was observed that the TPT NIV formulation had a high particle size when compared with empty NIVs while the TPT NIV size reported by Souza et al. (2011a) showed similar size results to the blank NIVs. This significant difference may be a result of differences in drug solubility in melted lipids and the amount of drug added to the formulations. previous studies explained the significant difference of empty niosomes compared to loaded niosomes and concluded that factors such as the degree of hydration of the hydrophilic head, the hydrophobic character of the surface active agent, the properties of the molecules in the bilayer, distance between the bilayers and the number of bilayers present have a significant effect to increase the size of niosomes (Ammar et al., 2017a, Hao et al., 2002). Furthermore, in this matter Hao *et al.,* (2002) concluded that a larger particle size of drug loaded niosomes compared to empty niosomes indicates a high encapsulation of drug by noisome system. Another research conducted by Arzani *et al.* (2015) found that niosomal carvedilol had a significant larger size than empty noisome and explained this deference to be due to the presence of a possible interaction between carvedilol and cholesterol, incorporated into the noisome system. This has also been previously observed in a niosomal formulation developed with cholesterol and carotenoids (Moghassemi and

Hadjizadeh, 2014). Another important previous research by Ammar et al. (2017b) studied niosomes with different types and ratios of Span (liquid surfactant) and found the mean particle size in the range of 1.45–1.59 μm (1450-1590 nm). Ammar et al. (2017b) concluded that the larger particle size of niosomes may be correlated to the higher HLB value which reflects higher contribution of its hydrophilic head that is well hydrated with water, where the use of more hydrophobic surfactant (such as Span 60) with low HLB value and surface free energy results in formation of smaller size vesicles.

The stability studies of TPT NIVs were performed on the basis of entrapment efficiency, size and ZP at two different temperatures (4°C and 25°C) over 28 days post preparation. The results of this stability study confirmed that the particle size was consistent and stable over time ($P > 0.05$). It was observed that temperature had no significant effects on size, ZP, or entrapment efficiency. Furthermore, no apparent changes in the physical appearance were observed that could indicate colloidal system instability such as sedimentation and flocculation.

Despite the fact that TPT is hydrophilic, all TPT NIV formulations used in the stability study showed EE values greater than 76% on day 0. Souza *et al*. (2011a) reported encapsulation of TPT in solid lipid nanoparticles using a microemulsion technique and showed EE values of greater than 90%. Another study of encapsulation of a hydrophilic drug into lipid nanoparticles was reported by Marquele-Oliveira *et al*. (2010) and the EE for this nitrosyl-ruthenium complex was 78.32%. It is imperative to note that in these cited reports, the surfactant and

lipid compositions had some similarities to those employed in this chapter. The high EE values observed in this study indicate that the lipid and surfactant compositions employed are suitable for TPT entrapment in the niosomal formulations prepared in this chapter. Encapsulating TPT in lipid vesicles can stabilize the lactone ring of TPT, since the lactone intercalates between the lipid acyl chains, shielding it from the aqueous media (Burke *et al*., 1993). However, the EE was significantly decreased on day 28 when compared to day 0 of this stability study.

Vesicular delivery systems (NIVs) can improve the delivery of cytotoxic drugs against cancer cells in a targeting manner by encapsulating active drugs efficiently (Hua, 2015). The main aim of this chapter was to determine whether the designed NIV formulations encapsulating drugs can effectively achieve greater cytotoxicity than free drugs. The empty NIV formulations tested on both cell lines in this research and were non-toxic when compared to untreated control. This result was in agreement with Rinaldi *et al.* (2017) that observed no cytotoxicity of empty niosomal formulation containing Span (surfactant) in dose range 50-100 μM when tested in *vitro* on human keratinocyte cells (HaCaT) using clonogenic assay, however, on mouse fibroblasts Balb/3T3 cells it was observed that empty niosomes produced significant cytotoxicity on Balb/3T3. Nematollahi *et al*. (2017) observed that the cytotoxic profiles of niosomes increased with the higher concentration of niosomes. Thus in this chapter the low concentration of niosomes (10-250 nM) did not achieve significant cytotoxicity when compared to untreated control.

The cytotoxic effects of free drugs alone (cisplatin and TPT) alone and drugs-loaded in niosomes against H460 cells (Figure 5.16) and A549 cells (Figure 5.18) were investigated, after 24h of treatment with either treatment alone or in combination, using clonogenic assay. In this study, it was clear that the cytotoxic effect of TPT-NIV formulation in both cell lines was superior in achieving greater cytotoxicity effects compared to free drugs ($p < 0.001/p < 0.05$). These observed significant differences in our study were in agreement with some published studies by (Burger *et al*., 2002, Velinova *et al*., 2004). Velinova *et al.* (2004) used different lipid nanoparticles (phosphatidylserine (PS)) and zwitterionic phosphatidylcholine (PC)) prepared from different negatively charged surfactant encapsulating cisplatin to be tested against human ovarian IGROV-1 tumour cells to examine their cytotoxicity in comparison to free cisplatin. Velinova *et al.* (2004) found that PC formulations display approximately similar cytotoxic activities as free cisplatin, whereas PS-containing formulation exhibits increased cytotoxic activity when compared to free drug. Furthermore, Burger *et al*., 2002 used lipid nanoparticles loded with cisplatin and found that the *in vitro* cytotoxicity was up to 1000-fold higher than with the free drug.

Nanoparticle technology has the potential to leverage the EPR effect to enhance the selective accumulation of cisplatin in tumour cells and to minimize toxicities *in vivo* (Guo *et al*., 2013). In this chapter, it was observed that TPT-NIVs alone was superior in achieving greater cytotoxicity than free TPT alone, whereas cisplatin-NIVs appeared to be superior to free cisplatin at only one dose (125nM). In contrast to single agents NIVs, the combination therapy showed that the NIV formulations of cisplatin in combination with TPT had similar cytotoxicity effects

of free drugs with an exception of one NIV combination dose (20nM TPT combined with 125nM cisplatin) tested on A549, this was odd that it was at some doses only and while this was achieved in replicate experiments the reason for this are unclear and require further interrogation in future work. The results in this chapter showed that treatment with cisplatin NIV formulations were superior with significant reductions at some doses in the survival fraction of A549 and H460 cells when compared with free drugs. One of the major obstacles of cisplatin for most formulation methods is its poor solubility in either organic or aqueous solutions (Souza *et al*., 2011b). Lee *et al*. (2010) encapsulated cisplatin with a lipid to stabilize the formulation for dispersion in an aqueous solution with the presence of 1,2-dioleoyl-sn-glycero-3-phosphate (DOPA). This cisplatin encapsulation significantly improved cell uptake and *in vitro* cytotoxicity.

In addition, previous studies by Li *et al.* (2006) and Souza *et al*. (2011a) were in agreement with TPT-NIVs results in this chapter. Li *et al*. (2006) concluded that the nanoencapsulation of TPT provided 90% enhancement of cytotoxic effects. Drummond *et al*. (2010) showed that a liposomal TPT formulation improved cell uptake under physiological conditions and, as a result, increased cytotoxic effects. As discussed earlier in chapter 5, the active lactone ring of TPT can be converted to the inactive carboxylate form due to a hydrolytic conversion caused by physiological pH (Hao *et al.*, 2010, Davies *et al*., 1997). The lactone form can be protected and this conversion can be prevented in an aqueous solution (Burke *et al*., 1993). Therefore, in this study, the improved TPT NIVs' cytotoxic effects against H460 and A549 cells observed at some doses using lipid encapsulation can potentially be attributed to both protection of the TPT lactone ring and an

increase in cellular uptake of TPT. In support of this, Souza *et al*. (2011b) measured *in vitro* release of lipid nanoparticles loaded with TPT and showed that after 2h of treatment lipid nanoparticles has not released TPT, but after 24h TPT was completely released from the nanoparticles. Therefore, at this stage, TPT was released into the acidic environment of the cytoplasmic organelles involved in the phagocytosis process resulting in an increase of TPT cellular uptake (Souza *et al*., 2011b) .

Chapter 6 . *In Vitro* Assessment of Non-Ionic Surfactant Vesicle (NIV) Formulations: Predicting Pulmonary Drug Deposition

6.1 Introduction

Lung cancer treatment by inhalation is more effective than parenteral injection due to its ability to target lung diseases specifically and its ability in concentrating the effect of toxic drugs to the lungs rather than systematic exposure (Kuzmov and Minko, 2015). Furthermore, pulmonary drug delivery avoids the first pass metabolism enzymes such as CYP450 by the liver (Patil and Sarasija, 2012, Carter and Puig, 2015).

The clinical effectiveness of a pulmonary drug delivery system depends on the capability of this system to generate residual particles (≤ 5 μm) that can efficiently deposit in the appropriate site of action within the lungs whereas larger particle size will be filtered and removed out of the lungs (Evans and Koo, 2009, Patil and Sarasija, 2012). Normally, during nebulization drug particles will deposit gradually depending on particle size from large to small in the primary bronchi, bronchi, terminal bronchi and finally the alveoli (Paranjpe and Müller, 2014). Pulmonary drug delivery also requires production of a safe and stable formulation that is capable of escaping the innate defence mechanisms in the lungs, such as mucociliary clearance and macrophage uptake before it reaches its target site of action within the lungs (Iyer *et al.*, 2015, Wenzler *et al*., 2016). Therefore, in this chapter delivering small particles (≤ 5 μm) indicate a successful formulation that able to escape the innate defence system of the lungs.

Previous research has shown that particle size and solubility are both physicochemical factors that potentially affect drug deposition within the lungs

during nebulization (El-Sherbiny *et al*., 2015). The smaller the particle size (≤ 5 μm), the more nanoparticles will be deposited into the micron-size aerosol droplets, thereby enhancing the delivery of the drug to the deep lung because of increased diffusional mobility, and the rate of drug absorption increases by providing more uniform drug distribution (Yang *et al*., 2008, Youngren-Ortiz e*t al.*, 2016). Therefore, our target delivery area of the lungs is the alveolar system because it is well connected to the systemic circulation via the pulmonary circulation system where the transepithelial drug transport takes place more effectively due to the presence of alveolar epithelial cells, the pulmonary blood-gas system, and the size of the pores (Palecanda and Kobzik, 2001, Patil and Sarasija, 2012).

Therefore, in this chapter we aimed l to determine the in *vitro* drug deposition and the aerosol particle size distribution (APSD) profiles of both TPT-NIVs and non-encapsulated TPT using an *in vitro* simulator device such as a Next Generation Impactor (NGI). However, cisplatin drug deposition patterns were not investigated in this study because previous research had been previously conducted by research colleagues at SIPBS and the results presented by Puig (2016).

6.1.1 Next Generation Impactor (NGI)

Measurements of aerosol particle size in *vitro* can be made using a lung simulator apparatus such as a Next Generation Impactor (NGI) as shown in Figure 6.1, which is the latest impactor described in the European Pharmacopoeia (Nichols *et al*., 2013). An NGI has seven stages and a micro orifice collector and is the only impactor that works horizontally to collect the aerosol droplets in cups of different cut-off diameters in which the aerosol separates into different size ranges depending on where it deposits in the impactor sections (Carter and Puig-Sellart, 2016). The aerosolised formulation is carried by the airflow inside the NGI and particles impact on a flat collecting plate present in each section. The NGI acts as synthetic lungs in relation to drug particles deposition, where particles with a high inertial force collide with the first stages of the NGI and are captured, whereas smaller particles are deposited in the lower stages (Mitchell *et al.*, 2007).

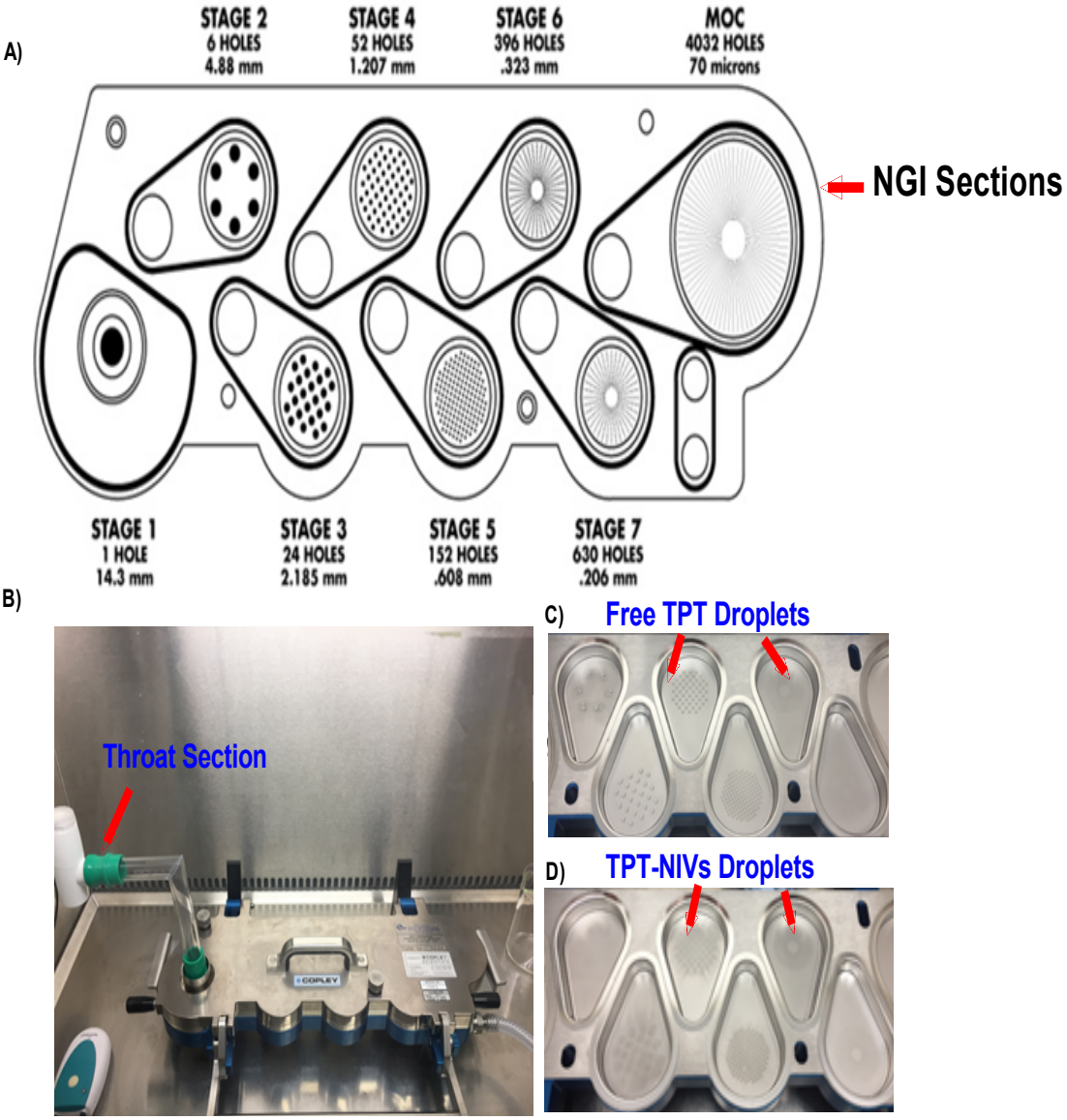

Figure 6.1 Next Generation Impactor. A) Schematic diagram showing sections in the NGI. The throat section simulates the mouth and throat. Trachea, bronchi and bronchioles are simulated by the NGI stages (Guo *et al*., 2008; Menzies *et al.,* 2007; Roberts and Romay, 2005). B) The NGI used in this project showing the invented simulator throat. C) Free TPT aerosol droplets deposited in NGI sections. D) TPT-NIV aerosol droplets deposited in NGI sections.

The NGI provides essential data that enables calculation of the aerodynamic aerosol size distribution after nebulizing an aerosolised formulation. From the particle size distribution data, two major indexes can be measured: the mass median aerodynamic diameter (MMAD) and fine particle fraction (FPF%). The MMAD of an active drug is the diameter at which 50% of the particles by mass are bigger than the other 50%. The MMAD is calculated when the log-normal distribution of the mass-weighted data is assumed by plotting a base ten logarithm cut-off diameter against cumulative percentage undersize (Carter and Puig-Sellart, 2016). Fine particle fraction (FPF < 5 μm) is the fraction of the aerosol mass contained in particles with an aerodynamic diameter smaller than 5 μm and larger than 0.98 μm. Achieving a low MMAD indicates a fine aerosol size with a tight size distribution. Electrostatic charge and fine particle adhesion on the walls of the apparatus and losses between stages may also disturb particle collection (Carter and Puig-Sellart, 2016).

6.2 Aims

The main aim was to use the next generation impactor (NGI) as an in *vitro* model to determine the lung drug deposition and the aerosol particle size distribution (APSD) profiles of TPT-NIVs and TPT aerosol solutions. From the particle size distribution, two major indexes were measured: MMAD and FPF%.

6.3 Results

6.3.1 Prediction of *in vitro* lung drug delivery and deposition

In order to determine the drug deposition by inhalation, an aerosol formulation containing 200 µg/ml 5% tartaric acid in 0.9% NaCl of either TPT NIVs or TPT solution were formulated as described in section 2.12. The aerosol was nebulized with a mesh nebulizer (Aerogen), and a breath simulator (throat section) was invented by a colleague (Abiy Desta) for this study to simulating the throat and passageway. A total of 1 ml of a formulation was nebulized over 1.20 minutes. An *in vitro* simulated lung model (NGI) was used to collect the aerosol particle size (aerosol formulation) of the active ingredient and then HPLC used to quantify the concentration of TPT that was deposited in each section of the NGI. For the aerosol particle size distribution, a major index was determined: FPF% (fine particle fraction) which represented the amount of aerosolized delivered drug in which the diameter was less than or equal to 5 µm. Particles of this size were considered to be respirable.

6.3.2.1 Determination of aerodynamic particle size distribution of TPT NIVs and TPT solution

The aerosol particle size distribution (APSD) profiles of TPT NIVs and TPT aerosol solutions from stage 1 to micro-orifice collector (MOC) are shown in Figure 6.4A. Figure 6.4B shows the APSD including the drug deposition in the invented breath simulator (throat and passageway).

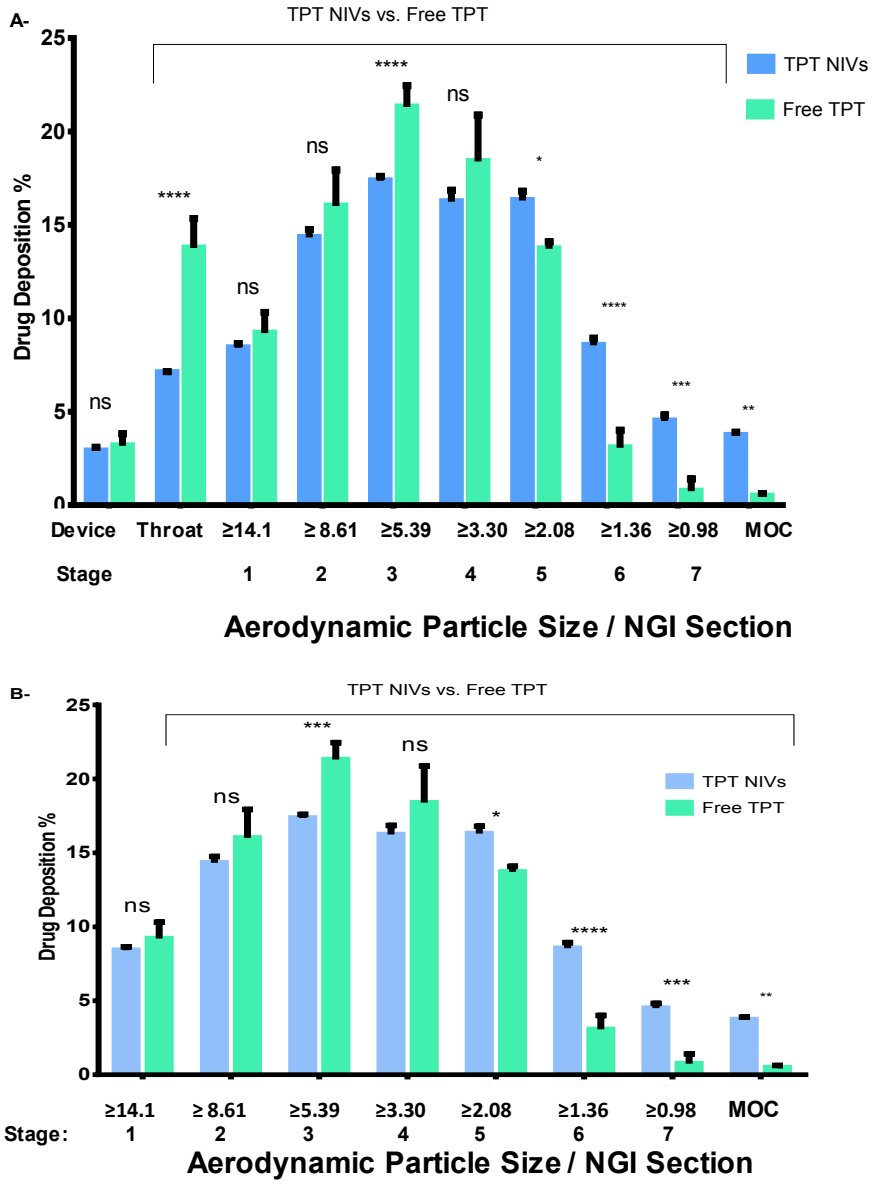

Figure 6.2 *In vitro* pulmonary drug deposition rate for TPT NIVs and free TPT solution in different stages.

The nebulization efficiency of the two formulations was evaluated using NGI. An aerosol formulation containing 200 µg/ml 5% tartaric acid in 0.9% NaCl of either niosomal topotecan or topotecan solution were nebulized over 1.20 minutes using a mesh nebulizer (Aerogen). T-test was used to statistically compare means of drug deposition of TPT NIVS with free TPT. ** = $p < 0.01$; *** = $p < 0.001$; **** = $p < 0.0001$; ns = no significance. Data are expressed as mean ± SD, n = 3.

Significant differences in the drug concentration and size distribution of the aerosols between the two formulations across NGI sections were found (Figure 6.4). The total active drug deposited in the lung with niosomal topotecan and topotecan solution were 176.48 µg (± 6.6) and 164.9 µg (± 3.7), respectively. It was observed at the throat and stage 3 (particle size > 5 µm) that the percentage of free TPT deposition was significantly higher than TPT-NIVs ($p < 0.0001$). At the throat, free TPT deposition was 13.76% (± 1.57, 22.69 µg) and TPT NIVs was 7.09% (± 0.04, 12.51 µg). At stage 3, free TPT deposition was 21.31% (± 1.14, 35.14 µg) and TPT NIVs 17.36% (± 0.238, 30.63 µg).

Interestingly, it was observed that TPT NIV deposition increased as the aerodynamic particle size decreased (≤ 2 µm). There were statistically significant differences in the drug deposition of TPT NIVs (16.30% ± 0.49, 28.76 µg) compared with free TPT (13.71% ± 0.37, 22.60 µg) at stage 5 (3.30-2.08 µm) ($p < 0.05$). Similarly, at stage 6 (2.08-1.36 µm) there was a significantly higher deposition of TPT NIVs (8.55% ±0.037, 15.08 µg) when compared with free TPT (3.06% ± 0.93, 5.04 µg) ($p < 0.0001$). At stage 7 (1.36-0.98 µm) there was a significantly higher deposition of TPT NIVs (4.50% ±0.031, 7.94 µg) when compared with free TPT (0.74% ± 0.65, 1.22 µg) ($p < 0.001$).

6.3.2.2 Determination of fine particle fraction (FPF %)

For calculating the fine particle fraction (FPF %), the data from the curve of drug deposition (Figure 6.2) in different stages of NGI was obtained. FPF% which represented the amount of aerosolized delivered drug in which the diameter was less than or equal to 5 µm. Particles of this size were considered to be respirable. FPF% results for both formulations are shown in Figure 6.3, and Table 6.1 show FPF%, and total drug deposition values.

Table 6.1 FPF% and drug deposition % values of TPT NIV formulation and free TPT. N = 3.

	FPF% (respirable)	**Total Drug Deposition %** **(Including device and throat)**
TPT NIV	49.34% (87.07 µg,± 6.12)	88.24 % (176.48 µg, ± 6.6)
TPT free	36.41 % (60.04 µg ,± 9.23)	82.46 % (164.92 µg, ± 3.7)

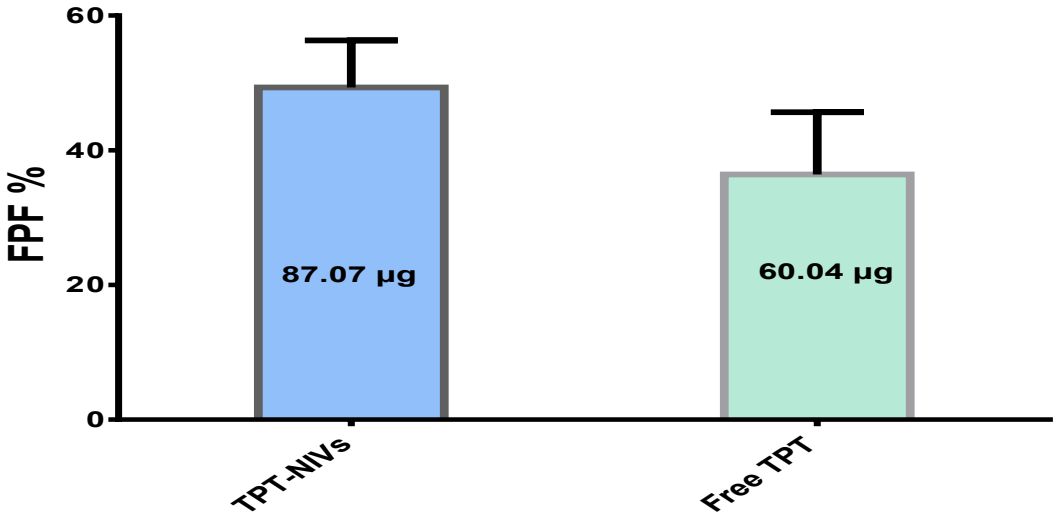

Figure 6.3 The FPF% of TPT NIVs and Free TPT

The FPF% of TPT NIVs was 49.34% (87.07µg, ± 6.12) and 36.41% (60.04 µg, ± 9.23) for free TPT aerosol. 49.34% of the TPT NIV formulation had a particle size of ≤ 5 µm indicating a successful delivery of respirable particles via simulated lung airways.

6.4 Discussion

It was vital to determine the drug deposition using a cascade impactor such as an NGI. Therefore, the second aim of this chapter was to determine the lung drug deposition and the aerosol particle size distribution (APSD) profiles of TPT NIVs and TPT aerosol solutions using an in *vitro* model such as NGI. Normally, during nebulization drug particles will gradually deposit in primary bronchi, bronchi, terminal bronchi and alveoli in accordance with the particle size from large to small, respectively (Mitchell and Nagel, 2004, Shekunov *et al*., 2007). Furthermore, drugs delivered in the upper airways of the lungs are inadequate due to a smaller surface area and minimal blood flow, as well as the presence of ciliated cells that cause propulsion of mucus out of the lung to clear foreign substances, resulting in a high capacity to filter and remove up to 90% of delivered drug particles (Evans and Koo, 2009, Patil and Sarasija, 2012). In contrast, 95% of the lung's surface area is made up of smaller airways and alveolar space and is well connected to the systemic circulation via the pulmonary circulation system. Here, transepithelial drug transport takes place more effectively due to the presence of alveolar epithelial cells, the pulmonary blood-gas system, and the size of the pores (Palecanda and Kobzik, 2001, Patil and Sarasija, 2012). Therefore, our target delivery area of the lungs is the alveolar system. The results in this chapter (Figure 6.2) showed significant differences in the amount and size distribution of the aerosols between the two formulations across NGI sections.

It was observed at the throat and stage 3 (particle size > 5 μm) that the percentage of free TPT deposition was significantly higher than TPT NIVs, whereas aerosol TPT NIVs ($p < 0.0001$) were deposited significantly more in stages with particle size < 5 μm when compared with free TPT solution. This suggests that TPT NIVs have a better ability to reach deeper into the lung. Particle size is one of the vital factors in the nebulization process; the smaller the particle size the more nanoparticles will be deposited into the micron-size aerosol droplets, thereby enhancing delivery of the drug to the deep lung because of the increased diffusional mobility (Mishra *et al.*, 2010). Another advantage of smaller particle size is that the rate of drug absorption increases by providing more uniform drug distribution (Yang *et al.*, 2008). From the characterisation study of TPT-NIVs conducted in chapter 5 that showed the particle size of TPT-NIVs was ranging 1.19 -1.26 μm, we can understand that TPT-NIVs had the potential to be deposited into micron-size aerosol droplets and eventually could deliver the drug into deeper champers of the NGI device more efficiently than free TPT.

Previous research showed that solubility as a physicochemical factor has the potential to affect the drug in the delivery system during nebulization: the air-flow may dry out aqueous particles leading to a large amount of drug particles being deposited on the early stages of a lung simulator device (O'Callaghan and Barry, 1997). The results in this chapter showed that encapsulating TPT with NIVs had a superior deposition efficiency in the deeper stages of the NGI compared with free TPT due to the presence of DCP and non-ionic surfactant in the NIV formulation which has a key role in reducing the inertial impaction between NIV

and enhancing the nebulisation efficiency. Chimote and Banerjee (2009) evaluated in *vitro* nebulization efficacy of isoniazid NIV formulation in comparison with free isoniazid using a lung simulator device. Chimote and Banerjee (2009) used dipalmitoylphosphatidylcholine (DPPC) as the surfactant lipid and showed that the NIV formulation had an improved capability to reduce the surface tension at the air-aqueous interface, resulting in a better spread of NIV into the lung simulating device and reaching deeper champers of device rather than adhering to the MP (throat) surface. Similarly, Pilcer *et al.* (2009) in a previous study using a different delivery system also showed that the addition of surfactant such as Na glycocholate had the potential to improve the deposition and dispersion properties of tobramycin nanosuspension into deeper parts of the MSLI device.

Therefore, the formulated TPT-NIVs in this research had the potential to be nebulised efficiently than free TPT in a targeting delivery system that is capable to reach the deeper size of lung simulating device and this can be further investigated in *in vivo* model to treat lung cancer tumour.

Chapter 7. Final Conclusions and Future Works

7.1 Final conclusions

The combination of cisplatin TPT as a double therapy confirmed a statistically significant decrease in the clonogenic survival of H460 in all of three schedules when compared to cisplatin or TPT alone indicating that TPT is a chemosinsitiser to cisplatin, further to this, the CI analysis showed a synergism interaction in all of the three schedules with CI values less than 1. However, the survival results for the combination of cisplatin and TPT on A549 cells showed a statistically significant deference in only schedule C (simultaneous administration of cisplatin and TPT) compared with cisplatin exposure alone. The in *vitro* investigations in this study of the CI between cisplatin and TPT in A549 cells underwent antagonistic effects in schedules A and B (CI > 1) and an additive to infra-additive effect was observed in schedule C. This observed synergistic interaction of cisplatin and TPT during simultaneous administration induced by the increased retention of DNA interstrand cross-links (ISCs) in the presence of topo I inhibitors. This combination may therefore have pharmacological implications in overcoming the cisplatin-induced resistance. Supporting this data, the results of the induction and repair of DNA damage by measurement of γ-H2AX foci in that confirmed a significant dose-dependent increase in γ-H2AX levels on H460 and A549 (Figure 3.8 and Figure 3.9, respectively) following cisplatin treatment alone it was observed that cisplatin induced DNA damage was significantly repaired after 24hrs. However, after combining TPT with cisplatin, the observed DNA damage repair was inhibited.

Cell exposure to cisplatin commonly results in G2/M phase arrest, which is induced and sustained by the transactivation of p53 genes as a result of exposure

to cisplatin while TPT results in S-phase and G2/M arrest. The results of the cell cycle analysis reported in this study confirmed that exposure to cisplatin alone resulted in G2/M arrest in a higher percentage of the cell population in H460 and A549 cell lines, whereas exposure to TPT alone resulted in S-phase and G2/M arrest in H460 and A549 cells. Interestingly, after combination treatment, there was a significant population of A549 cells were arrested in G1 and S-phase, and H460 cells displayed S and G2/M arrests. The arrest of cells at G1 phase in A549 cells minimises the population of cells that will enter S and G2/M phase. Nonetheless, the rationale for this observation is still unclear, as combinations are often still purely empirical.

The radiosensitisation potential of the triple therapy indicate that cisplatin and TPT act as radiosensitisers and the triple therapy of cisplatin and TPT in combination with radiation treatment showed a supra additive effect compared to double treatment of cisplatin and TPT in both cell lines, indicating that using triple therapy is in agreement with the initial hypothesis that aim to using low doses of triple therapy to achieve greater cytotoxicity than would be required to achieve therapeutic efficacy with a single agent while maintaining the potential antitumor activity, as an attempt to minimise the toxicities and the acquisition of cisplatin resistance.

Following NIVs characterization study, it was concluded that NIV formulation were capable of encapsulating cisplatin and TPT with an improved and stable physical properties such as uniform size distribution, charge and EE with no

apparent changes in the physical appearance were observed that could indicate colloidal system instability such as sedimentation and flocculation. The designed NIV formulations were effectively influenced the EPR effects improving cisplatin or TPT delivery in H460 and A549 cancer cells. As discussed earlier in chapter 5, the active lactone ring of TPT can be converted to the inactive carboxylate form due to a hydrolytic conversion caused by physiological pH (Hao *et al.*, 2010, Davies *et al*., 1997). The lactone form can be protected and this conversion can be prevented in an aqueous solution (Burke et al., 1993). Therefore, in this study, the improved TPT NIVs' cytotoxic effects against H460 and A549 cells observed at some doses using lipid encapsulation can be attributed to both protection of the TPT lactone ring and an increase in cellular uptake of TPT. Thus, the drug inhalation results (discussed in chapter 6) showed significant differences in the amount and size distribution in favour of the aerosols of TPT NIVs compared to free TPT solution. It was observed that aerosol TPT NIVs were deposited significantly more in stages with particle size < 5 μm when compared with free TPT solution, indicating that TPT NIVs have a better ability to reach deeper into the lung. Particle size is one of the vital factors in the nebulization process; the smaller the particle size the more nanoparticles will be deposited into the micron-size aerosol droplets, thereby enhancing delivery of the drug to the deep lung because of the increased diffusional mobility.

7.2 Future works

Future studies could start with addressing the problems that were reported to be associated with the present research and then expand research.

In characterisation studies, a 12 months stability study to study the physicochemical characters of TPT-NIVs would be recommended to assure best carrier system was designed. The use of an alternative methods, such as sonication or size extrusion, to reduce the particle size reduction of NIVs loaded with drugs.

It would be interesting to study cisplatin and TPT NIVs formulated with different type of surfactants and cholesterol concentrations to measure the change in size, charge and entrapment efficiency of these different formulations to recommend a suitable formulation technique when formulating NIVs. Visualisation using FFEM of the different NIVs formulations were not utilized in this study to define the structure and lamellarity of the vesicles studied. Therefore, it would be helpful to use these imaging techniques.

Chemical stability/reactivity study of cisplatin and TPT as a candidate to be co-formulated with each other would be important as an effective strategy to it was suggested to overcome the acquisition of cisplatin resistance, cisplatin to be combined and delivered simultaneously with TPT.

Pharmacokinetic study to determine the toxicities, distribution, metabolism, elimination of these drugs after pulmonary delivery using an in *vivo* model, would highly support the results of this study.

References

ABDELAZIZ, H. M., GABER, M., ABD-ELWAKIL, M. M., MABROUK, M. T., ELGOHARY, M. M., KAMEL, N. M., KABARY, D. M., FREAG, M. S., SAMAHA, M. W., MORTADA, S. M., ELKHODAIRY, K. A., FANG, J. Y. & ELZOGHBY, A. O. 2018. Inhalable particulate drug delivery systems for lung cancer therapy: Nanoparticles, microparticles, nanocomposites and nanoaggregates. *J Control Release,* 269**,** 374-392.

ABDELKADER, H., ALANI, A. W. & ALANY, R. G. 2014. Recent advances in non-ionic surfactant vesicles (niosomes): self-assembly, fabrication, characterization, drug delivery applications and limitations. *Drug Deliv,* 21**,** 87-100.

ADAMS, J. M. & CORY, S. 2007. The Bcl-2 apoptotic switch in cancer development and therapy. *Oncogene,* 26**,** 1324.

AG SELECI, D., SELECI, M., WALTER, J.-G., STAHL, F. & SCHEPER, T. 2016. Niosomes as Nanoparticular Drug Carriers: Fundamentals and Recent Applications. *Journal of Nanomaterials***,** 13.

AGNANTIS, N. J., PARASKEVAIDIS, E. & ROUKOS, D. 2004. Preventing Breast, Ovarian Cancer in BRCA Carriers: Rational of Prophylactic Surgery and Promises of Surveillance. *Annals of Surgical Oncology,* 11**,** 1030-1034.

AGUIRRE-GHISO, J. A. 2007. Models, mechanisms and clinical evidence for cancer dormancy. *Nat Rev Cancer,* 7**,** 834-46.

AHN, S. H., JEONG, E. H., LEE, T. G., KIM, S. Y., KIM, H. R. & KIM, C. H. 2014. Gefitinib induces cytoplasmic translocation of the CDK inhibitor

p27 and its binding to a cleaved intermediate of caspase 8 in non-small cell lung cancer cells. *Cell Oncol (Dordr),* 37**,** 377-86.

AHSAN, F., RIVAS, I. P., KHAN, M. A. & TORRES SUAREZ, A. I. 2002. Targeting to macrophages: role of physicochemical properties of particulate carriers--liposomes and microspheres--on the phagocytosis by macrophages. *J Control Release,* 79**,** 29-40.

AKUDUGU, J. M. & SLABBERT, J. P. 2008. Modulation of radiosensitivity in Chinese hamster lung fibroblasts by cisplatin. *Canadian Journal of Physiology and Pharmacology,* 86**,** 257-263.

ALAMGEER, M., GANJU, V. & WATKINS, D. N. 2013. Novel therapeutic targets in non-small cell lung cancer. *Curr Opin Pharmacol,* 13**,** 394-401.

ALCORN, S., WALKER, A. J., GANDHI, N., NARANG, A., WILD, A. T., HALES, R. K., HERMAN, J. M., SONG, D. Y., DEWEESE, T. L., ANTONARAKIS, E. S. & TRAN, P. T. 2013. Molecularly Targeted Agents as Radiosensitizers in Cancer Therapy—Focus on Prostate Cancer. *International Journal of Molecular Sciences,* 14**,** 14800-14832.

ALEXANDER, A., CAI, S.-L., KIM, J., NANEZ, A., SAHIN, M., MACLEAN, K. H., INOKI, K., GUAN, K.-L., SHEN, J., PERSON, M. D., KUSEWITT, D., MILLS, G. B., KASTAN, M. B. & WALKER, C. L. 2010. ATM signals to TSC2 in the cytoplasm to regulate mTORC1 in response to ROS. *Proceedings of the National Academy of Sciences,* 107**,** 4153-4158.

ALLALUNIS-TURNER, M. J., BARRON, G. M., DAY, R. S., 3RD, DOBLER, K. D. & MIRZAYANS, R. 1993. Isolation of two cell lines from a human

malignant glioma specimen differing in sensitivity to radiation and chemotherapeutic drugs. *Radiat Res,* 134**,** 349-54.

ALLEN, T. M. & CULLIS, P. R. 2013. Liposomal drug delivery systems: from concept to clinical applications. *Adv Drug Deliv Rev,* 65**,** 36-48.

ALSAADI, M. 2011. *Non-ionic surfactant vesicles as a delivery system for cisplatin.* Ph.D, Strathclyde University.

ALSAADI, M. M., CHRISTINE CARTER, K. & MULLEN, A. B. 2013. High performance liquid chromatography with evaporative light scattering detection for the characterisation of a vesicular delivery system during stability studies. *Journal of Chromatography A,* 1320**,** 80-85.

AMIRI, B., AHMADVAND, H., FARHADI, A., NAJMAFSHAR, A., CHIANI, M. & NOROUZIAN, D. 2018. Delivery of vinblastine-containing niosomes results in potent in vitro/in vivo cytotoxicity on tumor cells. *Drug Dev Ind Pharm,* 44**,** 1371-1376.

AMMAR, H. O., HAIDER, M., IBRAHIM, M. & EL HOFFY, N. M. 2017a. In vitro and in vivo investigation for optimization of niosomal ability for sustainment and bioavailability enhancement of diltiazem after nasal administration. *Drug Delivery,* 24**,** 414-421.

AMMAR, H. O., HAIDER, M., IBRAHIM, M. & EL HOFFY, N. M. 2017b. In vitro and in vivo investigation for optimization of niosomal ability for sustainment and bioavailability enhancement of diltiazem after nasal administration. *Drug Deliv,* 24**,** 414-421.

ANABOUSI, S., BAKOWSKY, U., SCHNEIDER, M., HUWER, H., LEHR, C. M. & EHRHARDT, C. 2006. In vitro assessment of transferrin-conjugated

liposomes as drug delivery systems for inhalation therapy of lung cancer. *Eur J Pharm Sci,* 29**,** 367-74.

ANAND, P., KUNNUMAKARA, A. B., SUNDARAM, C., HARIKUMAR, K. B., THARAKAN, S. T., LAI, O. S., SUNG, B. & AGGARWAL, B. B. 2008. Cancer is a Preventable Disease that Requires Major Lifestyle Changes. *Pharmaceutical Research,* 25**,** 2097-2116.

ANDRADE, F., DAS NEVES, J., GENER, P., SCHWARTZ, S., JR., FERREIRA, D., OLIVA, M. & SARMENTO, B. 2015. Biological assessment of self-assembled polymeric micelles for pulmonary administration of insulin. *Nanomedicine,* 11**,** 1621-31.

APEL, A., HERR, I., SCHWARZ, H., RODEMANN, H. P. & MAYER, A. 2008. Blocked Autophagy Sensitizes Resistant Carcinoma Cells to Radiation Therapy. *Cancer Research,* 68**,** 1485-1494.

ARZANI, G., HAERI, A., DAEIHAMED, M., BAKHTIARI-KABOUTARAKI, H. & DADASHZADEH, S. 2015. Niosomal carriers enhance oral bioavailability of carvedilol: effects of bile salt-enriched vesicles and carrier surface charge. *International Journal of Nanomedicine,* 10**,** 4797-4813.

ASAKA-AMANO, Y., TAKIGUCHI, Y., YATOMI, M., KUROSU, K., KASAHARA, Y., TANABE, N., TATSUMI, K. & KURIYAMA, T. 2007. Effect of Treatment Schedule on the Interaction of Cisplatin and Radiation in Human Lung Cancer Cells. *Radiation Research,* 167**,** 637-644.

AUBREY, B. J., KELLY, G. L., JANIC, A., HEROLD, M. J. & STRASSER, A. 2017. How does p53 induce apoptosis and how does this relate to p53-mediated tumour suppression? *Cell Death And Differentiation,* 25**,** 104.

AZHAR SHEKOUFEH BAHARI, L. & HAMISHEHKAR, H. 2016. The Impact of Variables on Particle Size of Solid Lipid Nanoparticles and Nanostructured Lipid Carriers; A Comparative Literature Review. *Advanced Pharmaceutical Bulletin,* 6**,** 143-151.

BAERLOCHER, G. M., OPPLIGER LEIBUNDGUT, E., OTTMANN, O. G., SPITZER, G., ODENIKE, O., MCDEVITT, M. A., RÖTH, A., DASKALAKIS, M., BURINGTON, B., STUART, M. & SNYDER, D. S. 2015. Telomerase Inhibitor Imetelstat in Patients with Essential Thrombocythemia. *New England Journal of Medicine,* 373**,** 920-928.

BAILLIE, A. J., COOMBS, G. H., DOLAN, T. F. & LAURIE, J. 1986. Non-ionic surfactant vesicles, niosomes, as a delivery system for the anti-leishmanial drug, sodium stibogluconate. *J Pharm Pharmacol,* 38**,** 502-5.

BANIN, S., MOYAL, L., SHIEH, S., TAYA, Y., ANDERSON, C. W., CHESSA, L., SMORODINSKY, N. I., PRIVES, C., REISS, Y., SHILOH, Y. & ZIV, Y. 1998. Enhanced phosphorylation of p53 by ATM in response to DNA damage. *Science,* 281**,** 1674-7.

BARNUM, K. J. & O'CONNELL, M. J. 2014. Cell Cycle Regulation by Checkpoints. *Methods in molecular biology (Clifton, N.J.),* 1170**,** 29-40.

BARR, M. P., GRAY, S. G., HOFFMANN, A. C., HILGER, R. A., THOMALE, J., O'FLAHERTY, J. D., FENNELL, D. A., RICHARD, D., O'LEARY, J. J. & O'BYRNE, K. J. 2013. Generation and characterisation of cisplatin-resistant non-small cell lung cancer cell lines displaying a stem-like signature. *PLoS One,* 8**,** e54193.

BARSOUM, N. & KLEEMAN, C. 2002. Now and then, the history of parenteral fluid administration. *Am J Nephrol,* 22**,** 284-9.

BARTEK, J. & LUKAS, J. 2007. DNA damage checkpoints: from initiation to recovery or adaptation. *Curr Opin Cell Biol,* 19**,** 238-45.

BARTELDS, R., NEMATOLLAHI, M. H., POLS, T., STUART, M. C. A., PARDAKHTY, A., ASADIKARAM, G. & POOLMAN, B. 2018. Niosomes, an alternative for liposomal delivery. *PLoS ONE,* 13**,** e0194179.

BASKAR, R. 2010. Emerging role of radiation induced bystander effects: Cell communications and carcinogenesis. *Genome Integr,* 1**,** 13.

BASKAR, R., DAI, J., WENLONG, N., YEO, R. & YEOH, K.-W. 2014. Biological response of cancer cells to radiation treatment. *Frontiers in Molecular Biosciences,* 1**,** 24.

BASKAR, R., LEE, K. A., YEO, R. & YEOH, K.-W. 2012. Cancer and Radiation Therapy: Current Advances and Future Directions. *International Journal of Medical Sciences,* 9**,** 193-199.

BASOURAKOS, S. P., LI, L., APARICIO, A. M., CORN, P. G., KIM, J. & THOMPSON, T. C. 2017. Combination Platinum-based and DNA Damage Response-targeting Cancer Therapy: Evolution and Future Directions. *Current medicinal chemistry,* 24**,** 1586-1606.

BATES, J. H. T. 2009. *Lung Mechanics: An Inverse Modeling Approach,* Cambridge, Cambridge University Press.

BECK-BROICHSITTER, M., MERKEL, O. M. & KISSEL, T. 2012. Controlled pulmonary drug and gene delivery using polymeric nano-carriers. *J Control Release,* 161**,** 214-24.

BERA, B. 2015. Nanoporous Silicon Prepared by Vapour Phase Strain Etch and Sacrificial Technique. *IJCA Proceedings on International Conference on Microelectronic Circuit and System,* MICRO 2015**,** 42-45.

BHATTACHARJEE, S. 2016. DLS and zeta potential – What they are and what they are not? *Journal of Controlled Release,* 235**,** 337-351.

BOECKMAN, H. J., TREGO, K. S., HENKELS, K. M. & TURCHI, J. J. 2005a. Cisplatin sensitizes cancer cells to ionizing radiation via inhibition of non-homologous end joining. *Mol Cancer Res,* 3**,** 277-85.

BOECKMAN, H. J., TREGO, K. S. & TURCHI, J. J. 2005b. Cisplatin Sensitizes Cancer Cells to Ionizing Radiation via Inhibition of Nonhomologous End Joining. *Molecular Cancer Research,* 3**,** 277-285.

BRAMBILLA, C., PUGATCH, B., GEISINGER, K. & AL, E. 2004. Tumours of the lung. Large cell carcinoma. Lyon: IARC.

BROUSTAS, C. G. & LIEBERMAN, H. B. 2014. DNA Damage Response Genes and the Development of Cancer Metastasis. *Radiation research,* 181**,** 111-130.

BROWN, J. M. & WOUTERS, B. G. 1999. Apoptosis, p53, and tumor cell sensitivity to anticancer agents. *Cancer Res,* 59**,** 1391-9.

BROWN, J. S. 2015. Chapter 27 - Deposition of Particles. *In:* PARENT, R. A. (ed.) *Comparative Biology of the Normal Lung (Second Edition).* San Diego: Academic Press.

BULBAKE, U., DOPPALAPUDI, S., KOMMINENI, N. & KHAN, W. 2017. Liposomal Formulations in Clinical Use: An Updated Review. *Pharmaceutics,* 9.

BURGER, K. N. J., STAFFHORST, R. W. H. M., DE VIJLDER, H. C., VELINOVA, M. J., BOMANS, P. H., FREDERIK, P. M. & DE KRUIJFF, B. 2002. Nanocapsules: lipid-coated aggregates of cisplatin with high cytotoxicity. *Nature Medicine,* 8**,** 81.

BURKE, T. G., MISHRA, A. K., WANI, M. C. & WALL, M. E. 1993. Lipid bilayer partitioning and stability of camptothecin drugs. *Biochemistry,* 32**,** 5352-5364.

BUSH, W. S. & MOORE, J. H. 2012. Chapter 11: Genome-Wide Association Studies. *PLoS Computational Biology,* 8**,** e1002822.

BUXTON, D. B. 2009. Nanomedicine for the management of lung and blood diseases. *Nanomedicine (Lond),* 4**,** 331-9.

BUZEA, C., PACHECO, II & ROBBIE, K. 2007. Nanomaterials and nanoparticles: sources and toxicity. *Biointerphases,* 2**,** MR17-71.

BYRNE, J. D., BETANCOURT, T. & BRANNON-PEPPAS, L. 2008. Active targeting schemes for nanoparticle systems in cancer therapeutics. *Adv Drug Deliv Rev.* Netherlands.

ÇAĞDAŞ., M., SEZER., A. D. & BUCAK., S. 2014. *Liposomes as Potential Drug Carrier Systems for Drug Delivery, Application of Nanotechnology in Drug Delivery,* Turkey, InTech.

CALSOU, P. & SALLES, B. 1993. Role of DNA repair in the mechanisms of cell resistance to alkylating agents and cisplatin. *Cancer Chemother Pharmacol,* 32**,** 85-9.

CAMIDGE, D. R., PAO, W. & SEQUIST, L. V. 2014. Acquired resistance to TKIs in solid tumours: learning from lung cancer. *Nature Reviews Clinical Oncology,* 11**,** 473.

CAPRANICO, G., MARINELLO, J. & CHILLEMI, G. 2017. Type I DNA Topoisomerases. *Journal of Medicinal Chemistry,* 60**,** 2169-2192.

CARTER, K. & PUIG, M. 2015. Nanocarriers made from non-ionic surfactants or natural polymers for pulmonary drug delivery. *strathprints:56154*.

CARTER, K. C. & PUIG-SELLART, M. 2016. Nanocarriers Made from Non-Ionic Surfactants or Natural Polymers for Pulmonary Drug Delivery. *Curr Pharm Des,* 22**,** 3324-31.

CHAACHOUAY, H., OHNESEIT, P., TOULANY, M., KEHLBACH, R., MULTHOFF, G. & RODEMANN, H. P. 2011. Autophagy contributes to resistance of tumor cells to ionizing radiation. *Radiother Oncol,* 99**,** 287-92.

CHAN, B. A. & HUGHES, B. G. M. 2015. Targeted therapy for non-small cell lung cancer: current standards and the promise of the future. *Translational Lung Cancer Research,* 4**,** 36-54.

CHANG, D. K., LIN, C. T., WU, C. H. & WU, H. C. 2009. A novel peptide enhances therapeutic efficacy of liposomal anti-cancer drugs in mice models of human lung cancer. *PLoS One,* 4**,** e4171.

CHEN, M., ZHANG, J., YU, S., WANG, S., ZHANG, Z., CHEN, J., XIAO, J. & WANG, Y. 2012. Anti-Lung-Cancer Activity and Liposome-Based Delivery Systems of β-Elemene. *Evidence-Based Complementary and Alternative Medicine,* 2012**,** 5.

CHENG, N., CHYTIL, A., SHYR, Y., JOLY, A. & MOSES, H. L. 2008. Transforming Growth Factor-β Signaling–Deficient Fibroblasts Enhance Hepatocyte Growth Factor Signaling in Mammary Carcinoma Cells to Promote Scattering and Invasion. *Molecular Cancer Research,* 6**,** 1521-1533.

CHHEANG, S. & BROWN, K. 2013. Lung Cancer Staging: Clinical and Radiologic Perspectives. *Seminars in Interventional Radiology,* 30**,** 99-113.

CHIMOTE, G. & BANERJEE, R. 2009. Evaluation of antitubercular drug-loaded surfactants as inhalable drug-delivery systems for pulmonary tuberculosis. *J Biomed Mater Res A,* 89**,** 281-92.

CHO, J., CHEN, L., SANGJI, N., OKABE, T., YONESAKA, K., FRANCIS, J. M., FLAVIN, R. J., JOHNSON, W., KWON, J., YU, S., GREULICH, H., JOHNSON, B. E., ECK, M. J., JÄNNE, P. A., WONG, K.-K. & MEYERSON, M. 2013. Cetuximab Response of Lung Cancer–Derived EGF Receptor Mutants Is Associated with Asymmetric Dimerization. *Cancer Research,* 73**,** 6770-6779.

CHONO, S., TANINO, T., SEKI, T. & MORIMOTO, K. 2006. Influence of particle size on drug delivery to rat alveolar macrophages following pulmonary administration of ciprofloxacin incorporated into liposomes. *J Drug Target,* 14**,** 557-66.

COLLADO, M. & SERRANO, M. 2010. Senescence in tumours: evidence from mice and humans. *Nature Reviews Cancer,* 10**,** 51.

D'ANNESSA, I., COLETTA, A., SUTTHIBUTPONG, T., MITCHELL, J., CHILLEMI, G., HARRIS, S. & DESIDERI, A. 2014. Simulations of DNA topoisomerase 1B bound to supercoiled DNA reveal changes in the flexibility pattern of the enzyme and a secondary protein–DNA binding site. *Nucleic Acids Research,* 42**,** 9304-9312.

DANAEI, M., DEHGHANKHOLD, M., ATAEI, S., HASANZADEH DAVARANI, F., JAVANMARD, R., DOKHANI, A., KHORASANI, S. & MOZAFARI, M. R. 2018a. Impact of Particle Size and Polydispersity Index on the Clinical Applications of Lipidic Nanocarrier Systems. *Pharmaceutics,* 10**,** 57.

DANAEI, M., DEHGHANKHOLD, M., ATAEI, S., HASANZADEH DAVARANI, F., JAVANMARD, R., DOKHANI, A., KHORASANI, S. & MOZAFARI, M. R. 2018b. Impact of Particle Size and Polydispersity Index on the Clinical Applications of Lipidic Nanocarrier Systems. *Pharmaceutics,* 10.

DASARI, S. & TCHOUNWOU, P. B. 2014. Cisplatin in cancer therapy: molecular mechanisms of action. *European journal of pharmacology,* 0**,** 364-378.

DAVIES, B. E., MINTHORN, E. A., DENNIS, M. J., ROSING, H. & BEIJNEN, J. H. 1997. The Pharmacokinetics of Topotecan and Its Carboxylate Form Following Separate Intravenous Administration to the Dog. *Pharmaceutical Research,* 14**,** 1461-1465.

DELBALDO, C., MICHIELS, S., SYZ, N., SORIA, J. C., LE CHEVALIER, T. & PIGNON, J. P. 2004. Benefits of adding a drug to a single-agent or a 2-agent chemotherapy regimen in advanced non-small-cell lung cancer: a meta-analysis. *Jama,* 292**,** 470-84.

DEMCHENKO, A. P. 2013. Beyond annexin V: fluorescence response of cellular membranes to apoptosis. *Cytotechnology,* 65**,** 157-172.

DEVALAPALLY, H., CHAKILAM, A. & AMIJI, M. M. 2007. Role of nanotechnology in pharmaceutical product development. *J Pharm Sci,* 96**,** 2547-65.

DOLLING, J. A., BOREHAM, D. R., BROWN, D. L., MITCHEL, R. E. & RAAPHORST, G. P. 1998. Modulation of radiation-induced strand break repair by cisplatin in mammalian cells. *Int J Radiat Biol,* 74**,** 61-9.

DONG, Y., ZHOU, L., TIAN, Q., ZHENG, Y. & SANCHE, L. 2017a. Chemoradiation Cancer Therapy: Molecular Mechanisms of Cisplatin Radiosensitization. *The Journal of Physical Chemistry C,* 121**,** 17505-17513.

DONG, Y. D., TCHUNG, E., NOWELL, C., KAGA, S., LEONG, N., MEHTA, D., KAMINSKAS, L. M. & BOYD, B. J. 2017b. Microfluidic preparation of drug-loaded PEGylated liposomes, and the impact of liposome size on tumour retention and penetration. *J Liposome Res***,** 1-9.

DRUMMOND, D. C., NOBLE, C. O., GUO, Z., HAYES, M. E., CONNOLLY-INGRAM, C., GABRIEL, B. S., HANN, B., LIU, B., PARK, J. W., HONG, K., BENZ, C. C., MARKS, J. D. & KIRPOTIN, D. B. 2010. Development of a highly stable and targetable nanoliposomal formulation of topotecan. *J Control Release,* 141**,** 13-21.

DUNCAN, R. 2003. The dawning era of polymer therapeutics. *Nat Rev Drug Discov.* England.

EL-SHERBINY, I. M., EL-BAZ, N. M. & YACOUB, M. H. 2015. Inhaled nano- and microparticles for drug delivery. *Global Cardiology Science & Practice,* 2015**,** 2.

ELDER, A., VIDYASAGAR, S. & DELOUISE, L. 2009. Physicochemical Factors that Affect Metal and Metal Oxide Nanoparticle Passage Across Epithelial Barriers. *Wiley Interdiscip Rev Nanomed Nanobiotechnol,* 1**,** 434-50.

ELKIND, M. E. & WHITMORE, G. F. 1967. *In vitro survival curves,* New York, Gordon and Breach.

ELMORE, S. 2007. Apoptosis: A Review of Programmed Cell Death. *Toxicologic pathology,* 35**,** 495-516.

ETTINGER, D. S., AKERLEY, W., BORGHAEI, H., CHANG, A. C., CHENEY, R. T., CHIRIEAC, L. R., D'AMICO, T. A., DEMMY, T. L., GOVINDAN, R., GRANNIS, F. W., JR., GRANT, S. C., HORN, L., JAHAN, T. M., KOMAKI, R., KONG, F. M., KRIS, M. G., KRUG, L. M., LACKNER, R. P., LENNES, I. T., LOO, B. W., JR., MARTINS, R., OTTERSON, G. A., PATEL, J. D., PINDER-SCHENCK, M. C., PISTERS, K. M., RECKAMP, K., RIELY, G. J., ROHREN, E., SHAPIRO, T. A., SWANSON, S. J., TAUER, K., WOOD, D. E., YANG, S. C., GREGORY, K. & HUGHES, M. 2013. Non-small cell lung cancer, version 2.2013. *J Natl Compr Canc Netw,* 11**,** 645-53; quiz 653.

EVANS, C. M. & KOO, J. S. 2009. Airway mucus: the good, the bad, the sticky. *Pharmacol Ther,* 121**,** 332-48.

EYVAZZADEH, N., NESHASTEH-RIZ, A. & MAHDAVI, S. R. 2015. DNA Damage of Glioblastoma Multiform Cells Induced by Beta Radiation of Iodine-131 in The Presence or Absence of Topotecan: A Picogreen and Colonogenic Assay. *Cell Journal (Yakhteh),* 17**,** 99-110.

FALCK, J., MAILAND, N., SYLJUASEN, R. G., BARTEK, J. & LUKAS, J. 2001. The ATM-Chk2-Cdc25A checkpoint pathway guards against radioresistant DNA synthesis. *Nature,* 410**,** 842-7.

FARKONA, S., DIAMANDIS, E. P. & BLASUTIG, I. M. 2016. Cancer immunotherapy: the beginning of the end of cancer? *BMC Medicine,* 14**,** 73.

FASSBERG, J. & STELLA, V. J. 1992. A kinetic and mechanistic study of the hydrolysis of camptothecin and some analogues. *J Pharm Sci,* 81**,** 676-84.

FENSKE, D. B., CHONN, A. & CULLIS, P. R. 2008. Liposomal nanomedicines: an emerging field. *Toxicol Pathol.* United States.

FINN, R. S., ALESHIN, A. & SLAMON, D. J. 2016. Targeting the cyclin-dependent kinases (CDK) 4/6 in estrogen receptor-positive breast cancers. *Breast Cancer Research,* 18**,** 17.

FISHLER, R., HOFEMEIER, P., ETZION, Y., DUBOWSKI, Y. & SZNITMAN, J. 2015. Particle dynamics and deposition in true-scale pulmonary acinar models. *Scientific Reports,* 5**,** 14071.

FLOREA, A.-M. & BÜSSELBERG, D. 2011. Cisplatin as an Anti-Tumor Drug: Cellular Mechanisms of Activity, Drug Resistance and Induced Side Effects. *Cancers,* 3**,** 1351-1371.

FONG, K., SEKIDO, Y., GAZDAR, A. & MINNA, J. 2003. Lung cancer: molecular biology of lung cancer: clinical implications. 58.

FRANKEN, N. A., OEI, A. L., KOK, H. P., RODERMOND, H. M., SMINIA, P., CREZEE, J., STALPERS, L. J. & BARENDSEN, G. W. 2013. Cell survival and radiosensitisation: modulation of the linear and quadratic parameters of the LQ model (Review). *Int J Oncol,* 42**,** 1501-15.

FUJIKANE, R., KOMORI, K., SEKIGUCHI, M. & HIDAKA, M. 2016. Function of high-mobility group A proteins in the DNA damage signaling for the induction of apoptosis. *Scientific Reports,* 6**,** 31714.

GABRIELA, A. L. & DANIELA, M. E. 2016. Treatment for small cell lung cancer, where are we now?—a review. *Translational Lung Cancer Research,* 5**,** 26-38.

GAZDAR, A. F. & BRAMBILLA, E. 2010. Preneoplasia of lung cancer. *Cancer biomarkers : section A of Disease markers,* 9**,** 385-396.

GELBARD, A., GARNETT, C. T., ABRAMS, S. I., PATEL, V., GUTKIND, J. S., PALENA, C., TSANG, K. Y., SCHLOM, J. & HODGE, J. W. 2006. Combination Chemotherapy and Radiation of Human Squamous Cell Carcinoma of the Head and Neck Augments CTL-Mediated Lysis. *Clin Cancer Res,* 12**,** 1897-905.

GERHARDS, N. M. & ROTTENBERG, S. 2018. New tools for old drugs: Functional genetic screens to optimize current chemotherapy. *Drug Resistance Updates,* 36**,** 30-46.

GERTH, M. & VOETS, I. K. 2017. Molecular control over colloidal assembly. *Chemical Communications,* 53**,** 4414-4428.

GROEN, H. J., SLEIJFER, S., MEIJER, C., KAMPINGA, H. H., KONINGS, A. W., DE VRIES, E. G. & MULDER, N. H. 1995. Carboplatin- and cisplatin-induced potentiation of moderate-dose radiation cytotoxicity in human lung cancer cell lines. *Br J Cancer,* 72**,** 1406-11.

GUNASEKARAN, T., HAILE, T., NIGUSSE, T. & DHANARAJU, M. D. 2014. Nanotechnology: an effective tool for enhancing bioavailability and bioactivity of phytomedicine. *Asian Pacific Journal of Tropical Biomedicine,* 4**,** S1-S7.

GUO, S., WANG, Y., MIAO, L., XU, Z., LIN, C. M., ZHANG, Y. & HUANG, L. 2013. Lipid-coated Cisplatin nanoparticles induce neighboring effect and exhibit enhanced anticancer efficacy. *ACS Nano,* 7**,** 9896-904.

GUPTA, S., KORU-SENGUL, T., ARNOLD, S. M., DEVI, G. R., MOHIUDDIN, M. & AHMED, M. M. 2011. Low-Dose Fractionated Radiation Potentiates the Effects of Cisplatin Independent of the Hyper-Radiation Sensitivity in Human Lung Cancer Cells. *Molecular Cancer Therapeutics,* 10**,** 292-302.

GURNEY, H. 2002. How to calculate the dose of chemotherapy. *British Journal of Cancer,* 86**,** 1297-1302.

GUTSCHNER, T. & DIEDERICHS, S. 2012. The hallmarks of cancer: A long non-coding RNA point of view. *RNA Biology,* 9**,** 703-719.

HAINAUT, P. & PLYMOTH, A. 2013. Targeting the hallmarks of cancer: towards a rational approach to next-generation cancer therapy. *Current Opinion in Oncology,* 25**,** 50-51.

HALL, E. J. 2000. *Cell survival curves,* Philadelphia, Lippincott.

HALL, E. J. 2007. Cancer caused by x-rays—a random event? *The Lancet Oncology,* 8**,** 369-370.

HANAHAN, D. & FOLKMAN, J. 1996. Patterns and Emerging Mechanisms of the Angiogenic Switch during Tumorigenesis. *Cell,* 86**,** 353-364.

HANAHAN, D. & WEINBERG, R. A. 2011a. Hallmarks of cancer: the next generation. *Cell,* 144**,** 646-74.

HANAHAN, D. & WEINBERG, ROBERT A. 2011b. Hallmarks of Cancer: The Next Generation. *Cell,* 144**,** 646-674.

HANAHAN., D. & WEINBERG., R. 2000. The hallmarks of cancer. Cell.

HAO, Y., ZHAO, F., LI, N., YANG, Y. & LI, K. 2002. Studies on a high encapsulation of colchicine by a niosome system. *Int J Pharm,* 244**,** 73-80.

HAO, Y. L., DENG, Y. J., CHEN, Y., HAO, A. J., ZHANG, Y. & WANG, K. Z. 2010. In-vitro cytotoxicity, in-vivo biodistribution and anti-tumour effect of PEGylated liposomal topotecan. *Journal of Pharmacy and Pharmacology,* 57**,** 1279-1287.

HEIN, A. L., OUELLETTE, M. M. & YAN, Y. 2014. Radiation-induced signaling pathways that promote cancer cell survival (review). *Int J Oncol,* 45**,** 1813-9.

HERMANN, R. M., RAVE-FRÄNK, M. & PRADIER, O. 2008. Combining radiation with oxaliplatin: A review of experimental results. *Cancer/Radiothérapie,* 12**,** 61-67.

HOFFMAN, SCHORGE, BRADSHAW, HALVORSON & CORTON 2016. Principles of Chemotherapy. Williams Gynecology.

HORITA, N., YAMAMOTO, M., SATO, T., TSUKAHARA, T., NAGAKURA, H., TASHIRO, K., SHIBATA, Y., WATANABE, H., NAGAI, K., INOUE, M., NAKASHIMA, K., USHIO, R., SHINKAI, M., KUDO, M. & KANEKO, T. 2015. Topotecan for Relapsed Small-cell Lung Cancer: Systematic Review and Meta-Analysis of 1347 Patients. *Scientific Reports,* 5**,** 15437.

HOUSMAN, G., BYLER, S., HEERBOTH, S., LAPINSKA, K., LONGACRE, M., SNYDER, N. & SARKAR, S. 2014. Drug Resistance in Cancer: An Overview. *Cancers,* 6**,** 1769-1792.

HUA, S. 2015. Lipid-based nano-delivery systems for skin delivery of drugs and bioactives. *Frontiers in Pharmacology,* 6**,** 219.

HUANG, C.-Y., JU, D.-T., CHANG, C.-F., MURALIDHAR REDDY, P. & VELMURUGAN, B. K. 2017. A review on the effects of current chemotherapy drugs and natural agents in treating non–small cell lung cancer. *BioMedicine,* 7**,** 23.

HUANG, L. & FU, L. 2015. Mechanisms of resistance to EGFR tyrosine kinase inhibitors. *Acta Pharmaceutica Sinica B,* 5**,** 390-401.

HUNG, L. B., PARCHER, J. F., SHORES, J. C. & WARD, E. H. 1988. Theoretical and experimental foundation for surface-coverage programming in gas-solid chromatography with an adsorbable carrier gas. *Analytical Chemistry,* 60**,** 1090-1096.

IONESCU 2013a. The Human Respiratory System. Springer.

IONESCU, C. M. 2013b. The Human Respiratory System. *In:* IONESCU, C. M. (ed.) *The Human Respiratory System: An Analysis of the Interplay*

between Anatomy, Structure, Breathing and Fractal Dynamics. London: Springer London.

IRBY, D., DU, C. & LI, F. 2017. Lipid–Drug Conjugate for Enhancing Drug Delivery. *Molecular Pharmaceutics,* 14**,** 1325-1338.

IYER, R., HSIA, C. C. W. & NGUYEN, K. T. 2015. Nano-Therapeutics for the Lung: State-of-the-Art and Future Perspectives. *Current pharmaceutical design,* 21**,** 5233-5244.

JAAFAR-MAALEJ, C., DIAB, R., ANDRIEU, V., ELAISSARI, A. & FESSI, H. 2010. Ethanol injection method for hydrophilic and lipophilic drug-loaded liposome preparation. *J Liposome Res,* 20**,** 228-43.

JACKSON, S. P. & BARTEK, J. 2009. The DNA-damage response in human biology and disease. *Nature,* 461**,** 1071-8.

JAIN, A., GULBAKE, A., JAIN, A., SHILPI, S., HURKAT, P., KASHAW, S. & JAIN, S. K. 2014a. Development and Validation of the HPLC Method for Simultaneous Estimation of Paclitaxel and Topotecan. *Journal of Chromatographic Science,* 52**,** 697-703.

JAIN, K. K. 2009. The role of nanobiotechnology in drug discovery. *Adv Exp Med Biol,* 655**,** 37-43.

JAIN, S., JAIN, V. & MAHAJAN, S. C. 2014b. Lipid Based Vesicular Drug Delivery Systems. *Advances in Pharmaceutics,* 2014**,** 12.

JIN, J.-F., ZHU, L.-L., CHEN, M., XU, H.-M., WANG, H.-F., FENG, X.-Q., ZHU, X.-P. & ZHOU, Q. 2015. The optimal choice of medication administration route regarding intravenous, intramuscular, and subcutaneous injection. *Patient preference and adherence,* 9**,** 923-942.

JIN, Y.-J., ZHENG, C. & JI, H.-B. 2012. 20 - Molecular and Cellular Characteristics of Small Cell Lung Cancer: Implications for Molecular-Targeted Cancer Therapy A2 - Liu, Xin-Yuan. *In:* PESTKA, S. & SHI, Y.-F. (eds.) *Recent Advances in Cancer Research and Therapy.* Oxford: Elsevier.

JOSHI, M. D. & MULLER, R. H. 2009. Lipid nanoparticles for parenteral delivery of actives. *Eur J Pharm Biopharm,* 71**,** 161-72.

KALEMKERIAN, G. P. 2011. Staging and imaging of small cell lung cancer. *Cancer Imaging,* 11**,** 253-258.

KAR, A. 2007. *Pharmaceutical Drug Analysis*, New Age International.

KARASAWA, T. & STEYGER, P. S. 2015. An integrated view of cisplatin-induced nephrotoxicity and ototoxicity. *Toxicology letters,* 237**,** 219-227.

KASTAN, M. B. & BARTEK, J. 2004. Cell-cycle checkpoints and cancer. *Nature,* 432**,** 316-23.

KATZUNG, B., MASTERS, S. & TREVOR, A. 2009. *Basic and Clinical Pharmacology, 11th Edition*, Mcgraw-hill.

KATZUNG, B. G., MASTERS, S. B. & TREVOR, A. J. 2012. *Basic and Clinical Pharmacology,* New York, McGraw-Hill Medical.

KAUFMANN, S. H., PEEREBOOM, D., BUCKWALTER, C. A., SVINGEN, P. A., GROCHOW, L. B., DONEHOWER, R. C. & ROWINSKY, E. K. 1996. Cytotoxic Effects of Topotecan Combined With Various Anticancer Agents in Human Cancer Cell Lines. *JNCI: Journal of the National Cancer Institute,* 88**,** 734-741.

KAUR, K. 2016. 2 - Functional nutraceuticals: past, present, and future. *In:* GRUMEZESCU, A. M. (ed.) *Nutraceuticals.* Academic Press.

KAZI, K. M., MANDAL, A. S., BISWAS, N., GUHA, A., CHATTERJEE, S., BEHERA, M. & KUOTSU, K. 2010. Niosome: A future of targeted drug delivery systems. *Journal of Advanced Pharmaceutical Technology & Research,* 1**,** 374-380.

KEARNEY, C. J. & MOONEY, D. J. 2013. Macroscale delivery systems for molecular and cellular payloads. *Nat Mater,* 12**,** 1004-17.

KHAWAJA, M. Z., CAFFERKEY, C., RAJANI, R., REDWOOD, S. & CUNNINGHAM, D. 2013. Cardiac complications and manifestations of chemotherapy for cancer. *Heart*.

KIM, E. H., KIM, M.-S., LEE, K.-H., SAI, S., JEONG, Y. K., KOH, J.-S. & KONG, C.-B. 2017. Effect of low- and high-linear energy transfer radiation on in vitro and orthotopic in vivo models of osteosarcoma by activation of caspase-3 and -9. *International Journal of Oncology,* 51**,** 1124-1134.

KODA-KIMBLE, M. A., YOUNG, L. Y., KRADJAN, W. A. & AL, E. 2008. *Applied Therapeutics: The Clinical Use of Drugs,* Maryland, USA.

KOL, A., TERWISSCHA VAN SCHELTINGA, A., POOL, M., GERDES, C., DE VRIES, E. & DE JONG, S. 2017. ADCC responses and blocking of EGFR-mediated signaling and cell growth by combining the anti-EGFR antibodies imgatuzumab and cetuximab in NSCLC cells. *Oncotarget,* 8**,** 45432-45446.

KOSTOVA, I. 2006. Platinum complexes as anticancer agents. *Recent Pat Anticancer Drug Discov,* 1**,** 1-22.

KOU, L., SUN, J., ZHAI, Y. & HE, Z. 2013. The endocytosis and intracellular fate of nanomedicines: Implication for rational design. *Asian Journal of Pharmaceutical Sciences,* 8**,** 1-10.

KRAFT, J. C., FREELING, J. P., WANG, Z. & HO, R. J. Y. 2014. Emerging Research and Clinical Development Trends of Liposome and Lipid Nanoparticle Drug Delivery Systems. *Journal of pharmaceutical sciences,* 103**,** 29-52.

KRAWCZYK, P., KOWALSKI, D. M., RAMLAU, R., KALINKA-WARZOCHA, E., WINIARCZYK, K., STENCEL, K., POWRÓZEK, T., RESZKA, K., WOJAS-KRAWCZYK, K., BRYL, M., WÓJCIK-SUPERCZYŃSKA, M., GŁOGOWSKI, M., BARINOW-WOJEWÓDZKI, A., MILANOWSKI, J. & KRZAKOWSKI, M. 2017. Comparison of the effectiveness of erlotinib, gefitinib, and afatinib for treatment of non-small cell lung cancer in patients with common and rare EGFR gene mutations. *Oncology Letters,* 13**,** 4433-4444.

KUBIK, T., BOGUNIA-KUBIK, K. & SUGISAKA, M. 2005. Nanotechnology on duty in medical applications. *Curr Pharm Biotechnol,* 6**,** 17-33.

KURASHIGE, T., SHIMAMURA, M. & NAGAYAMA, Y. 2016. Differences in quantification of DNA double-strand breaks assessed by 53BP1/γH2AX focus formation assays and the comet assay in mammalian cells treated with irradiation and N-acetyl-L-cysteine. *Journal of Radiation Research,* 57**,** 312-317.

KUZMOV, A. & MINKO, T. 2015. Nanotechnology approaches for inhalation treatment of lung diseases. *Journal of Controlled Release,* 219**,** 500-518.

KYDD, J., JADIA, R., VELPURISIVA, P., GAD, A., PALIWAL, S. & RAI, P. 2017. Targeting Strategies for the Combination Treatment of Cancer Using Drug Delivery Systems. *Pharmaceutics,* 9**,** 46.

LANTUEJOUL, S. & BRAMBILLA, E. 2018. 27 - Neuroendocrine Neoplasms A2 - Zander, Dani S. *In:* FARVER, C. F. (ed.) *Pulmonary Pathology (Second Edition).* Philadelphia: Content Repository Only!

LEE, S. M., O'HALLORAN, T. V. & NGUYEN, S. T. 2010. Polymer-caged nanobins for synergistic cisplatin-doxorubicin combination chemotherapy. *J Am Chem Soc,* 132**,** 17130-8.

LEFEMINE, V. & SWEETLAND, H. 2012. The role of surgeons in cancer management. *Surgery (Oxford),* 30**,** 181-185.

LEIVA, M. C., ORTIZ, R., CONTRERAS-CÁCERES, R., PERAZZOLI, G., MAYEVYCH, I., LÓPEZ-ROMERO, J. M., SARABIA, F., BAEYENS, J. M., MELGUIZO, C. & PRADOS, J. 2017. Tripalmitin nanoparticle formulations significantly enhance paclitaxel antitumor activity against breast and lung cancer cells in vitro. *Scientific Reports,* 7**,** 13506.

LI, X., LU, W. L., LIANG, G. W., RUAN, G. R., HONG, H. Y., LONG, C., ZHANG, Y. T., LIU, Y., WANG, J. C., ZHANG, X. & ZHANG, Q. 2006. Effect of stealthy liposomal topotecan plus amlodipine on the multidrug-resistant leukaemia cells in vitro and xenograft in mice. *European Journal of Clinical Investigation,* 36**,** 409-418.

LIAN, T. & HO, R. J. 2001. Trends and developments in liposome drug delivery systems. *J Pharm Sci,* 90**,** 667-80.

LIANG, N., JIA, L., LIU, Y., LIANG, B., KONG, D., YAN, M., MA, S. & LIU, X. 2013. ATM pathway is essential for ionizing radiation-induced autophagy. *Cell Signal,* 25**,** 2530-9.

LIN, C.-H., CHEN, C.-H., LIN, Z.-C. & FANG, J.-Y. 2017. Recent advances in oral delivery of drugs and bioactive natural products using solid lipid nanoparticles as the carriers. *Journal of Food and Drug Analysis,* 25**,** 219-234.

LIN, X. & HOWELL, S. B. 2006. DNA mismatch repair and p53 function are major determinants of the rate of development of cisplatin resistance. *Molecular Cancer Therapeutics,* 5**,** 1239-1247.

LIU, J. J., HONG, R. L., CHENG, W. F., HONG, K., CHANG, F. H. & TSENG, Y. L. 2002. Simple and efficient liposomal encapsulation of topotecan by ammonium sulfate gradient: stability, pharmacokinetic and therapeutic evaluation. *Anticancer Drugs,* 13**,** 709-17.

LIU, M. I. N., MA, S., LIU, M., HOU, Y., LIANG, B., SU, X. U. & LIU, X. 2014. Synergistic killing of lung cancer cells by cisplatin and radiation via autophagy and apoptosis. *Oncology Letters,* 7**,** 1903-1910.

LOPEZ, M. 2015. Stem cell division theory of cancer. *Cell Cycle,* 14**,** 2547-8.

MADER, S. S. 2004. *Human Biology*, McGraw Hill Publishing.

MAIRS, R. J. & BOYD, M. 2011. Preclinical Assessment of Strategies for Enhancement of Metaiodobenzylguanidine Therapy of Neuroendocrine Tumors. *Seminars in Nuclear Medicine,* 41**,** 334-344.

MANAIA, E. B., ABUÇAFY, M. P., CHIARI-ANDRÉO, B. G., SILVA, B. L., OSHIRO JUNIOR, J. A. & CHIAVACCI, L. A. 2017. Physicochemical

characterization of drug nanocarriers. *International Journal of Nanomedicine,* 12**,** 4991-5011.

MARASINI, N., GHAFFAR, K. A., SKWARCZYNSKI, M. & TOTH, I. 2017. Chapter Twelve - Liposomes as a Vaccine Delivery System. *In:* SKWARCZYNSKI, M. & TOTH, I. (eds.) *Micro and Nanotechnology in Vaccine Development.* William Andrew Publishing.

MARCHESINI, R., COLOMBO, A., CASERINI, C., PEREGO, P., SUPINO, R., CAPRANICO, G., TRONCONI, M. & ZUNINO, F. 1996. Interaction of ionizing radiation with topotecan in two human tumor cell lines. *Int J Cancer,* 66**,** 342-6.

MARQUELE-OLIVEIRA, F., SANTANA, D. C., TAVEIRA, S. F., VERMEULEN, D. M., DE OLIVEIRA, A. R., DA SILVA, R. S. & LOPEZ, R. F. 2010. Development of nitrosyl ruthenium complex-loaded lipid carriers for topical administration: improvement in skin stability and in nitric oxide release by visible light irradiation. *J Pharm Biomed Anal,* 53**,** 843-51.

MARTINELLI, E., DE PALMA, R., ORDITURA, M., DE VITA, F. & CIARDIELLO, F. 2009. Anti-epidermal growth factor receptor monoclonal antibodies in cancer therapy. *Clinical and Experimental Immunology,* 158**,** 1-9.

MATSUOKA, S., HUANG, M. & ELLEDGE, S. J. 1998. Linkage of ATM to cell cycle regulation by the Chk2 protein kinase. *Science,* 282**,** 1893-7.

MAYER, E. L. 2015. Targeting Breast Cancer with CDK Inhibitors. *Current Oncology Reports,* 17**,** 20.

MIHLON, F., RAY, C. E. & MESSERSMITH, W. 2010. Chemotherapy Agents: A Primer for the Interventional Radiologist. *Seminars in Interventional Radiology,* 27**,** 384-390.

MILLER, R. P., TADAGAVADI, R. K., RAMESH, G. & REEVES, W. B. 2010. Mechanisms of Cisplatin Nephrotoxicity. *Toxins,* 2**,** 2490-2518.

MINNA, J. D., ROTH, J. A. & GAZDAR, A. 2002. Focus on lung cancer. 1.

MINNA., JOHN., D., ROTH, JACK., A., GAZDAR. & ADI., F. 2002. Focus on lung cancer. 1.

MISHRA, B., PATEL, B. B. & TIWARI, S. 2010. Colloidal nanocarriers: a review on formulation technology, types and applications toward targeted drug delivery. *Nanomedicine.* United States: 2010 Elsevier Inc.

MITCHELL, J. & NAGEL, M. 2004. Particle Size Analysis of Aerosols from Medicinal Inhalers. *KONA Powder and Particle Journal,* 22**,** 32-65.

MITCHELL, J., NEWMAN, S. & CHAN, H.-K. 2007. In vitro and in vivo aspects of cascade impactor tests and inhaler performance: A review. *AAPS PharmSciTech,* 8**,** 237-248.

MOGHASSEMI, S. & HADJIZADEH, A. 2014. Nano-niosomes as nanoscale drug delivery systems: an illustrated review. *J Control Release,* 185**,** 22-36.

MOLERÓN, R. Chemoradiation: Why, what, for whom? *Reports of Practical Oncology & Radiotherapy,* 18**,** S7-S8.

MOLNÁR, I. & HORVÁTH, C. 1976. Reverse-phase chromatography of polar biological substances: separation of catechol compounds by high-performance liquid chromatography. *Clinical Chemistry,* 22**,** 1497-1502.

MÜLLER, R. H., MÄDER, K. & GOHLA, S. 2000. Solid lipid nanoparticles (SLN) for controlled drug delivery – a review of the state of the art. *European Journal of Pharmaceutics and Biopharmaceutics,* 50**,** 161-177.

MURALIDHARAN, P., MALAPIT, M., MALLORY, E., HAYES, D. & MANSOUR, H. M. 2015. Inhalable nanoparticulate powders for respiratory delivery. *Nanomedicine: Nanotechnology, Biology and Medicine,* 11**,** 1189-1199.

NEMATOLLAHI, M. H., PARDAKHTY, A., TORKZADEH-MAHANAI, M., MEHRABANI, M. & ASADIKARAM, G. 2017. Changes in physical and chemical properties of niosome membrane induced by cholesterol: a promising approach for niosome bilayer intervention. *RSC Advances,* 7**,** 49463-49472.

NGOUNE, R., PETERS, A., VON ELVERFELDT, D., WINKLER, K. & PÜTZ, G. 2016. Accumulating nanoparticles by EPR: A route of no return. *Journal of Controlled Release,* 238**,** 58-70.

NICHOLS, S. C., MITCHELL, J. P., SHELTON, C. M. & ROBERTS, D. L. 2013. Good Cascade Impactor Practice (GCIP) and considerations for "in-use" specifications. *AAPS PharmSciTech,* 14**,** 375-390.

NURWIDYA, F., TAKAHASHI, F. & TAKAHASHI, K. 2016. Gefitinib in the treatment of nonsmall cell lung cancer with activating epidermal growth factor receptor mutation. *Journal of Natural Science, Biology, and Medicine,* 7**,** 119-123.

O'CALLAGHAN, C. & BARRY, P. W. 1997. The science of nebulised drug delivery. *Thorax,* 52**,** S31-S44.

OHNESEIT, P. A., PRAGER, D., KEHLBACH, R. & RODEMANN, H. P. 2005. Cell cycle effects of topotecan alone and in combination with irradiation. *Radiother Oncol,* 75**,** 237-45.

OJINI, I. & GAMMIE, A. 2015. Rapid Identification of Chemoresistance Mechanisms Using Yeast DNA Mismatch Repair Mutants. *G3: Genes|Genomes|Genetics,* 5**,** 1925-1935.

PADMA, V. V. 2015. An overview of targeted cancer therapy. *BioMedicine,* 5**,** 19.

PALUMBO, M. O., KAVAN, P., MILLER, W. H., PANASCI, L., ASSOULINE, S., JOHNSON, N., COHEN, V., PATENAUDE, F., POLLAK, M., JAGOE, R. T. & BATIST, G. 2013. Systemic cancer therapy: achievements and challenges that lie ahead. *Frontiers in Pharmacology,* 4**,** 57.

PANDITA, A. & SHARMA, P. 2013. Pharmacosomes: An Emerging Novel Vesicular Drug Delivery System for Poorly Soluble Synthetic and Herbal Drugs. *ISRN Pharmaceutics,* 2013**,** 348186.

PARANJPE, M. & MULLER-GOYMANN, C. C. 2014. Nanoparticle-mediated pulmonary drug delivery: a review. *Int J Mol Sci,* 15**,** 5852-73.

PARANJPE, M. & MÜLLER, C. C. 2014. Nanoparticle-Mediated Pulmonary Drug Delivery: A Review. *International Journal of Molecular Sciences,* 15**,** 5852-5873.

PARASHAR, B., ARORA, S. & WERNICKE, A. G. 2013. Radiation Therapy for Early Stage Lung Cancer. *Seminars in Interventional Radiology,* 30**,** 185-190.

PATIL, J. S. & SARASIJA, S. 2012. Pulmonary drug delivery strategies: A concise, systematic review. *Lung India : Official Organ of Indian Chest Society,* 29**,** 44-49.

PATTON, J. S. & BYRON, P. R. 2007. Inhaling medicines: delivering drugs to the body through the lungs. *Nat Rev Drug Discov,* 6**,** 67-74.

PENG, T., LIN, S., NIU, B., WANG, X., HUANG, Y., ZHANG, X., LI, G., PAN, X. & WU, C. 2016. Influence of physical properties of carrier on the performance of dry powder inhalers. *Acta Pharmaceutica Sinica B,* 6**,** 308-318.

PILCER, G., VANDERBIST, F. & AMIGHI, K. 2009. Spray-dried carrier-free dry powder tobramycin formulations with improved dispersion properties. *J Pharm Sci,* 98**,** 1463-75.

POMMIER, Y., SUN, Y., HUANG, S. N. & NITISS, J. L. 2016. Roles of eukaryotic topoisomerases in transcription, replication and genomic stability. *Nat Rev Mol Cell Biol,* 17**,** 703-721.

PRIESTMAN, T. 2008. *Cancer Chemotherapy in Clinical Practice*.

PUIG, M. 2016. *Development of non-ionic surfactant vesicles for inhaled drug delivery.* Ph.D., Strathclyde University.

QI, S.-S., SUN, J.-H., YU, H.-H. & YU, S.-Q. 2017. Co-delivery nanoparticles of anti-cancer drugs for improving chemotherapy efficacy. *Drug Delivery,* 24**,** 1909-1926.

RAICA, M., CIMPEAN, A. M. & RIBATTI, D. 2009. Angiogenesis in pre-malignant conditions. *European Journal of Cancer,* 45**,** 1924-1934.

RAMISHETTI, S. & HUANG, L. 2012. Intelligent design of multifunctional lipid-coated nanoparticle platforms for cancer therapy. *Ther Deliv,* 3**,** 1429-45.

RAVISANKAR, P., NAVYA, N., PRAVALLIKA1 & SRI, N. 2015. A Review on Step-by-Step Analytical Method Validation. *IOSR Journal Of Pharmacy,* 5**,** 07-19.

RINALDI, F., DEL FAVERO, E., RONDELLI, V., PIERETTI, S., BOGNI, A., PONTI, J., ROSSI, F., DI MARZIO, L., PAOLINO, D., MARIANECCI, C. & CARAFA, M. 2017. pH-sensitive niosomes: Effects on cytotoxicity and on inflammation and pain in murine models. *Journal of Enzyme Inhibition and Medicinal Chemistry,* 32**,** 538-546.

RIVERA, A. M., STRAUSS, K. W., VAN ZUNDERT, A. & MORTIER, E. 2005. The history of peripheral intravenous catheters: how little plastic tubes revolutionized medicine. *Acta Anaesthesiol Belg,* 56**,** 271-82.

ROSE, P. G., BUNDY, B. N., WATKINS, E. B., THIGPEN, J. T., DEPPE, G., MAIMAN, M. A., CLARKE-PEARSON, D. L. & INSALACO, S. 1999. Concurrent cisplatin-based radiotherapy and chemotherapy for locally advanced cervical cancer. *N Engl J Med,* 340**,** 1144-53.

RUBIN, B. P., SINGER, S., TSAO, C., DUENSING, A., LUX, M. L., RUIZ, R., HIBBARD, M. K., CHEN, C. J., XIAO, S., TUVESON, D. A., DEMETRI, G. D., FLETCHER, C. D. & FLETCHER, J. A. 2001. KIT activation is a ubiquitous feature of gastrointestinal stromal tumors. *Cancer Res,* 61**,** 8118-21.

RUCKMANI, K. & SANKAR, V. 2010. Formulation and Optimization of Zidovudine Niosomes. *AAPS PharmSciTech,* 11**,** 1119-1127.

SAHOO, R. K., BISWAS, N., GUHA, A., SAHOO, N. & KUOTSU, K. 2014. Nonionic Surfactant Vesicles in Ocular Delivery: Innovative Approaches and Perspectives. *BioMed Research International,* 2014**,** 12.

SAINI, P. K., JAIN, C. L., SINGH, R. M., MATHUR, S. C. & SINGH, G. N. 2010. Development and Validation of a RP-Ultra performance liquid chromatographic Method for Quantification of Topotecan Hydrochloride in Bulk and Injection Dosage Form. *Indian J Pharm Sci,* 72**,** 494-7.

SARIN, N., ENGEL, F., KALAYDA, G. V., MANNEWITZ, M., CINATL, J., JR., ROTHWEILER, F., MICHAELIS, M., SAAFAN, H., RITTER, C. A., JAEHDE, U. & FROTSCHL, R. 2017. Cisplatin resistance in non-small cell lung cancer cells is associated with an abrogation of cisplatin-induced G2/M cell cycle arrest. *PLoS One,* 12**,** e0181081.

SAVAS, P., HUGHES, B. & SOLOMON, B. 2013. Targeted therapy in lung cancer: IPASS and beyond, keeping abreast of the explosion of targeted therapies for lung cancer. *J Thorac Dis,* 5 Suppl 5**,** S579-92.

SCHEIDEGGER, S., FUCHS, H. U., ZAUGG, K., BODIS, S. & FÜCHSLIN, R. M. 2013. Using State Variables to Model the Response of Tumour Cells to Radiation and Heat: A Novel Multi-Hit-Repair Approach. *Computational and Mathematical Methods in Medicine,* 2013**,** 587543.

SCHINAZI, R. F., CHOU, T. C., SCOTT, R. T., YAO, X. J. & NAHMIAS, A. J. 1986. Delayed treatment with combinations of antiviral drugs in mice infected with herpes simplex virus and application of the median effect method of analysis. *Antimicrob Agents Chemother,* 30**,** 491-8.

SEARS, C. R., COONEY, S. A., CHIN-SINEX, H., MENDONCA, M. S. & TURCHI, J. J. 2016a. DNA damage response (DDR) pathway engagement in cisplatin radiosensitization of non-small cell lung cancer. *DNA Repair (Amst),* 40**,** 35-46.

SEARS, C. R., COONEY, S. A., CHIN-SINEX, H., MENDONCA, M. S. & TURCHI, J. J. 2016b. DNA damage response (DDR) pathway engagement in cisplatin radiosensitization of non-small cell lung cancer. *DNA repair,* 40**,** 35-46.

SEIWERT, T. Y., SALAMA, J. K. & VOKES, E. E. 2007. The concurrent chemoradiation paradigm--general principles. *Nat Clin Pract Oncol,* 4**,** 86-100.

SEKIGUCHI, I., SUZUKI, M., TAMADA, T., SHINOMIYA, N., TSURU, S. & MURATA, M. 1996. Effects of cisplatin on cell cycle kinetics, morphological change, and cleavage pattern of DNA in two human ovarian carcinoma cell lines. *Oncology,* 53**,** 19-26.

SEMALTY, A., SEMALTY, M., RAWAT, B. S., SINGH, D. & RAWAT, M. S. 2009. Pharmacosomes: the lipid-based new drug delivery system. *Expert Opin Drug Deliv,* 6**,** 599-612.

SEVER, R. & BRUGGE, J. S. 2015. Signal Transduction in Cancer. *Cold Spring Harbor Perspectives in Medicine,* 5**,** a006098.

SHABIR, G. A. 2003. Validation of high-performance liquid chromatography methods for pharmaceutical analysis. Understanding the differences and similarities between validation requirements of the US Food and Drug

Administration, the US Pharmacopeia and the International Conference on Harmonization. *J Chromatogr A,* 987**,** 57-66.

SHAGAM, J. Y. 2010. Cancer-focused molecular imaging. *Radiol Technol,* 82**,** 59-80.

SHAKER, S., GARDOUH, A. R. & GHORAB, M. M. 2017. Factors affecting liposomes particle size prepared by ethanol injection method. *Research in Pharmaceutical Sciences,* 12**,** 346-352.

SHARMA, P. & ALLISON, J. P. 2015a. Immune checkpoint targeting in Cancer Therapy: toward combination strategies with curative potential. *Cell,* 161.

SHARMA, P. & ALLISON, J. P. 2015b. Immune checkpoint targeting in cancer therapy: toward combination strategies with curative potential. *Cell,* 161**,** 205-14.

SHARMA, P., WAGNER, K., WOLCHOK, J. D. & ALLISON, J. P. 2011. Novel cancer immunotherapy agents with survival benefit: recent successes and next steps. *Nat Rev Cancer,* 11**,** 805-12.

SHEKUNOV, B. Y., CHATTOPADHYAY, P., TONG, H. H. & CHOW, A. H. 2007. Particle size analysis in pharmaceutics: principles, methods and applications. *Pharm Res,* 24**,** 203-27.

SHEN, D.-W., POULIOT, L. M., HALL, M. D. & GOTTESMAN, M. M. 2012. Cisplatin Resistance: A Cellular Self-Defense Mechanism Resulting from Multiple Epigenetic and Genetic Changes. *Pharmacological Reviews,* 64**,** 706-721.

SHI, J., KANTOFF, P. W., WOOSTER, R. & FAROKHZAD, O. C. 2017. Cancer nanomedicine: progress, challenges and opportunities. *Nature reviews. Cancer,* 17**,** 20-37.

SHI, J., VOTRUBA, A. R., FAROKHZAD, O. C. & LANGER, R. 2010. Nanotechnology in drug delivery and tissue engineering: from discovery to applications. *Nano Lett,* 10**,** 3223-30.

SIEGEL, R., DESANTIS, C., VIRGO, K. & AL, E. 2012. Cancer treatment and survivorship statistics, 2012. *Cancer Journal for Clinicians,* 62**,** 220-241.

SIEGLER, E. L., KIM, Y. J. & WANG, P. 2016. Nanomedicine targeting the tumor microenvironment: Therapeutic strategies to inhibit angiogenesis, remodel matrix, and modulate immune responses. *Journal of Cellular Immunotherapy,* 2**,** 69-78.

SMOLA, M., VANDAMME, T. & SOKOLOWSKI, A. 2008. Nanocarriers as pulmonary drug delivery systems to treat and to diagnose respiratory and non respiratory diseases. *International Journal of Nanomedicine,* 3**,** 1-19.

SORENSON, C. M., BARRY, M. A. & EASTMAN, A. 1990. Analysis of events associated with cell cycle arrest at G2 phase and cell death induced by cisplatin. *J Natl Cancer Inst,* 82**,** 749-55.

SOUZA, L. G., SILVA, E. J., MARTINS, A. L., MOTA, M. F., BRAGA, R. C., LIMA, E. M., VALADARES, M. C., TAVEIRA, S. F. & MARRETO, R. N. 2011a. Development of topotecan loaded lipid nanoparticles for chemical stabilization and prolonged release. *Eur J Pharm Biopharm,* 79**,** 189-96.

SOUZA, L. G., SILVA, E. J., MARTINS, A. L. L., MOTA, M. F., BRAGA, R. C., LIMA, E. M., VALADARES, M. C., TAVEIRA, S. F. & MARRETO, R. N.

2011b. Development of topotecan loaded lipid nanoparticles for chemical stabilization and prolonged release. *European Journal of Pharmaceutics and Biopharmaceutics,* 79**,** 189-196.

STAKER, B. L., HJERRILD, K., FEESE, M. D., BEHNKE, C. A., BURGIN, A. B. & STEWART, L. 2002. The mechanism of topoisomerase I poisoning by a camptothecin analog. *Proceedings of the National Academy of Sciences of the United States of America,* 99**,** 15387-15392.

STETEFELD, J., MCKENNA, S. A. & PATEL, T. R. 2016. Dynamic light scattering: a practical guide and applications in biomedical sciences. *Biophysical Reviews,* 8**,** 409-427.

STEWART, B. & WILD, C. P. 2014. World Cancer Report 2014. International Agency for Research on Cancer.

STEWART, D. 2010. *Lung Cancer Prevention, Management, and Emerging Therapies,* New York, Springer.

STRATTON, M. R., CAMPBELL, P. J. & FUTREAL, P. A. 2009. The cancer genome. *Nature,* 458**,** 719-724.

TAKIMOTO, C. H. & ARBUCK, S. G. 1997. Clinical status and optimal use of topotecan. *Oncology (Williston Park),* 11**,** 1635-46; discussion 1649-51, 1655-7.

TANIDA, S., MIZOSHITA, T., OZEKI, K., TSUKAMOTO, H., KAMIYA, T., KATAOKA, H., SAKAMURO, D. & JOH, T. 2012. Mechanisms of Cisplatin-Induced Apoptosis and of Cisplatin Sensitivity: Potential of BIN1 to Act as a Potent Predictor of Cisplatin Sensitivity in Gastric Cancer Treatment. *International Journal of Surgical Oncology,* 2012**,** 862879.

TILLEY, A. E., WALTERS, M. S., SHAYKHIEV, R. & CRYSTAL, R. G. 2015. Cilia Dysfunction in Lung Disease. *Annual review of physiology,* 77**,** 379-406.

TIRUMANI, S. H., FAIRCHILD, A., KRAJEWSKI, K. M., NISHINO, M., HOWARD, S. A., BAHETI, A. D., ROSENTHAL, M. H., JAGANNATHAN, J. P., SHINAGARE, A. B. & RAMAIYA, N. H. 2015. Anti-VEGF Molecular Targeted Therapies in Common Solid Malignancies: Comprehensive Update for Radiologists. *RadioGraphics,* 35**,** 455-474.

TOLIS, C., PETERS, G. J., FERREIRA, C. G., PINEDO, H. M. & GIACCONE, G. 1999. Cell cycle disturbances and apoptosis induced by topotecan and gemcitabine on human lung cancer cell lines. *Eur J Cancer,* 35**,** 796-807.

TOMASETTI, C., LI, L. & VOGELSTEIN, B. 2017. Stem cell divisions, somatic mutations, cancer etiology, and cancer prevention. *Science,* 355**,** 1330-1334.

TORCHILIN, V. P. 2005. Recent advances with liposomes as pharmaceutical carriers. *Nat Rev Drug Discov,* 4**,** 145-60.

TOULANY, M., MIHATSCH, J., HOLLER, M., CHAACHOUAY, H. & RODEMANN, H. P. 2014. Cisplatin-mediated radiosensitization of non-small cell lung cancer cells is stimulated by ATM inhibition. *Radiother Oncol,* 111**,** 228-36.

TRAVIS, W. D., BRAMBILLA, E., MÜLLER-HERMELINK, H. K. & HARRIS, C. C. 2004. World Health Organization Classification of Tumours: Tumours of the Lung, Pleura,Thymus and Heart. World Health Organization.

TSENG., C.-L., YANG., K.-C., YEN., K.-C., WU., S. Y.-H. & LIN., F.-H. 2011. Preparation and Characterization of Cisplatin-Incorporated Gelatin Nanocomplex for Cancer Treatment. *Current Nanoscience,* 7**,** 932 - 937.

TSIM, S., O'DOWD, C. A., MILROY, R. & DAVIDSON, S. 2010. Staging of non-small cell lung cancer (NSCLC): A review. *Respiratory Medicine,* 104**,** 1767-1774.

UPPONI & TORCHILIN 2014. Passive vs. Active Targeting: An Update of the EPR Role in Drug Delivery to Tumors. Springer, Cham.

UTSUMI, H. & ELKIND, M. M. 2001. Requirement for repair of DNA double-strand breaks by homologous recombination in split-dose recovery. *Radiat Res,* 155**,** 680-6.

VELEZ, A. M. A. & HOWARD, M. S. 2015. Tumor-suppressor Genes, Cell Cycle Regulatory Checkpoints, and the Skin. *North American Journal of Medical Sciences,* 7**,** 176-188.

VELINOVA, M. J., STAFFHORST, R. W. H. M., MULDER, W. J. M., DRIES, A. S., JANSEN, B. A. J., DE KRUIJFF, B. & DE KROON, A. I. P. M. 2004. Preparation and stability of lipid-coated nanocapsules of cisplatin: anionic phospholipid specificity. *Biochimica et Biophysica Acta (BBA) - Biomembranes,* 1663**,** 135-142.

VENNEPUREDDY, A., ATALLAH, J.-P. & TERJANIAN, T. 2015. Role of Topotecan in Non-Small Cell Lung Cancer: A Review of Literature. *World Journal of Oncology,* 6**,** 429-436.

VINCENT, B. 2012. Early (pre-DLVO) studies of particle aggregation. *Advances in Colloid and Interface Science,* 170**,** 56-67.

VISACRI, M. B., PINCINATO, E. D. C., FERRARI, G. B., QUINTANILHA, J. C. F., MAZZOLA, P. G., LIMA, C. S. P. & MORIEL, P. 2017. Adverse drug reactions and kinetics of cisplatin excretion in urine of patients undergoing cisplatin chemotherapy and radiotherapy for head and neck cancer: a prospective study. *DARU Journal of Pharmaceutical Sciences,* 25**,** 12.

VISCONTI, R., DELLA MONICA, R. & GRIECO, D. 2016. Cell cycle checkpoint in cancer: a therapeutically targetable double-edged sword. *Journal of Experimental & Clinical Cancer Research : CR,* 35**,** 153.

VISCONTI, R. & GRIECO, D. 2009. New insights on oxidative stress in cancer. *Curr Opin Drug Discov Devel,* 12**,** 240-5.

VITORINO, C., CARVALHO, F. A., ALMEIDA, A. J., SOUSA, J. J. & PAIS, A. A. C. C. 2011. The size of solid lipid nanoparticles: An interpretation from experimental design. *Colloids and Surfaces B: Biointerfaces,* 84**,** 117-130.

VIVANCO, I. & SAWYERS, C. L. 2002. The phosphatidylinositol 3-Kinase–AKT pathway in human cancer. *Nature Reviews Cancer,* 2**,** 489.

VIVEK, K., REDDY, H. & MURTHY, R. S. R. 2007. Investigations of the effect of the lipid matrix on drug entrapment, in vitro release, and physical stability of olanzapine-loaded solid lipid nanoparticles. *AAPS PharmSciTech,* 8**,** 16-24.

VOUSDEN, K. H. & LU, X. 2002. Live or let die: the cell's response to p53. *Nat Rev Cancer,* 2**,** 594-604.

WANG, J.-S., WANG, H.-J. & QIAN, H.-L. 2018. Biological effects of radiation on cancer cells. *Military Medical Research,* 5**,** 20.

WANG, Y.-F., LIU, L., XUE, X. & LIANG, X.-J. 2017. Nanoparticle-based drug delivery systems: What can they really do in vivo? *F1000Research,* 6**,** 681.

WANG, Y., HA, M., LIU, J., LI, P., ZHANG, W. & ZHANG, X. 2016. Role of BCL2-associated athanogene in resistance to platinum-based chemotherapy in non-small-cell lung cancer. *Oncol Lett,* 11**,** 984-990.

WELLS, B. G., DIPIRO, J. T., SCHWINGHAMMER, T. L. & DIPIRO, C. V. 2009. *Pharmacotherapy Handbook*, McGraw-Hill.

WENZLER, E., FRAIDENBURG, D. R., SCARDINA, T. & DANZIGER, L. H. 2016. Inhaled Antibiotics for Gram-Negative Respiratory Infections. *Clinical Microbiology Reviews,* 29**,** 581-632.

WEYEL, D., SEDLACEK, H. H., MÜLLER, R. & BRÜSSELBACH, S. 2000. Secreted human β-glucuronidase: a novel tool for gene-directed enzyme prodrug therapy. *Gene Therapy,* 7**,** 224.

WINDMAIER, P. W. R., H. STRANG, T.S. 2004. *Vander, Sherman, & Luciano's Human Physiology,*, Mcgraw-Hill.

WONG, E. T. & BERKENBLIT, A. 2004. The role of topotecan in the treatment of brain metastases. *Oncologist,* 9**,** 68-79.

WRIGHT, J. R., JR. 2013. Charles Emmanuel Sédillot and Émile Küss: The first cancer biopsy. *International Journal of Surgery,* 11**,** 106-107.

WU, H.-M., JIANG, Z.-F., DING, P.-S., SHAO, L.-J. & LIU, R.-Y. 2015. Hypoxia-induced autophagy mediates cisplatin resistance in lung cancer cells. *Scientific Reports,* 5**,** 12291.

XIAODAN, S., XUEJUN, W., XIA, D., HUA, W., DI, D. & LINHUA, W. 2007. Preparation of beta-elemene liposomes and their tissue distribution in rats. *Chinese Pharmaceutical Journal,* 42**,** 1480–1482.

XU, G. & MCLEOD, H. L. 2001. Strategies for Enzyme/Prodrug Cancer Therapy. *Clinical Cancer Research,* 7**,** 3314-3324.

YADDANAPUDI, K., MITCHELL, R. A. & EATON, J. W. 2013. Cancer vaccines: Looking to the future. *Oncoimmunology,* 2**,** e23403.

YANG, W., PETERS, J. I. & WILLIAMS, R. O., 3RD 2008. Inhaled nanoparticles--a current review. *Int J Pharm,* 356**,** 239-47.

YILMAZ, M. & CHRISTOFORI, G. 2009. EMT, the cytoskeleton, and cancer cell invasion. *Cancer Metastasis Rev,* 28**,** 15-33.

YOU, Y. N., LAKHANI, V. T. & WELLS, S. A. 2007. The Role of Prophylactic Surgery in Cancer Prevention. *World Journal of Surgery,* 31**,** 450-464.

YOUNGREN-ORTIZ, S. R., GANDHI, N. S., ESPAÑA-SERRANO, L. & CHOUGULE, M. B. 2016. Aerosol Delivery of siRNA to the Lungs. Part 1: Rationale for Gene Delivery Systems. *KONA Powder and Particle Journal,* 33**,** 63-85.

ZAPPA, C. & MOUSA, S. A. 2016. Non-small cell lung cancer: current treatment and future advances. *Translational Lung Cancer Research,* 5**,** 288-300.

ZHANG, Y. L., YUAN, J. Q., WANG, K. F., FU, X. H., HAN, X. R., THREAPLETON, D., YANG, Z. Y., MAO, C. & TANG, J. L. 2016. The

prevalence of EGFR mutation in patients with non-small cell lung cancer: a systematic review and meta-analysis. *Oncotarget,* 7**,** 78985-78993.

ZHAO, H. & DARZYNKIEWICZ, Z. 2017. Rapid Detection of DNA Strand Breaks in Apoptotic Cells by Flow- and Image-Cytometry. *Methods Mol Biol,* 1644**,** 139-149.

ZHAO, L., WIENTJES, M. G. & AU, J. L. 2004. Evaluation of combination chemotherapy: integration of nonlinear regression, curve shift, isobologram, and combination index analyses. *Clin Cancer Res,* 10**,** 7994-8004.

ZHU, H., SUN, G., DONG, J. & FEI, L. 2017. The role of PRRX1 in the apoptosis of A549 cells induced by cisplatin. *American Journal of Translational Research,* 9**,** 396-402.

Appendix A

1. **Chromatographic conditions of the evaluated HPLC method for cisplatin detection**. Conditions include type of instrument and column, constituent of mobile phase, flow rate, wave lengths, and size of injected sample.

Instrument	Gynkotek® HPLC pump series P580 and autosampler model GINA 50 (Macclesfield, UK) operated by Chromeleon™ software version 6.30 SP3 Build 594, Dionex (Surrey, UK).
Column	Luna 3 µm C18(2) 100A – 150 x 4.60 mm 3 micron
Mobile phase	Water:acetonitrile:methanol 29:31:40 v/v/v
Flow rate	1.4 ml/min
Detector wave length	254 nm
Sample size	20 µg

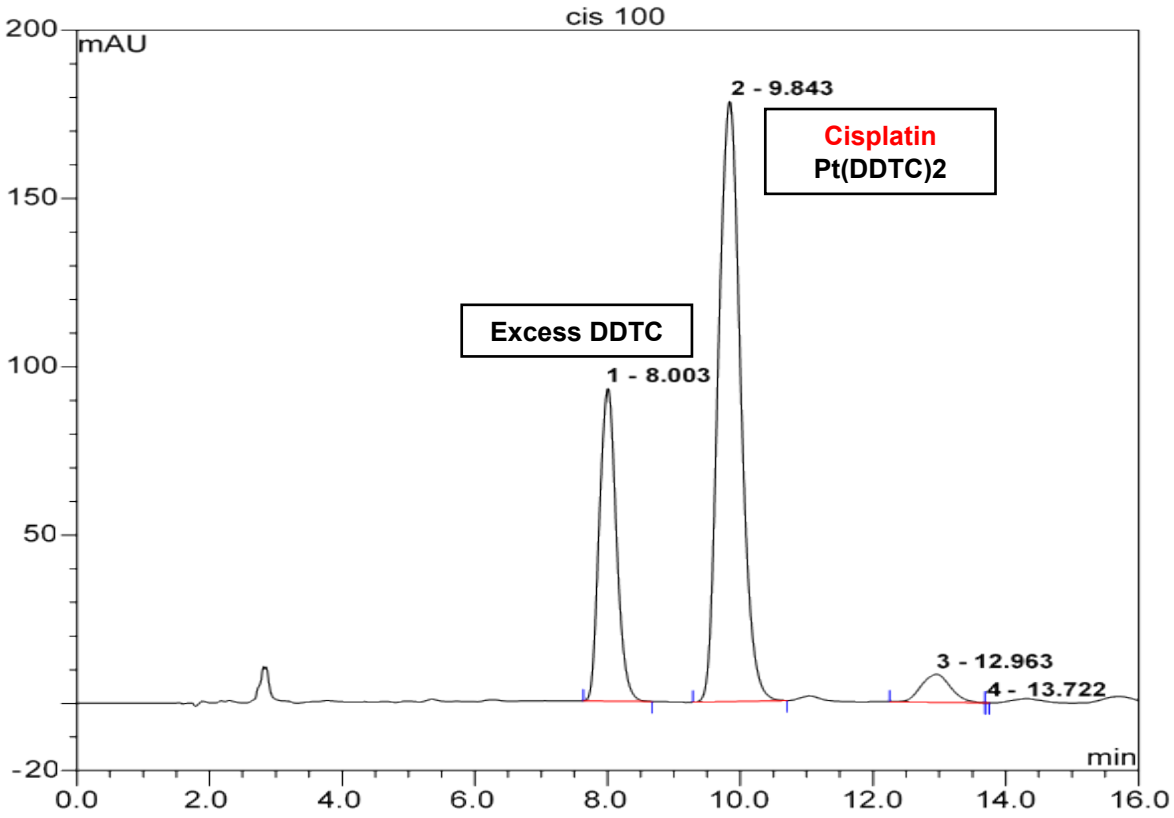

2. A chromatogram illustrating the separation and elution of excess DDTC, Pt(DDTC)2 and Ni(DDTC)2 at 8, 9.8 and 12.9 min, respectively. The sample was prepared from a 0.9% w/v NaCl solution containing 100 µg/ml cisplatin.

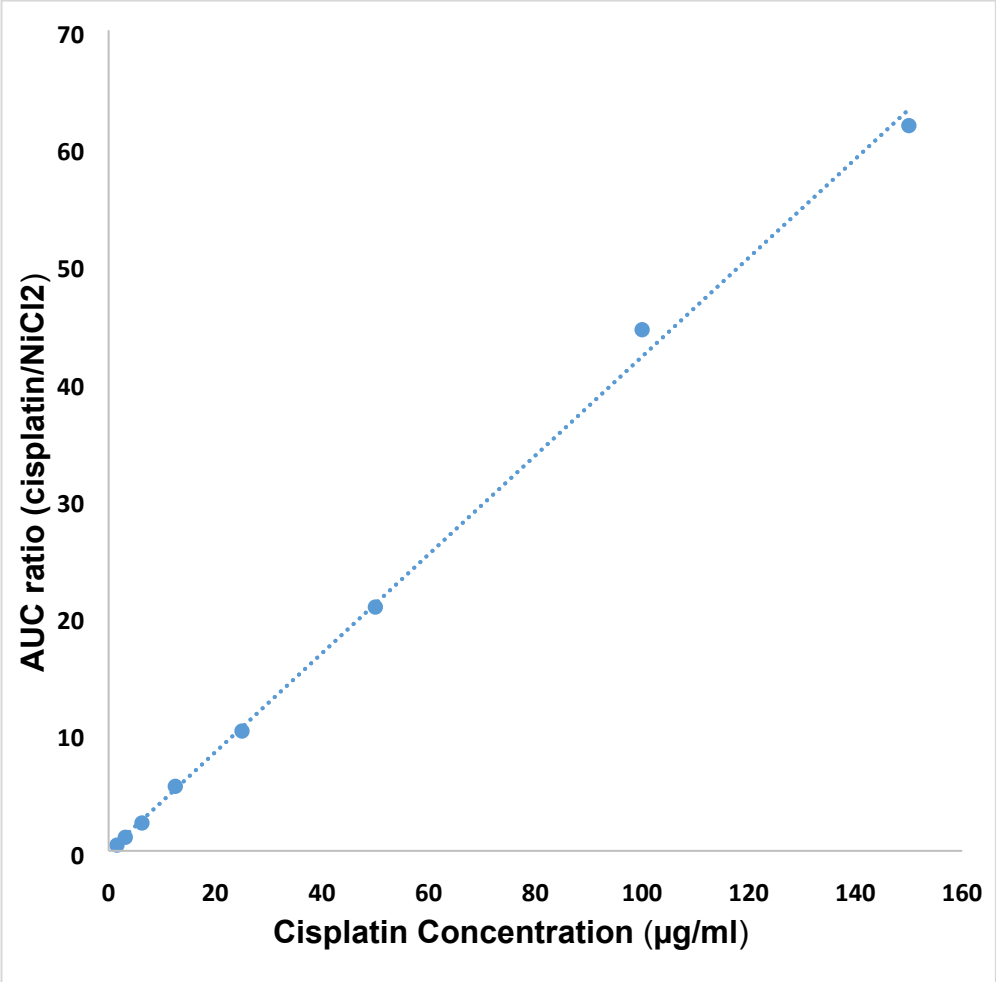

3. A typical calibration curve obtained for the quantification of platinum. Concentrations used to establish the calibration curve were 0, 1.56, 3.125, 6.25, 12.5, 25, 50, 100 and 150 µg/ml in 0.9% w/v NaCl (n=1).

5. The intraday and interday precision of the analysis of cisplatin standard concentrations in 0.9% w/v NaCl. Values are representative as % RSD. Two sets of standards were analysed in triplicate for intraday precision and three sets of standards were analysed in triplicate for interday precision.

Concentration (µg/ml)	Intra-day precision (% RSD) (n = 2)	Inter-day precision (% RSD) (n = 3)
1.56	1.5396	2.8359
3.125	1.6032	2.96511
6.25	1.05	2.9911
12.5	1.3826	2.4539
25	1.475	2.4435
50	1.2479	2.1728
100	0.4069	2.616
150	0.342	1.193

6. Accuracy of method III in the detection of platinum using three concentrations prepared in 0.9% w/v NaCl and analysed in triplicate.

Concentration (µg/ml)	Mean % recovery ± SD (n = 1)
3.125	94.6133 (± 3.5077)
25	96.71667 (± 2.4742)
150	97.79667 (± 1.1679)